

**SYNTHESIS, CHARACTERIZATION AND
CATALYTIC APPLICATIONS OF
TRANSITION METAL INCORPORATED
MESOPOROUS SBA MOLECULAR SIEVES**

A THESIS

SUBMITTED TO THE
UNIVERSITY OF PUNE
FOR THE DEGREE OF
DOCTOR OF PHILOSOPHY

IN
CHEMISTRY

BY
ANUJ KUMAR

UNDER THE GUIDANCE OF
DR. D. SRINIVAS

CATALYSIS DIVISION
NATIONAL CHEMICAL LABORATORY
PUNE - 411 008, INDIA

JANUARY 2013

CERTIFICATE

This is to certify that the work incorporated in the thesis entitled “**Synthesis, Characterization and Catalytic Applications of Transition Metal Incorporated Mesoporous SBA Molecular Sieves**” submitted by **Mr. Anuj Kumar**, to the University of Pune, for the degree of Doctor of Philosophy in Chemistry, was carried out by the candidate under my supervision at Catalysis Division, National Chemical Laboratory, Pune – 411 008, India. Such material as has been obtained from other sources has been duly acknowledged in the thesis. To the best of my knowledge, the present work or any part thereof has not been submitted to any other university for the award of any other degree or diploma.

Place: Pune

Date:

Dr. D. Srinivas

Research Guide

DECLARATION

I hereby declare that the work described in the thesis entitled “**Synthesis, Characterization and Catalytic Applications of Transition Metal Incorporated Mesoporous SBA Molecular Sieves**” submitted for the **Degree of Doctor of Philosophy in Chemistry** to the University of Pune, has been carried out by me at the Catalysis Division, National Chemical Laboratory, Pune – 411 008, India, under the supervision of **Dr. D. Srinivas**. Such material as has been obtained from other sources has been duly acknowledged in this thesis. The work is original and has not been submitted in part or full by me for any other degree or diploma to this or any other University.

Place: Pune

Date:

Anuj Kumar

Research Scholar

***..... Dedicated to
My
Beloved Family
& Teachers***

Acknowledgments

First, I would like to acknowledge my research guide, Dr. D. Srinivas, for his constant inspiration, invaluable guidance and constructive criticism which helped me a lot to focus my views in a proper perspective. I take this opportunity to express my intense reverence towards him for guiding me in the right direction throughout the course of this work. My deepest personal regards are due for him forever.

I wish to express my sincere gratitude to Dr. Paul Ratnasamy, Former Director, National Chemical Laboratory, Pune, for his thought provoking valuable discussions and suggestions during my research work.

I would like to express my profound gratitude to Dr. A.P. Singh, Chairman of Catalysis Division for providing all facilities required for my work.

My heartfelt thanks are due to Dr. (Mrs.) S.A. Pardhy, Dr. (Mrs.) S.S. Deshpande, Dr. S.P. Mirajkar, Dr. C.V.V. Satyanarayana, Dr. T. Raja, Dr. Subhangi Umberkar, Dr. Nandini Devi, Mr. R.K. Jha, Ms. Violet Samuel, Mr. Gaikwad, Mr. P.K. Purushothaman, Mr. Madhu, Mr. Milind and all other scientific and non-scientific staff of the Catalysis Division and NCL for their valuable help and cooperation during my tenure as a research student.

I sincerely thank all my friends especially Lakshi, Jitendra, Mehjabeen, Rahul, Mufsir, Hamza, Bhogesh, Joby, Unnikrishnan, Devadutta, Poonam, Rakesh, Chitra, Anand, Chand, Atul, Ajay, Sahu, Umesh, Malvi, Adhish, Gupta, Prince, Ajeet, Deepak, Ankush, Prakash, Hanmant, Nishita, Trupti, Vaibhav, Thushara, Edwin, Rajesh, Jijil, Prabhakar, Alok, Varun, Birju, Kheria, Ravi, Vilas, Suneel, Sanjay, Himadri, Nem Singh, Roshan, Srikant, Rajeev, Kamal and many others for their valuable help and cooperation during my tenure as a research scholar.

I am extremely grateful to my parents, my late elder brother Shri Chandrasen Maurya, younger brothers Pradeep, Hari Shankar and sister Sushma, for their love, support, patience, encouragement and blessings.

It is indeed my privilege to thank the former and present Director, NCL, Dr. Sivaram and Dr. Sourav Pal for allowing me this opportunity and extending all possible infrastructural facilities at NCL for the research work.

Finally I thank the Council of Scientific and Industrial Research (CSIR), New Delhi for financial support.

Anuj Kumar

TABLE OF CONTENTS

Chapter – 1: General Introduction	1
1.1. Porous Materials	2
1.2. Mesoporous Silica	2
1.3. SBA-Mesoporous Molecular Sieves	3
1.3.1. Three-dimensional Molecular Sieves	4
1.3.1.1. SBA-12	6
1.3.1.2. SBA-16	6
1.4. Mechanisms of Formation of Mesoporous Materials	7
1.4.1. Liquid Crystal Templating (LCT) Mechanism	8
1.4.2. Charge Density Matching and Folding-Sheets Mechanisms	10
1.4.3. Generalized Liquid Crystal Templating Mechanisms	11
1.4.3.1. Ionic Route (Electrostatic Interaction)	11
1.4.3.2. Neutral Templating Route (Hydrogen Bonding Interaction)	12
1.5. Modification of Mesoporous Molecular Sieves	14
1.5.1. Incorporation of Heteroatoms by Direct Hydrothermal Synthesis Method	15
1.5.2. Post Synthesis Method (Grafting/Impregnation of Heteroatoms)	17
1.6. Catalytic Oxidations	18
1.6.1. Epoxidation	19
1.6.2. Hydroxylation	20
1.6.3. Oxidation of Amines	21
1.7. Acid Catalyzed Reactions	21
1.7.1. Aminolysis of Epoxides	21
1.7.2. Esterifications of Acids	22
1.8. Scope and Objectives of the Thesis	22
1.9. Organization of the Thesis	23
1.10. References	24

Chapter – 2: Material Preparation and Characterization		34
2.1.	Introduction	35
2.2.	Materials	35
2.3.	Synthesis of Mesoporous Silica Molecular Sieves	38
2.3.1.	SBA-12	38
2.3.2.	SBA-16	38
2.3.3.	SBA-15	39
2.3.4.	MCM-41	39
2.4.	Synthesis and Characterization of Titanosilicate Molecular Sieves	39
2.4.1.	Synthesis	39
2.4.1.1.	Ti-SBA-12	40
2.4.1.2.	Ti-SBA-16	40
2.4.1.3.	Ti-SBA-15	41
2.4.1.4.	Ti-MCM-41	41
2.4.1.5.	TS-1	41
2.4.2.	Characterization Techniques	42
2.4.2.1.	Chemical Composition	44
2.4.2.2.	X-ray Powder Diffraction (XRD)	44
2.4.2.3.	N ₂ -Physisorption	52
2.4.2.4.	Scanning Electron Microscopy (SEM)	59
2.4.2.5.	High Resolution Transmission Electron Microscopy (HRTEM)	59
2.4.2.6.	Diffuse Reflectance Ultraviolet Visible Spectroscopy (DRUV-vis)	59
2.4.2.7.	Electron Paramagnetic Resonance Spectroscopy (EPR)	63
2.4.2.8.	Fourier Transform Infrared Spectroscopy (FTIR)	65
2.4.2.9.	Fourier Transform Raman Spectroscopy (FT-Raman)	66
2.4.2.10.	²⁹ Si MAS NMR Spectroscopy	66
2.4.2.11.	Thermal Analysis (TGA)	71
2.4.2.12.	Acidic Properties	74

2.5.	Synthesis and Characterization of Manganese-containing SBA-12 and SBA-16 Molecular Sieves	77
2.5.1.	Synthesis	77
2.5.1.1.	Mn-SBA-12	77
2.5.1.2.	Mn-SBA-16	77
2.5.2.	Characterization	78
2.5.2.1.	Chemical Composition	78
2.5.2.2.	X-ray Powder Diffraction (XRD)	78
2.5.2.3.	N ₂ -Physisorption	78
2.5.2.4.	Scanning Electron Microscopy (SEM)	80
2.5.2.5.	High Resolution Transmission Electron Microscopy (HRTEM)	80
2.5.2.6.	Diffuse Reflectance Ultraviolet Visible Spectroscopy (DRUV-vis)	80
2.5.2.7.	Electron Paramagnetic Resonance Spectroscopy (EPR)	84
2.5.2.8.	Fourier Transform Infrared Spectroscopy (FTIR)	85
2.5.2.9.	Fourier Transform Raman Spectroscopy (FT-Raman)	86
2.5.2.10.	Thermal analysis (TGA)	87
2.5.2.11.	NH ₃ -TPD	88
2.6.	Synthesis and Characterization of Vanadium-containing SBA-12 Molecular Sieves	88
2.6.1.	Synthesis	88
2.6.1.1.	V-SBA-12	88
2.6.2.	Characterization	89
2.6.2.1.	Chemical Composition	89
2.6.2.2.	X-ray Powder Diffraction (XRD)	89
2.6.2.3.	N ₂ -Physisorption	91
2.6.2.4.	Scanning Electron Microscopy (SEM)	95
2.6.2.5.	High Resolution Transmission Electron Microscopy (HRTEM)	95
2.6.2.6.	Diffuse Reflectance Ultraviolet Visible	95

	Spectroscopy (DRUV-vis)	
2.6.2.7.	Fourier Transform Infrared Spectroscopy (FTIR)	96
2.6.2.8.	²⁹ Si MAS NMR Spectroscopy	96
2.6.2.9.	Thermal Analysis (TGA)	96
2.6.2.10.	NH ₃ -TPD	97
2.7.	Synthesis and Characterization of Fe-SBA-12 Molecular Sieves	99
2.7.1.	Synthesis	99
2.7.1.1.	Fe-SBA-12	99
2.7.2.	Characterization	99
2.7.2.1.	X-ray Powder Diffraction (XRD)	99
2.7.2.2.	N ₂ -Physisorption	100
2.7.2.3.	Diffuse Reflectance Ultraviolet-Visible Spectroscopy (DRUV-vis)	101
2.7.2.4.	Fourier Transform Infrared Spectroscopy (FTIR)	102
2.7.2.5.	NH ₃ -TPD	102
2.8.	Conclusions	103
2.9.	References	103

Chapter – 3: Catalytic Properties of Ti-SBA-12 and Ti-SBA-16 in Oxidation Reactions 108

3.1.	Introduction	109
3.2.	Epoxidation of Cyclic Olefins	111
3.2.1.	Experimental Section	112
3.2.1.1.	Reaction Procedure	112
3.2.1.2.	Product Analysis	112
3.2.2.	Catalytic Activity	114
3.2.2.1.	Epoxidation of Cyclohexene	114
3.2.2.1.1.	Influence of Different Titanosilicates	114
3.2.2.1.2.	Influence of Reaction Time	115
3.2.2.1.3.	Influence of Reaction Temperature, Si/Ti and Oxidant/Substrate Molar Ratio	117
3.2.2.1.4.	Influence of Solvent and Oxidant	118
3.2.2.2.	Epoxidation of Cyclooctene	118

3.2.2.3.	Tentative Reaction Mechanism	121
3.3.	Hydroxylation of Phenol	123
3.3.1.	Experimental Section	125
3.3.1.1.	Reaction Procedure	125
3.3.1.2.	Product Analysis	125
3.3.2.	Catalytic Activity	125
3.3.2.1.	Influence of Si/Ti Molar Ratio	126
3.3.2.2.	Influence of Reaction Time and Temperature	126
3.3.2.3.	Influence of Catalyst and Oxidant Amount	128
3.3.2.4.	Comparative Catalytic Activity of Ti-SBA-12 and Ti-SBA-16	129
3.3.2.5.	Catalyst Reusability Study	131
3.4.	Conclusions	135
3.5.	References	135

Chapter – 4: Acid Catalyzed Reactions over Ti-SBA-12 & Ti-SBA-16 141

4.1.	Introduction	142
4.2.	Ring-Opening of Epoxides with Amines	143
4.2.1.	Experimental Section	145
4.2.1.1.	Reaction Procedure	145
4.2.1.2.	Product Analysis	145
4.2.2.	Catalytic Activity	145
4.2.2.1.	Aminolysis of Styrene oxide with Aniline over Different Catalysts	146
4.2.2.2.	Influence of Si/Ti Molar Ratio	147
4.2.2.3.	Influence of Method of Preparation	148
4.2.2.4.	Influence of Reaction Time and Pore Structure	149
4.2.2.5.	Influence of Reaction Temperature	150
4.2.2.6.	Influence of Solvent	150
4.2.2.7.	Influence of Substrate Structure	152
4.2.2.8.	Catalyst Reusability	158
4.2.2.9.	Structure-Activity Correlations	159

4.2.2.10.	Tentative Reaction Mechanisms	159
4.3.	Esterification of Oleic Acid with Methanol	161
4.3.1.	Experimental Section	162
4.3.1.1.	Reaction Procedure	162
4.3.1.2.	Product Analysis	162
4.3.2.	Catalytic Activity	163
4.3.2.1.	Influence of Si/Ti Molar Ratio	163
4.3.2.2.	Influence of Reaction Time and Temperature	165
4.3.2.3.	Catalyst Reusability	166
4.4.	Conclusions	167
4.5.	References	168
<hr/>		
Chapter – 5: Aerobic Oxidation of Amines to Amides		180
<hr/>		
5.1.	Introduction	181
5.2.	Experimental Section	182
5.2.1.	Reaction Procedure	183
5.2.2.	Product Analysis	183
5.3.	Catalytic Activity	183
5.3.1.	Influence of Si/Mn Molar Ratio	183
5.3.2.	Influence of Different Catalysts	184
5.3.3.	Influence of Reaction Time	185
5.3.4.	Influence of Reaction Temperature	185
5.3.5.	Influence of Reaction Pressure	187
5.3.6.	Reaction Mechanism and Structure - Activity Relationship	187
5.4.	Conclusions	190
5.5.	References	190
<hr/>		
Chapter – 6: Summary and Overall Conclusions		192
<hr/>		
List of Research Publications and Patents		

LIST OF TABLES

Table No.	Table Caption	Page No.
1.1.	List of Ordered Three-Dimensional (3-D) Mesoporous Silica Materials	5
1.2.	Synthesis of Various Mesoporous Materials under Different Synthesis Conditions	13
2.1.	Chemicals Used in the Present Work	35
2.2.	Composition and Structural Properties of Ti-SBA-12 and Ti-SBA-16	50
2.3.	Composition, Structure and Textural properties of TS-1, Ti-MCM-41 and Ti-SBA-15	51
2.4.	Textural Properties of SBA-12, Ti-SBA-12, SBA-16 and Ti-SBA-16	57
2.5.	²⁹ Si MAS NMR, Thermogravimetry, NH ₃ -TPD and DRUV-vis Spectral Data of Ti-SBA-12 and Ti-SBA-16	72
2.6.	Composition, Structure and Textural Properties of Mn-SBA-12 and Mn-SBA-16	81
2.7.	Thermogravimetric Analysis (TGA) and NH ₃ -TPD Data of Mn-SBA-12 and Mn-SBA-16	88
2.8.	Composition, Structure and Textural properties of V-SBA-12	93
2.9.	²⁹ Si MAS NMR, Thermogravimetry (TG) and NH ₃ -TPD Data of V-SBA-12	98
3.1.	Oxidation of Cyclohexene over Different Titanosilicates	114
3.2.	Influence of Solvent, Oxidant and Silica Structure on the Oxidation of Cyclohexene	119
3.3.	Influence of Amount of Solvent on the Oxidation of Cyclohexene with TBHP (5.5 M in Decane)	120
3.4.	Oxidation of Cyclooctene: Influence of Reaction Conditions	122
3.5.	Hydroxylation of Phenol over Ti-SBA-12 and Ti-SBA-16 Catalysts: Influence of Si/Ti Molar Ratio	127
3.6.	Influence of Catalyst and Oxidant Amounts on the Hydroxylation	129

	of Phenol over Ti-SBA-12	
3.7.	Comparative Catalytic Activity Data of Ti-SBA-12 and TS-1 for the Hydroxylation of Phenol	130
4.1.	Aminolysis of Styrene Oxide with Aniline over Different Catalysts	146
4.2.	Effect of Si/Ti Molar Ratio on the Aminolysis of Styrene Oxide	147
4.3.	Influence of Method of Preparation on the Aminolysis of Styrene Oxide with Aniline	148
4.4.	Effect of Solvent on the Reaction of Styrene Oxide with Aniline	151
4.5.	Aminolysis of Epoxides over Ti-SBA-12 and Ti-SBA-16	153
4.6.	Catalyst Reusability Studies: Reaction of Styrene Oxide with Aniline	157
4.7.	Catalytic Activity of Ti-SBA-12 and Ti-SBA-16 for Esterification of Oleic Acid with Methanol	164
5.1.	Influence of Si/Mn Molar Ratio on the Conversion of Benzylamine and Product Selectivity	184
5.2.	Influence of Different Catalysts on the Conversion of Benzylamine and Product Selectivity	185
5.3.	Influence of Reaction Time on the Conversion of Benzylamine and Product Selectivity	186
5.4.	Influence of Reaction Temperature	186
5.5.	Influence of Reaction Pressure on the Conversion of Benzylamine and Product Selectivity	187

LIST OF SCHEMES

Scheme No.	Scheme Caption	Page No.
3.1.	Oxidation of cyclohexene and their products	113
3.2.	Oxidation of cyclooctene and their products	113
3.3.	Hydroxylation of phenol and their products	124
4.1.	Regio- and stereoselective ring opening of epoxides with amines	144
5.1.	Oxidation of benzylamine and the possible reaction products	183

LIST OF FIGURES

Fig. No.	Figure Caption	Page No.
1.1.	Three-dimensional mesopore architecture of SBA-12	6
1.2.	Direct image of 3-D pore structure of SBA-16: (a) Electrostatic potential map of SBA-16 parallel to (110) plane through the centre of the cell, (b) 3-D arrangement of a cavity and its interconnection; block corresponds to the cavity, and (c) Mean cavity surface for SBA-16	7
1.3.	Liquid crystal templating mechanism proposed for the formation of MCM-41: (A) Liquid crystal phase initiated and (B) Silicate anion initiated	8
1.4.	Silicate rod assembly mechanisms for the formation of MCM-41	9
1.5.	Mechanisms proposed for the transformation of surfactant-silicate systems from lamellar to hexagonal mesophases: (A) hexagonal mesophase obtained by charge density matching, and (B) folding of kanemite silicate sheets around intercalated surfactant molecules	10
1.6.	Strategies for the functionalization of mesoporous silica: where M is the catalytically active metals (e.g., Ti, Mn, V etc.), A is the non-active Si atoms of mesoporous silica and L is the ligand	18
2.1.	Low-angle XRD patterns of (a) SBA-12 & Ti-SBA-12, and (b) SBA-16 & Ti-SBA-16 prepared using 2 M HCl, (c) XRD patterns of Ti-SBA-12 (Si/Ti = 30) prepared using varying molar concentration of HCl (0.05 – 2 M)	45
2.2.	Variation of unit cell parameters and unit cell volume as a function of Ti content in Ti-SBA-12 and Ti-SBA-16	46
2.3.	Effect of HCl concentration used in the synthesis gel on output Ti content in Ti-SBA-12 and Ti-SBA-16	46
2.4.	Low-angle XRD patterns: (a) MCM-41 and Ti-MCM-41 with Si/Ti molar ratio of 30 and 40, (b) SBA-15 and Ti-SBA-15 with Si/Ti molar ratio of 20, 30 and 40 prepared using 2 M HCl, (c) wide-angle XRD pattern of TS-1 (Si/Ti = 30)	47

- 2.5. XRD profiles in the wide-angle region: (a) Ti-SBA-12 and (b) Ti-SBA-16 (Si/Ti = 20 – 80, prepared using 2 M HCl), (c) Ti-SBA-12 and (d) Ti-SBA-16 (Si/Ti = 30, prepared using 0.05 – 2 M HCl). Peaks marked by asterisk correspond TiO₂ phase 49
- 2.6. Nitrogen adsorption-desorption isotherms of SBA-12 and Ti-SBA-12 with varying Si/Ti molar ratio (Si/Ti = 20 – 80) prepared using 2 M HCl in the synthesis gel 53
- 2.7. Nitrogen adsorption-desorption isotherms of Ti-SBA-12 (Si/Ti = 30) prepared using varying molar concentration of HCl (1 - 0.05 M) in the synthesis gel 54
- 2.8. Nitrogen adsorption-desorption isotherms of SBA-16 and Ti-SBA-16 with varying Si/Ti molar ratio (Si/Ti = 20 – 80) and their pore size distribution (inset) prepared using 2 M HCl 55
- 2.9. Nitrogen sorption isotherms and pore size distribution (inset) of (a) TS-1 (b) Ti-MCM-41 (c) SBA-15 and (d) Ti-SBA-15 58
- 2.10. SEM images of SBA-12, Ti-SBA-12, SBA-16 and Ti-SBA-16 60
- 2.11. HRTEM images of neat SBA-12, Ti-SBA-12 (Si/Ti = 20, 30, 40 and 50), neat SBA-16 and Ti-SBA-16 (Si/Ti = 20, 30 and 50) prepared in 2 M HCl 61
- 2.12. Diffuse reflectance UV-visible spectra: (a) and (b) neat SBA-12, Ti-SBA-12, neat SBA-16 and Ti-SBA-16 prepared using 2 M HCl, (c) and (d) Ti-SBA-12 and Ti-SBA-16 (Si/Ti = 30) prepared using varying molar concentration of HCl (0.05 – 2 M) 62
- 2.13. Diffuse reflectance UV-visible spectra of (a) TS-1 (Si/Ti = 30), (b) Ti-MCM-41 (Si/Ti = 30) and (c) Ti-SBA-15 (Si/Ti = 30) prepared with 2 M HCl 63
- 2.14. EPR spectra of superoxo-Ti generated on TS-1, Ti-MCM-41, Ti-SBA-12 and Ti-SBA-16 with 30% aqueous H₂O₂ 64
- 2.15. Influence of concentration of HCl used in the synthesis on EPR signal intensity of superoxo-titanium Ti(O₂⁻) species generated on Ti-SBA-12 (Si/Ti = 30) contacting with 30% H₂O₂ 65
- 2.16. FTIR spectra of (a) SBA-12 and Ti-SBA-12 (b) SBA-16 and Ti-SBA-16, prepared using 2 M HCl, (c) Ti-SBA-12 (Si/Ti = 30) 67

- prepared using 0.05 – 1 M HCl, and (d) TS-1, Ti-MCM-41 and Ti-SBA-15 with Si/Ti = 30
- 2.17. FT-Raman spectra: (a) SBA-12 & Ti-SBA-12 (Si/Ti = 30, 50) 68 prepared using 2 M HCl, (b) SBA-16 & Ti-SBA-16 (Si/Ti = 20 – 80) prepared using 2 M HCl, and (c) Ti-SBA-12 (Si/Ti = 30) prepared using 0.05 – 1 M HCl. * indicates bands due to TiO₂ (anatase)
- 2.18. ²⁹Si MAS NMR spectra of (a) Ti-SBA-12 and (b) Ti-SBA-16 with 69 Si/Ti = 20 – 80 prepared using 2 M HCl
- 2.19. TGA plots of (a) SBA-12 and Ti-SBA-12, (b) SBA-12 and Ti- 70 SBA-12 (Si/Ti = 30) prepared in varying molar concentration of HCl (0.05 to 2 M), (c) SBA-16 & Ti-SBA-16, (a) and (c) were for Si/Ti = 20 – 80 prepared using 2 M HCl
- 2.20. Water adsorption capacity (up to 523 K from thermal analysis) of 71 Ti-SBA-12 (Si/Ti = 30) and Ti-SBA-16 (Si/Ti = 30) prepared using 0.05 – 2 M HCl
- 2.21. Variation of (a) intensity ratio of Q⁴/(Q³+Q²) (from ²⁹Si MAS 73 NMR), (b) water adsorption capacity (up to 523 K from thermal analysis) as a function of Ti-content in Ti-SBA-12 and Ti-SBA-16 prepared using 2 M HCl, and (c) correlation of water adsorption capacity with Q⁴/(Q³+Q²) in these titanosilicates
- 2.22. NH₃-TPD plots of (a) Ti-SBA-12 and (b) Ti-SBA-16 prepared 74 using 2 M HCl
- 2.23. spectra of adsorbed pyridine on (a) Ti-SBA-12 and (b) Ti-SBA-16 75 with varying Si/Ti molar ratio prepared using 2 M HCl
- 2.24. DRIFT spectra of adsorbed pyridine at different temperatures: (a) 76 Ti-SBA-12 (Si/Ti = 30), (b) Ti-SBA-16 (Si/Ti = 50), and (c) Ti-SBA-16 (Si/Ti = 80) prepared using 2 M HCl
- 2.25. Low and wide-angle XRD patterns: (a) Mn-SBA-12 (Si/Mn = 20), 79 (b) & (c) Mn-SBA-16 with different Si/Mn molar ratios
- 2.26. Nitrogen adsorption-desorption isotherms of Mn-SBA-16 (Si/Mn = 82 20 – 80) and Mn-SBA-12 (Si/Mn = 20) and their pore size distribution curves (inset)

2.27.	SEM images of Mn-SBA-12 (Si/Mn = 20) and Mn-SBA-16 with Si/Mn molar ratio of 30, 50 and 80	83
2.28.	HRTEM images of (a) Mn-SBA-12 (Si/Mn = 20) and (b) Mn-SBA-16 (Si/Mn = 20)	83
2.29.	DRUV-vis spectra of (a) Mn-SBA-12(Si/Mn = 20) prepared using 0.1 M HCl and (b) Mn-SBA-16 (Si/Mn = 20 – 80) prepared in 2 M HCl	84
2.30.	EPR spectra of Mn-SBA-12 and Mn-SBA-16	85
2.31.	FTIR spectra of Mn-SBA-12 and Mn-SBA-16	86
2.32.	FT-Raman spectra of (a) SBA-16, (b) Mn-SBA-16 (Si/Mn = 80), (c) Mn-SBA-16 (Si/Mn = 50), (d) Mn-SBA-16 (30) and (e) Mn-SBA-12 (Si/Mn = 20)	86
2.33.	Thermogravimetric analysis plots of Mn-SBA-12 and Mn-SBA-16	87
2.34.	NH ₃ -TPD plots of Mn-SBA-12 and Mn-SBA-16	87
2.35.	Low-angle XRD patterns of (a) V-SBA-12 (Si/V = 20, 2 M), (b) V-SBA-12 (Si/V = 30, 2 M), (c) V-SBA-12 (Si/V = 40, 2 M), (d) V-SBA-12 (Si/V = 50, 2 M), (e) V-SBA-12 (Si/V = 80, 2 M), and (f) V-SBA-12 (Si/V = 30, 1 M)	90
2.36.	Wide-angle XRD patterns: (a) V-SBA-12 (Si/V =20 - 80) prepared using 2 M HCl, (b) V-SBA-12 (Si/V = 30) prepared using varying concentrations of HCl	91
2.37.	N ₂ adsorption-desorption isotherms of V-SBA-12 (Si/V = 20 – 80) prepared using 2 M HCl and V-SBA-12 (Si/V = 30) prepared using 1 M HCl	92
2.38.	SEM images of V-SBA-12	94
2.39.	HRTEM images of V-SBA-12	94
2.40.	DRUV-vis spectra of (a) V-SBA-12 (Si/V = 20 – 80) prepared using 2 M HCl and (b) V-SBA-12 (Si/V = 30) prepared using 0.1 to 2 M HCl	95
2.41.	FTIR spectra of V-SBA-12 (Si/V = 20 – 80) prepared in 2 M HCl	96
2.42.	²⁹ Si MAS NMR of V-SBA-12 mesoporous molecular sieves	97
2.43.	TGA graph of V-SBA-12	97
2.44.	NH ₃ -TPD plots of V-SBA-12 prepared using 2 M HCl	99

2.45.	Low and wide-angle XRD patterns of Fe-SBA-12 (Si/Fe = 20) prepared using 0.1 M HCl	100
2.46.	N ₂ adsorption-desorption isotherms and BJH pore size distribution plot (inset) of Fe-SBA-12 (Si/Fe = 20) prepared using 0.1 M HCl	101
2.47.	DRUV-visible spectra of Fe-SBA-12 (Si/Fe = 20)	101
2.48.	FTIR spectrum of Fe-SBA-12 (Si/Fe = 20)	102
2.49.	NH ₃ -TPD profile of Fe-SBA-12 (Si/Fe = 20)	102
3.1.	Comparative catalytic activities of Ti-SBA-12 (Si/Ti = 30) and Ti-SBA-16 (Si/Ti = 30) in the oxidation of cyclohexene with TBHP (5.5 M in decane)	115
3.2.	Influence of reaction parameters on the oxidation of cyclohexene over Ti-SBA-16 (Si/Ti = 30)	116
3.3.	Correlation of catalytic activity (cyclohexene conversion) with variation in molar ratio of Ti, unit cell volume (XRD) and area of tetrahedral Ti (diffuse reflectance UV-visible spectroscopy)	117
3.4.	Tentative mechanism of oxidation of cyclic olefins over Ti-SBA-12 and Ti-SBA-16 catalysts	123
3.5.	Effect of reaction time and temperature on phenol conversion and products selectivity	128
3.6.	Variation of HQ/CAT molar ratio as a function of phenol conversion: (Left) for Ti-SBA-12 and Ti-SBA-16, data and reaction conditions taken from Table 3.5 and (Right) for Ti-SBA-12 and TS-1, data and reaction conditions taken from Table 3.7	131
3.7.	Catalyst reusability study in the hydroxylation of phenol	132
3.8.	Low-angle X-ray diffraction (XRD), thermal analysis and FTIR of fresh and spent Ti-SBA-12 (Si/Ti = 20) catalyst after 5 th recycle	133
4.1.	Catalytic activity of different titanosilicate catalysts in the aminolysis of styrene oxide with aniline	149
4.2.	Effect of reaction temperature on the aminolysis of styrene oxide with aniline	150
4.3.	Influence of dielectric constant of solvent on the conversion of styrene oxide in the aminolysis reaction with aniline over Ti-SBA-12 (Si/Ti = 30, 0.1 M) and Ti-SBA-16 (Si/Ti = 20, 2 M) catalysts	152

4.4.	Correlation between turnover frequency (TOF) and (a) acidity (from NH ₃ -TPD), (b) tetrahedral Ti content (from ICP-OES and DRUV-vis.), (c) water adsorption capacity (thermogravimetric analysis) and (d) ²⁹ Si MAS NMR signal intensity of Ti-SBA-12 catalysts	158
4.5.	Tentative reaction mechanism for the ring-opening of epoxides with amines	160
4.6.	DRUV-vis. spectra of Ti-SBA-12 and Ti-SBA-16 contacted with water, styrene oxide, aniline and the mixture of styrene oxide and aniline (1:1)	160
4.7.	Effect of reaction time and temperature on the esterification of oleic acid with methanol	166
4.8.	Arrhenius plots for the calculation of energy of activation (E _a)	166
4.9.	Catalyst reusability study in the esterification of oleic acid (OA) with methanol	167
5.1.	Possible reaction mechanisms for the formation of primary amides from primary amines	188
5.2.	Correlation between product selectivity and acidity of Mn-SBA-16 catalyst	189

LIST OF ABBREVIATIONS

MCM	Mobil's Crystalline Material
SBA	Santa Barbara Amorphous
CTMABr	Cetyltrimethylammonium bromide
CMC	Critical micelle concentration
XRD	X-ray diffraction
BET	Braunauer-Emmett-Teller
FSM	Folded sheet material
BJH	Barrett-Joyner-Halenda
SEM	Scanning electron microscopy
MSU	Michigan State University
HMS	Hexagonal mesoporous silica
HRTEM	High-resolution transmission electron microscopy
FTIR	Fourier transform infrared
DRIFT	Diffuse reflectance infrared Fourier transform
DRUV-vis	Diffuse reflectance ultraviolet visible
TBHP	<i>tert.</i> -Butylhydroperoxide
ISR	Integrated sphere attachment
TEOS	Tetraethyl orthosilicate
EPR	Electron paramagnetic resonance
GC	Gas chromatography
GC-MS	Gas chromatography-mass spectrometry
FID	Flame ionization detector
ICP-OES	Inductively coupled plasma-optical emission spectroscopy
MAS	Magic angle spinning
LCT	Liquid crystal templating
TGA	Thermogravimetric analysis
DTA	Differential thermal analysis
TOF	Turn over frequency
Boc	<i>tert.</i> -Butoxycarbonylgroup

CHAPTER – 1

General Introduction

1.1. Porous Materials

Porous materials have attracted much attention in academic research as well as in industry due to their applications as adsorbents and catalysts [1]. These materials have high surface area than the analogous of non-porous materials. Other important characteristics of porous solids are crystallinity, pore size distribution and the nature of pore walls. These properties of such porous materials should be tailored to suit to desired application. Silica-based porous materials show up such kind of flexibility and have been found wide industrial applications in catalysis and separation science [1].

According to the IUPAC classification [2], porous materials can be classified into three categories, based on their average pore size:

Classification	Pore diameter (nm)
Microporous	: < 2
Mesoporous	: 2 - 50
Macroporous	: > 50

Zeolites are the important class of microporous materials which have pore sizes between 0.2 and 1.0 nm. They have been extensively used as adsorbents, catalysts and catalyst supports due to their highly crystalline structure, high internal surface area, uniform pores of one or more discrete sizes and good thermal stability. Zeolites are long been used in petroleum refining industry and in laboratory research for the transformation of organics and shape selective properties [3]. But their applications are limited due to their small pore sizes (< 1 nm) and they can only deal with molecules which have molecular dimension smaller than about < 1 nm. Despite many industrial applications of zeolites, there has been a persistent demand for crystalline mesoporous materials because of their possible application as catalysts for the transformation of bulky molecules.

1.2. Mesoporous Silica

The discovery of surfactant-templated mesostructure molecular sieves opened up new opportunities in the area of chemistry and material science [4-7]. The invention of a new family of mesoporous silica/aluminosilicate molecular sieves has attracted worldwide interest in many areas of physical, chemical, and engineering sciences. The first synthesis of an ordered mesoporous material was reported in the US patent in 1969 [8(a)]. However, due to lack of proper analysis, this material was

not fully recognized [8(b)]. In the early 1990s, Japanese researchers at Waseda University reported the first successful synthesis of novel periodic mesostructured material denoted as KSW-1 [9]. In 1992, Mobil Corporation scientists have discovered M41S type (MCM-41 or Mobil Composition of Matter No. 41) mesoporous materials [10]. These M41S type mesoporous silicate materials possess extremely high surface area, pore size, pore volume and well-ordered pore structure with narrow uniform pore size distribution and can be used in catalysis, separation and as host material for inclusion compounds. However, the weak hydrothermal stability of M41S type materials which is due to their thin and amorphous pore wall structure, greatly limits their extensive use. Many efforts have been made to improve the stability of MCM-41 and to prepare other stable mesoporous materials [11].

Inagaki et al. [12] independently prepared, virtually at the same time as M41S materials were synthesized, mesoporous silica designated as FSM-16 from the sodium form of layered polysilicate, kanemite ($\text{NaHSi}_2\text{O}_5 \cdot 3\text{H}_2\text{O}$) and alkyltrimethylammonium ions. Kanemite, a layered silicate, served as the silica source; the pathway leading to the ordered mesoporous material is thought to proceed *via* surfactant intercalation into the silicate sheets, wrapping of the sheets and transformation to the hexagonally packed material. The obtained materials were designated as Folded Sheet Mesoporous Material-*n* (FSM-*n*). Here, *n* is the number of carbon atoms in the surfactant alkyl chain used to synthesize the material.

Tanev and Pinnavaia [13] used neutral surfactants such as primary amines and polyethylene oxide (PEO, $\text{C}_{11-15}\text{EO}_{9-30}$), as structure directing agents to prepare a series of (disordered) mesoporous silicate structures through hydrogen-bonding interactions. They include HMS, MSU-*n* ($n = 1 - 4$), MSU-V and MSU-G. In 1996, yet another approach by Ryoo et al. [14] involving the addition of ethylenediaminetetraacetic acid to a high pH synthesis gel resulted in hydrothermally stable mesoporous silicates designated as KIT-1, with disordered interconnected pore channels.

1.3. SBA-Mesoporous Molecular Sieves

A variety of mesoporous silica materials with different structures have been synthesized by using the cooperative organization of ionic surfactants and ionic silica species in water [4-14]. In 1998, Zhao et al. [6] reported the synthesis of SBA-*n* (where $n = 11, 12, 15, 16$ etc., Santa Barbara Amorphous, University of California)

family mesoporous silica materials by using non-ionic alkyl poly(ethylene oxide) (PEO) oligomeric surfactants (for example, Brij76) and poly(alkylene oxide) block copolymers (for example, P123 and F127) as a structure directing agent (SDA) in acid media. These SBA family types of mesoporous silica opened up new and exciting opportunities in adsorbents, catalysis and material science. Non-ionic surfactants are a convenient alternative to primary amines and have demonstrated advantageous in solving the problems of ionic surfactants, since these surfactants are neutral, non-toxic, biodegradable and inexpensive. The SBA series mesoporous silica has improved stability. They have larger wall thickness due to the absence of electrostatic or charge-matching effects in the synthesis medium and thus have high thermal and hydrothermal stability than those of M41S family mesoporous materials.

1.3.1. Three-dimensional Molecular Sieves

Zeolites are crystalline microporous silicates or aluminosilicates formed through the linkages of oxygen atoms, possessing three-dimensional (3-D) networks within which channels and cavities of molecular dimensions are embedded. The three-dimensional networks of well-defined zeolitic micropores serve as spaces for shape-selective reactions and adsorptions. But their small pore size (< 1 nm) restricts their applications for large molecules. As discussed above, mesoporous materials (pore size: 2 to 50 nm) could solve this problem for bulky molecules of pharmaceutical interest. In general, all types of mesoporous silica do not possess three-dimensional pore architecture. After the success of using non-ionic surfactants for the synthesis of highly ordered mesostructures, a series of new three-dimensional mesoporous silicas (SBA series) with different structures were synthesized. Among the SBA family, SBA-12, SBA-15 and SBA-16 attract much attention due to their thicker pore walls and outstanding thermal and hydrothermal stability as compared to M41S type mesoporous materials. While SBA-15 has two-dimensional hexagonal pore arrangement with $p6mm$ space group, SBA-12 and SBA-16 have three-dimensional, hexagonal and cubic pore structure with $p6_3/mmc$ and $Im\bar{3}m$ space groups, respectively [6].

Three-dimensional mesopore architecture can provide better mass transfer kinetics (diffusion of the molecules in the pores) than two-dimensional pore architect materials (MCM-41 and SBA-15, 2-D hexagonal). 3-D materials can provide easy accessibility of active sites in the modified 3-D mesoporous silica as compared

Table 1.1. List of Ordered Three-Dimensional (3-D) Mesoporous Silica Materials

Space group	Material	Structure directing agent (SDA)	Synthesis medium	Ref.
$P6_3/mmc$ (3-D, hexagonal)	SBA-2	C_{n-3-1} ($n = 12-18$) and C_{n-6-1} ($n = 16, 18$)	Acidic or Basic	[16]
	SBA-7	C_{n-3-1} ($n = 12-18$) and C_{n-6-1} ($n = 16, 18$)	Basic	[6, 17]
	SBA-12	Brij76 ($C_{18}EO_{10}$)	Acidic	[6,15]
$Im\bar{3}m$ (3-D, cubic)	SBA-16	F127 ($EO_{106}PO_{70}EO_{106}$)	Acidic	[6]
	FDU-1	B50-6600 ($EO_{39}BO_{47}EO_{39}$)	Acidic	[18]
$Pm\bar{3}m$ (3-D, cubic)	SBA-11	Brij56 ($C_{16}EO_{10}$)	Acidic	[6]
$Pm\bar{3}n$ (3-D cubic)	SBA-1	$C_{16}TEABr$ or C_{16-3-1}	Acidic	[19]
	SBA-6	$18B_{4-3-1}$	Basic	[20]
$Ia\bar{3}d$ (3-D, cubic)	MCM-48	C_nTMA^+ ($n = 14-18$)	Basic	[4, 5]
	KIT-6	P123 ($EO_{20}PO_{70}EO_{20}$) or F127 ($EO_{106}PO_{70}EO_{106}$)	Acidic	[21]
	FDU-5	P123 ($EO_{20}PO_{70}EO_{20}$)	Acidic	[22]
$Fm\bar{3}m$ (3-D, cubic)	FDU-12	F127 ($EO_{106}PO_{70}EO_{106}$)	Acidic	[23]
	KIT-5	F127 ($EO_{106}PO_{70}EO_{106}$)	Acidic	[24]
$Fd\bar{3}m$ (3-D, cubic)	FDU-2	$C_{m-2-3-1}$ ($m = 14, 16, 18$)	Basic	[25]

EO = ethylene oxide, PO = propylene oxide, BO = butylene oxide, $C_{n-3-1} = [CH_3(CH_2)_{n-1}N^+(CH_3)_2(CH_2)_3N^+(CH_3)_3 \cdot 2Br^-]$, $C_{n-6-1} = [CH_3(CH_2)_{n-1}N^+(CH_3)_2(CH_2)_6N^+(CH_3)_3 \cdot 2Br^-]$, $18B_{4-3-1} = C_{18}H_{37}OC_6H_4OC_4H_8N(CH_3)_2C_3H_6N(CH_3)_3Br_2$, $C_{16-3-1} =$ dicationic Gemini surfactant $[CH_3(CH_2)_{15}N(CH_3)_2(CH_2)_3N(CH_3)_3]Br_2$, $C_{m-2-3-1} = [C_mH_{2m+1}N^+(CH_3)_2CH_2CH_2N^+(CH_3)_2CH_2CH_2CH_2N^+-(CH_3)_3 \cdot 3Br^-]$

to the 2-D mesoporous molecular sieves. The interaction of reactant molecules with active sites present in the two dimensional system is less as compared to the 3-dimensional system. Table 1.1 provides the list of some 3-D mesoporous silicas.

1.3.1.1. SBA-12

SBA-12 is a member of the SBA family mesoporous silicas. It has three-dimensional, hexagonal, pore architecture with the space group of $P6_3/mmc$ [6]. SBA-12 can be synthesized hydrothermally in acidic medium using non-ionic surfactant, Brij76 as a structure directing agent [6]. Electron crystallographic analysis revealed that SBA-12 is having a mixture of two types of mesophase intergrowth, hexagonal and cubic phase (*hcp* and *ccp*) [15]. SBA-12 has outstanding thermal and hydrothermal stability [6]. Fig. 1.1 shows the three-dimensional pore architecture of SBA-12.

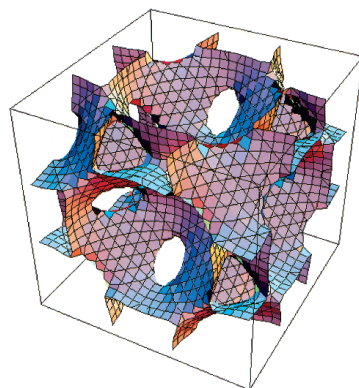


Fig. 1.1. Three-dimensional mesopore architecture of SBA-12 [15]

1.3.1.2. SBA-16

Of late, there is a worldwide interest in the design and synthesis of new materials with three-dimensional, cubic cage-like interconnected mesopore architecture. Such types of 3-D mesostructured porous materials are expected to be superior to 2-D, hexagonal structures. SBA-16 is a three-dimensional, body-centered cubic (bcc), cage-like interconnected mesoporous structure with space group of $Im\bar{3}m$ symmetry [6, 20]. SBA-16 can be synthesized in acidic medium using non-ionic pluronic F127 ($EO_{106}PO_{70}EO_{106}$) surfactant as a structure directing agent. The structure of SBA-16 can be described by a triply periodic minimal surface

of I-WP (body centered, wrapped package) as represented in Fig. 1.2 (c). The mesophase might also be a triply periodic minimal surface. As suggested by electron crystallography studies [20], each mesopore is connected to eight neighboring mesopores for SBA-16, thus forming a multidirectional pore network system.

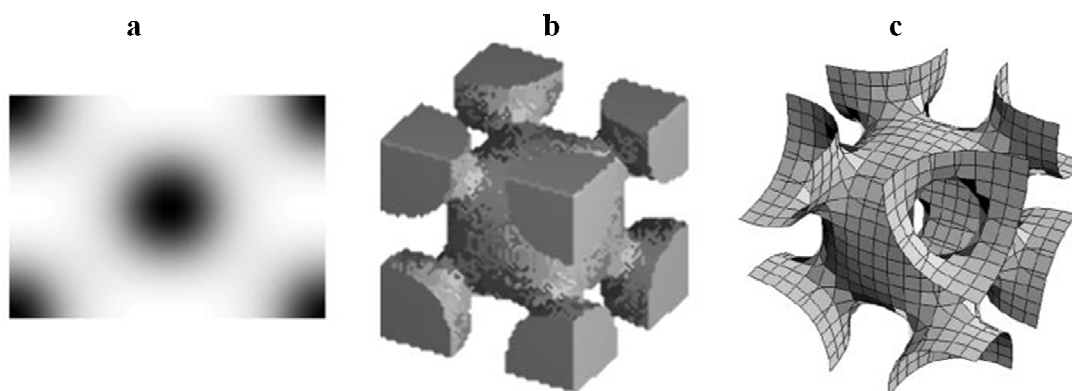


Fig. 1.2. Direct image of 3-D pore structure of SBA-16: (a) Electrostatic potential map of SBA-16 parallel to (110) plane through the centre of the cell, (b) 3-D arrangement of a cavity and its interconnection; block corresponds to the cavity, and (c) Mean cavity surface for SBA-16 [20]

SBA-16 possesses high hydrothermal stability due to its thick pore wall. This 3-D cage structure has a promising application in catalysis and materials science. SBA-16 has ink-bottle type mesopore in which their neck (pore entrance) size is smaller than their pore body size. The open frameworks and tunable porosities endow SBA-16 mesoporous material with accessibility to metal ions and reagents. These characteristics are extremely important in the field of catalysis.

1.4. Mechanisms of Formation of Mesoporous Materials

A number of mechanisms have been proposed for the formation of mesoporous silica materials. All these mechanisms are based on the presence and the role of surfactants in solution to guide the formation of inorganic mesostructures by different routes. Surfactants having two parts within the same molecule (hydrophilic head group and long chain hydrophobic tail group) aggregate and self organize in solution in such a way as to minimize contact between the incompatible ends. The type of interaction between the surfactant and the inorganic precursor under different synthesis conditions needs careful attention and is a subject of much discussion. A few of these mechanisms are discussed below.

1.4.1. Liquid Crystal Templating (LCT) Mechanism

In order to explain the synthesis mechanism of ordered mesoporous materials, Mobil scientists proposed a liquid crystal templating (LCT) mechanism, based on the similarity between liquid crystalline surfactant assemblies (i.e. lyotropic phases) and M41S [4, 5]. The mesostructure formation depends on the hydrocarbon chain length of the surfactant tail group [26], surfactant concentration and on additional organic swelling agents. The lowest concentration at which surfactant molecules aggregate to form spherical isotropic micelles is called critical micelle concentration (CMC1). Further increase in the surfactant concentration initiates aggregation of spherical into cylindrical or rod-like micelles (CMC2). There are three main liquid crystalline phases with hexagonal, cubic and lamellar structures.

The hexagonal phase is the result of hexagonal packing of cylindrical micelles, the lamellar phase corresponds to the formation of surfactant bilayers and the cubic phase may be regarded as a bicontinuous structure. The structure of the mesophase depends on the composition of the mixture, the pH and the temperature. Two mechanistic pathways were postulated for the formation of M41S type materials (Fig. 1.3): The silicate condensation is not the dominant factor in the formation of the mesoporous structure.

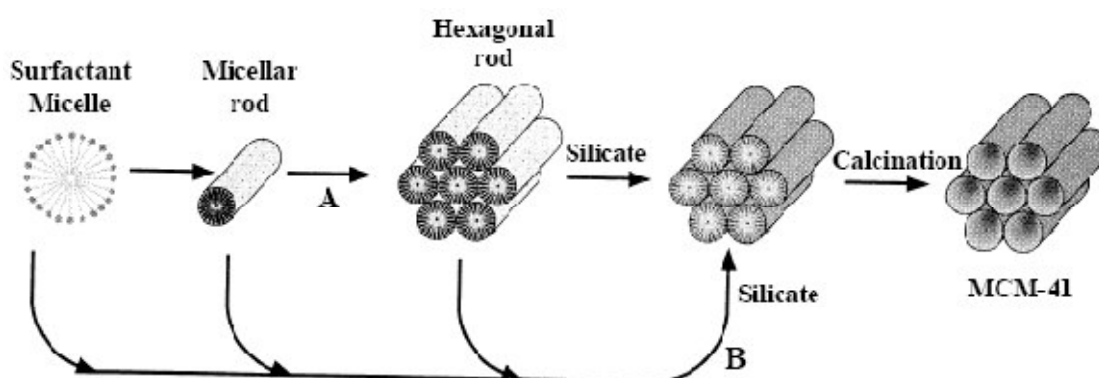


Fig. 1.3. Liquid crystal templating mechanism proposed for the formation of MCM-41: (A) Liquid crystal phase initiated and (B) Silicate anion initiated [5]

In the first pathway, it is considered that first there is a formation of the surfactant hexagonal liquid-crystal phase around which the growth of the inorganic materials is directed. The $C_nH_{2n+1}(CH_3)_3N^+$ surfactant micelles aggregate to form hexagonal arrays of rods. Silicate anions present in the reaction mixture interact with

the surfactant cationic head groups. Condensation of the silicate species leads to the formation of an inorganic polymer. On calcination, the organic template is burnt off, leaving inorganic hollow cylinders in hexagonal arrangement. However, this pathway did not get much support in the literature. It has been observed that at lower concentrations only micelles exist in solution [27]. Moreover, *in situ* ^{14}N -NMR spectra revealed that the hexagonal liquid-crystalline phase of CTMA ions was not present at any time during MCM-41 formation [10, 28]. Thus the first synthesis scheme proposed by Beck et al. and Zhao et al. [5, 6] was abandoned (Fig. 1.3).

In the second pathway, it has been proposed that the randomly ordered rod like micelles interact with silicate species by coulombic interactions in the reaction mixture to produce approximately two or three monolayers of silicate around the external surfaces of the micelles. These randomly ordered composite species spontaneously pack into a highly ordered mesoporous phase with an energetically favorable hexagonal arrangement, accompanied by silicate condensation. With the increase in heating time, the inorganic wall continues to condense. The investigation on the formation mechanism [28, 29] using XRD, ^{29}Si NMR, *in situ* ^{14}N NMR, and thermogravimetric analysis (TGA) techniques proves the absence of hexagonal liquid crystalline mesophases, either in the synthesis gel or in the surfactant solution used as template. It was therefore, concluded that formation of MCM-41 phase is possibly *via* pathway 2 (Fig. 1.4) rather than pathway 1. Yuan and Zhou [30] gave weak evidence for this mechanism, because they observed a single rod on the edge of samples in different synthetic periods using TEM. This mechanism is, however, unconvincing due to the difficulty of assembling long rods.

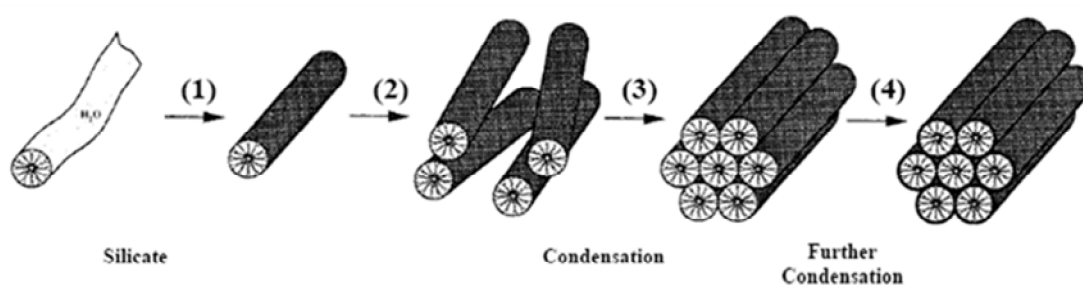


Fig. 1.4. Silicate rod assembly mechanisms for the formation of MCM-41 [29]

1.4.2. Charge Density Matching and Folding-Sheets Mechanisms

Fig. 1.5 shows the charge-density and folding-sheets mechanisms for the formation of mesoporous silica. Both the charge density matching and folded sheet mechanistic models are based on the transformation of lamellar phase to hexagonal phases. The ‘charge density matching’ model proposed by Stucky and co-workers [31] suggested that condensation occurs between initially formed silicate species by the electrostatic interactions between the anionic silicates and the cationic surfactant head groups.

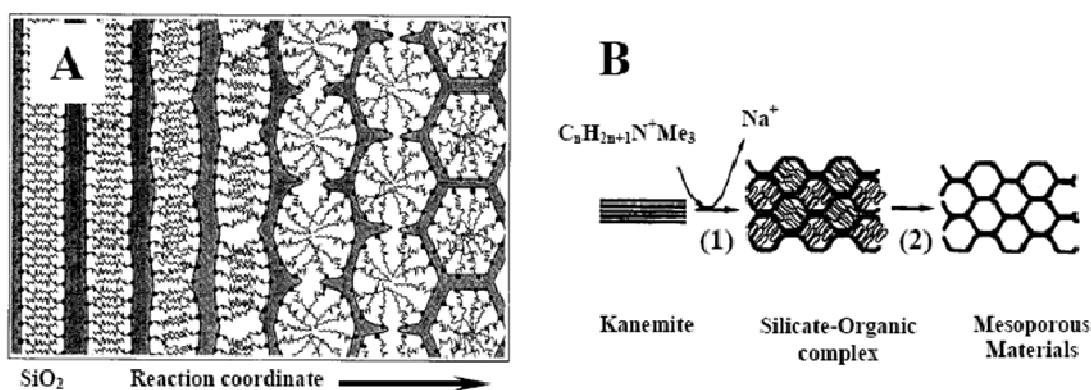


Fig. 1.5. Mechanisms proposed for the transformation of surfactant-silicate systems from lamellar to hexagonal mesophases: (A) hexagonal mesophase obtained by charge density matching [31], and (B) folding of kanemite silicate sheets around intercalated surfactant molecules [12]

This eventually reduces the charge density and therefore, curvature was introduced into the layers to maintain the charge density balance with the surfactant head groups, which leads to transformation of the lamellar mesostructure into the hexagonal one (Fig. 1.5A).

The ‘folded-sheet mechanism’ postulated by Inagaki et al. [12] indicated the presence of intercalated silicate phases in the synthesis medium of the reaction products. The flexible silicate layers of kanemite fold around the surfactant cations and cross-linking of the interlayer occur by condensation of silanol groups on adjacent silicate sheets. This folding and cross-linking process is facilitated by the flexibility of the single-layered kanemite sheets. On increase of pH, the amount of occluded alkyltrimethylammonium cations in kanemite increases and as a result, the interlayers of kanemite expand to form a regular hexagonal structure called FSM-16. The undissolved portion of kanemite converts to FSM-16 materials whereas the

dissolved species yield amorphous silica (Fig. 1.5B). However, this mechanism is not general, and the layered intermediate is unnecessary in the formation of hexagonal mesostructure MCM-41. It is also unclear whether the two hexagonal mesostructures, namely, FSM-16 generated by layered kanemite and MCM-41, are identical.

1.4.3. Generalized Liquid Crystal Templating Mechanisms

This generalized liquid crystal templating mechanism is based on the interaction between organic templates and inorganic precursors used in the synthesis. Many researchers have tried to explain the possible ways by which a surfactant species interact with the silica species under various synthesis conditions for the development of mesoporous materials having interesting textural and structural properties. These ordered mesoporous materials can be synthesized by different routes: (i) Ionic route (electrostatic interaction) and (ii) Neutral templating route or non-ionic route (hydrogen bonding interaction). A brief summary of the possible interactions between surfactant and silicate species is discussed in this section and a summary of the various syntheses opted under different pathways are depicted in Table 1.2.

1.4.3.1. Ionic Route (Electrostatic Interaction)

Huo et al. [32] proposed a generalized mechanism for the formation of mesostructures, which was based on specific types of electrostatic interaction between an inorganic precursor (I) and a surfactant head group (S). In this concept, four different approaches were proposed to synthesize mesoporous materials. The first route involves the charge density matching between surfactant cations and inorganic anions (S^+I^-). In the first route, silicate polyanions such as silicate oligomers interact with positively charged groups in cationic surfactants driven by Coulomb forces. The silicate species at the interface polymerize and cross-link and further change the charge density of the inorganic layers. With the proceeding of the reaction, the arrangements of surfactants and the charge density between inorganic and organic species influence each other. Hence, the compositions of inorganic-organic hybrids differ to some degree. It is the matching of charge density at the surfactant/inorganic species interfaces that governs the assembly process. The final mesophase is the ordered 3-D arrangement with the lowest interface energy. The transformation of the isotropic micellar solutions of CTAB into hexagonal or

lamellar phases when mixed with anionic silicate oligomers in highly alkaline solutions was indeed detected through a combination of correlated solution state ^1H , ^{13}C , and ^{29}Si nuclear magnetic resonance (NMR) spectroscopy, small-angle X-ray scattering (SAXS), and polarized optical microscopy measurements [33, 34]. The mechanism in different surfactant systems has been studied using NMR techniques [35].

The second route deals with the charge-reversed situation, *i.e.*, anionic surfactant and cationic inorganic species (S^-T^+) (Table 1.2). Both the third and fourth routes are counter-ion mediated pathways. The third one demonstrates the assembly of cationic species *via.*, halide ions ($\text{S}^-\text{X}^+\text{T}^+$), while the fourth one depicts the assembly of anionic species *via.*, alkali metal ions ($\text{S}^+\text{X}^-\text{T}^+$). These synthesis strategies are acceptable for the formation of wide variety of hexagonal, cubic or lamellar mesophases, but a common problem encountered was the instability of the inorganic framework after the removal of template.

1.4.3.2. Neutral Templating Route (Hydrogen Bonding Interaction)

Hydrogen-bonding interaction mechanisms, *viz.*, $\text{S}^\circ\text{I}^\circ$ or $\text{N}^\circ\text{I}^\circ$, were proposed by Tanev and Pinnavaia [13] for preparing mesoporous silicates under neutral conditions. N° are neutral amines, S° are non-ionic surfactants, and I° are hydrated silicate oligomers from tetraethyl orthosilicate (TEOS). It should be noted that amines and PEO-derived molecules are different. Organic long-chain alkyl amines, such as primary alkylamines (dodecylamine, hexadecylamine, etc.) and N,N-dimethylalkylamines (N,N-dimethyldodecylamine; N,N-dimethylhexadecylamine, etc.) have hydrophobic hydrocarbon chains and hydrophilic amine groups, similar to surfactants. However, ethanol has to be added in the synthesis batch for mesoporous silicas due to the insolubility of these amines [36]. Only disordered worm-like mesoporous silicas were obtained. Silicate oligomers are negatively charged in neutral solution. Neutral amines (N°) and non-ionic surfactants (S°) are probably partially protonated or charged. Later on, the synthesis of mesoporous silica like SBA-12, SBA-15 and SBA-16 was carried out under strongly acidic conditions by using tri-block copolymer Brij76, P123 or F127 as a template. It is more likely a double-layer hydrogen bonding $\text{S}^\circ\text{H}^+\text{X}^-\text{T}^+$ interaction exists [7, 37].

Table 1.2. Synthesis of Various Mesoporous Materials under Different Synthesis Conditions [37]

Interaction	Template source	Pathway	Examples
<i>Strong Electrostatic Interactions</i>			
Direct interaction	Ammonium surfactants	S^+I^-	MCM-41, MCM-48, FSM-16, KIT-1
	Anionic surfactants	S^-I^+	Mesoporous alumina
Anion mediated interaction	Ammonium surfactants	$S^+X^-I^+$	SBA-1, SBA-2, SBA-3
	Triblock copolymers	$(S^{\circ}H^+)X^-I^+$	SBA-15, SBA-16
	Ethylene oxides	$(S^{\circ}H^+)X^-I^+$	SBA-11, 12, 14
<i>Weak Van der Waals Interactions</i>			
Hydrogen bonding interaction	Amine surfactants	$N^{\circ}I^{\circ}$	HMS
Hydrogen bonding interaction	Non-ionic ethylene oxides	$S^{\circ}I^{\circ}$	MSU- <i>n</i>
Covalent bond interactions	Cationic surfactants containing silicate, e.g., $C_{16}H_{33}N(CH_3)_2OSi(OC_2H_5)_3Br$	$S^+ - I^-$	Mesoporous silica

S^+ = surfactant cations, S^- = surfactant anions, S° = Non-ionic surfactant, N° = Neutral amines, I^+ = inorganic precursor cations, I^- = inorganic precursor anions, I° = hydrated silicate oligomer, X^+ = cationic counterions, and X^- = anionic counterions

The cooperative formation mechanism in a non-ionic surfactant system was investigated by *in situ* techniques. Goldfarb and co-workers [38, 39] investigated the formation mechanism of mesoporous silica SBA-15, which are templated by triblock copolymer P123 (EO₂₀PO₇₀EO₂₀) by using direct imaging and freeze-fracture replication cryo-TEM techniques, *in situ* electron paramagnetic resonance (EPR) spectroscopy, and electron spin-echo envelope modulation (ESEEM) experiments. They found a continuous transformation from spheroidal micelles into threadlike

micelles. Bundles were then formed with dimensions that are similar to those found in the final materials.

The elongation of micelles is a consequence of the reduction of polarity and water content within the micelles due to the adsorption and polymerization of silicate species. Before the hydrothermal treatment, a majority of PEO chains insert into silicate frameworks, which generate micropores after the removal of templates. Moreover, they found that the extent of the PEO chains located within the silica micropores depended on both the hydrothermal aging temperature and the Si/P123 molar ratio. The formation dynamics of SBA-15 was studied by Flodstrom et al. [40] on the basis of time-resolved *in situ* ^1H NMR and TEM investigations. They observed four stages during the cooperative assembly, which are the adsorption of silicates on globular micelles, the association of globular micelles into flocs, the precipitation of flocs, and the micelle-micelle coalescence. Khodakov et al. [41] proposed a structure with a hydrophobic PPO core and a PEO-water silicate corona in the first stage, then the cylindrical micelles pack into large domains. At the same time, solvents are replaced by condensed silicate species.

1.5. Modification of Mesoporous Molecular Sieves

The advantages of using ordered mesoporous materials in catalysis are due to the relatively large pores, which facilitate mass transfer, and the very high surface area, which allow a high concentration of active sites per mass of the material [1, 42]. Although, mesoporous materials possess unique textural as well as morphological features, siliceous M41S or SBA-n mesoporous family materials show limited catalytic activity in various organic transformations and hence, ample modifications are necessary to make them as suitable candidates for various catalytic organic transformations. In general, ordered mesoporous silicas are not often used as catalysts as such. The incorporation of hetero atoms into the framework of pure siliceous mesoporous materials is an important route to modify the nature of the framework and to make them potential catalytic materials. The catalytic properties of such materials are closer to those of metal substituted amorphous silica than to those of framework substituted zeolites. These catalytic active sites can be created either directly or *via* post-synthesis methods. The catalytic properties of such materials are variable and controllable, depending on the synthetic procedure. The active sites of these materials prepared by two different routes are not necessarily identical. While

the direct hydrothermal synthesis method typically results in a relatively homogeneous incorporation (isomorphous substitution) of the hetero element, post-synthesis treatment primarily modifies the wall surface and thus, leads to an increased concentration of the hetero element as metal oxide on the surface of the catalyst. However, there are many possible pathways to modify pure siliceous mesoporous materials when one wants to give them a new catalytic function. Some of them are discussed below.

1.5.1. Incorporation of Heteroatoms by Direct Hydrothermal Synthesis Method

Currently, there is worldwide interest for the incorporation of heteroatoms into the framework or matrix of mesoporous silica by direct hydrothermal synthesis method. Transition metal ions incorporated mesoporous silicates have received great attention, because of their excellent catalytic properties. Surprisingly, the majority of studies on hetero atom incorporated mesoporous silicates, published so far, deal with phases having two-dimensional pore system such as MCM-41 and SBA-15, respectively. However, mesoporous materials with three-dimensional pore systems can offer a lot of advantages especially in catalysis, because they allow a faster diffusion of reactants or molecules than a one-dimensional array of pores and tend easy access to all adsorption catalytic active sites.

Isomorphous substitution of metals into the framework or matrix of mesoporous silica (MCM-41, SBA-12, SBA-16, SBA-15, etc.) by direct hydrothermal synthesis is the simplest way to create catalytically active sites into the materials (Fig. 1.6). However, it is very difficult to incorporate metal ions into SBA-12 or SBA-16 directly under the strong acidic conditions, as the metal ions will exist as cations and the formation of corresponding oxo species will be difficult and so difficult will be the formation of M-O-Si bonds for effective inclusion of metal in the structure [43]. Highly acidic conditions of preparation of Si-SBA-12, SBA-15 or SBA-16 normally prohibit the incorporation of Ti^{4+} , V^{5+} , Mn^{n+} , Fe^{3+} , Al^{3+} , Sn^{4+} , etc., from the synthesis gel due to the high solubility of their precursors. It is still a challenge to find a one-step route of metal incorporation into SBA-12 or SBA-16 in order to increase the acidity without changing its structural order or increasing the complexity of the synthesis.

Isomorphous substitution of trivalent cations like Al^{3+} , B^{3+} , Ga^{3+} and Fe^{3+} for silicon in the framework of the mesoporous silica creates negative charges that can

be compensated by protons providing acid sites. The types of acid sites, acid density (concentration) and strength depend on the amount and nature of the incorporated metal. These materials are useful in acid catalyzed reactions and have potential applications in various industrial processes [44]. When other metal cations like Ti^{4+} , Mn^{n+} (where $n = 2, 3, \text{ or } 4$) and V^{5+} etc. are incorporated, the corresponding mesoporous materials can be used in various oxidation reactions. However, there are only a few reports in the open literature regarding metal-containing SBA-12 silica despite its three-dimensional hexagonal structure. Campelo et al. [45] reported the highly active and dispersed metal nanoparticles (Ag, Au and Pd) on SBA-12 mesoporous support, prepared by conventional microwave method. These catalysts were highly active and selective in the oxidation of styrene and benzylalcohol [45]. Zelenak et al. [46] reported the synthesis of amine modified SBA-12 silica and used in the capture of carbon dioxide and they found that amine modified SBA-12 three-dimensional hexagonal mesoporous silica is more active than that of two-dimensional amine modified SBA-15 silica materials. While there are many reports on the modification of three-dimensional cubic cage like SBA-16 mesoporous silica. Al [47], Ti [48], V [49], Cu [50], Zr and Sn [51] and Fe-containing SBA-16 were prepared by the one-pot hydrothermal synthesis method and some of them were prepared under weak acidic conditions [52]. Bérubé et al. [53(a)] and Vinu et al. [53(b)] prepared Ti-SBA-15 by direct hydrothermal synthesis by adjusting pH or changing the HCl molar concentration (from 2 to 0.1 M) in the synthesis gel. Synthesis under weak acidic conditions through adjusting the H_2O to HCl molar ratio of the synthesis gel enabled controlled hydrolysis of tetraalkylorthosilicate (TMOS or TEOS) and condensation in presence of other metal cations [53]. Ti-containing microporous molecular sieves have been widely investigated due to their remarkable catalytic activity for oxidation reactions at mild conditions using aqueous H_2O_2 as oxidant [54]. However, the application of microporous titanosilicates (TS-1 or TS-2) is limited to molecules with smaller dimensions due to inherent constraints on pore size (< 1 nm). Ti-containing mesoporous SBA-12 and SBA-16 are expected to be superior to the other known titanium silicates because of their three-dimensional mesopore architecture.

1.5.2. Post Synthesis Method (Grafting/Impregnation of Heteroatoms)

The direct hydrothermal synthesis method for metallosilicate molecular sieves is difficult because the employed synthesis is in strong acidic medium (2 M HCl). One of the alternative routes involves the post-synthesis modification of purely siliceous SBA-n ($n = 12, 15$ or 16) family materials to generate acid sites on the inner walls of the mesoporous materials. This is possible because the walls of mesoporous silica molecular sieves are quasi-amorphous and possess high density of silanol groups.

It is widely accepted that guest species are grafted onto the surface of SBA-n molecular sieves *via* silanol groups. The silanol groups on the internal walls of SBA family materials are suggested to be the sites for metal incorporation. In this method, functionality is directly introduced through the reaction of silanol groups [55]. Ti-grafted materials have been prepared by this method for the oxidation of alkenes [56]. Recently, many efforts have been made to incorporate Al, Ti, V and Mn into the walls of SBA-15 and SBA-16 by post-synthesis grafting procedures [57-59] (Fig. 1.6). There are also reports about Al-SBA-16 supported manganese oxide catalysts prepared by impregnation methods [60]. The post-synthesis method is still overwhelmingly used in spite of the fact that the “post-synthesis” way always needs complex experimental conditions, especially for Ti and V (inside a glove-box under flowing of nitrogen). Another drawback of “post-synthesis” is that the metals in the form of metal oxides always reside in the channels or external surface of the catalysts, which would block the channels partially or fully, thereby reducing the surface area, pore volume and pore diameter and not allow the reactant molecules to access the active sites for the reaction to occur [61].

The high surface area and three-dimensional mesopore structure, high wall thickness of SBA family mesoporous silica favor high dispersion of the active species and provide easy accessibility to large molecules making them attractive supports and catalysts. These mesoporous materials with narrow and uniform pore size distribution may replace zeolite catalysts in some commercial applications. In a few research applications, they were already reported to possess superior performance compared to conventional microporous zeolites.

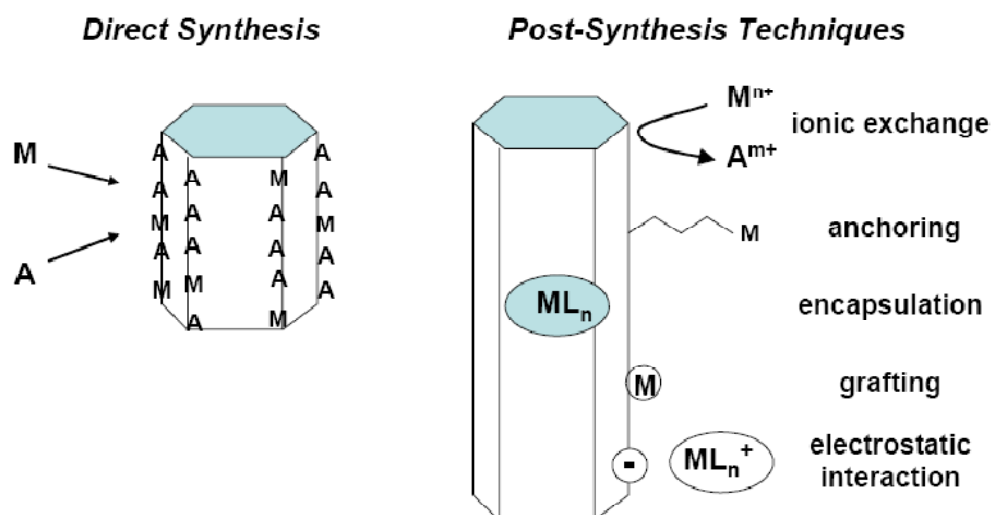


Fig. 1.6. Strategies for the functionalization of mesoporous silica: where M is the catalytically active metals (e.g., Ti, Mn, V etc.), A is the non-active Si atoms of mesoporous silica and L is the ligand [62]

1.6. Catalytic Oxidations

Selective oxidation of organics to their corresponding oxygenates is one of the most important and challenging transformations in the fine chemical industry [63-66]. Oxidation reactions have often been conducted by using stoichiometric metal-containing oxidants such as permanganate or chromium (VI) reagents [64, 67, 68]. These stoichiometric metal oxidants produce a large amount of heavy metal waste as by-product and further, their effective oxygen content is very low. The use of molecular oxygen or peroxides as oxidants in oxidation reactions is an alternative way to make the process environmentally benign [64-66]. Many efforts have been made in the last decades to search for newer, more efficient and acceptable, environmental benign oxidation catalysts. Zeolites have attracted great attention in the field of catalysis due to their unique pore structure, high internal surface area and high thermal and hydrothermal stability [69].

During the 1980s, 1990s and to date, synthesis and application of metal containing aluminophosphate (M-AIPO) molecular sieves (redox catalysts) have also been extensively studied for selective oxidations using hydrogen peroxide, organic peroxide or air as oxidizing agent [70]. Various transition metal (Ti, V, Mn, Fe, Mo and W, etc.) based homogeneous inorganic complexes [71-73], encapsulated or anchored metal complexes on microporous and mesoporous materials [74, 75] and

polymer supported metal complexes [76] have been investigated for the oxidation reactions. However, the use of supported metal complexes in liquid phase oxidation reactions creates leaching problems of transition metals in the reaction. Such single site-encapsulated catalysts allow access of only those reactant molecules small enough to diffuse through the windows of the zeolitic cage and prevent any of those products, which, if formed, are too large, from leaving the sphere of reaction. More importantly, the encapsulation protects the active site entity from losing its intrinsic catalytic performance because of dimerization or other complicating side reactions.

In 1983, the discovery of crystalline microporous titanium silicates (TS-1) by Taramasso et al. [77] was a breakthrough in the zeolite oxidation catalysis. TS-1 is an important heterogeneous catalyst and can oxidize a variety of organic compounds using hydrogen peroxide as oxidant at mild conditions [65(a) and (b), 66(a), 54(a)]. However, the pore size of TS-1 catalyst ($< \sim 0.6$ nm) restricts the application in the oxidation of bulky molecules. After the discovery of TS-1, many transition metals incorporated or grafted zeolite and mesoporous silica molecular sieves have been extensively investigated for these types of reactions [42(a), 65(a), 78, 79].

1.6.1. Epoxidation

Epoxides also called oxiranes, are cyclic ethers with three-membered ring. The basic structure of an epoxide contains an oxygen atom attached to two adjacent carbon atoms of a hydrocarbon. The epoxidation of alkenes is an electrophilic addition of oxygen to a carbon–carbon double bond in the presence of a catalysts and remains as one of the most significant challenges in synthetic chemistry. The formed epoxides are the building block intermediates that can be converted to a variety of products [80]. Epoxidation of cyclic olefins is an important organic transformation and could be used as intermediates in the synthesis of fine chemicals and pharmaceuticals. Various olefins can be converted into their epoxide using environmental benign oxidants like molecular oxygen, hydrogen peroxide or organic peroxides (TBHP). Among several solid catalysts as discussed above, microporous TS-1 showed remarkable catalytic activity in the oxidation of organic molecules at mild reaction conditions but its application is limited to small molecular transformations because of its small pore size ($< \sim 0.6$ nm) [54(a),77]. Most of the known mesoporous titanosilicates including Ti-MCM-41 and Ti-SBA-15 are less active and selective. Development of more efficient mesoporous Ti-molecular sieves

is a challenge. Titanosilicates (Ti-SBA-12 and Ti-SBA-16) with 3-D pore architecture would be ideal catalysts due to easy accessibility of catalytic active sites and easy mass transfer kinetics as compared to the 2-D counterparts (Ti-MCM-41 and Ti-SBA-15).

1.6.2. Hydroxylation

The catalytic direct hydroxylation (insertion of side-chain hydroxyl group to the aromatic ring) of aromatic compounds (e.g., benzene, phenol and naphthalene) in the presence of an oxidant is one of the most important and challenging industrial processes [81]. Hydroxylated products of aromatic compounds are widely used as photography chemicals, antioxidants, polymerization inhibitors, flavouring agents and drug intermediates [81]. Since the 1970s, hydroxylation of aromatics (benzene and phenol, for example) has been widely investigated using various homogeneous and heterogeneous catalysts [82]. The problem associated with homogeneous catalysts is separation and their reusability. The homogeneously catalysed liquid-phase reaction proceeds *via* $\cdot\text{OH}$ radicals giving very low conversion and product selectivity [82(c), 83]. Several supported metal catalysts (Pd, Pt, etc.) to activate oxygen with redox metals (Cu, Ti, and V etc.) were used for the oxidation of aromatics but still there was only a little improvement in conversion and product selectivity [84]. TS-1 with MFI structure opens up a new way for the hydroxylation of aromatics using environmentally benign oxidant H_2O_2 in which water is the only by-product [54(a), 77, 85]. Direct hydroxylation of aromatics to their corresponding phenols was reported by Moltz et al. [86] over H-[Al]ZSM-5 zeolites. In several other studies, iron was replaced by redox metals. Fe-ZSM-5 catalysts have also been reported for the oxidation of aromatics using N_2O as oxidant [87]. Vanadium and Tin containing silicates have been investigated for the hydroxylation reactions [88]. Various metal complexes encapsulated in zeolites and mesoporous silica have been investigated [74(d), 89]. Various transition metal incorporated as well as supported (as metal oxides) mesoporous silica have also been reported for the hydroxylation [90, 91]. Still there is a need to develop more efficient and stable, mesoporous titanosilicate catalyst for the hydroxylation of bulky molecules with 30% aqueous H_2O_2 .

1.6.3. Oxidation of Amines

Aerobic oxidation of amines to amides is one of the most important reactions because amides are valuable synthetic intermediates in chemistry as well as in biology [92]. There are a few reports on the synthesis of amides from amines [93-95]. Amides can be prepared in numerous ways. Traditional methods for the preparation of amides require stoichiometric amount of (hazardous) reagents and generate equimolar quantities of byproducts [96, 97]. Therefore, there is a need to develop an environmentally benign process for the synthesis of amides.

1.7. Acid Catalyzed Reactions

Acid-catalyzed reactions form one of the most extensively studied areas for the application of heterogeneous catalysis in the fine chemical industry [100]. However, to some extent, homogeneous catalysts are still being used in the fine chemical synthesis. But most of the processes are replaced by solid acid heterogeneous catalysts due to their advantages of separation and reusability. Various Solid acid catalysts such as zeolites, aluminophosphates, mixed metal oxides, resins, sulfonic acid functionalized mesoporous silica, sulfated metal oxides and metal containing micro and mesoporous molecular sieves have been used for many organic transformations in the fine chemical and pharmaceutical industries [99-101]. Transition metal containing micro and mesoporous molecular sieves act as Lewis solid acid catalysts and can be used for various acid catalyzed reactions.

1.7.1. Aminolysis of Epoxides

Aminolysis of epoxides yields β -amino alcohols which are versatile intermediates for the synthesis of various biologically active natural products, unnatural amino acids, β -blockers, insecticidal agents, chiral auxiliaries and oxazolines [102]. Among several synthetic strategies, the most straightforward approach for the synthesis of β -amino alcohols is the direct reaction of epoxide with an excess amount of amine at elevated temperatures and in the presence of solvents. This approach is not always favourable especially when the reactants contain temperature-sensitive functional groups. Further, this method is less effective for weakly nucleophilic amines and yields low regioselectivity. Several Lewis and Brønsted acid catalysts have been reported to catalyze this transformation [103]. However, many of these methods suffer from one or more of the following

disadvantages: poor regio-selectivity, requirement of extended reaction times, elevated temperatures, high pressures and stoichiometric amount of catalyst and the use of expensive reagents or catalysts. Hence, there is need to develop more efficient and reusable solid catalysts that are active at *low* temperatures and *avoid* the use of solvent. The discovery of an efficient solid acid catalyst for the aminolysis of epoxides will contribute to the eco-friendly manufacture of many β -amino alcohol compounds for the pharmaceuticals.

1.7.2. Esterifications of Acids

Esterification is a classical organic reaction for the preparation of esters through the reaction of carboxylic acids and alcohols in the presence of a catalyst. Esters are generally used as solvents, plasticizers, perfumes and precursors for pharmaceuticals and agrochemicals [104]. The esterification of free fatty acids with lower molecular weight alcohols is an important industrial reaction for the production of fatty acid alkyl esters (biodiesel). In conventional esterification processes, strong acids such as H_2SO_4 , HF, and HNO_3 are used as catalysts when the vegetable oil contains a large amounts of free fatty acids and water [105]. But these homogeneous strong mineral acids have the problems such as corrosiveness, difficulty in separation and reusability [104, 106]. Various solid acid catalysts have been investigated for the esterification of free fatty acids with alcohols such as zeolites, resins, tungstated and sulfated zirconia, sulphated tin oxide, heteropolyacids, acidic ionic liquid, etc. [107]. Ti-SBA-12 and Ti-SBA-16 could be the ideal alternative for these catalysts mentioned above due to their high surface area, pore volume, pore size and three-dimensional pore architectures.

1.8. Scope and Objectives of the Thesis

Development of a highly active and stable mesoporous metallosilicate for catalytic transformation of bulky organic molecules of pharmaceutical interest is a challenging task in catalysis research. In pursuit of this, the scope and objectives of this thesis are to prepare metal ion (Ti^{4+} , V^{5+} , Mn^{n+} (where $n = 2$ or 3) and Fe^{3+}) incorporated SBA-12 and SBA-16 molecular sieves by direct hydrothermal synthesis method, to characterize them by various physicochemical techniques and to investigate their catalytic properties in selective oxidation and acid-catalyzed reactions. Accordingly, Ti-SBA-12 and Ti-SBA-16 catalysts with varying Si/Ti

molar ratio are synthesized and used as catalysts for selective epoxidation of cyclic olefins (cyclohexene and cyclooctene), hydroxylation of phenol, aminolysis of epoxides and esterification of oleic acid with methanol producing methyl oleate esters for application as biodiesel. Mn-incorporated SBA-16 and Mn-, V-, Fe-incorporated SBA-12 are studied for the oxidation of benzylamine to benzamide using air as oxidant. Factors influencing the activity of these catalysts are investigated.

1.9. Organization of the Thesis

The thesis is divided into six chapters. **Chapter 1** provides a general introduction and historical background of mesoporous silica, synthesis strategies of metal-containing mesoporous silicates, formation mechanisms and their possible catalytic applications for the transformation of organics. This chapter also describes the scope and objective of the thesis.

Chapter 2 describes the synthesis and characterization of transition metal (Ti, V, Mn and Fe) containing SBA-12 and SBA-16 molecular sieves. Ti containing MCM-41 and SBA-15 are also prepared according to the reported procedure for the sake of comparison. These catalysts are characterized by various physicochemical techniques.

Chapter 3 deals with the catalytic properties of Ti-SBA-12 and Ti-SBA-16 in two different oxidation reactions viz., epoxidation of cyclic olefins (cyclohexene and cyclooctene) and hydroxylation of phenol. Oxidation of cyclic olefins was carried using different oxidizing agents like 30% aqueous hydrogen peroxide, 70% aqueous *tert.*-butylhydroperoxide (TBHP) and non-aqueous TBHP (5.5 M in decane). The catalytic oxidation properties of these three-dimensional titanosilicates were compared with those of microporous TS-1 and mesoporous Ti-MCM-41 and Ti-SBA-15. The catalysts of this study (Ti-SBA-12 and Ti-SBA-16) show high catalytic activity and selectivity than hitherto known solid titanosilicate mesoporous catalysts. The possible causes for the high catalytic oxidation activity of these catalysts were examined.

Chapter 4 presents the catalytic activity of Ti-SBA-12 and Ti-SBA-16 in acid-catalyzed reactions viz., aminolysis of epoxides and esterification of oleic acid with methanol. A range of β -amino alcohols were synthesized by the aminolysis of epoxides viz., cyclohexene oxide and styrene oxide with aniline and its derivatives

over Ti-SBA-12 and Ti-SBA-16 solid acid catalysts. The three-dimensional architecture of mesopores results in high conversion and selectivity due to easy access of the active sites and mass transfer kinetics. Esterification of oleic acid with methanol was carried out over these titanosilicates for the production of fatty acid methyl ester (FAME) or biodiesel. Effects of reaction parameters in these transformations were studied.

Chapter 5 describes the aerobic oxidation of benzylamine to benzamide over Mn-containing SBA-16 and Mn-, V- and Fe-containing SBA-12 molecular sieves. The role of acidity and oxidation state of metal on product selectivity was investigated.

Chapter 6 provides an overall summary and conclusions of the work presented in the thesis.

By and large, the work presented in this thesis reports the synthesis, characterization and catalytic applications of Ti-, Mn-, V- and Fe-containing SBA-12 and/or SBA-16 molecular sieves. These mesoporous metallosilicates have been found to be more efficient than microporous TS-1 and other known mesoporous metallosilicates in certain industrially relevant organic transformations. The catalysts of the investigation were reusable. Structure-function correlations revealed that the framework substituted metal ions as well as the unique pore structure and hydrophilic-hydrophobic properties are responsible for the high activity of the investigated three-dimensional, mesoporous metal-containing SBA-molecular sieves. In general, the work presented in this thesis contributes to the area of new materials and sustainable catalytic processes.

1.10. References

1. A. Corma, Chem. Rev. 97 (1997) 2373.
2. K.S.W. Sing, D.H. Everett, R.A.W. Haul, L. Moscou, R.A. Pierotti, J. Rouquerol, T. Siemieniowska, Pure Appl. Chem. 57 (1985) 603.
3. K. Tanabe, W.F. Hölderich, Appl. Catal. A: Gen. 181 (1999) 399.
4. C.T. Kresge, M.E. Leonowicz, W.J. Roth, J.C. Vartuli, J.S. Beck, Nature 359 (1992) 710.
5. J.S. Beck, J.C. Vartuli, W.J. Roth, M.E. Leonowicz, C.T. Kresge, K.D. Schmitt, C.T.W. Chu, D.H. Olson, E.W. Sheppard, S.B. McCullen, J.B.

- Higgins, J.L. Schlenker, *J. Am. Chem. Soc.* 114 (1992) 10834.
6. (a) D. Zhao, J. Feng, Q. Huo, N. Molish, G.H. Fredrickson, B.F. Chmelka, G.D. Stucky, *Science* 279 (1998) 548. (b) D. Zhao, Q. Huo, J. Feng, B.F. Chmelka, G.D. Stucky, *J. Am. Chem. Soc.* 120 (1998) 6024.
 7. (a) M.I. Clerc, P. Davidson, A. Davidson, *J. Am. Chem. Soc.* 122 (2000) 11925. (b) R. Ryoo, C.H. Ko, *J. Phys. Chem. B* 104 (2000) 11465.
 8. (a) V. Chiola, J.E. Ritsko, C.D. Vanderpool, US Patent No. 3,556,725, 1971. (b) F.D. Renzo, H. Cambon, R. Dutartre, *Micropor. Mater.* 10 (1997) 283.
 9. T. Yanagisawa, T. Shimizu, K. Kuroda, C. Kato, *Bull. Chem. Soc. Jpn.* 63 (1990) 988.
 10. (a) C.T. Kresge, M.E. Leonowicz, W.J. Roth, J.C. Vartuli, U.S. Patent 5,098,684 (1992). (b) J.S. Beck, C.T. Chu, I.D. Johnson, C.T. Kresge, M.E. Leonowicz, W.J. Roth., J.C. Vartuli, U. S. Patent, 5,108,725 (1992). (c) J.S. Beck, D.C. Calabro, S.B. McCullen, B.P. Pelrine, K.D. Schmitt, J.C. Vartuli, U.S. Patent, 5,145,816 (1992). (d) J.S. Beck, C.T. Kresge, M.E. Leonowicz, W.J. Roth, J.C. Vartuli, U.S. Patent, 5,264,203 (1993). (e) J.C. Vartuli, C.T. Kresge, M.E. Leonowicz, A.S. Chu, S.B. McCullen, I.D. Johnson, E.W. Sheppard, *Chem. Mater.* 6 (1994) 2070.
 11. (a) R. Ryoo, S. Jun, *J. Phys. Chem. B* 101 (1997) 317. (b) D. Das, C.-M. Tsai, S. Cheng, *Chem. Commun.* (1999) 473. (c) Q.-H. Xia, K. Hidajat, S. Kawi, *Mater. Lett.* 42 (2000) 102. (d) X.S. Zhao, G.Q. Lu, X. Hu, *Micropor. Mesopor. Mater.* 41 (2000) 37. (e) R. Anwender, I. Nagl, M. Widenmeyer, *J. Phys. Chem. B* 104 (2000) 3532. (f) P. Selvam, S.K. Bhatia, C.G. Sonwane, *Ind. Eng. Chem. Res.* 40 (2001) 3237.
 12. S. Inagaki, Y. Fukushima, K. Kuroda, *J. Chem. Soc. Chem. Commun.* (1993) 680.
 13. P.T. Tanev, T.J. Pinnavaia, *Science* 267 (1995) 865.
 14. R. Ryoo, J.M. Kim, C.H. Ko, C.H. Shin, *J. Phys. Chem.* 100 (1996) 17718-.
 15. Y. Sakamoto, I. Díaz, O. Terasaki, D. Zhao, J. Pérez-Pariente, J.M. Kim, G.D. Stucky, *J. Phys. Chem. B* 106 (2002) 3118.
 16. Q.S. Huo, D.I. Margolese, G.D. Stucky, *Chem. Mater.* 8 (1996) 1147.
 17. A.E.G. Bennett, S. Williamson, P.A. Wright, I.J. Shannon, *J. Mater. Chem.*, 12 (2002) 3533.

18. C.Z. Yu, Y.H. Yu, D.Y. Zhao, *Chem. Commun.* (2000) 575.
19. Q.S. Huo, D.I. Margolese, U. Ciesla, P.Y. Feng, T.E. Gier, P. Sieger, R. Leon, P.M. Petroff, F. Schuth, G.D. Stucky, *Nature* 368 (1994) 317.
20. Y. Sakamoto, M. Kaneda, O. Terasaki, D. Zhao, J.M. Kim, G.D. Stucky, H.J. Shim, R. Ryoo, *Nature* 408 (2000) 449.
21. F. Kleitz, S.H. Choi, R. Ryoo, *Chem. Commun.* (2003) 2136.
22. X.Y. Liu, B.Z. Tian, C.Z. Yu, F. Gao, S.H. Xie, B. Tu, R.C. Che, M.L. Peng, D. Zhao, *Angew. Chem. Int. Ed.* 41 (2002) 3876.
23. J. Fan, C.Z. Yu, T. Gao, J. Lei, B.Z. Tian, L.M. Wang, Q. Luo, B. Tu, W.Z. Zhou, D. Zhao, *Angew. Chem., Int. Ed.* 42 (2003) 3146.
24. (a) F. Kleitz, D.N. Liu, G.M. A. Kumar, I.S. Park, L.A. Solovyov, A.N. Shmakov, R. Ryoo, *J. Phys. Chem. B* 107 (2003) 14296. (b) D.H. Chen, Z. Li, Y. Wan, X.J. Tu, Y.F. Shi, Z.X. Chen, W. Shen, C.Z. Yu, B. Tu, D.Y. Zhao, *J. Mater. Chem.* 16 (2006) 1511.
25. S.D. Shen, Y.Q. Li, Z.D. Zhang, J. Fan, B. Tu, W.Z. Zhou, D. Zhao, *Chem. Commun.* (2002) 2212.
26. J.S. Beck, J.C. Vartulli, G.J. Kennedy, C.T. Kresge, W.J. Roth, S.E. Schramm, *Chem. Mater.* 6 (1994) 1816.
27. C.F. Cheng, H. He, W. Zhou, J. Klinowski, *Chem. Phys. Lett.* 244 (1995) 117.
29. A. Steel, S.W. Carr, M.W. Anderson, *J. Chem. Soc. Chem. Commun.* (1994) 1571.
29. C.-Y. Chen, S.L. Burkett, H.Y. Li, M.E. Davis, *Microporous Mater.* 2 (1993) 27.
30. Z.Y. Yuan, W.Z. Zhou, *Chem. Phys. Lett.* 333 (2001) 427.
31. (a) A. Monnier, F. Schuth, Q. Huo, D. Kumar, D. I. Margolese, R.S. Maxwell, G.D. Stucky, M. Krishnamurthy, P. Petroff, A. Firouzi, M. Janicke, B.F. Chmelka, *Science* 261 (1993) 1299. (b) G.D. Stucky, A. Monnier, F. Schuth, Q. Huo, D.I. Margolese, D. Kumar, M. Krishnamurthy, P. Petroff, A. Firouzi, M. Janicke, B.F. Chmelka, *Mol. Cryst. Liq. Cryst.* 240 (1994) 187.
32. Q.S. Huo, D.I. Margolese, U. Ciesla, P.Y. Feng, T.E. Gier, P. Sieger, R. Leon, P.M. Petroff, F. Schuth, G.D. Stucky, *Nature* 368 (1994) 317.
33. A. Firouzi, D. Kumar, L.M. Bull, T. Besier, P. Sieger, Q. Huo, S.A. Walker,

- J.A. Zasadzinski, C. Glinka, J. Nicol, D. Margolese, G.D. Stucky, B.F. Chmelka, *Science* 267 (1995) 1138.
34. A. Firouzi, F. Atef, A.G. Oertli, G.D. Stucky, B.F. Chmelka, *J. Am. Chem. Soc.* 119 (1997) 3596.
35. J.D. Epping, B.F. Chmelka, *Curr. Opin. Colloid Interface Sci.* 11 (2006) 81.
36. K. Cassiers, P.V. Voort, T. Linssen, E.F. Vansant, O. Lebedev, J.V. Landuyt, *J. Phys. Chem. B* 107 (2003) 3690.
37. Y. Wan, D. Zhao, *Chem. Rev.* 107 (2007) 2821.
38. S. Ruthstein, V. Frydman, S. Kababya, M. Landau, D. Goldfarb, *J. Phys. Chem. B* 107 (2003) 1739.
39. S. Ruthstein, J. Schmidt, E. Kesselman, Y. Talmon, D. Goldfarb, *J. Am. Chem. Soc.* 128 (2006) 3366.
40. K. Flodstrom, H. Wennerstrom, V. Alfredsson, *Langmuir* 20 (2004) 680.
41. A.Y. Khodakov, V.L. Zholobenko, M.I. Clerc, D. Durand, *J. Phys. Chem. B* 109 (2005) 22780.
42. A. Sayari, *Chem. Mater.* 8 (1996) 1840.
43. (a) S. Wu, Y. Han, Y.-C. Zou, J.-W. Song, L. Zhao, Y. Di, S.-Z. Liu, F.-S. Xiao, *Chem. Mater.* 16 (2004) 486. (b) N.N. Trukhan, V.N. Romannikov, A.N. Shmakov, M.P. Vanina, E.A. Paukshtis, V.I. Bukhtiyarov, V.V. Kriventsov, I.Y. Danilov, O.A. Kholdeeva, *Micropor. Mesopor. Mater.* 59 (2003) 73. (c) J.A. Melero, J.M. Arsuaga, P.de Frutos, J. Iglesias, J. Sainz, S. Blazquez, *Micropor. Mesopor. Mater.* 86 (2005) 364.
44. (a) W.A Adams, M.G. Bakker, T. Macias, I.A. Jefcoat, *J. Hazardous Mater.* 112 (2004) 253. (b) J.L. Casci, *Stud. Surf. Sci. Catal.* 85 (1994) 329.
45. J.M. Campelo, T.D. Conesa, M.J. Gracia, *Green Chem.* 10 (2008) 853.
46. V. Zelenak, M. Badanicova, D. Halamova, *Chem. Eng. J.* 144 (2008) 336.
47. J.M.R. Gallo, C. Bisio, L. Marchese, H.O. Pastore, *Micropor. Mesopor. Mater.* 145 (2011) 124.
48. (a) S. Shen, Y. Deng, G. Zhu, D. Mao, Y. Wang, G. Wu, J. Li, X.Z. Liu, G. Lu, D. Zhao, *J. Mater. Sci.* 42 (2007) 7057. (b) A.T. Shah, B. Li, Z.E.A. Abdalla, *J. Colloid Interface Sci.* 336 (2009) 707.
49. (a) B.R. Jermy, S.-Y. Kim, K.V. Bineesh, D.-W. Park, *Micropor. Mesopor. Mater.* 117 (2009) 661. (b) L. Zhao, Y. Dong, X. Zhan, Y. Cheng, Y. Zhu, F.

- Yuan, H. Fu, *Catal. Lett.* 142 (2012) 619.
50. Y. Dong, X. Niu, Y. Zhu, *Catal. Lett.* 141 (2011) 242.
51. N. Jiang, J.-B. Koo, S.C. Han, S.-E. Park, *Resear. Chem. Intermed.* 34 (2008) 507.
52. (a) B.R. Jermy, S.-Y. Kim, K.V. Bineesh, M. Selvaraj, D.-W. Park, *Micropor. Mesopor. Mater.* 121 (2009) 103. (b) B.R. Jermy, S.-Y. Kim, *J. Ind. Eng. Chem.* 17 (2011) 130. (c) A.T. Shah, B. Li, Z. E.A. Abdalla, *Micropor. Mesopor. Mater.* 130 (2010) 248.
53. (a) F. Bérubé, F. Kleitz, S. Kaliaguine, *J. Phys. Chem. C* 112 (2008) 14403. (b) A. Vinu, V. Murugesan, W. Böhlmann, M. Hartmann, *J. Phys. Chem. B* 108 (2004) 11496. (c) A. Vinu, P. Srinivasu, M. Miyahara, K. Ariga, *J. Phys. Chem. B* 110 (2006) 801. (d) A. Vinu, V. Murugesan, *Chem. Lett.* 33 (2004) 588. (e) X. Cui, W.C. Zin, W.J. Cho, C.S. Ha, *Mater. Lett.* 59 (2005) 2257. (f) Y. Li, Z. Feng, Y. Lian, K. Sun, L. Zhang, G. Jia, Q. Yang, C. Li, *Micropor. Mesopor. Mater.* 84 (2005) 41.
54. (a) P. Ratnasamy, D. Srinivas, H. Knözinger, *Adv. Catal.* 48 (2004) 1. (b) B. Notari, *Adv. Catal.* 41 (1996) 253. (c) J.E. Gallot, S. Kaliaguine, *Can. J. Chem. Eng.* 76 (1998) 833.
55. (a) L. Mercier, T.J. Pinnavaia, *Adv. Mater.* 9 (1997) 500. (b) A. Cauvel, G. Renard, D. Brunel, *J. Org. Chem.* 62 (1997) 749.
56. T. Maschmeyer, F. Rey, G. Sanker, J. M. Thomas, *Nature* 378 (1995) 159.
57. (a) J. Ma, L. Qiang, X. Tang, H. Li, *Catal. Lett.* 138 (2010) 88. (b) J. Ma, L. Qiang, J. Wang, D. Tang, X. Tang, *Catal. Lett.* 141 (2011) 356. (c) R. Bulánek, A. Kaluzová, M. S. cka, A. Zukal, P. Cîcmanec, J. Mayerová, *Catal. Today* 179 (2012) 149. (d) M. Cheng, Z. Wang, K. Sakurai, F. Komata, T. Saito, T. Komatsu, T. Yashima, *Chem. Lett.* (1999) 131. (e) Z. Luan, M. Hartmann, Maes, D. Zhao, W. Zhou, L. Kevan, *Chem. Mater.* 11 (1999) 1621.
58. (a) Z. Luan, E.M. Maes, P.A.W.V. Heide, D. Zhao, R.S. Czernuszewicz, L. Kevan, *Chem. Mater.* 11 (1999) 3680. (b) P. Wuy, T. Tatsumi, T. Komatsu, T. Yashima, *Chem. Mater.* 14 (2002) 1657.
59. Z. Luan, J.Y. Bae, L. Kevan, *Chem. Mater.* 12 (2000) 3202.
60. J.H. Park, J.M. Kim, J.-K. Jeon, S.-S. Kim, S.H. Park, S.C. Kim, Y.-K. Park,

- Nanoscale Res. Lett. 7 (2012) 1.
61. R. Murugavel, H.W. Roesky, *Angew. Chem. Int. Ed. Engl.* 109 (1997) 4491.
 62. V.D. Santo, F. Liguori, C. Pirovano, M. Guidotti, *Molecules* 15 (2010) 3829.
 63. (a) R.A. Sheldon, J.K. Kochi, “Metal-Catalyzed Oxidations of Organic Compounds” Academic Press, New York, 1981. (b) R.A. Sheldon, *Heterogeneous Catalytic Oxidation and Fine Chemicals*, *Stud. Surf. Sci. Catal.* 66 (1991) 33.
 64. A. Corma, H. García, *Chem. Rev.* 102 (2002) 3837.
 65. (a) I.W.C.E. Arends, R.A. Sheldon, *Appl. Catal. A: Gen.* 212 (2001) 175. (b) J.M. Thomas, G. Sankar, *Acc. Chem. Res.*, 34 (2001) 571. (c) K. Shimizu, T. Kaneko, T. Fujishima, T. Kodama, H. Yoshida, Y. Kitayama, *Appl. Catal. A: Gen.* 225 (2002) 185.
 66. (a) B. Notari, *Adv. Catal.* 41 (1996) 253. (b) Z. Du, J. Ma, J. Gao, J. Xu, *Green Chemistry* 12 (2010) 590.
 67. (a) J. Muzart, *Chem. Rev.* 92 (1992) 113. (b) B.S. Lane, K. Burgess, *Chem. Rev.* 103 (2003) 2457.
 68. R.A. Sheldon, in: L.I. Simandi (Ed.), *Dioxygen Activation and Homogeneous Catalytic Oxidation*, Elsevier, Amsterdam, 199, p. 573.
 69. G.J. Suppes, M.A. Dasari, E.J. Doskocil, P. J. Mankidy, M.J. Goff, *J. Appl. Catal. A: Gen.* 257 (2004) 213.
 70. (a) B.M. Weckhuysen, R.R. Rao, R.A. Schoonheydt, *Europ. Open. J. Chem.* 4 (1999) 565. (b) A. Sayari, I. Moudrakovski, J.S. Reddy, C.I. Ratcliffe, J.A. Ripmeester, K.F. Preston, *Chem. Mater.* 8 (1996) 2080.
 71. (a) P.S.E. Dai, R.H. Petty, C.W. Ingram, R. Szostak, *Appl. Catal. A: Gen.* 143 (1996) 101. (b) M.H.Z. Niaki, M.P. Kapoor, S. Kaliaguine, *J. Catal.* 177 (1998) 231. (c) J.M.L. Nieto, *Top. Catal.* 15 (2001) 189. (d) F. Corà, C.R.A. Catlow, A. D’Ercole, *J. Mol. Catal. A: Chem.* 166 (2001) 87. (e) M. Hartmann, L. Kevan, *Res. Chem. Intermed.* 28 (2002) 625. (f) S.K. Mohapatra, F. Hussain, P. Selvam, *Catal. Commun.* 4 (2003) 57. (g) S.-O. Lee, R. Raja, D.M.H. Kenneth, J.M. Thomas, F.G.J. Brain, G. Sankar, *Angew. Chem. Int. Ed.* 42 (2003) 1520. (h) W. Fan, B. Fan, M. Song, T. Chen, R. Li, T. Dou, T. Tatsumi, B.M. Weckhuysen, *Micropor. Mesopor.*

- Mater. 94 (2006) 348.
72. (a) L. Raboin, J. Yano, T.D. Tilley, J. Catal. 285 (2012) 168. (b) L.G. Hortigüela, F. Corá, C.R.A. Catlow, ACS Catal. 1 (2011) 18. (c) C.N. Kato, K. Hayashi, S. Negishi, K. Nomiya, J. Mol. Catal. A: Chem. 262 (2007) 25. (d) M. Fujiwara, H. Wessel, P.H.-Suh, H.W. Roesky, Tetrahedron, 58 (2002) 239. (e) G.B.-Brieva, M.C.C.-Sanchez, J.M.C.-Martín, J.L.G. Fierro, E.J. Ledesma, L. Adrini, F.G. Requejo, Adv. Syn. Catal. 345 (2003) 1314. (f) G.B. Shul'pin, J. Mol. Catal. A: Chem. 189 (2002) 39. (g) M. Vandichel, K. Leus, P.V. D. Voort, M. Waroquier, V. V. Speybroeck, J. Catal. 294 (2012) 1.
73. (a) D.E. De Vos, B.F. Sels, P.A. Jacobs, Adv. Catal. 46 (2001) 1. (b) D.E. De Vos, B.F. Sels, P.A. Jacobs, Adv. Synth. Catal. 345 (2003) 457. (c) C.A. Sureshan, P.K. Bhattacharya, J. Mol. Catal. A: Chem. 136 (1998) 285.
74. (a) R. Raja, P. Ratnasamy, Appl. Catal. A: Gen. 143 (1996) 145. (b) C.R. Jacob, S.P. Varkey, P. Ratnasamy, Micropor. Mesopor. Mater. 22 (1998) 465. (c) P. Ratnasamy, R. Raja, D. Srinivas, Phil. Trans. R. Soc. A 363 (2005) 1001. (d) P. Ratnasamy, D. Srinivas, Catal. Today 141 (2009) 3. (e) P. P. Knoosgerrits, D. Devos, F. Thibaultstarzyk, P. A. Jacobs, Nature 369 (1994) 543. (f) A.B. Sorokin, E.V. Kudrik, Catal. Today 159 (2011) 37. (g) N. Sehlotho, T. Nyokong, J. Mol. Catal. A: Chem. 209 (2004) 51.
75. (a) N.K.K. Raj, S.S. Deshpande, R.H. Ingle, T. Raja, P. Manikandan, Catal. Lett. 98 (2004) 217. (b) R.L. Brutchey, B.V. Mork, D.J. Sirbully, P.D. Yang, T.D. Tilley, J. Mol. Catal. A: Chem. 238 (2005) 1. (c) Sujandi, S.-C. Han, D.S. Han, M.J. Jin, S.E. Park, J. Catal. 243 (2006) 410. (d) S.V. Sirotnin, A.Y. Tolbin, I.F. Moskovskaya, S.S. Abramchuk, L.G. Tomilova, B.V. Romanovsky, J. Mol. Catal. A: Chem. 319 (2010) 39. (e) E.A. Prasetyanto, S.E. Park, Bull. Korean Chem. Soc. 29 (2008) 1033. (f) H. Yang, X. Han, Z. Ma, R. Wang, J. Liu, X. Ji, Green Chem. 12 (2010) 441.
76. (a) L. Zhang, H.C.L. Abbenhuis, G. Gerritsen, N. Nij, Bhriain, P.C.M.M. Magusin, B. Mezari, W. Han, R.A. van Santen, Q. Yang, C. Li, Chem. Eur. J. 13 (2007) 1210. (b) D.C. Sherrington, S. Simpson, J. Catal. 131 (1991) 115. (c) G. Olason, D.C. Sherrington, React. Funct. Polym. 42 (1999) 163. (d) D.C. Sherrington, Catal. Today, 57 (2000) 87. (e) A.B. Sorokin, E.V. Kudrik, Catal. Today, 159 (2011) 37.

77. M. Taramasso, G. Perego, B. Notari, US Pat. 4,410,501, 1983 to SNAM Progetti.
78. (a) R.A. Sheldon, I.W.C.E. Arends, H.E.B. Lempers, *Catal. Today* 41 (1998) 387. (b) G. Bellussai, M.S. Rigitto, *Stud. Surf. Sci. Catal.* 85 (1994) 177. (c) B. Sulikowski, *Heterogeneous Chem. Rev.* 3 (1996) 203. (d) I.W.C.E. Arends, R.A. Sheldon, M. Wallau, U. Schuchardt, *Angew. Chem. Int. Ed. Engl.* 36 (1997) 1144. (e) M. Hartman, L. Kevan, *Chem. Rev.* 99 (1999) 635. (f) M. Dusi, T. Mallat, A. Baiker, *Catal. Rev. Sci. Eng.*, 42 (2000) 213. (g) A. Corma, *J. Catal.* 216 (2003) 298. (h) W.A. Carvalho, P.B. Varaldo, M. Wallau, U. Schuchardt, *Zeolites* 18 (1997) 408.
79. (a) K.K. Kang, W.S. Ahn, *J. Mol. Catal. A: Chem.* 159 (2000) 403. (b) K. Chaudhari, R. Bal, D. Srinivas, A.J. Chandwadkar, S. Sivasanker, *Micropor. Mesopor. Mater.* 50 (2001) 209. (c) S. Shylesh, A.P. Singh, *J. Catal.* 228 (2004) 333. (d) J.S. Choi, S.S. Yoon, S.H. Jang, W.S. Ahn, *Catal. Today* 111 (2006) 280. (e) F. Chiker, F. Launay, J.P. Nogier, J.L. Bonardet, *Green Chem.* 5 (2003) 318. (f) P.J. Cordeiro, T.D. Tilley, *Langmuir* 27 (2011) 6295.
80. (a) Ullmann's Encyclopedia of Industrial Chemistry, 6th Edition (Electronic Release), Wiley/VCH, New York/Weinheim, 1998. (b) K. Bauer, D. Garbe, H. Surburg, *Common Fragrance and Flavor Materials*, Wiley/VCH, New York/Weinheim, 1997.
81. H. Fiegel, H.-W. Voges, T. Hamamoto, S. Umemura, T. Iwata, H. Miki, Y. Fujita, H.-J. Buysch, D. Garbe, W. Paulus, *Phenol Derivatives in Ullmann's Encyclopedia of Industrial Chemistry*; Wiley-VCH: New York, 2002; Vol. 26, p 521.
82. (a) P. Maggioni, F. Minisci, *Chim. Ind. (Milan)* 59 (1977) 239. (b) F. Bourdin, M. Costantini, M. Jouffret, G. Lartigan, *Ger. Pat. DE 064,497* (1971), assigned to Rhone-Paulenc, France. (c) G.A. Hamilton, J.P. Friedman, P.M. Campbell, *J. Am. Chem. Soc.* 88 (1966) 5266. (d) A. Thangaraj, R. Kumar, P. Ratnasamy, *Appl. Catal.* 57 (1990) L1.
83. J. Varagnat, *Ind. Eng. Chem. Prod. Res. Dev.* 15 (1976) 212.
84. (a) Y. Kuroda, M. Mori, A. Itoh, T. Kitano, F. Yamaguchi, K. Sasaki. M. Nitta, *J. Mol. Catal. A: Chem.* 73 (1992) 237. (b) T. Tatsumi, K. Yuasa, H. Tominaga, *J. Chem. Soc. Chem. Commun.* (1992) 1446. (c) H. Ehrich, H.

- Berndt, M.-M. Pohl, K. Jähnisch, M. Baerns, *Appl. Catal. A: Gen.* 230 (2002) 271. (d) T. Miyake, M. Hamada, H. Niwa, M. Nishizuka, M. Oguri, *J. Mol. Catal. A: Chem.* 2002, 178, 199.
85. A. Thangraj, R. Kumar, P. Ratnasamy, *J. Catal.* 131 (1991) 294.
86. J.L. Moltz, H. Heinichen, W.F. Holderich, *J. Mol. Catal. A: Chem.* 136 (1998) 175.
87. (a) A. Ribera, I.W.C.E. Arends, S.D. Vries, J.P. Ramírez, R.A. Sheldon, *J. Catal.* 195 (2000) 287. (b) A.L. Villa, C.A. Caro, C.M.de Correa, *J. Mol. Catal. A: Chem.* 228 (2005) 233.
88. (a) A. Tuel, Y.B. Tarrit, *Appl. Catal. A: Gen.* 102 (1993) 201. (b) A.V. Ramaswamy, S. Sivasanker, *Catal. Lett.* 22 (1993) 239. (c) P.S. Niphadkar, M.S. Kotwal, S.S. Deshpande, V.V. Bokade, P.N. Joshi, *J. Mater. Chem. Phys.* 114 (2009) 344. (d) N.K. Mal, A.V. Ramaswamy, *J. Mol. Catal. A: Chem.* 105 (1996) 149.
89. (a) S. Seelan, A.K. Sinha, *Appl. Catal. A: Gen.* 238 (2003) 201. (b) D. Srinivas, S. Sivasanker, *Catal. Surv. Asia* 7 (2003) 121. (c) S. Raya, S.F. Mapolie, J. Darkwa, *J. Mol. Catal. A: Chem.* 267 (2007) 143.
90. (a) K.M. Parida, S. Singha, P.C. Sahoo, *Catal. Lett.* 136 (2010) 155. (b) W. Zhao, Y. Luo, P. Deng, Q. Li, *Catal. Lett.* 73 (2001) 199. (c) I. Sobczak, M. Ziolk, M. Renn, P. Decyk, I. Nowak, M. Daturi, J.C. Lavalley, *Micropor. Mesoporor. Mater.* 74 (2004) 23. (d) S.V. Sirotnin, I.F. Moskovskaya, B.V. Romanovsky, *Catal. Sci. Technol.* 1 (2011) 971.
91. (a) Y. Han, F. Xiao, S. Wu, Y. Sun, X. Meng, D. Li, S. Lin, *J. Phys. Chem. B* 105 (2001) 7963. (b) L. Wang, A. Kong, B. Chen, H. Ding, Y. Shan, M. He, *J. Mol. Catal. A: Chem.* 230 (2005) 143. (c) Y. Zhu, Y. Dong, L. Zhao, F. Yuan, *J. Mol. Catal. A: Chem.* 315 (2010) 205. (d) Y. Dong, X. Y. Niu, Y. Zhu, F. Yuan, H. Fu, *Catal. Lett.* 141 (2011) 242. (e) L. Zhao, Y. Dong, X. Zhan, Y. Cheng, Y. Zhu, F. Yuan, H. Fu, *Catal. Lett.* 142 (2012) 619.
92. (a) C.E. Mabermann in *Encyclopedia of Chemical Technology*, Vol. 1 (Eds.: J.I. Kroschwitz), Wiley, New York, 1991, p. 251. (b) D. Lipp in *Encyclopedia of Chemical Technology*, Vol. 1 (Eds.: J. I. Kroschwitz), Wiley, New York, 1991, p. 266. (c) R. Opsahl in *Encyclopedia of Chemical Technology*, Vol. 2 (Eds.: J. I. Kroschwitz), Wiley, New York, 1991, p. 346.

93. J.W. Kim, K. Yamaguchi, N. Mizuno, *Angew. Chem. Int. Ed.* 47 (2008) 9249.
94. Y. Wang, H. Kobayashi, K. Yamaguchi, N. Mizuno, *N. Chem. Commun.* 48 (2012) 2642.
95. M.T. Schumperli, C. Hammond, I. Hermans, *ACS Catal.* 2 (2012) 1108.
96. A. Nishinaga, T. Shimizu, T. Matsuura, *J. Chem. Soc. Chem. Commun.* (1979) 970.
97. K.-I. Tanaka, S. Yoshifuji, Y. Nitta, *Chem. Pharm. Bull.*, 36 (1988) 3125.
98. A. Corma, H. Garcia, *Catal. Today* 38 (1997) 267.
99. G. Busca, *Chem. Rev.* 107 (2007) 5366.
100. K. Tanabe, W.F. Hölderich, *Appl. Catal. A: Gen.* 181 (1999) 399.
101. R.A. Sheldon, *Pure Appl. Chem.* 72 (2000) 1233.
102. (a) O. Mitsunobu, in: B. M. Trost, I. Fleming (Eds.), *Comprehensive Organic Synthesis*, vol. 6, Springer, New York, 1991, p. 88. (b) E. J. Corey, F.-Y. Zhang, *Angew. Chem. Int. Ed. Engl.* 38 (1999) 1931. (c) D. J. Ager, I. Prakash, D. R. Schaad, *Chem. Rev.* 96 (1996) 835.
103. (a) A. Procopio, M. Gaspari, M. Nardi, M. Oliverio, O. Rosati, *Tetrahedron Lett.* 49 (2008) 2289. (b) J. Agarwal, A. Duley, R. Rani, R. Peddinti, *Synthesis* 16 (2009) 2790.
104. (a) D. Srinivas, J.K. Satyarthi, *Catal. Surv. Asia* 15 (2011) 145. (b) J.K. Satyarthi, D. Srinivas, *Energy Fuels* 25 (2011) 4106. (c) M. Kouzu, A. Nakagaito, J.-S. Hidaka, *Appl. Catal. A: Gen.* 405 (2011) 36.
105. (a) U.R. Unnithan, K.K. Tiwari, *Indian J. Technol.* 25 (1987) 477. (b) B. Chemseddine, R. Audinos, *Catal. Today* 25 (1995) 417.
106. A. Endalew, Y. Kiros, R. Zanzi, *Biomass Bioenergy* 35 (2011) 3787.
107. (a) J. Pérez-Pariente, I. Díaz, F. Mohino, E. Sastre, *Appl. Catal. A: Gen.* 254 (2003) 173. (b) S.A. Fernandes, A.L. Cardoso, da Silva, M. Jose, *Fuel Process. Technol.* 96 (2012) 98. (c) W.D. Bossaert, D.E. De Vos, W.M.V. Rhijn, J. Bullen, P.J. Grobet, P.A. Jacobs, *J. Catal.* 182 (1999) 156. (d) I. Diaz, C. Marquez-Alvarez, F. Mohino, *J. Catal.* 193 (2000) 295.

CHAPTER – 2
Material Preparation and
Characterization

2.1. Introduction

This chapter describes the synthesis of various catalyst materials investigated in this work. Transition metals like Ti, Mn, V and Fe were incorporated into the structure of three-dimensional, mesoporous silicas, SBA-12 and SBA-16 by direct hydrothermal synthesis method. The formation, structural integrity and textural properties of metallosilicates were investigated by various physicochemical techniques including X-ray powder diffraction (XRD), diffuse reflectance ultraviolet-visible spectroscopy (DRUV-vis), scanning electron microscopy (SEM), high-resolution transmission electron microscopy (HRTEM), temperature-programmed desorption (TPD), thermogravimetric analysis (TGA), Fourier-transform infrared spectroscopy (FTIR), diffuse reflectance infrared Fourier transform (DRIFT) spectroscopy, Fourier transform laser Raman spectroscopy (FT-Raman), liquid and solid state (magic angle spinning) nuclear magnetic resonance spectroscopy (MAS NMR), electron paramagnetic resonance spectroscopy (EPR), N₂-physisorption and inductively coupled plasma-optical emission spectroscopy (ICP-OES). Catalytic activities of these materials for oxidation and acid-catalyzed reactions were investigated. The oxidation reactions include epoxidation of cyclic olefins (cyclohexene and cyclooctene) and hydroxylation of phenol with peroxides and oxidation of amines with aerial oxygen. The acid-catalyzed reactions include aminolysis of epoxides and esterification of oleic acid, a representative fatty acid, with methanol. These SBA-type metallosilicate have been investigated as catalysts, for the first time, in the above-said reactions.

2.2. Materials

Table 2.1 provides the list of various chemicals used in the synthesis and catalytic reactions

Table 2.1. Chemicals Used in the Present Work

S. No.	Chemical	Grade	Remarks
1.	Acetone	AR, 99.5%	Thomas Baker
2.	Acetonitrile	AR, 99.5%	Thomas Baker
3.	Methanol	AR, 99.8%	Thomas Baker
4.	Toluene	AR, 99.5%	Thomas Baker
5.	Dichloromethane	AR, 99.5%	Thomas Baker

6.	Chloroform	AR, 99.4%	Thomas Baker
7.	1,2-Dichloroethane	AR	Thomas Baker
8.	Carbon tetrachloride	GR	Merck Ltd., India
9.	Brij76 (Polyethylene glycol octadecyl ether)	Average M_n ~711	Aldrich
10.	Pluronic 123 (EO ₂₀ PO ₇₀ EO ₂₀)	Average M_n ~5800	Aldrich
11.	Pluronic F127 (EO ₁₀₆ PO ₇₀ EO ₁₀₆)	Average M_n ~12600	Aldrich
12.	Cetyltrimethylammonium bromide (CTMABr)	98%, Average M_n ~364.45	Aldrich
13.	Tetraethyl orthosilicate	98%	Aldrich
14.	Hydrochloric acid	35.4%	Thomas Baker
15.	Sodium hydroxide pellets	97%	Merck Ltd., India
16.	Sulphuric acid	98%	Thomas Baker
17.	Titanium tetraisopropoxide	98%	Spectrochem Pvt. Ltd. (Mumbai), India
18.	Isopropanol	99.7%	Thomas Baker
19.	Hydrogen peroxide solution (30% aq.)	GR	Loba Chemie Pvt. Ltd. India
20.	<i>tert.</i> -Butylhydroperoxide (TBHP)	70% in water	Aldrich
21.	<i>tert.</i> -Butylhydroperoxide (TBHP)	~5.5 M in decane	Aldrich
22.	Hydrofluoric acid	40%	Thomas Baker
23.	Manganese nitrate tetrahydrate	97%	Thomas Baker
24.	Ammonium metavanadate	98%	Thomas Baker
25.	Iron(III) chloride anhydrous	96%	Merck Ltd., India
26.	Potassium iodide	GR, 99.8%	Merck Ltd., India
27.	Sodium thiosulfate	99%	Qualigens Fine Chemicals (India)

28.	Ammonium molybdate	GR, 99%	Loba Chemie Pvt. Ltd. India
29.	Ammonium nitrate	98.5%	Loba Chemie Pvt. Ltd. India
30.	Ammonia solution	AR, 25% aq.	Thomas Baker
31.	Potassium dichromate	GR, 99.5%	Merck Ltd., India
32.	Diethylether	AR	Thomas Baker
33.	Ethyl acetate	AR	Thomas Baker
34.	Petroleum ether	AR	Thomas Baker
35.	Chloroform-d	99.8 atom % D	Aldrich
36.	Dimethylformamide	AR, 99.5%	Thomas Baker
37.	Dimethylsulphoxide	99%	Loba Chemie Pvt. Ltd. India
38.	Benzonitrile	98%	Aldrich
39.	Cyclohexene	99%	S.D. Fine-Chem. Ltd., India
40.	Cyclooctene	95%	Spectrochem Pvt. Ltd. (Mumbai), India
41.	Phenol	AR, 99.5%	Thomas Baker
42.	Benzylamine	99%	Loba Chemie Pvt. Ltd. India
43.	Pyridine	99.5%	Merck Ltd., India
44.	Potassium bromide	IR grade	Merck Ltd., Germany
45.	Styrene oxide	97%	Aldrich
46.	Cyclohexene oxide	98%	Aldrich
47.	Cyclooctene oxide	99%	Aldrich
48.	1,4-dioxane	AR, 99.5%	Thomas Baker
49.	Benzaldehyde	99.5 %	Merck Ltd., India
50.	Benzoic acid	AR, 99.9%	Thomas Baker
51.	Catechol	GR, 99%	Loba Chemie Pvt. Ltd. India
52.	Hydroquinone	GR, 99%	Loba Chemie Pvt. Ltd. India
53.	p-Benzoquinone	99%	Loba Chemie Pvt. Ltd. India
54.	Aniline	GR, 99.5%	Merck Ltd., India
55.	o-Toluidine	GR, 99.5%	Loba Chemie Pvt. Ltd. India
56.	m-Toluidine	99%	S.D. Fine-Chem. Ltd., India
57.	p-Toluidine	99.5%	S.D. Fine-Chem. Ltd., India
58.	p-Chloroaniline	98%	Loba Chemie Pvt. Ltd. India
59.	p-Methoxyaniline	99%	S.D. Fine-Chem. Ltd., India

60.	Morpholine	98.5%	Loba Chemie Pvt. Ltd. India
61.	2-Aminophenol	99%	Aldrich
62.	Cyclohexylamine	99%	Merck Ltd., India
63.	n-Butylamine	99%	Loba Chemie Pvt. Ltd. India
64.	Dibutylamine	98%	Aldrich
65.	Oleic acid	Extra pure	Loba Chemie Pvt. Ltd. India
66.	Titanium dioxide	GR, 99.5%	Loba Chemie Pvt. Ltd. India
67.	Aluminium(III) chloride anhydrous	98%	Merck Ltd., India
68.	Zinc chloride	95%	Merck Ltd., India
69.	Manganese(II) chloride tetrahydrate	GR, 98%	Loba Chemie Pvt. Ltd. India
70.	Starch soluble	Extra pure	Thomas Baker
71.	Silica gel	100-200 mesh	Thomas Baker

2.3. Synthesis of Mesoporous Silica Molecular Sieves

2.3.1. SBA-12

SBA-12 was prepared by a modified procedure of Zhao et al. [1]. In a typical preparation, 160 g of 2 M HCl and 40 g of distilled water were taken in a polypropylene beaker. Then, 8 g of Brij76 [$C_{18}H_{37}(OCH_2CH_2)_{10}OH$] was dissolved in it while stirring the mixture at 313 K for 2 h. Later, 17.6 g of tetraethyl orthosilicate (TEOS) was added over 30 min. Stirring was continued for 20 h. The gel formed was transferred into a Teflon-lined stainless-steel autoclave and heated at 373 K for 24 h. The solid (as-synthesized SBA-12) formed was filtered, washed thoroughly with distilled water (2 - 3 L) and dried at 373 K for 12 h. Then, it was calcined at 823 K for 8 h to remove all the organic matter in it. The calcined SBA-12 was white in color. Yield = 94%.

2.3.2. SBA-16

In a typical synthesis of SBA-16, 7.4 g of Pluronic F127 block-copolymer ($EO_{106}PO_{70}EO_{106}$) was dissolved in 384.3 g of 2 M HCl solution at 313 K while stirring for 2 h. To it, 28.34 g of TEOS was added over 30 min. The stirring was continued for 24 h. The gel formed was transferred into a Teflon-lined stainless steel autoclave. It was crystallized at 353 K for 48 h. The solid formed was filtered,

washed with distilled water (2 - 3 L), dried overnight at 373 K and calcined at 823 K for 8 h. The calcined SBA-16 [1, 2] was white in color. Yield = 96%.

2.3.3. SBA-15

SBA-15 was prepared hydrothermally according to the reported procedure [1, 3]. In a typical synthesis of SBA-15, 8.0 g of non-ionic surfactant Pluronic P123 (EO₂₀PO₇₀EO₂₀) was dissolved in 60 g of distilled water and 240 g of 2 M HCl solution while stirring at 313 K. To it, 17.0 g of tetraethyl orthosilicate (TEOS) was added over 30 min. Stirring was continued for 24 h. The gel formed was transferred into a Teflon-lined stainless-steel autoclave. It was aged at 373 K for 48 h. The solid formed was separated by filtration, washed with distilled water (2 - 3 L), dried overnight at 373 K and calcined in air at 823 K for 6 h. The calcined SBA-15 was white in color. Yield ~ 98%.

2.3.4. MCM-41

MCM-41 was synthesized by modifying the reported procedure [4]. In a typical synthesis, 2.67 g of sodium hydroxide was dissolved in 147 g of distilled water. To that, 5.94 g of cetyltrimethylammonium bromide (CTMABr) was added. Then, 14.17 g of tetraethyl orthosilicate (TEOS) was added slowly while stirring over a period of 30 min. The stirring was continued for another 1 h. After that, pH of the gel was maintained at 9-10 by using dilute H₂SO₄ solution. The resultant gel was stirred for further 5 h at 298 K. It was then transferred into a Teflon-lined stainless steel autoclave and heated to 373 K for 48 h. The solid product was filtered, washed with distilled water and dried overnight at 353 K and calcined at 823 K for 6 h to remove the organic template from the solid. The obtained silica material was white in color and yield was 94%.

2.4. Synthesis and Characterization of Titanosilicate Molecular Sieves

2.4.1. Synthesis

Different titanosilicate materials with varying Si/Ti molar ratio were prepared by direct hydrothermal synthesis method.

2.4.1.1. Ti-SBA-12

In the preparation of Ti-SBA-12 (with Si/Ti input molar ratio of 30), 8 g of Brij76 was dissolved in 40 g of distilled water and 160 g of 2 M HCl taken in a polypropylene beaker. The mixture was stirred at 313 K for 2 h. Then, 17.6 g of TEOS was added over 30 min. Later, 0.8 g of titanium iso-propoxide dissolved in 10 mL of iso-propanol was added. Stirring was continued for 20 h. The gel formed was transferred into a Teflon-lined stainless steel autoclave and heated at 373 K for 24 h. The solid formed was recovered by filtration, washed thoroughly with distilled water (2 - 3 L), dried at 373 K for 12 h and calcined at 823 K for 8 h. The calcined Ti-SBA-12 (30) was white in color. Yield = 93%.

Ti-SBA-12 with Si/Ti input molar ratios of 80, 50, 40 and 20 were prepared in a similar manner as described above using appropriate quantities of Si and Ti sources. Also, the catalysts with Si/Ti molar ratio of 30 were prepared using HCl of concentration 1, 0.5, 0.2, 0.1 and 0.05 M (instead of 2 M) in the synthesis ([see Appendix at the end of this chapter](#)).

2.4.1.2. Ti-SBA-16

In a typical synthesis of Ti-SBA-16 (with Si/Ti input molar ratio of 30), 7.4 g of Pluronic F127 was dissolved in 384.3 g of 2 M HCl solution at 313 K. After 2 h of stirring, 28.34 g of TEOS was added drop-wise over 30 min and stirred for 4 h. Then, 1.28 g of titanium iso-propoxide dissolved in 10 mL of iso-propanol was added slowly. Stirring was continued for another 20 h. The gel formed was transferred into a Teflon-lined stainless-steel autoclave. It was heated at 353 K for 48 h. The solid formed was separated by filtration, washed with distilled water (2 - 3 L), dried overnight at 373 K and calcined in air at 823 K for 8 h. The calcined Ti-SBA-16 was white in color. Yield = 95%.

Ti-SBA-16 with Si/Ti input ratios of 80, 50, 40 and 20 were prepared in a similar manner as described above using appropriate quantities of Si and Ti sources. Also, the catalysts with Si/Ti molar ratio of 30 were prepared using HCl of concentration 1, 0.5, 0.2, 0.1 and 0.05 M (instead of 2 M) in the synthesis ([see Appendix at the end of this chapter](#)).

2.4.1.3. Ti-SBA-15

Ti-SBA-15 catalysts with different Si/Ti molar ratio of 20, 30 and 40 were prepared by direct hydrothermal synthesis method. In a typical synthesis of Ti-SBA-15 (with input Si/Ti molar ratio of 30), 8.0 g of Pluronic P123 was dispersed in 60 g of distilled water and 240 g of 2 M HCl solution while stirring at 313 K. To it, 17.0 g of TEOS was added over 30 min. Then, 0.77 g of titanium iso-propoxide dissolved in 10 mL of iso-propanol was added slowly. Stirring was continued for another 24 h. The gel formed was transferred into a Teflon-lined stainless-steel autoclave. It was aged at 373 K for 48 h. The solid formed was separated by filtration, washed with distilled water (2 - 3 L), dried overnight at 373 K and calcined in air at 823 K for 6 h. The calcined Ti-SBA-15 (Si/Ti = 30) was white in color. Yield = 96%.

Ti-SBA-15 with Si/Ti input molar ratios of 20 and 40 were prepared in a similar manner as described above using appropriate quantities of Si and Ti sources.

2.4.1.4. Ti-MCM-41

In a typical synthesis of Ti-MCM-41 (with Si/Ti input ratio of 30) [4], 2.67 g of sodium hydroxide was dissolved in 147 g of distilled water. To that, 5.94 g of cetyltrimethylammonium bromide was added. Then, 14.17 g of TEOS was added slowly while stirring over a period of 30 min. The stirring was continued for another 1 h. After that, pH of the gel was maintained at 9-10 by using dilute H₂SO₄ solution. Then, 0.64 g of titanium iso-propoxide dissolved in 10 mL of iso-propanol (Thomas Baker) was added over a period of 15 min. The resultant gel was stirred for further 5 h at 298 K. It was then transferred into a Teflon-lined stainless steel autoclave and heated to 373 K for 48 h. The solid product was filtered, washed with distilled water, dried at 353 K and finally, calcined at 823 K for 6 h to remove the organic materials (surfactant) from the solid. Ti-MCM-41 with Si/Ti input ratio of 20 and 40 were also prepared in a similar manner by taking appropriate amounts of silicon and titanium sources.

2.4.1.5. TS-1

Microporous titanosilicate, TS-1 (with Si/Ti input molar ratio of 30) was supplied by the Catalyst Pilot Plant, National Chemical Laboratory, Pune. TS-1 catalyst was prepared according to the reported procedure [5].

2.4.2. Characterization Techniques

The physical, chemical and spectroscopic properties of the prepared materials were investigated using various physicochemical techniques. Ti content in titanosilicate samples was determined using an inductively coupled plasma-optical emission spectrometer (Spectro Arcos ICP-OES). X-ray diffraction (XRD) patterns of the powder samples were recorded on a PANalytical (X'pert Pro) diffractometer equipped with Ni-filtered Cu-K α radiation ($\lambda = 0.15418$ nm, 40 kV and 30 mA) and a proportional counter detector. The diffraction patterns in the small-angle region ($2\theta = 0.5 - 5/10^\circ$) were recorded at a scan rate of $0.2^\circ/\text{min}$ and with a step-size of 0.02° . Those data in the wide-angle region ($2\theta = 10^\circ - 80^\circ$) were recorded at a scan rate of $4^\circ/\text{min}$. The N $_2$ adsorption-desorption isotherms were measured at 77 K using a Quantachrome USA (Autosorb-1C) equipment. Prior to N $_2$ adsorption, the samples were evacuated at 573 K for 5 h. The specific surface area of the samples was determined by the Brunauer, Emmett and Teller (BET) method using the data points in the relative pressure (P/P_0) region of 0.05 - 0.3. The total pore volume was determined from the uptake of adsorbate (N $_2$) at a relative pressure (P/P_0) of 0.99. A reference alumina sample (supplied by Quantachrome, USA) was used to calibrate the instrument. The average pore diameter was determined from the isotherms using the Barret-Joyner-Halenda (BJH) model. Scanning electron micrographs (SEM) were collected using a Leica STEREOSCAN 440, LEO Microscopy, Cambridge, UK instrument. High-resolution transmission electron micrograph (HRTEM) images of the samples were collected on a FEI Technai-F30 instrument with a 300 kV field emission gun.

Diffuse reflectance UV-visible (DRUV-vis.) measurements were conducted on a Shimadzu UV-2550 spectrophotometer equipped with an integrating sphere attachment (ISR 2200). Spectral grade BaSO $_4$ was used as a reference material. The electron paramagnetic resonance (EPR) spectra were recorded taking the samples in suprasil quartz tubes (~ 4 mm o.d.). Prior to EPR measurements, the powder samples were activated at 373 K, in air. Oxo-titanium species in titanosilicate molecular sieves were generated *in situ* contacting a known amount of activated sample (45 mg) with aqueous H $_2$ O $_2$ or TBHP (~ 0.1 mL) at 77 K. It was ensured that the whole sample in EPR tube was completely soaked in the oxidant medium. Concentrations of paramagnetic oxo-species were estimated by double integration of the first-derivative EPR plots. Diphenylpicrylhydrazine (DPPH) was used as a standard.

Fourier transform infrared (FTIR) spectra were recorded on a Shimadzu 8300 spectrophotometer in the region 400 – 4000 cm^{-1} (spectral resolution = 4 cm^{-1} ; number of scans = 300). Samples were prepared in the form of KBr pellets (1 wt%). FT-Raman spectra were recorded on a Horiba JY LabRaman HR 800 MicroRaman spectrometer using 630 nm wavelength generated by a He-Ne laser operating at 20 mV. ^{29}Si magic-angle spinning nuclear magnetic resonance (MAS NMR) spectra were recorded at 59.63 MHz on a Bruker AV300 NMR spectrometer with 4 mm sample rotors. Samples were spun at a frequency of 10 kHz. A single pulse sequence was applied and the measurements were performed at 293 K. Thermogravimetric and differential thermal analyses (TG-DTA) of the samples were done under nitrogen (50 mL/min) using a PerkinElmer Diamond TG-DTA instrument at a ramp rate of 10 K/min in the temperature range of 298 – 1273 K.

Acidic properties of titanosilicates were determined using ammonia and pyridine as probe molecules. Diffuse reflectance infrared Fourier transform (DRIFT) spectroscopy enabled determination of the type of acid sites present in the catalysts. In DRIFT measurements (Shimadzu SSU 8000), the samples were initially activated at 723 K. The temperature was brought down to 323 K and pyridine was adsorbed. Then, the temperature of the sample was raised and held at 373 K for 0.5 h before starting the measurements (spectral resolution = 2 cm^{-1} ; number of scans = 200). Difference FTIR spectra were obtained by subtracting the spectrum of the catalyst from that of the sample adsorbed with pyridine. Temperature-programmed desorption of ammonia (NH_3 -TPD; Micromeritics Auto Chem 2910 instrument) quantified the density of acid sites. In a typical experiment, 0.1 g of catalyst was taken in a U-shaped, flow-through, quartz sample tube. Prior to measurements, the catalyst was pretreated in He (30 mL/min) at 823 K for 1 h. A mixture of NH_3 in He (10 v%) was passed (30 mL/min) at 298 K for 1 h. Then, the sample was, subsequently flushed with He (30 mL/min) at 373 K for 1 h. The TPD measurements were carried out in the range 373 – 1073 K at a heating rate of 10 K/min. Ammonia concentration in the effluent was monitored with a gold-plated, filament thermal conductivity detector. The amount of desorbed ammonia was determined based on the area under the peak. Detailed characterization results are presented in the following sections.

All these techniques were used also for the characterization of other metallosilicates: Mn-SBA-12, Mn-SBA-16, V-SBA-12 and Fe-SBA-12.

2.4.2.1. Chemical Composition

The Si/Ti (input) content in these titanosilicate materials was varied from 20 to 80. Several factors including type of inorganic precursor, mode of addition of reagents, temperature, aging time, ionic strength, etc., have been known to influence the characteristics of the zeolite and mesoporous materials [6]. In the present study, the concentration of HCl used in the synthesis was varied and its influence was studied. Chemical analysis by ICP-OES (Table 2.2) revealed that only 45 to 62 mol% of the input Ti was incorporated in the final compositions when the synthesis was carried out using 2 M HCl. When the molarity of HCl was decreased from 2 to 0.05 M, the amount of input Ti incorporated in the final products increased from about 50 [for Ti-SBA-12 (30)] and 57 [for Ti-SBA-16 (30)] to 90 mol% (Table 2.2). In other words, this study reveals that by adjusting HCl concentration, one could alter the extent of Ti incorporation in the final compositions. The Si/Ti output molar ratio of Ti-MCM-41 (Si/Ti = 30) and TS-1 (Si/Ti = 30) was found to be 33 by ICP analysis (Table 2.3).

2.4.2.2. X-ray Powder Diffraction (XRD)

The crystallinity and phase purity of prepared titanosilicates were confirmed from the XRD pattern. Fig. 2.1 shows representative XRD patterns of SBA-12, Ti-SBA-12, SBA-16 and Ti-SBA-16 in the small-angle region ($2\theta = 0.5 - 5^\circ$). SBA-12 (prepared using 2 M HCl) showed an intense main peak at 1.68° corresponding to (002) reflection and two well-resolved, weak peaks at 2.9° and 3.28° attributable to (112) and (300) reflections, respectively (Fig. 2.1 (a)). A weak shoulder (to the main peak) at 1.47° due to (100) reflection was also observed. All these characteristics of SBA-12 correspond to the ordered, three-dimensional, hexagonal mesoporous structure with a space group of $p6_3/mmc$ [1, 3]. SBA-16 (prepared using 2 M HCl) showed a strong peak at 0.92° attributable to (110) reflection and two poorly-resolved, weak peaks at 1.2° and 1.9° due to (200) and (211) reflections, respectively (Fig. 2.1 (b)). These diffraction patterns of SBA-16 can be indexed to an ordered, three-dimensional, mesoporous, cubic structure with space group of $Im\bar{3}m$ [1, 2, 7-9]. Ti incorporation did not alter the integrity of the framework structure. But the peaks shifted to lower 2θ values. The unit cell parameters (a and c for the hexagonal Ti-SBA-12 and a for the cubic Ti-SBA-16) increased with increasing Ti content (Table 2.2).

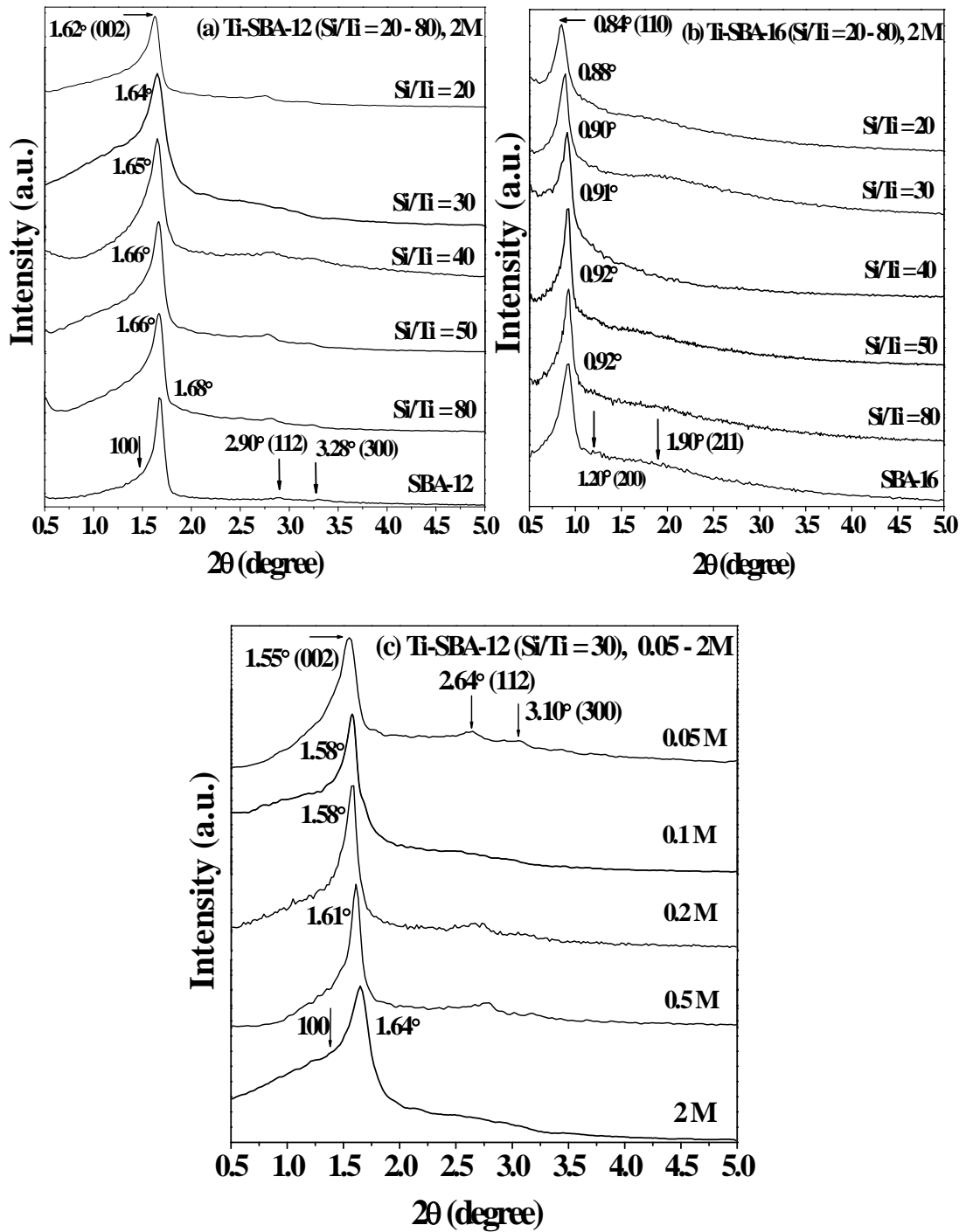


Fig. 2.1. Low-angle XRD patterns of (a) SBA-12 & Ti-SBA-12, and (b) SBA-16 & Ti-SBA-16 prepared using 2 M HCl, (c) XRD patterns of Ti-SBA-12 (Si/Ti = 30) prepared using varying molar concentration of HCl (0.05 – 2 M)

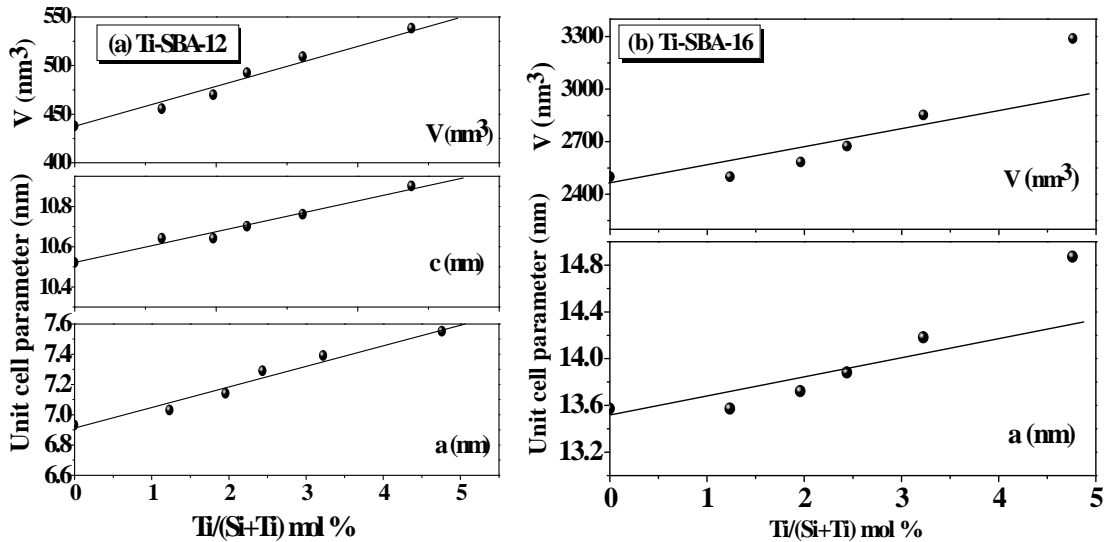


Fig. 2.2. Variation of unit cell parameters and unit cell volume as a function of Ti content in Ti-SBA-12 and Ti-SBA-16

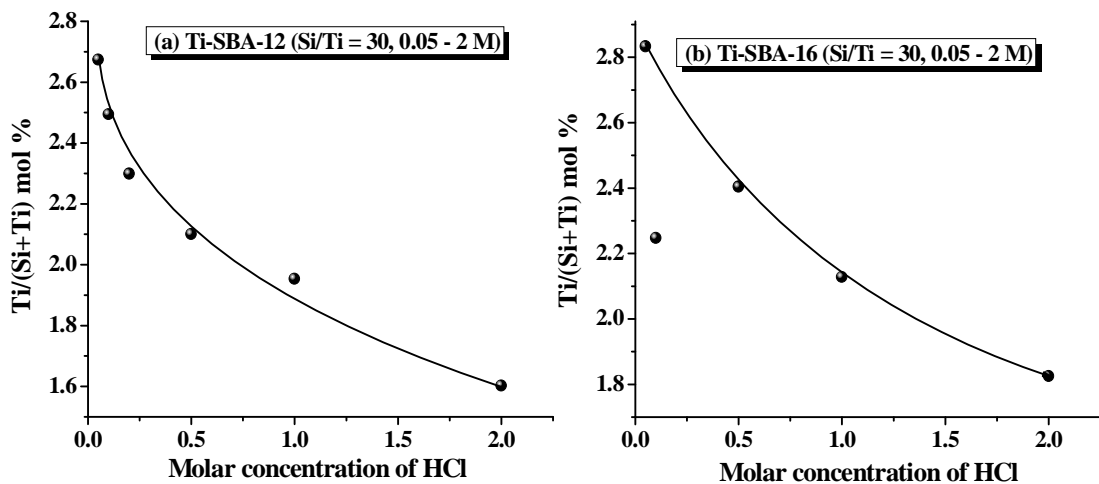


Fig. 2.3. Effect of HCl concentration used in the synthesis gel on output Ti content in Ti-SBA-12 and Ti-SBA-16

A similar effect was noticed also when the molarity of HCl used was decreased from 2 to 0.05 M (Fig. 2.1 (c) and Fig. 2.3). It may be noted that the ionic radii of Ti is larger (0.061 nm) than that of Si (0.04 nm). With increasing Ti content, the unit cell parameters and unit cell volume (V) of Ti-SBA-12 increased linearly up to a Ti/(Si+Ti) molar ratio of 0.033. This observation can be considered as an unequivocal evidence for the substitution of Ti (for Si) in the framework of mesoporous Ti-SBA-12. Similar relation holds good even in the case of Ti-SBA-16 materials (Fig. 2.2).

Fig. 2.4 shows the low-angle XRD patterns of MCM-41, Ti-MCM-41, SBA-15, Ti-SBA-15 and wide-angle XRD of TS-1. The XRD pattern of MCM-41 (Fig. 2.4, (a)) shows an intense peak at 2.52° due to (100) reflection and two less intense peaks at 4.36° and 5.04° due to (110) and (200) reflections, respectively. These XRD patterns can be indexed for a hexagonal type of material with $p6mm$ space group. Upon titanium incorporation, these peaks shifted towards lower 2θ value (Fig. 2.4 (a)). The increase in unit cell parameters (Table 2.3) of these hexagonal materials confirms Ti incorporation in the framework position of MCM-41.

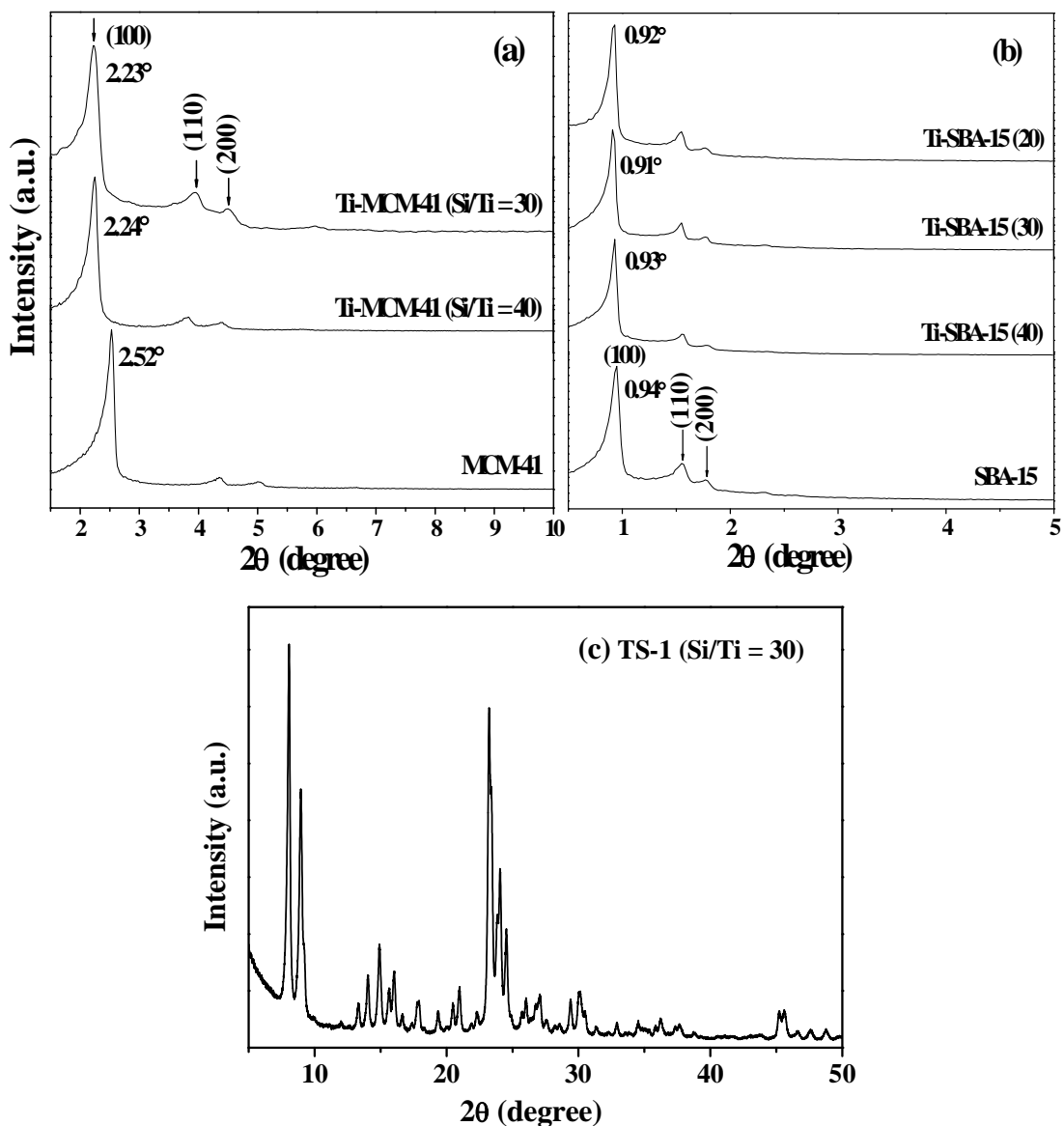


Fig. 2.4. Low-angle XRD patterns: (a) MCM-41 and Ti-MCM-41 with Si/Ti molar ratio of 30 and 40, (b) SBA-15 and Ti-SBA-15 with Si/Ti molar ratio of 20, 30 and 40 prepared using 2 M HCl, (c) wide-angle XRD pattern of TS-1 (Si/Ti = 30)

Low-angle XRD pattern of SBA-15 (Fig. 2.4, (b)) shows an intense peak at 0.94° corresponding to (100) reflection and two less intense peak at 1.56° and 1.78° arising from (110) and (200) reflections, respectively. These XRD patterns can be indexed to a hexagonal type of material with $p6mm$ space group. After titanium incorporation these peaks shifted to lower 2θ values (Fig. 2.4 (b)). The increase in unit cell parameters (Table 2.3) of these hexagonal materials confirms Ti incorporation in the framework position of SBA-15 mesoporous silica.

Wide-angle XRD pattern of TS-1 (Si/Ti = 30) (Fig. 2.4 (c)) shows MFI structure with orthorhombic symmetry which is indicative of titanium in the framework of silicalite-1 [10]. Pure silicalite-1 sample shows XRD pattern typical of monoclinic symmetry [11, 12]. There is no separate phase due to the crystalline TiO_2 in the XRD pattern. Expansion of unit cell parameters and unit cell volume was observed due to titanium incorporation (ionic radii of Ti is larger than that of Si) in the framework position of TS-1 with MFI structure [5, 13].

All these mesoporous materials (Ti-SBA-12 and Ti-SBA-16) showed a diffused XRD peak in the wide-angle region at 23° (Fig. 2.5) indicative of the presence of amorphous silica. Weak, additional peaks (marked by asterisk in Fig. 2.5) characteristic of a rutile TiO_2 (JCPDS Nos. 86-0148 and 78-1510) were observed at 27.4 , 36.1 and 54.3° in Ti-SBA-12 (prepared using 2 M HCl) with Si/Ti ≤ 40 (Fig. 2.5 (a)). Such an aggregated TiO_2 phase was not detected in the samples of Ti-SBA-16 prepared under similar acidic conditions (Fig. 2.5 (b)). At molar concentration of HCl < 2 , the presence of a TiO_2 phase was detected in both Ti-SBA-12 and Ti-SBA-16 (Figs. 2.5 (c) and 2.5 (d)). Lower concentrations of HCl stabilized anatase structure for TiO_2 showing characteristic peaks at 25.3 , 37.9 , 48 , 54.6 and 55.3° (JCPDS Nos. 86-1155 and 83-2243). The average crystallite size of TiO_2 (determined using Scherrer equation) was 2.6 and 3 nm for Ti-SBA-12 (30) and Ti-SBA-16 (30), respectively, prepared using lower molar concentration of HCl. This size is much smaller than the domain size of the mesostructure implying that there is no phase separation of titania crystals and silicate mesostructure. The XRD data in small- and wide-angle regions, thus, reveal that part of input Ti ions were substituted for Si in framework locations (unit cell parameters and unit cell volume increased with increasing Ti content) and the remaining were located inside the mesopores as dispersed TiO_2 particles, their proportion was dependent on the concentration of HCl and Si/Ti input molar ratio.

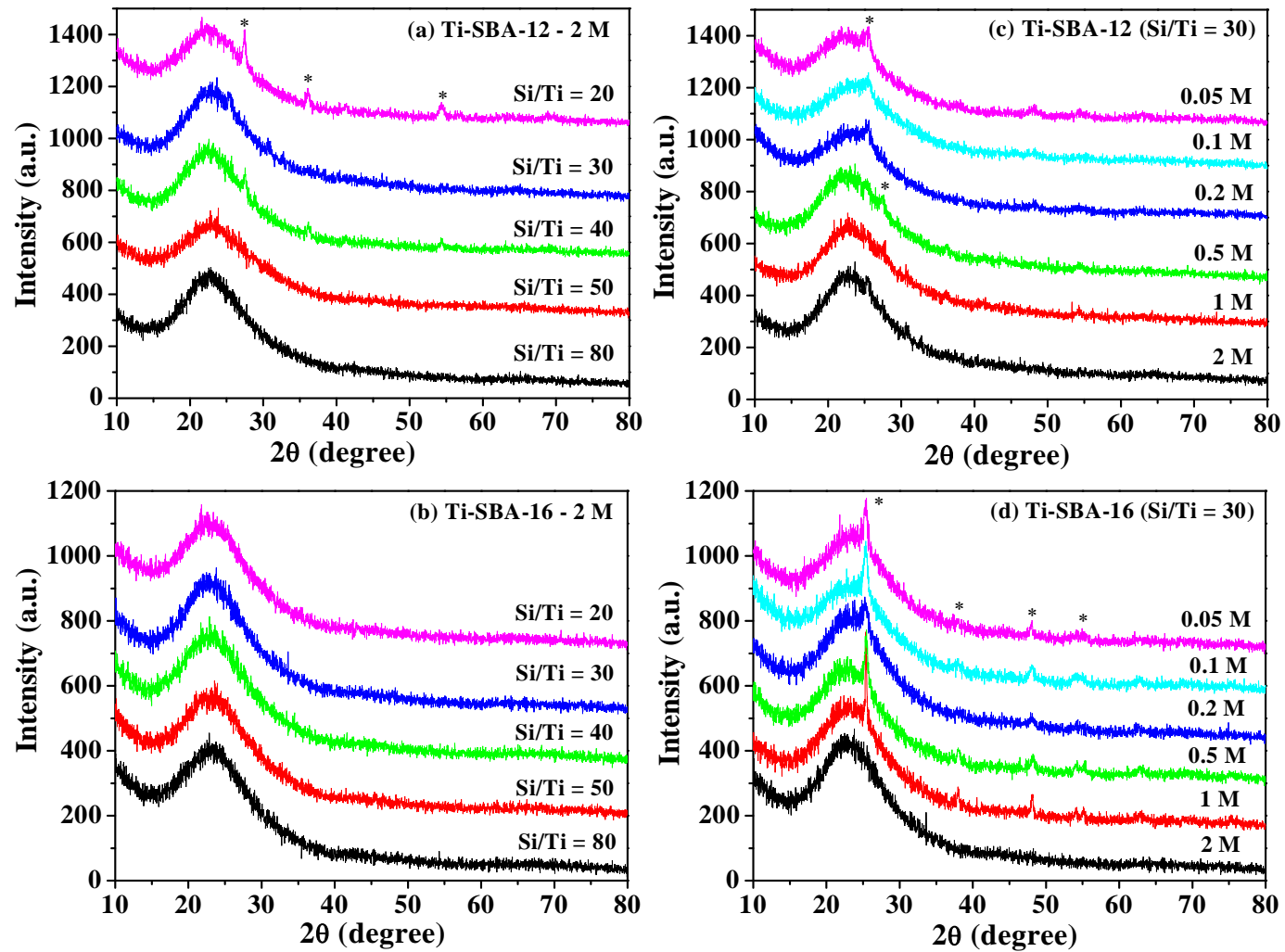


Fig. 2.5. XRD profiles in the wide-angle region: (a) Ti-SBA-12 and (b) Ti-SBA-16 (Si/Ti = 20 – 80, prepared using 2 M HCl), (c) Ti-SBA-12 and (d) Ti-SBA-16 (Si/Ti = 30, prepared using 0.05 – 2 M HCl). Peaks marked by asterisk correspond TiO₂ phase

Table 2.2. Composition and Structural Properties of Ti-SBA-12 and Ti-SBA-16

Catalyst	Conc. of HCl used in synthesis (M)	Si/Ti molar ratio			Structural data (XRD) ^a				
		Input	Output (ICP-OES)	Input Ti incorporated (mol%)	Interplanar spacing (nm)			Unit cell parameter (nm)	
					d ₁₀₀	d ₀₀₂	d ₁₁₀	a	c
SBA-12	2	∞	∞	-	6.00	5.26	-	6.93	10.52
Ti-SBA-12 (80)	2	80	146	55.1	6.09	5.32	-	7.03	10.64
Ti-SBA-12 (50)	2	50	80.2	62.8	6.18	5.32	-	7.14	10.64
Ti-SBA-12 (40)	2	40	68.7	58.8	6.31	5.35	-	7.29	10.70
Ti-SBA-12 (30)	2	30	61.4	49.7	6.40	5.38	-	7.39	10.76
Ti-SBA-12 (20)	2	20	45.7	45.0	6.54	5.45	-	7.55	10.90
Ti-SBA-12 (30)	1	30	50.2	60.6	6.40	5.52	-	7.39	11.04
Ti-SBA-12 (30)	0.5	30	46.6	65.1	6.50	5.49	-	7.50	10.98
Ti-SBA-12 (30)	0.2	30	42.5	71.3	6.54	5.60	-	7.55	11.20
Ti-SBA-12 (30)	0.1	30	39.1	77.3	6.54	5.60	-	7.55	11.20
Ti-SBA-12 (30)	0.05	30	36.4	89.9	6.95	5.70	-	8.02	11.40
SBA-16	2	∞	∞	-	-	-	9.6	13.57	-
Ti-SBA-16 (80)	2	80	150.2	53.5	-	-	9.6	13.57	-
Ti-SBA-16 (50)	2	50	80.5	62.6	-	-	9.7	13.72	-
Ti-SBA-16 (40)	2	40	70.6	57.3	-	-	9.82	13.88	-
Ti-SBA-16 (30)	2	30	53.8	56.6	-	-	10.04	14.18	-
Ti-SBA-16 (20)	2	20	40.6	50.5	-	-	10.52	14.87	-
Ti-SBA-16 (30)	1	30	46.0	66.0	-	-	11.12	15.72	-
Ti-SBA-16 (30)	0.5	30	40.6	74.5	-	-	11.20	15.73	-
Ti-SBA-16 (30)	0.2	30	50.8	59.9	-	-	11.33	16.02	-
Ti-SBA-16 (30)	0.1	30	43.5	69.7	-	-	11.12	15.72	-
Ti-SBA-16 (30)	0.05	30	34.3	90.4	-	-	11.18	15.81	-

^aSBA-12 and Ti-SBA-12 are described by a hexagonal system with space group of $p6_3/mmc$. SBA-16 and Ti-SBA-16 are defined by a cubic system with space of $Im\bar{3}m$. Unit cell parameter $a = 2d_{100}/\sqrt{3}$ and $c = 2d_{002}$ (for SBA-12 and Ti-SBA-12) and $a = \sqrt{2} \times d_{110}$ (for SBA-16 and Ti-SBA-16)

Table 2.3. Composition, Structure and Textural properties of TS-1, Ti-MCM-41 and Ti-SBA-15

Materials	Si/Ti molar ratio		Structural data (XRD) ^a			Textural properties (N ₂ physisorption)			
	Input	Output (ICP-OES)	Interplanar spacing (nm)	Unit cell parameter (nm)	S _{BET} (m ² /g)	Average pore diameter (nm)	Total pore volume (cc/g)	Wall thickness (nm)	
									d ₁₀₀
TS-1 (30) ^b	30	33	-	-	532	-	-	-	
MCM-41	∞	∞	3.50	4.04	994	3.50	0.87	0.54	
Ti-MCM-41 (40)	40	33	3.94	4.55	-	-	-	-	
Ti-MCM-41 (30)	30	-	3.96	4.57	1531	2.32	0.89	2.25	
SBA-15	∞	∞	9.40	10.85	800	8.10	0.91	2.75	
Ti-SBA-15 (40)	40	-	9.50	10.97	-	-	-	-	
Ti-SBA-15 (30)	30	-	9.70	11.20	892	8.80	1.14	2.40	
Ti-SBA-15 (20)	20	-	9.60	11.08	-	-	-	-	

^aMCM-41, Ti-MCM-41, SBA-15 and Ti-SBA-15 are described by a hexagonal system with space group of $p6mm$. Unit cell parameter $a = 2d_{100}/\sqrt{3}$ and wall thickness = $a - \text{average pore diameter (BJH)}$. ^bTS-1 (Titanium silicalite-1) is defined by orthorhombic space group (MFI topology)

2.4.2.3. N₂-Physisorption

Figs. 2.6 - 2.8 show the N₂ adsorption-desorption isotherms of SBA-12, Ti-SBA-12, SBA-16 and Ti-SBA-16 materials. Capillary condensation of gases within mesoporous materials is often distinguished by a distinct step in the adsorption isotherm accompanied by a hysteresis loop [14]. SBA-12 and Ti-SBA-12 showed typical type-IV N₂ adsorption-desorption isotherms with a H₁-hysteresis loop, which is characteristic of a hexagonal mesoporous materials (Figs. 2.6 and 2.7) [1]. SBA-16 and Ti-SBA-16 showed type IV isotherms with broad H₂-hysteresis loop, which is characterized by a steep desorption branch and a smooth increasing adsorption branch (Fig. 2.8). This has been corresponded to the existence of ink-bottle-type pores [15-19], viz., pores consisting of wide bodies fitted with narrow necks. At the heart of this mechanism lies the supposition that capillary condensation during adsorption in such pores is governed by the radius of curvature of the wide body of the pores, while capillary evaporation, during desorption, of the capillary condensate in the pores is obstructed by liquid remaining condensed in the nano necks (pore blocking). Porous glasses and silica gels give rise to the hysteresis loop of type H₂ [20, 21]. The N₂-adsorption-desorption behaviours of SBA-16 and Ti-SBA-16 are typical of cage-like uniform mesopores interconnected by relatively narrow aperture (Fig. 2.8) [19]. All these materials showed a narrow BJH pore size distribution with an average pore size of 3.8 to 6.9 nm for SBA-12 (Fig. 2.6 and 2.7, inset) and 3.4 to 6.4 nm for SBA-16 materials (Fig. 2.8, inset).

Ti incorporation and HCl molar concentration influenced the textural properties (Table 2.4). At a particular HCl concentration (ca., 2 M), the specific surface area of both SBA-12 and SBA-16 increased with increasing Ti content and beyond a certain value it started decreasing. A similar variation was found also for the average pore diameter and total pore volume. The catalysts with Si/Ti = 50 were found to have higher values of these parameters (Table 2.4). It may be recalled from the XRD results that the incorporated Ti in SBA-12 and SBA-16 was present in two types of locations – framework sites and as TiO₂ agglomerates in extra-framework sites. The latter were visible at Si/Ti ≤ 40. While the substituted Ti possibly increased the surface area and pore dimensions, the titania agglomerates formed inside the mesopores are the possible cause for the decreased values of textural parameters at Si/Ti ≤ 40. Although an increase in specific surface area was observed, pore volume and average pore diameter increased initially and then decreased with

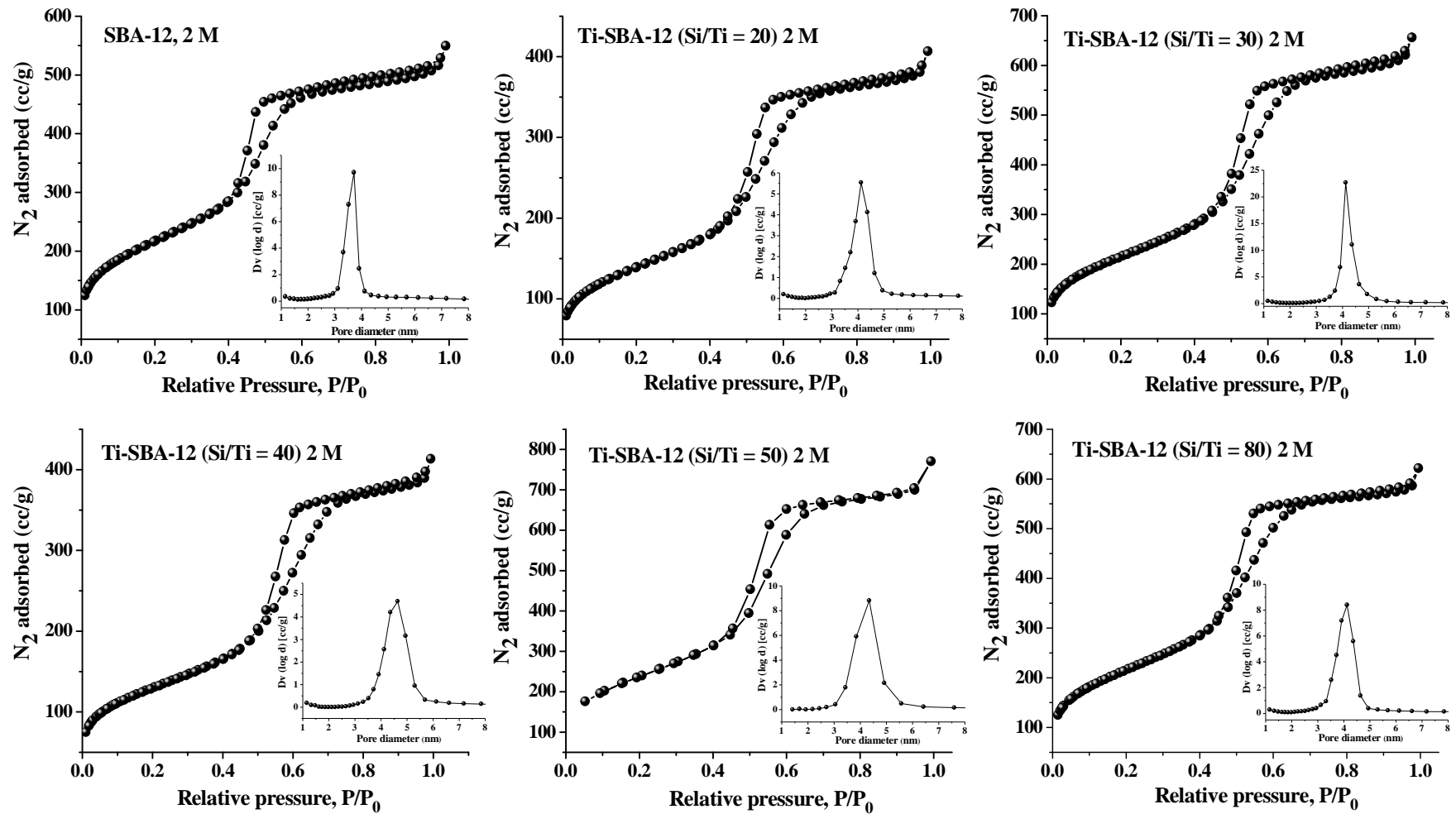


Fig. 2.6. Nitrogen adsorption-desorption isotherms of SBA-12 and Ti-SBA-12 with varying Si/Ti molar ratio (Si/Ti = 20 – 80) prepared using 2 M HCl in the synthesis gel

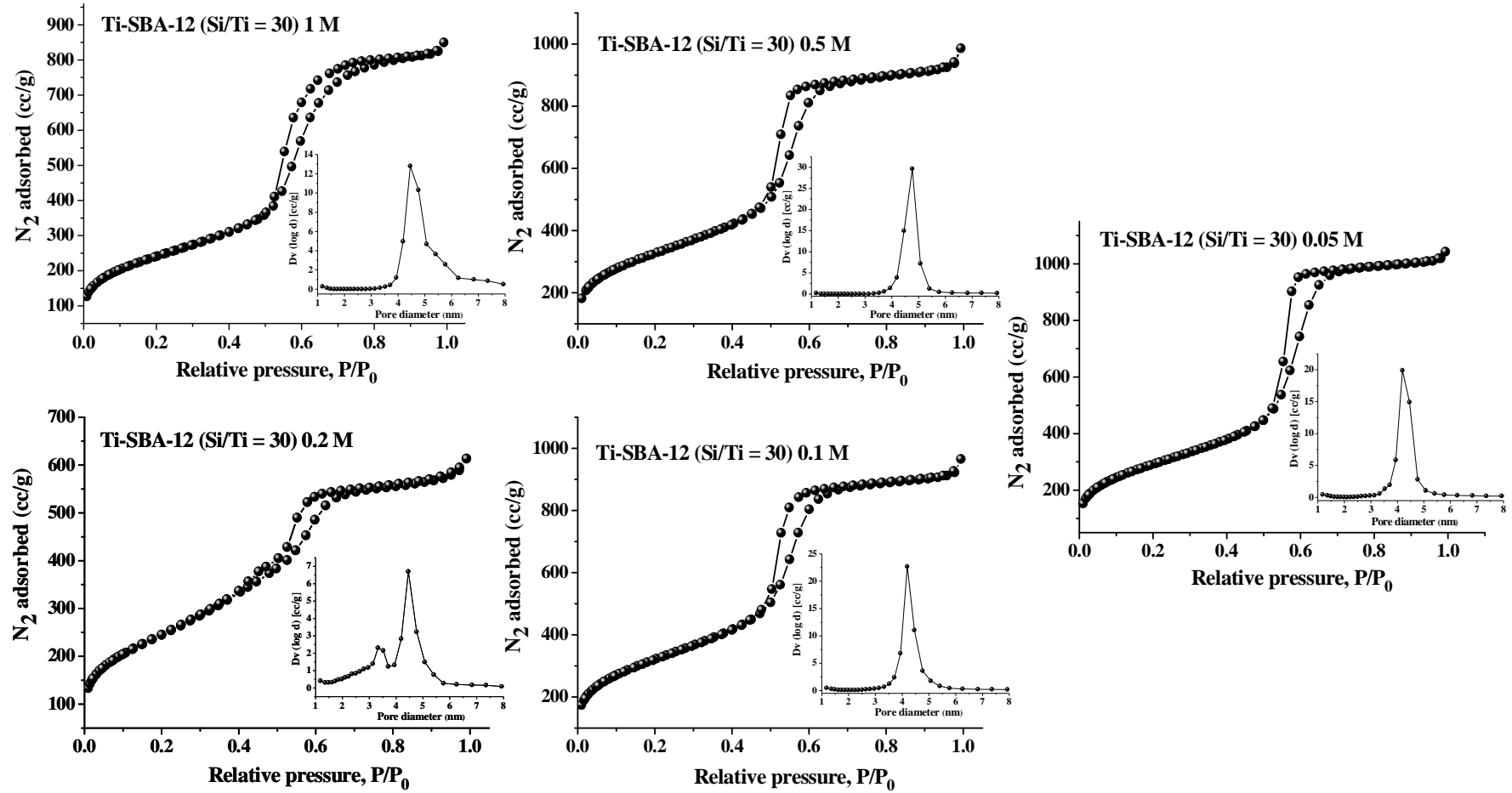


Fig. 2.7. Nitrogen adsorption-desorption isotherms of Ti-SBA-12 (Si/Ti = 30) prepared using varying molar concentration of HCl (1 - 0.05 M) in the synthesis gel

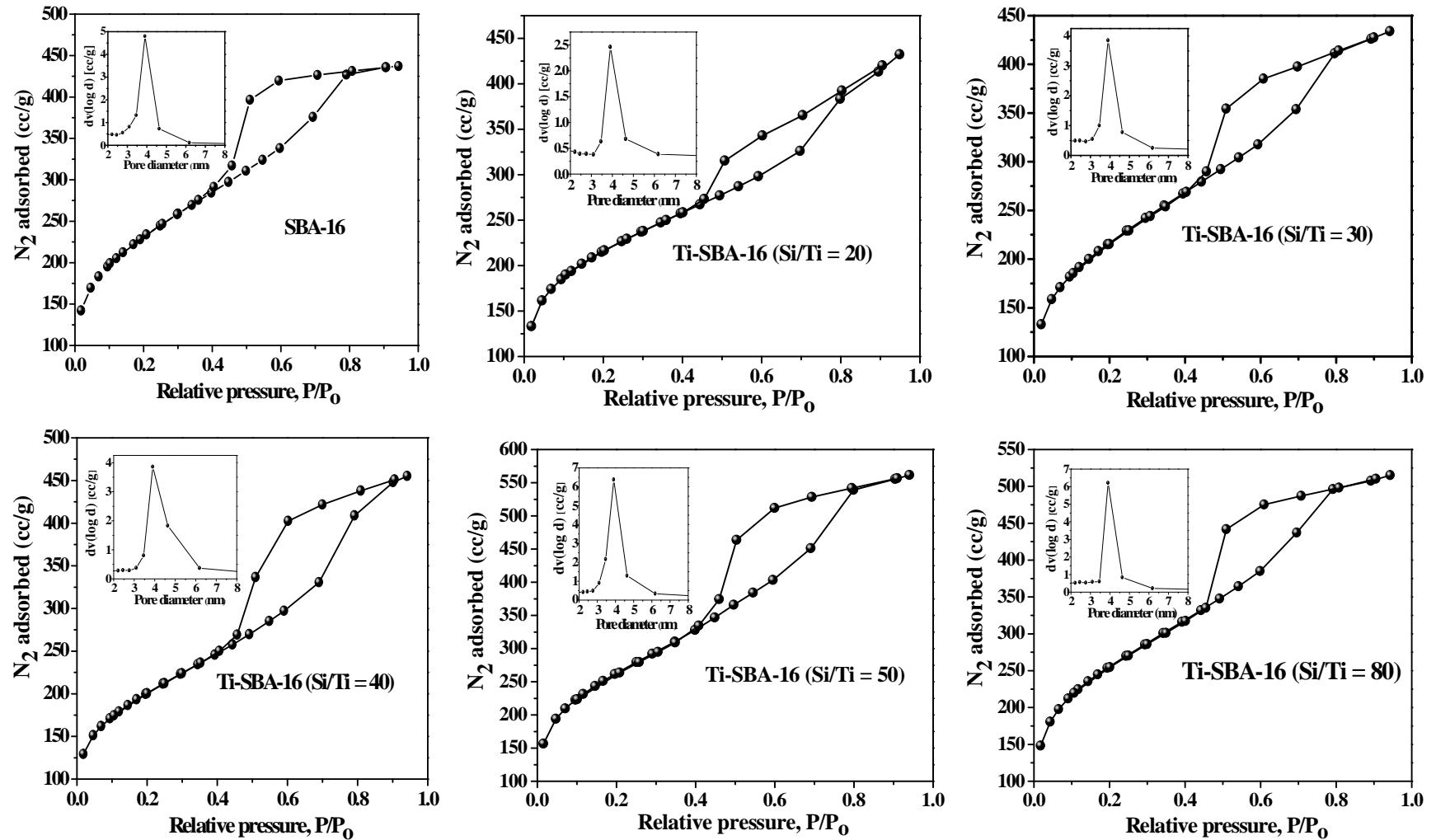


Fig. 2.8. Nitrogen adsorption-desorption isotherms of SBA-16 and Ti-SBA-16 with varying Si/Ti molar ratio (Si/Ti = 20 – 80) and their pore size distribution (inset) prepared using 2 M HCl

decreasing concentration of HCl from 2 to 0.05 M. Again, formation of titania agglomerates at lower concentration of HCl is the possible cause for this behaviour of textural properties. In other words, both Ti-content and molarity of HCl influenced the textural properties. The pore wall thickness of SBA-12 and Ti-SBA-12 were calculated as the difference of unit cell parameter c (XRD data) and average pore diameter (N_2 physisorption data) and that of SBA-16 and Ti-SBA-16 were determined using the formula:

$$\text{Pore wall thickness} = \sqrt{3}a/2 - \text{average pore diameter}$$

where a is the unit cell parameter as calculated from the XRD data. It may be noted from Table 2.4 that the wall thickness of Ti-SBA-16 materials is higher (8.0 – 10.6 nm) than that of Ti-SBA-12 (4.1 – 6.4 nm). Interestingly, the magnitude of wall thickness is same as that of pore diameter for Ti-SBA-12 and it is more than double for Ti-SBA-16. It may be mentioned here that the walls of Ti-SBA-12 and Ti-SBA-16 are more than 5 and 8 times thicker, respectively, than MCM-41 and MCM-48 [22]. The higher thickness of the walls of mesoporous materials of the current study make them thermally more stable than the MCM materials (Table 2.3).

Fig. 2.9 shows the N_2 adsorption-desorption isotherms of TS-1, Ti-MCM-41, SBA-15 and Ti-SBA-15 and their BJH pore size distribution (inset). TS-1 (Fig. 2.9 (a)) shows the type-I isotherm which is indicative of microporous material. TS-1 with Si/Ti molar ratio of 30 has a specific (S_{BET}) surface area of $532 \text{ m}^2/\text{g}$ (Table 2.3). N_2 adsorption-desorption isotherms of Ti-MCM-41, SBA-15 and Ti-SBA-15 showed type-IV isotherm and exhibit a H_1 hysteresis loop, which is the characteristics of mesoporous solid materials (Figs. 2.9) [21]. These materials (MCM-41, Ti-MCM-41, SBA-15 and Ti-SBA-15) showed a narrow BJH pore size distribution with uniform mesopore structure (Fig. 2.9, inset). The textural parameters of MCM-41, Ti-MCM-41, SBA-15 and Ti-SBA-15 are given in Table 2.3. Ti-MCM-41 (Si/Ti = 30) showed high specific BET surface area, average pore diameter, pore volume and wall thickness as compared to the pure MCM-41 (Table 2.3). Ti-SBA-15 (Si/Ti = 30) has larger specific BET surface area, average pore diameter and pore volume compared to SBA-15. However the wall thickness of Ti-SBA-15 (30) is relatively less as compared to the neat SBA-15 mesoporous silica (Table 2.3).

Table 2.4. Textural Properties of SBA-12, Ti-SBA-12, SBA-16 and Ti-SBA-16

Catalyst	Conc. of HCl used in the synthesis (M)	Textural properties (N ₂ physisorption)					
		S _{BET} (m ² /g)	Pore volume (cc/g)			Average pore diameter (nm) ^a	Wall thickness (nm) ^b
			Micro	Meso	Total		
SBA-12	2	672	0.01	0.63	0.64	3.8 (5.4)	6.72
Ti-SBA-12 (80)	2	767	0	0.96	0.96	5.0	5.64
Ti-SBA-12 (50)	2	857	0	1.20	1.20	5.6	5.04
Ti-SBA-12 (40)	2	460	0.02	0.62	0.64	5.5	5.20
Ti-SBA-12 (30)	2	765	0.03	0.98	1.01	5.3 (5.8)	5.46
Ti-SBA-12 (20)	2	500	0.02	0.61	0.63	5.0	5.90
Ti-SBA-12 (30)	1	759	0	1.31	1.31	6.9	4.14
Ti-SBA-12 (30)	0.5	980	0.03	1.58	1.61	6.6	4.38
Ti-SBA-12 (30)	0.2	775	0.08	0.87	0.95	4.9	6.30
Ti-SBA-12 (30)	0.1	1015	0	1.49	1.49	5.9	5.30
Ti-SBA-12 (30)	0.05	1085	0.04	1.49	1.53	5.6	5.80
SBA-16	2	800	0.16	0.51	0.67	3.4 (3.6)	8.35
Ti-SBA-16 (80)	2	886	0.15	0.64	0.79	3.6	8.15
Ti-SBA-16 (50)	2	910	0.11	0.75	0.86	3.8	8.08
Ti-SBA-16 (40)	2	709	0.10	0.60	0.70	4.0	8.02
Ti-SBA-16 (30)	2	765	0.15	0.52	0.67	3.5 (3.4)	8.78
Ti-SBA-16 (20)	2	780	0.18	0.49	0.67	3.4	9.47
Ti-SBA-16 (30)	1	796	0.03	0.99	1.02	5.1	8.51
Ti-SBA-16 (30)	0.5	780	0.01	1.23	1.24	6.4	7.22
Ti-SBA-16 (30)	0.2	856	0.14	0.58	0.72	3.4	10.47
Ti-SBA-16 (30)	0.1	950	0.17	0.61	0.78	3.3	10.31
Ti-SBA-16 (30)	0.05	1022	0.22	0.78	1.0	3.7	10.00

^aValues in parentheses are those obtained from HRTEM measurements. ^bWall thickness = c – average pore diameter (for SBA-12 and Ti-SBA-12) and $\sqrt{3}/2 a$ – average pore diameter (for SBA-16 and Ti-SBA-16). Unit cell parameter values c (for SBA-12 and Ti-SBA-12) and a (for SBA-16 and Ti-SBA-16) has taken from [Table 2.1](#) for the calculation of wall thickness of the materials

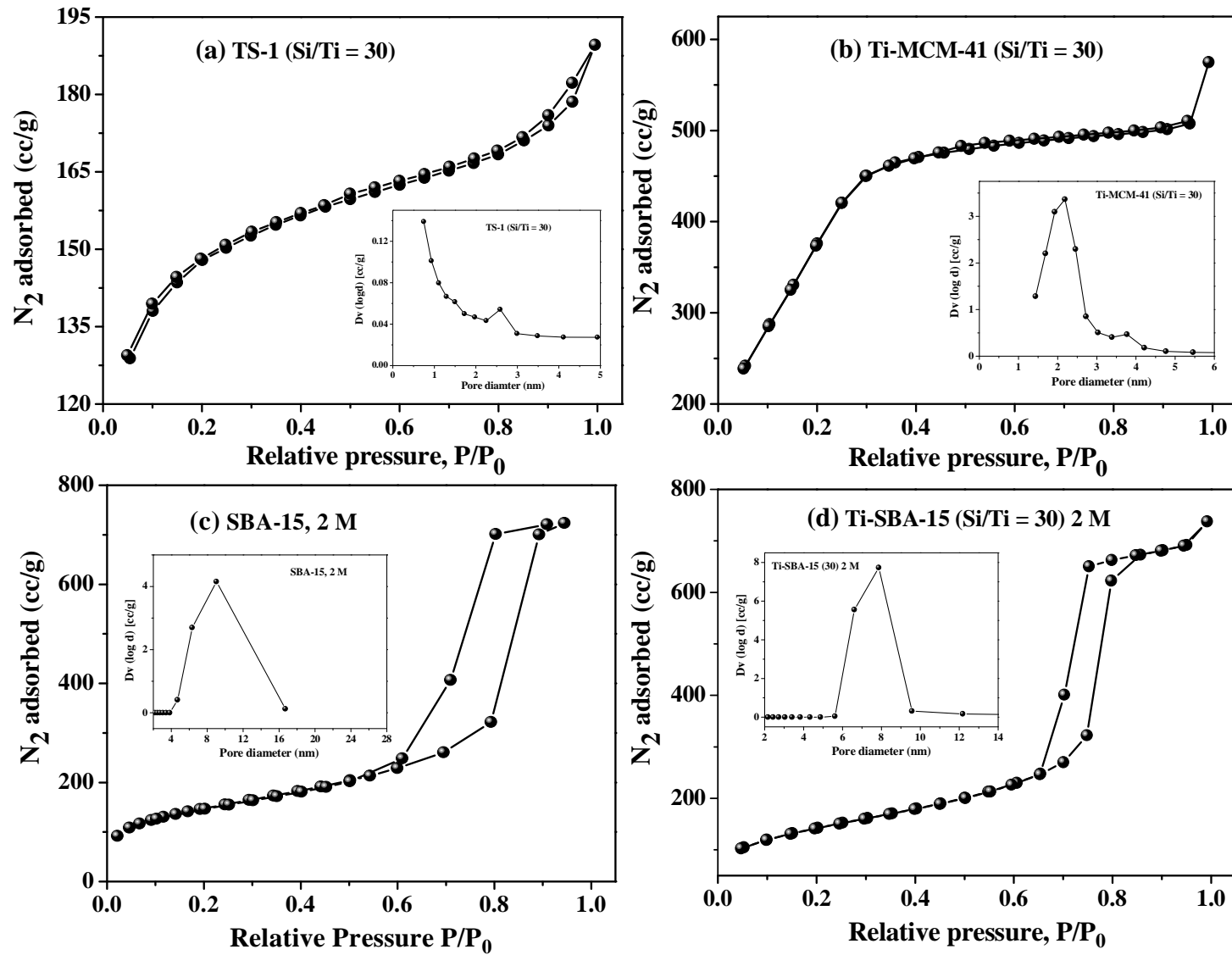


Fig. 2.9. Nitrogen sorption isotherms and pore size distribution (inset) of (a) TS-1 (b) Ti-MCM-41 (c) SBA-15 and (d) Ti-SBA-15

2.4.2.4. Scanning Electron Microscopy (SEM)

Fig. 2.10 shows the SEM images of SBA-12, Ti-SBA-12, SBA-16 and Ti-SBA-16 with Si/Ti molar ratios of 20, 40 and 50. While SBA-12 crystals have elliptical morphology, those of Ti-SBA-12 have a spherical morphology (SEM). However, Ti-SBA-12 with Si/Ti molar ratio of 20 has some agglomerated particles. The particle size of the latter is larger (4 – 6 μm) than that of the former (2 – 3 μm). Pure SBA-16 showed planar and somewhat spherical type of morphology particles size in the range 10 – 25 μm . Ti-SBA-16 formed as planar sheets and worm-like morphologies with particles size of 7 – 15 μm (Fig. 2.10). Ti-content and HCl concentration had no marked effect on the size and shape of titanosilicate particles.

2.4.2.5. High Resolution Transmission Electron Microscopy (HRTEM)

HRTEM images (Fig. 2.11) confirmed the long-range, three-dimensional, mesoporous ordering in these materials. While Ti-SBA-12 has hexagonally arranged pores, Ti-SBA-16 has cubic, cage-like interconnected pore arrangement. No separate bulk TiO_2 particles were detected in the HRTEM images.

2.4.2.6. Diffuse Reflectance Ultraviolet Visible Spectroscopy (DRUV-vis)

The nature and coordination of titanium in Ti-SBA-12 and Ti-SBA-16 was investigated by DRUV-vis spectroscopy (Fig. 2.12). Prior to spectral measurements, the samples were activated at 473 K for 2 h. Special care was taken to avoid contact with atmosphere. Pure silica samples, SBA-12 and SBA-16 showed no absorption bands in the UV-vis region. The activated Ti-SBA-12 and Ti-SBA-16 showed an absorption band maximum at 210 nm and a shoulder band at 217 – 220 nm which were attributed to mono-atomically dispersed Ti^{4+} ions in tetra-coordinated geometry. While the band at 210 nm was corresponded to $\text{Ti}(\text{OSi})_4$ structure, that at 217 – 220 nm was attributed to $\text{Ti}(\text{OH})(\text{OSi})_3$ structure [23].

All these absorption bands arise due to ligand-to-metal ($\text{O}^{2-} \rightarrow \text{Ti}^{4+}$) charge transfer transitions. The electronic transition for $\text{Ti}(\text{OH})(\text{OSi})_3$ occurs at lower energy (217 – 220 nm) than that for $\text{Ti}(\text{OSi})_4$ (210 nm) due to differences in electron donating capacities of OH^- and OSi^- ligand groups. The HO^- group has more electron donating capacity than SiO^- . Hence, the energy gap between oxygen and Ti molecular orbitals is lower in the case of $\text{Ti}(\text{OH})(\text{OSi})_3$ than in $\text{Ti}(\text{OSi})_4$. Thus, the

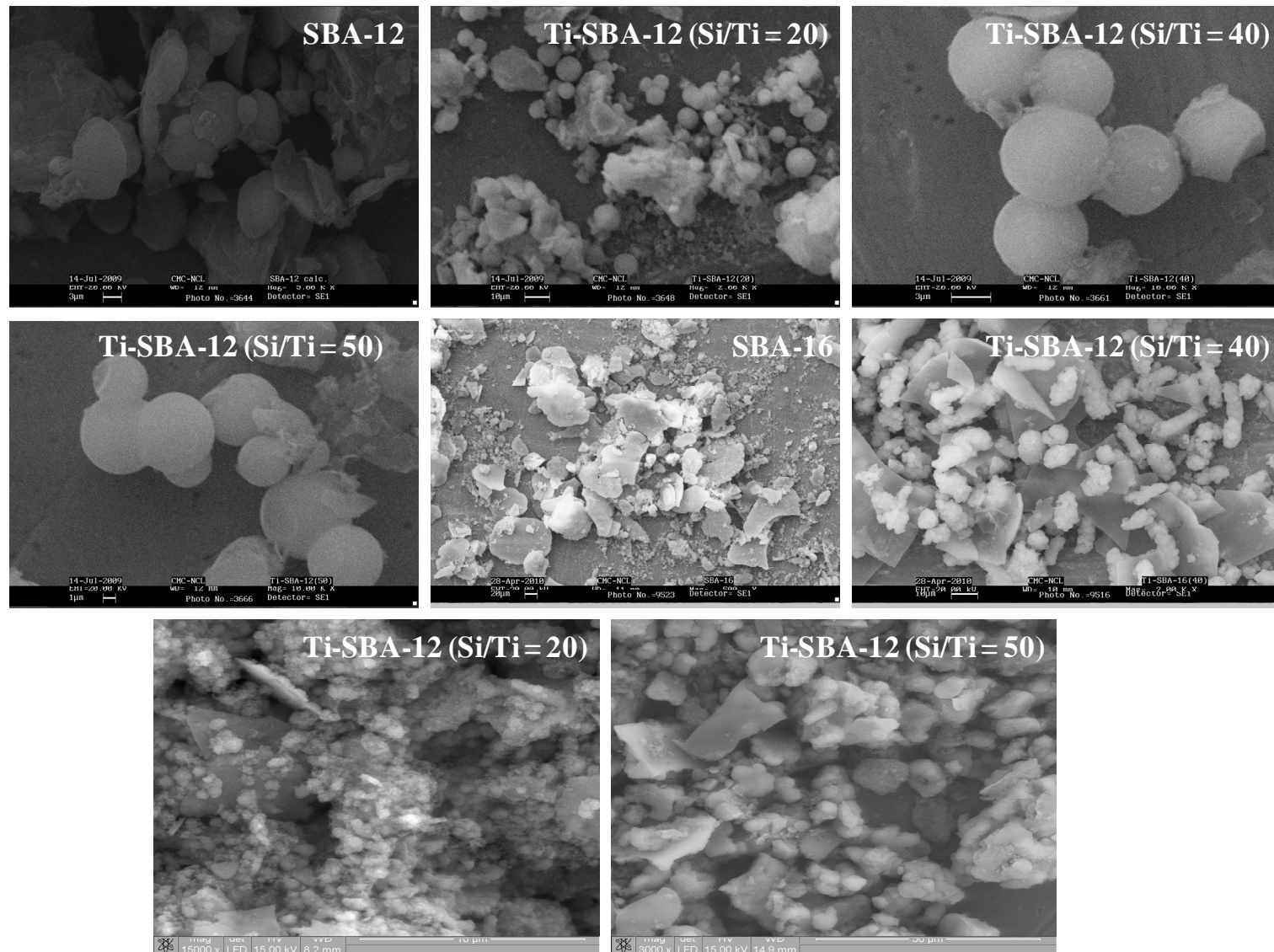


Fig. 2.10. SEM images of SBA-12, Ti-SBA-12, SBA-16 and Ti-SBA-16

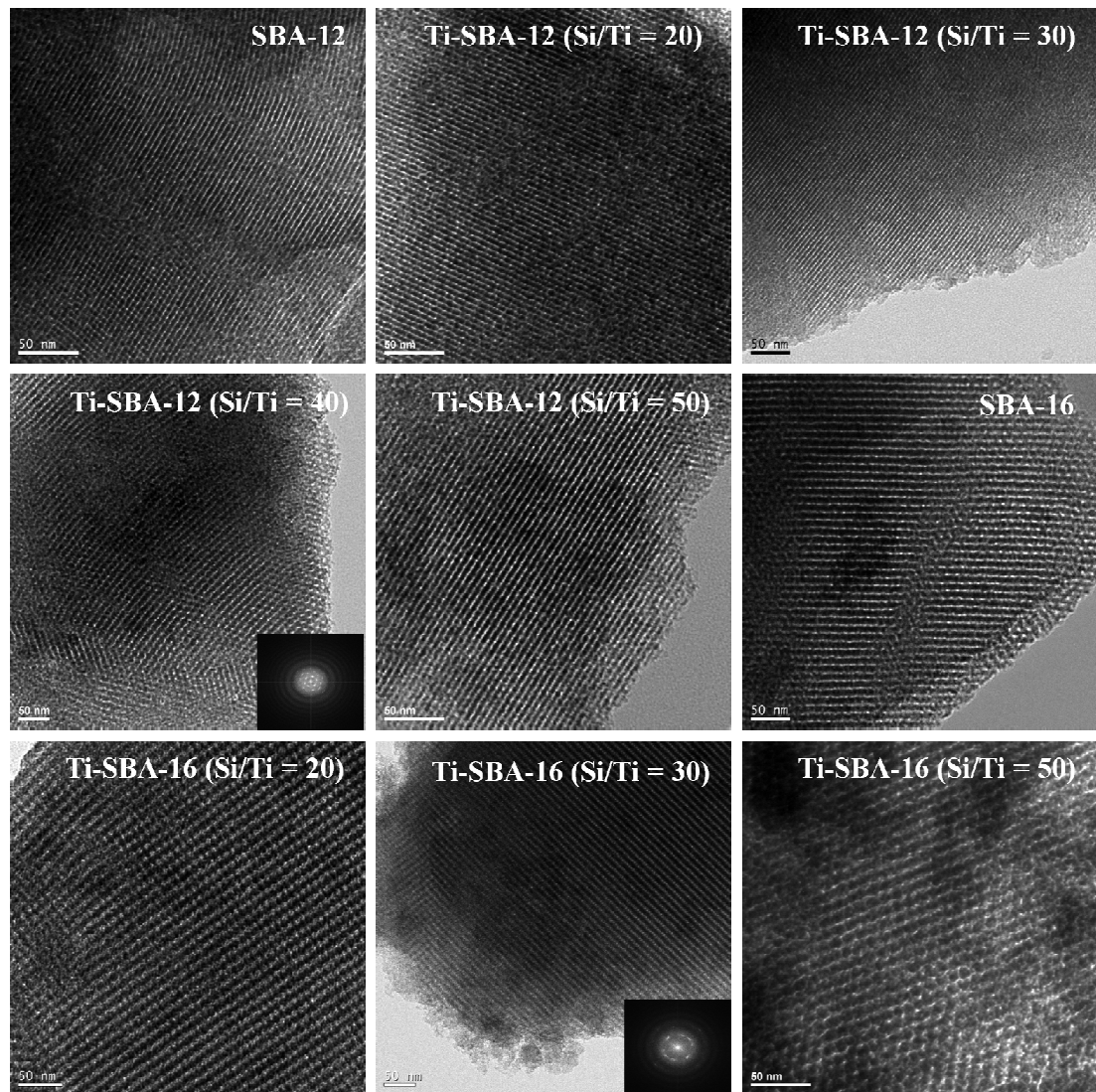


Fig. 2.11. HRTEM images of neat SBA-12, Ti-SBA-12 (Si/Ti = 20, 30, 40 and 50), neat SBA-16 and Ti-SBA-16 (Si/Ti = 20, 30 and 50) prepared in 2 M HCl

the charge transfer band is observed at 217 – 220 nm for $\text{Ti}(\text{OH})(\text{OSi})_3$ and at 210 nm for $\text{Ti}(\text{OSi})_4$ species. In Ti-SBA-12 samples with higher Ti content ($\text{Si}/\text{Ti} \leq 40$), an additional weak absorption band at 335 nm corresponding to the presence of agglomerated hexacoordinated titania phase was detected. This anatase phase was absent in Ti-SBA-16 prepared using 2 M HCl. These conclusions are in good agreement with those from the XRD analysis.

The DRUV-vis spectra were deconvoluted. Assuming same value of extinction coefficient for the absorption bands of both the framework and extraframework Ti ions, the percentage of framework substituted Ti species was

estimated (Table 2.5). Concentration of this Ti species (with UV bands at 210 and 217 nm) was found higher in Ti-SBA-16 than in Ti-SBA-12.

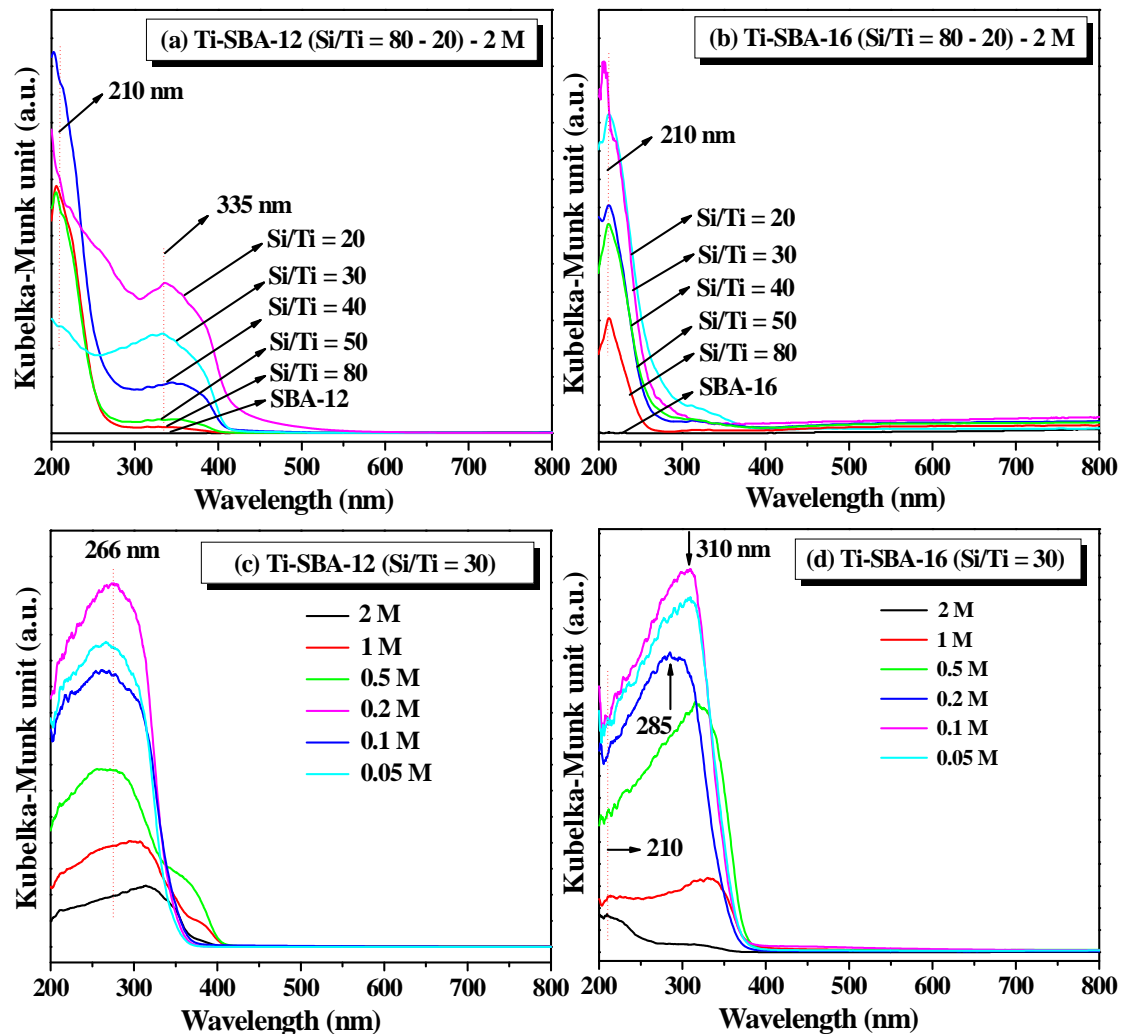


Fig. 2.12. Diffuse reflectance UV-visible spectra: (a) and (b) neat SBA-12, Ti-SBA-12, neat SBA-16 and Ti-SBA-16 prepared using 2 M HCl, (c) and (d) Ti-SBA-12 and Ti-SBA-16 (Si/Ti = 30) prepared using varying molar concentration of HCl (0.05 – 2 M)

Fig. 2.13 shows the DRUV-vis spectra of TS-1, Ti-MCM-41 and Ti-SBA-15 with Si/Ti molar ratio of 30. The absorption band at 210 nm for TS-1, 215 nm for Ti-MCM-41 and 220 nm for Ti-SBA-15 is due to isolated titanium ions in tetrahedral framework position [23]. The absorption band at 233 nm in Ti-MCM-41 is due to the pentacoordinated titanium and absorption band at 329 nm in Ti-SBA-15 is due to the hexacoordinated extra-framework titanium.

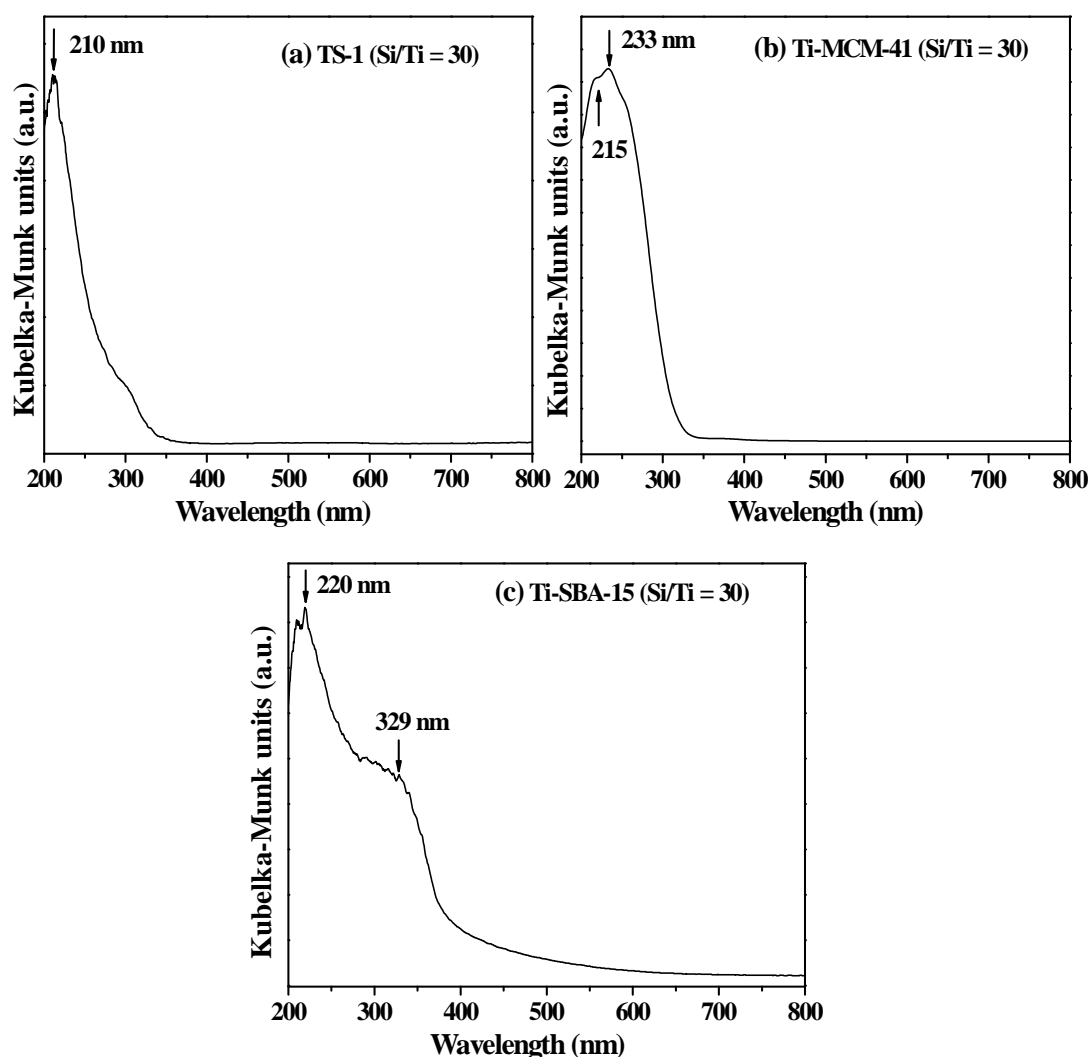


Fig. 2.13. Diffuse reflectance UV-visible spectra of (a) TS-1 (Si/Ti = 30), (b) Ti-MCM-41 (Si/Ti = 30) and (c) Ti-SBA-15 (Si/Ti = 30) prepared with 2 M HCl

2.4.2.7. Electron Paramagnetic Resonance Spectroscopy (EPR)

Fig. 2.14 shows the EPR spectra of TS-1, Ti-MCM-41, Ti-SBA-12 and Ti-SBA-16. Ti-SBA-12 and Ti-SBA-16 were EPR-silent consistent with the +4 oxidation state of titanium in these catalysts. Reactive oxygen species viz., hydroperoxo-, peroxy- and superoxo-Ti were generated on contact with aq. H_2O_2 (30%). While the former two types of oxo-Ti species are diamagnetic, the superoxo-titanium $\text{Ti}(\text{O}_2^{\cdot-})$ are paramagnetic and detectable by EPR spectroscopy [19]. These reactive oxo-Ti species are in equilibrium and one gets converted to the other as the temperature is varied [19]. The spectra of superoxo-titanium $\text{Ti}(\text{O}_2^{\cdot-})$ generated on Ti-SBA-12 and Ti-SBA-16 are shown in Fig. 2.14. From the spectral features, the presence of two types of $\text{Ti}(\text{O}_2^{\cdot-})$ species, A and B, arising from tetrapodal, and

tripodal titanium sites ($\text{Ti}(\text{OSi})_4$ and $\text{Ti}(\text{OH})(\text{OSi})_3$, respectively) can be discerned [16]. They are characterized by a rhombic EPR spectrum and differed in their g_{zz} value (species A: $g_{zz} = 2.038$, $g_{yy} = 2.008$ and $g_{xx} = 2.002$; species B: $g_{zz} = 2.024$, $g_{yy} = 2.008$ and $g_{xx} = 2.002$). From the spectral deconvolution, the relative concentration of the A-type species was found higher in the case of Ti-SBA-16 than in Ti-SBA-12. It may be noted that neat SBA-12, SBA-16 and bulk TiO_2 could not generate such reactive oxo-Ti species. Solvent influences the relative concentration of A and B species. It was found earlier, in the case of TS-1 samples that a direct correlation of oxidation activity and epoxide selectivity with the concentration of the A-type species exists [19–21]. Even in the present systems (Ti-SBA-12 and Ti-SBA-16), these differences in A and B species concentrations are expected to reflect on their catalytic activity performances (Chapter 3).

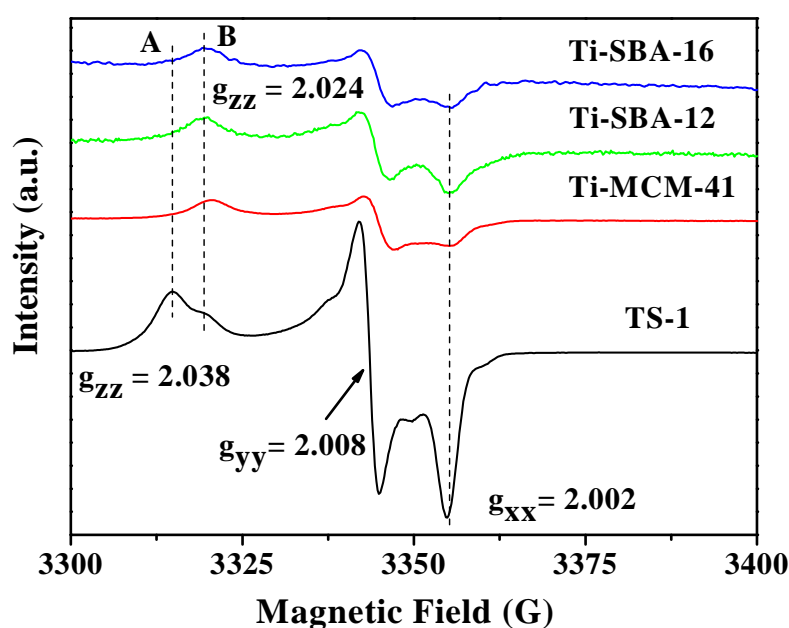


Fig. 2.14. EPR spectra of superoxo-Ti generated on TS-1, Ti-MCM-41, Ti-SBA-12 and Ti-SBA-16 with 30% aqueous H_2O_2

Fig. 2.15 shows the influence of HCl concentration (0.05 – 2 M) which was used in the synthesis of Ti-SBA-12 ($\text{Si}/\text{Ti} = 30$) on the intensity of superoxo-Ti signals. As discussed earlier that concentration of HCl affects the titanium content in titanosilicate materials (Table 2.2). Ti-SBA-12 (30) prepared using 0.1 M HCl concentration showed highest EPR signal intensity.

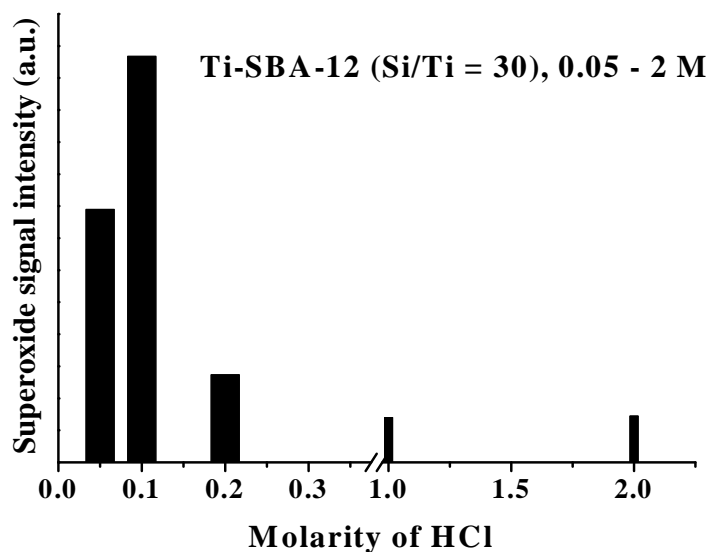


Fig. 2.15. Influence of concentration of HCl used in the synthesis on EPR signal intensity of superoxo-titanium $\text{Ti}(\text{O}_2^{\cdot-})$ species generated on Ti-SBA-12 (Si/Ti = 30) contacting with 30% H_2O_2

2.4.2.8. Fourier Transform Infrared Spectroscopy (FTIR)

Fig. 2.16 shows the FTIR spectra of pure silica materials (SBA-12, SBA-16) and different titanosilicates (Ti-SBA-12, Ti-SBA-16, TS-1, Ti-MCM-41 and Ti-SBA-15). Pure siliceous materials SBA-12 and SBA-16 showed vibrational bands at 961 cm^{-1} which can be assigned to Si-O-Si vibration. The intensity of these bands increased after Ti incorporation. All these titanosilicates showed vibrational bands at 961 cm^{-1} which can be assigned to the Si-O-Ti stretching vibration (Fig. 2.16) [5, 23, 24]. FTIR spectra of Ti-SBA-12 (Si/Ti = 30) prepared using varying molar concentration of HCl showed vibrational band at 961 cm^{-1} . The intensity of this band increased with decreasing molar concentration of HCl (1 – 0.05 M) (Fig. 2.16 (c)). TS-1, Ti-MCM-41 and Ti-SBA-15 with Si/Ti molar ratio of 30, also showed vibrational bands at 961 cm^{-1} (Fig. 2.16 (d)). The samples showed characteristic absorption bands at 458 , 805 and 1078 cm^{-1} assigned to $\delta(\text{Si-O-Si})$, $\nu_s(\text{Si-O-Si})$ and $\nu_{as}(\text{Si-O-Si})$, respectively. The absorption band at 1640 cm^{-1} is due to the deformation mode of adsorbed water. The absorption bands at 3449 and 3664 cm^{-1} were assigned to hydrogen-bonded surface silanol or titanol (Si/Ti-OH) groups [23, 25]. These FTIR spectra were recorded in atmospheric air at room temperature.

2.4.2.9. Fourier Transform Raman Spectroscopy (FT-Raman)

Fig. 2.17 shows the FT-Raman spectra of SBA-12, Ti-SBA-12, SBA-16 and Ti-SBA-16 materials. Pure mesoporous silica materials showed a FT-Raman band at 981 cm^{-1} assignable to Si-O-Si vibrations. The Ti-containing materials showed a new band at 955 cm^{-1} in the FT-Raman spectrum attributable to Si-O-Ti vibrations. TiO_2 anatase shows characteristic FT-Raman bands at 144, 397, 515 and 639 cm^{-1} [26]. From Figs. 2.17 (a) and (b), it can be noted that there are no bands due to bulk titania in the spectra of Ti-SBA-12 and Ti-SBA-16 prepared using 2 M HCl. However, Ti-SBA-12 (Si/Ti = 30) prepared using 0.05 M HCl showed an intense Raman band at 144 cm^{-1} which is due to the anatase titania. These FT-Raman spectral studies reveal that Ti in Ti-SBA-12 and Ti-SBA-16 is in an isolated, tetrahedral state.

2.4.2.10. ^{29}Si MAS NMR Spectroscopy

Fig. 2.18 shows ^{29}Si MAS NMR spectra of SBA-12, Ti-SBA-12, SBA-16 and Ti-SBA-16. Ti incorporation didn't alter the overall shape of the NMR spectrum. In general, ordered silica materials show ^{29}Si MAS NMR signals at around -91 , -101 , and -110 ppm which are attributed to three chemically and magnetically distinct tetracoordinated Si species, Q^2 , Q^3 and Q^4 with molecular formula of $\text{Si}(\text{OSi})_2(\text{OH})_2$, $\text{Si}(\text{OSi})_3(\text{OH})$ and $\text{Si}(\text{OSi})_4$, respectively [27, 28]. SBA-12 and Ti-SBA-12 showed these peaks at -91.8 , -100.9 and -110.6 ppm, respectively (Fig. 2.18). Interestingly, SBA-16 and Ti-SBA-16 showed only two of these peaks at -98.1 and -108.5 ppm attributable to Q^3 and Q^4 species, respectively (Fig. 2.18). Ti-SBA-16 showed downfield shift of Q^3 and Q^4 signals compared to Ti-SBA-12. This deshielding effect on the position of ^{29}Si MAS NMR signals is possibly due to differences in the structures of Ti-SBA-12 and Ti-SBA-16. In the past, experimental and theoretical studies on zeolites showed correlations between chemical shifts and Si-O-Si bond angles [29-31]. While the intensity of Q^3 signal is higher than that of Q^4 in SBA-12 materials, the reverse is the case for SBA-16 materials (Table 2.5). Silanol groups in Q^2 and Q^3 are the sites for water adsorption and render the silica surface to be hydrophilic. On the contrary, lower number of these groups (as is the case in SBA-16 and Ti-SBA-16) make the surface hydrophobic. The NMR plots were deconvoluted and the signal intensity ratio $\text{Q}^4/(\text{Q}^3 + \text{Q}^2)$, a representative of surface hydrophobicity, was determined (Table 2.5, Fig. 2.21(a)). It was found that Ti content has an effect on this ratio, with its highest value being at Si/Ti = 80.

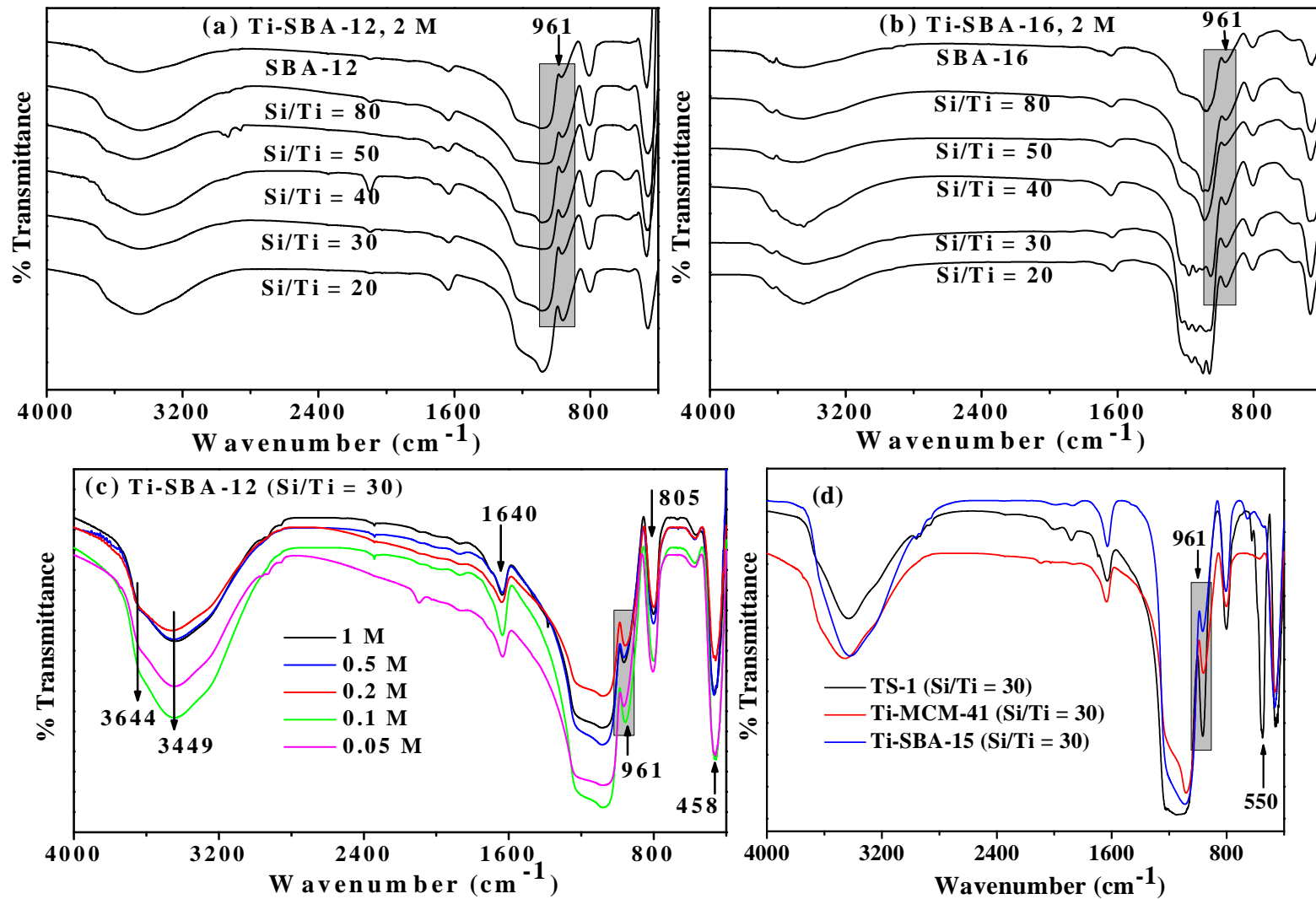


Fig. 2.16. FTIR spectra of (a) SBA-12 and Ti-SBA-12 (b) SBA-16 and Ti-SBA-16, prepared using 2 M HCl, (c) Ti-SBA-12 (Si/Ti = 30) prepared using 0.05 – 1 M HCl, and (d) TS-1, Ti-MCM-41 and Ti-SBA-15 with Si/Ti = 30

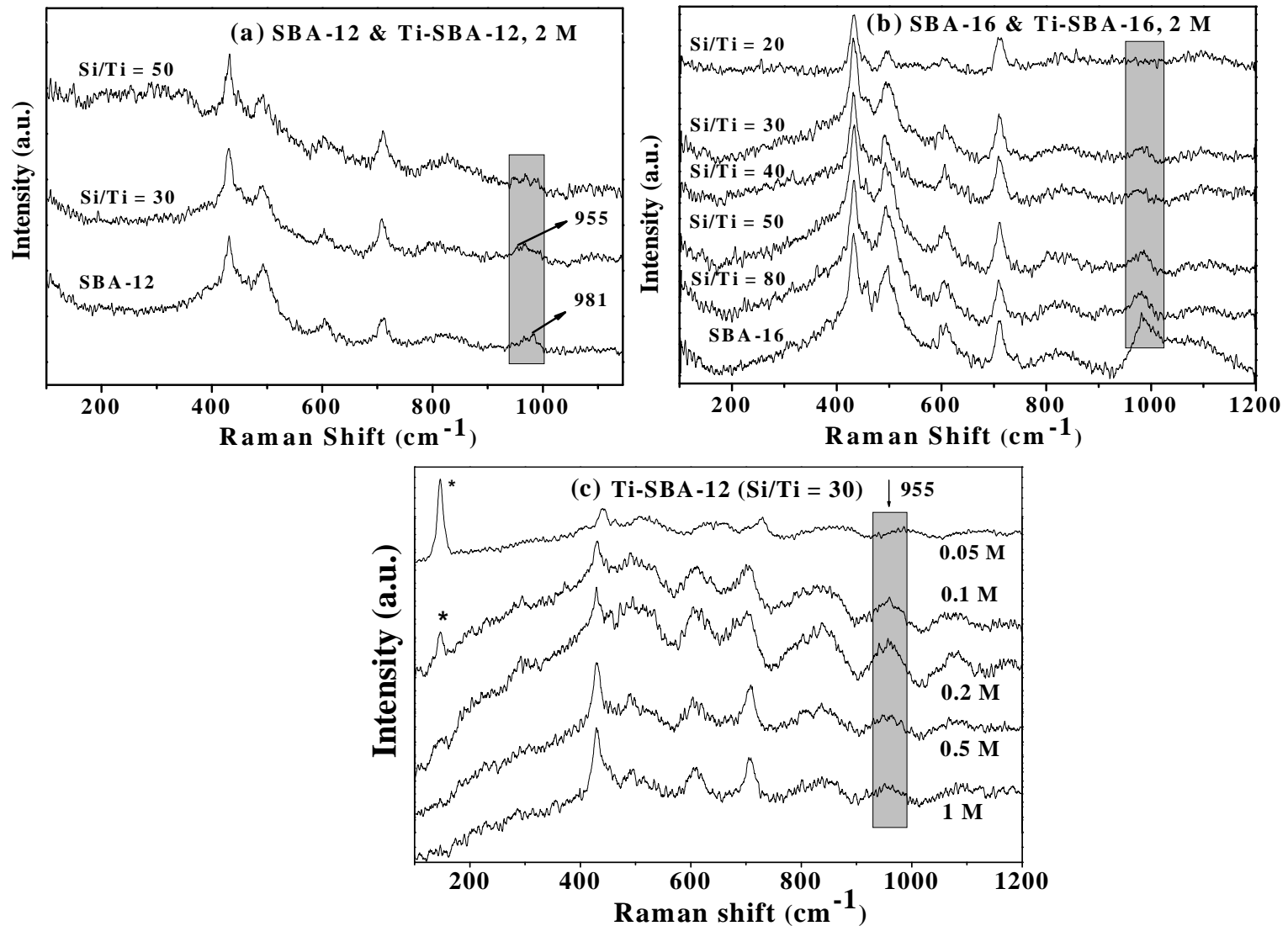


Fig. 2.17. FT-Raman spectra: (a) SBA-12 & Ti-SBA-12 (Si/Ti = 30, 50) prepared using 2 M HCl, (b) SBA-16 & Ti-SBA-16 (Si/Ti = 20 – 80) prepared using 2 M HCl, and (c) Ti-SBA-12 (Si/Ti = 30) prepared using 0.05 – 1 M HCl. * indicates bands due to TiO₂ (anatase)

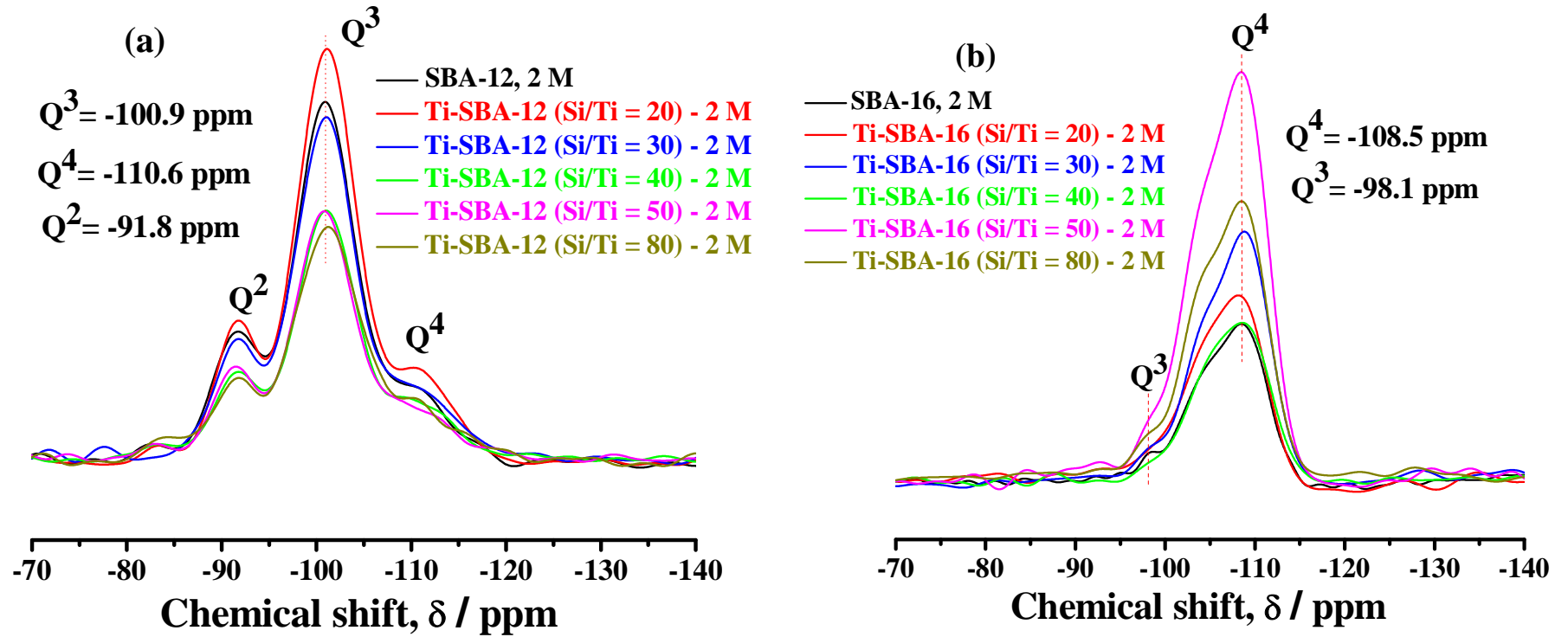


Fig. 2.18. ^{29}Si MAS NMR spectra of (a) Ti-SBA-12 and (b) Ti-SBA-16 with Si/Ti = 20 – 80 prepared using 2 M HCl

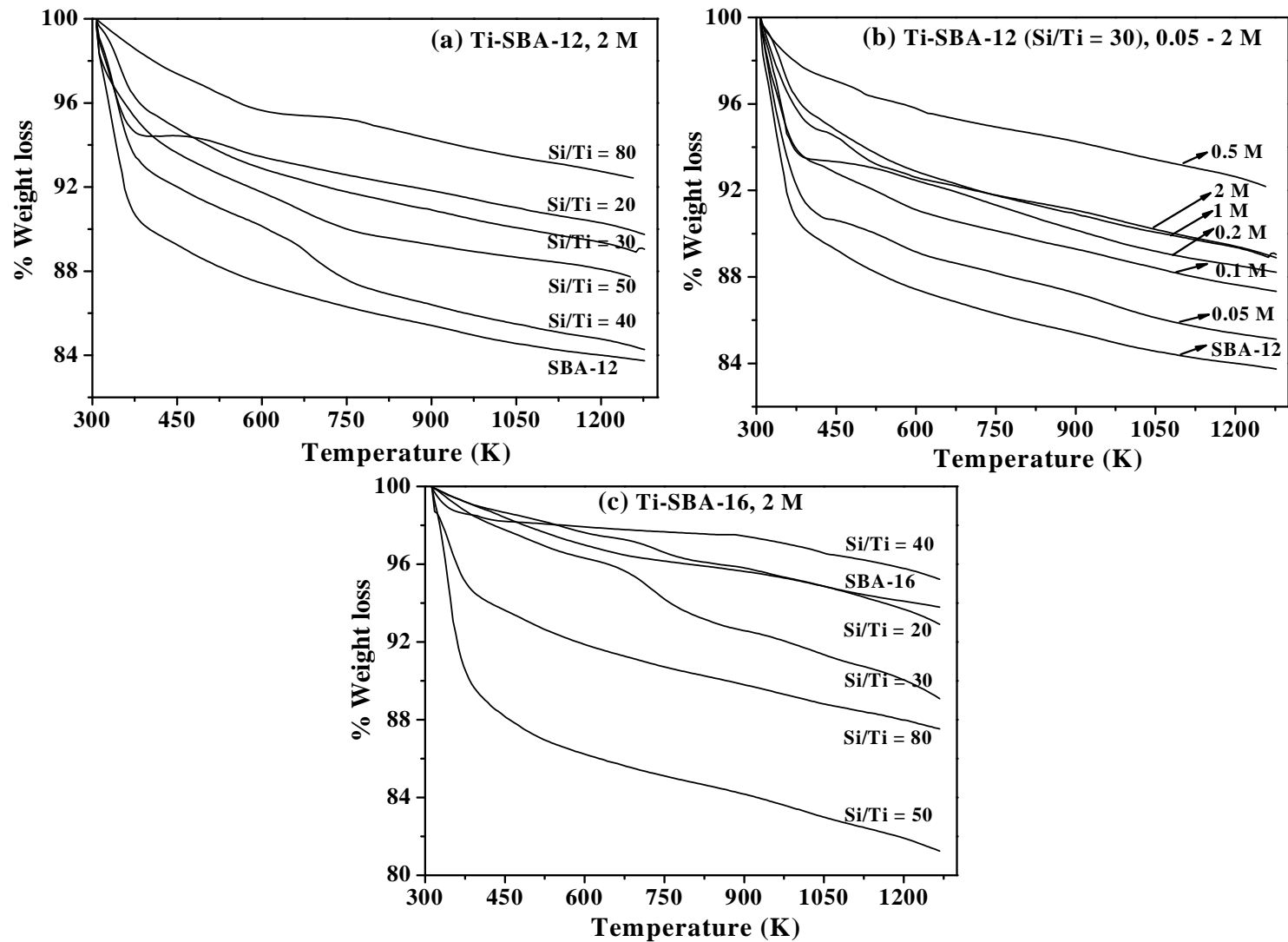


Fig. 2.19. TGA plots of (a) SBA-12 and Ti-SBA-12, (b) SBA-12 and Ti-SBA-12 (Si/Ti = 30) prepared in varying molar concentration of HCl (0.05 to 2 M), (c) SBA-16 & Ti-SBA-16, (a) and (c) were for Si/Ti = 20 – 80 prepared using 2 M HCl

These values for SBA-16 are one order of magnitude higher than that of SBA-12 (Table 2.5). In other words, SBA-16 materials are expected to be more hydrophobic than SBA-12 materials.

2.4.2.11. Thermal Analysis (TGA)

To rationalize the above fact, thermogravimetric analysis of all these materials was conducted (Fig. 2.19). Calcined samples were exposed to water vapour at ambient conditions and the weight loss due to adsorbed water was followed as a function of temperature (Table 2.5). This value monitored up to 523 K for different Ti-containing samples is plotted in Fig. 2.21 (b). It could be noted that Ti content has an effect on water adsorption capacity. The material with Si/Ti = 80 has the lowest capacity of water adsorption compared to materials with other ratios. SBA-12 adsorbed 6.6 times higher amount of water than SBA-16. The amount of water adsorbed correlated linearly with $Q^4/(Q^3 + Q^2)$ ratio (Fig. 2.21 (c)) indicating that the intensity ratio of ^{29}Si NMR signals is a good indicator to probe the surface properties of silica materials. Both these studies confirm that Ti-SBA-16 is relatively more hydrophobic than Ti-SBA-12. Water adsorption studies revealed that the materials prepared using lower concentrations of HCl are relatively less hydrophobic than those prepared using 2 M HCl (Fig. 2.20). This effect of HCl concentration is more marked in case of Ti-SBA-16 than in Ti-SBA-12.

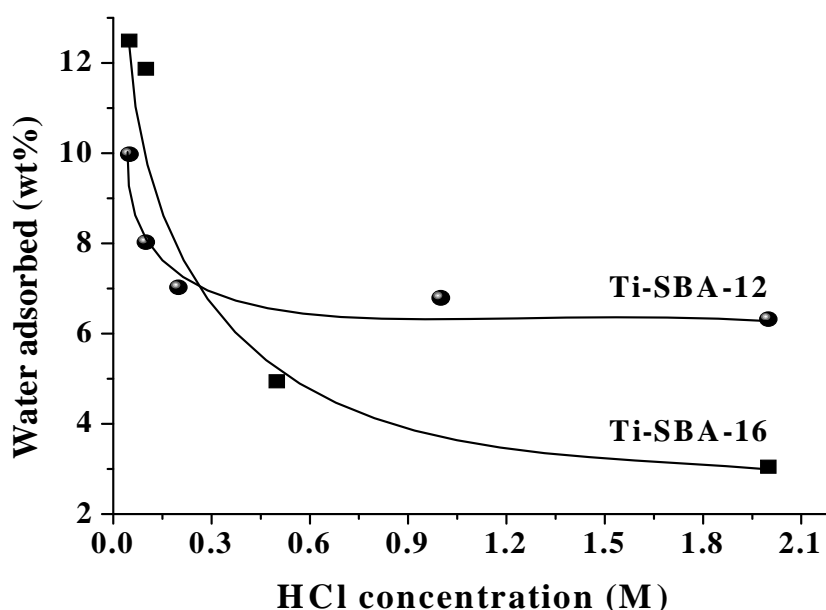


Fig. 2.20. Water adsorption capacity (up to 523 K from thermal analysis) of Ti-SBA-12 (Si/Ti = 30) and Ti-SBA-16 (Si/Ti = 30) prepared using 0.05 – 2 M HCl

Table 2.5. ^{29}Si MAS NMR, Thermogravimetry, NH_3 -TPD and DRUV-vis Spectral Data of Ti-SBA-12 and Ti-SBA-16

Catalyst (Si/Ti) input ratio	Concentration of HCl used in the synthesis (M)	% Intensity distribution of ^{29}Si MAS NMR signals				% Weight loss (TG) ^a		NH_3 -TPD (mmol/g)	Framework Ti species (% of total Ti present, DRUV-vis.)
		Q ²	Q ³	Q ⁴	Q ⁴ /Q ² + Q ³	< 523 K	523-1273 K		
SBA-12	2	16.14	78.16	5.70	0.06	11.70	4.50	0.03	-
Ti-SBA-12 (80)	2	26.15	43.32	30.53	0.30	3.48	4.05	0.08	95.2
Ti-SBA-12 (50)	2	18.76	57.10	24.14	0.32	7.33	4.87	0.10	89.3
Ti-SBA-12 (40)	2	19.20	62.10	18.70	0.23	8.90	6.77	0.12	81.3
Ti-SBA-12 (30)	2	18.56	62.28	19.16	0.24	6.26	4.74	0.12	79.4
Ti-SBA-12 (20)	2	16.34	67.87	15.79	0.18	5.84	4.34	0.13	78.7
Ti-SBA-12 (30)	1	-	-	-	-	6.74	4.20	0.10	79.4
Ti-SBA-12 (30)	0.5	-	-	-	-	3.67	4.08	0.10	82.6
Ti-SBA-12 (30)	0.2	-	-	-	-	6.90	4.80	0.11	82.6
Ti-SBA-12 (30)	0.1	-	-	-	-	7.97	4.56	0.14	86.2
Ti-SBA-12 (30)	0.05	-	-	-	-	9.93	4.85	0.08	86.2
SBA-16	2	0	24.10	75.90	3.15	1.77	4.44	0.04	-
Ti-SBA-16 (80)	2	0	20.30	79.70	3.93	7.28	5.20	0.09	100
Ti-SBA-16 (50)	2	0	23.36	76.64	3.38	6.50	4.60	0.09	100
Ti-SBA-16 (40)	2	0	17.15	82.85	4.83	6.30	9.46	0.10	100
Ti-SBA-16 (30)	2	0	22.70	77.30	3.40	3.0	7.82	0.11	97.1
Ti-SBA-16 (20)	2	0	25.52	74.48	2.92	2.35	4.72	0.12	88.5
Ti-SBA-16 (30)	1	-	-	-	-	12.33	8.51	0.14	75.2
Ti-SBA-16 (30)	0.5	-	-	-	-	5.0	4.83	0.13	67.6
Ti-SBA-16 (30)	0.2	-	-	-	-	14.14	5.52	0.18	66.7
Ti-SBA-16 (30)	0.1	-	-	-	-	11.86	7.49	0.16	68.5
Ti-SBA-16 (30)	0.05	-	-	-	-	12.56	6.16	0.15	68.5

^aWeight loss below 523 K is due to loss of adsorbed water and between 523 and 1273 K is due to condensation of silanol groups

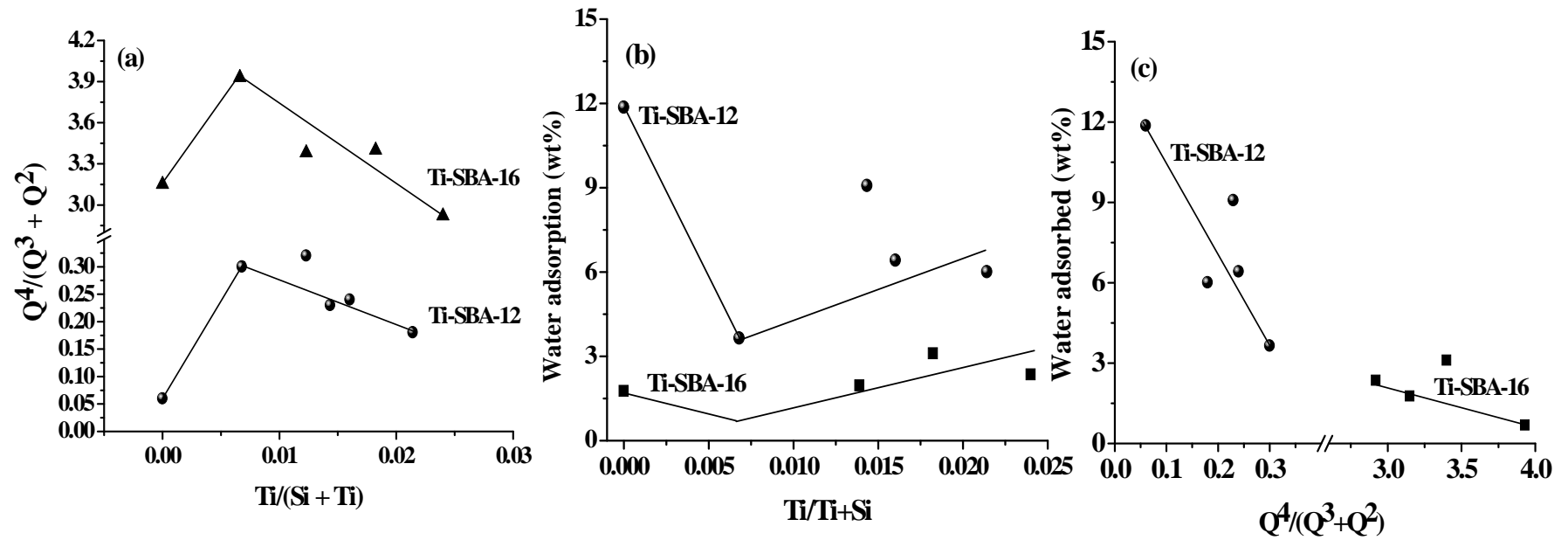


Fig. 2.21. Variation of (a) intensity ratio of $Q^4/(Q^3+Q^2)$ (from ^{29}Si MAS NMR), (b) water adsorption capacity (up to 523 K from thermal analysis) as a function of Ti-content in Ti-SBA-12 and Ti-SBA-16 prepared using 2 M HCl, and (c) correlation of water adsorption capacity with $Q^4/(Q^3+Q^2)$ in these titanosilicates

2.4.2.12. Acidic Properties

The type and density of acid sites were determined by NH_3 -TPD and DRIFT spectroscopy of adsorbed pyridine. Two desorption peaks with maxima at 461 and 627 K for Ti-SBA-12 and 408 and 567 K for Ti-SBA-16 were observed in NH_3 -TPD studies (Fig. 2.22). While the former is attributed to ammonia desorbed from weaker acid centers like silanols/titanols, the latter is attributed to that desorbed from relatively stronger acid centers like isolated, framework-substituted, tetrahedral Ti^{4+} ions. Intensity of the former peak is higher in Ti-SBA-12 than in Ti-SBA-16. This is because Ti-SBA-12 contained larger number of silanol groups (higher intensity of Q^2 and Q^3 signals, Fig. 2.18) than Ti-SBA-16. The position of these desorption peaks provides an indication of the strength of acid sites. These peaks occurring at higher temperatures in the case of Ti-SBA-12 than in Ti-SBA-16 suggest that the relative strength of acid sites in the former catalyst is higher than those in the latter. Difference in local framework structure is the possible cause for difference in acidity of these titanosilicates.

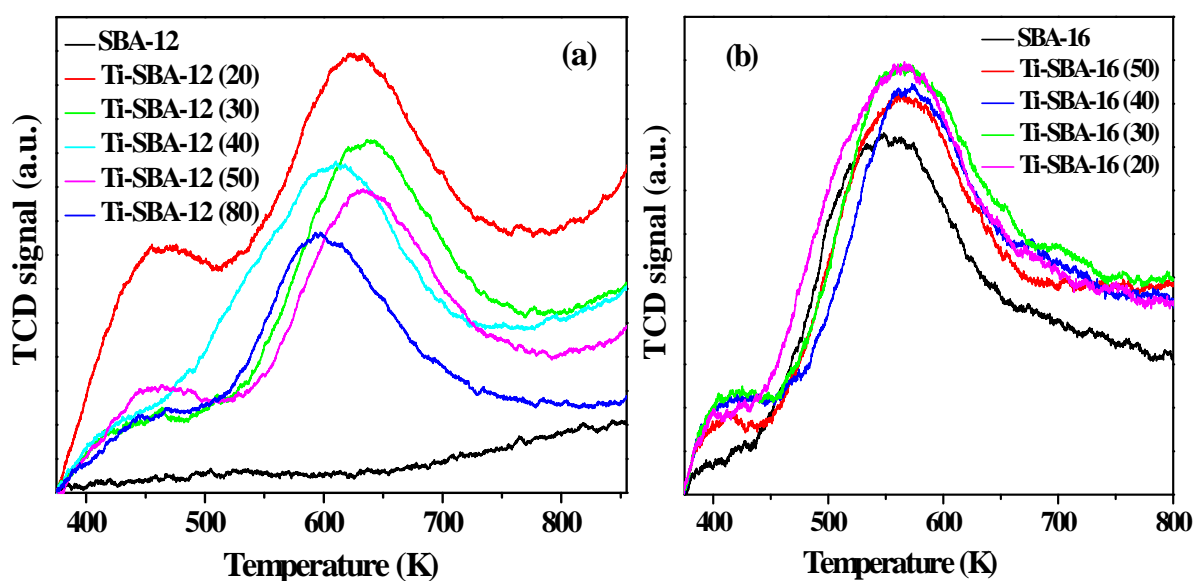


Fig. 2.22. NH_3 -TPD plots of (a) Ti-SBA-12 and (b) Ti-SBA-16 prepared using 2 M HCl

DRIFT spectroscopy of adsorbed pyridine revealed IR peaks at 1621, 1594, 1580, 1488, 1455 and 1445 cm^{-1} (Fig. 2.23 and Fig. 2.24). In this case, the measurements were done under nitrogen atmosphere. While the peaks at 1594 and 1445 cm^{-1} are attributed to H-bonded pyridine, those at 1580 and 1488 cm^{-1} are attributed to pyridine coordinated to weak

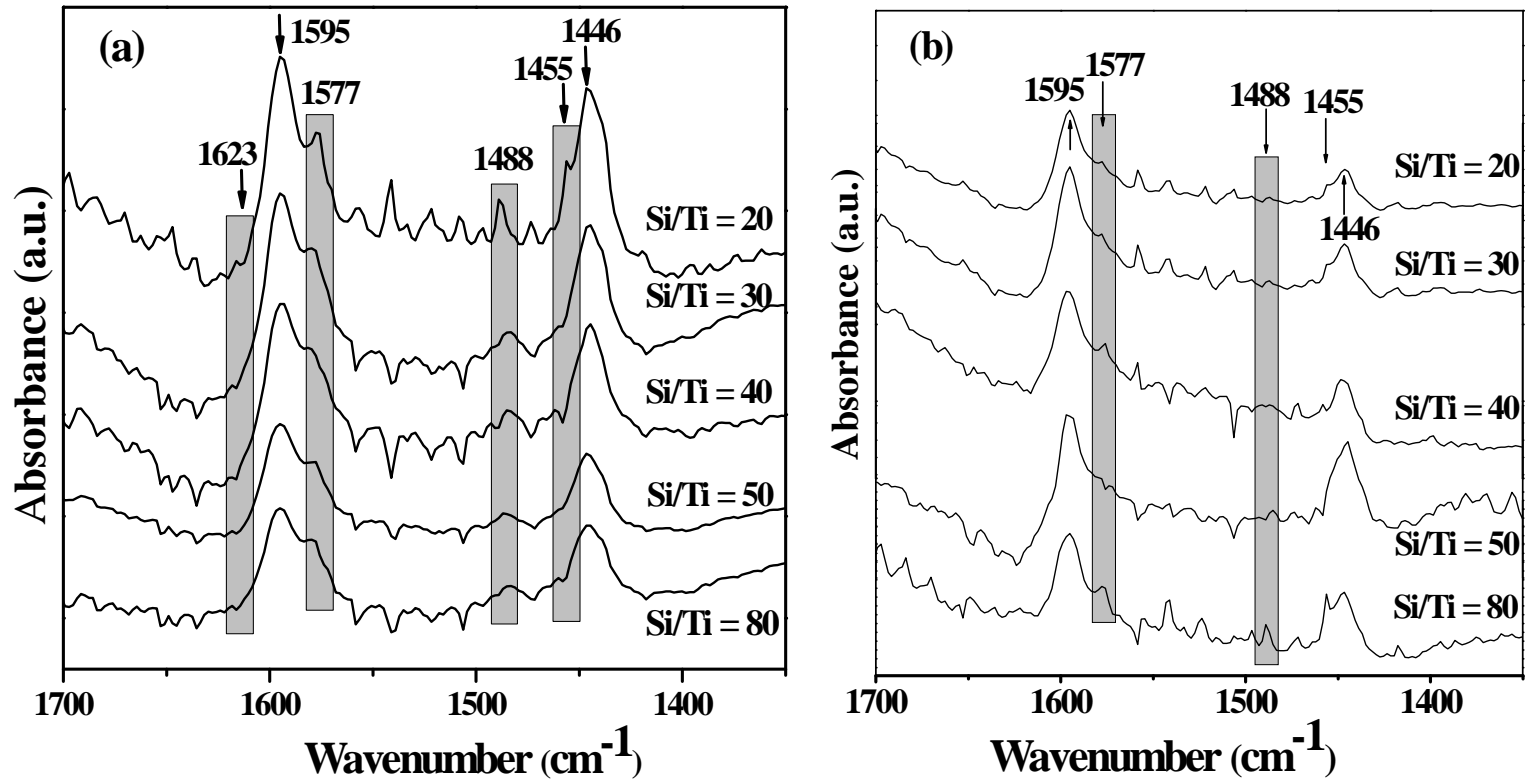


Fig. 2.23. DRIFT spectra of adsorbed pyridine on (a) Ti-SBA-12 and (b) Ti-SBA-16 with varying Si/Ti molar ratio prepared using 2 M HCl

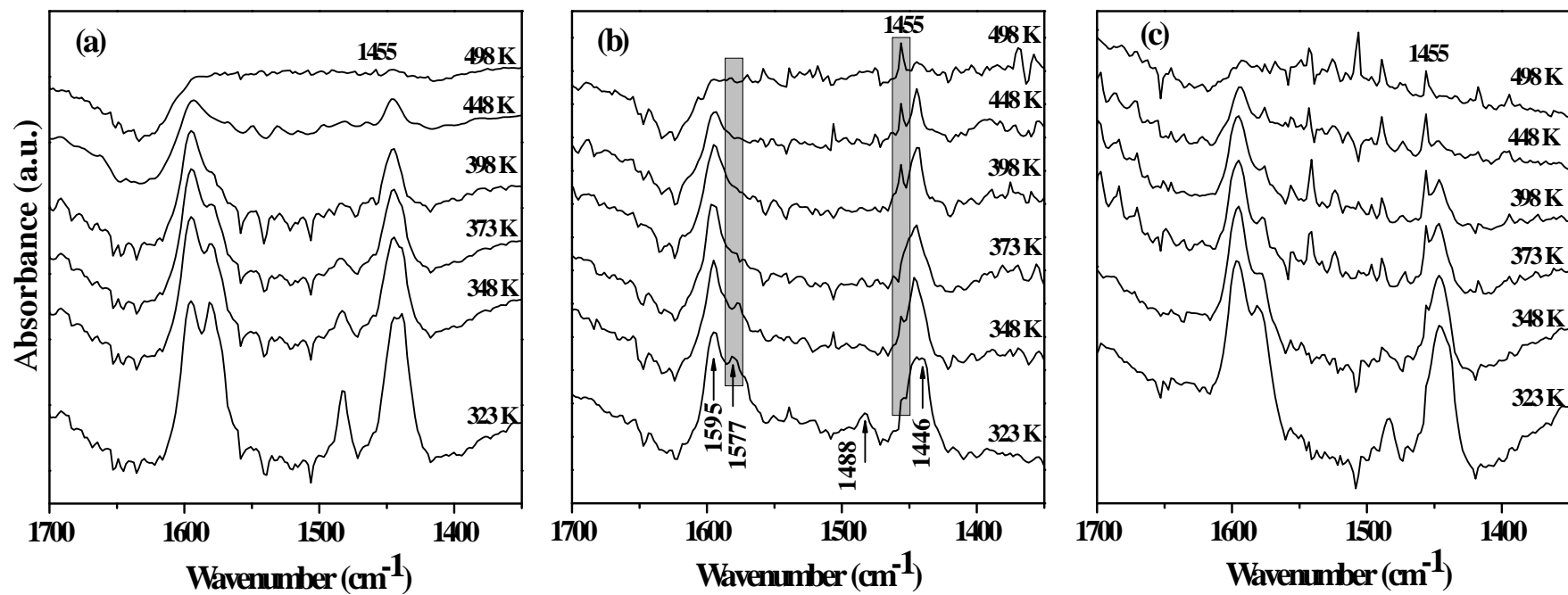


Fig. 2.24. DRIFT spectra of adsorbed pyridine at different temperatures: (a) Ti-SBA-12 (Si/Ti = 30), (b) Ti-SBA-16 (Si/Ti = 50), and (c) Ti-SBA-16 (Si/Ti = 80) prepared using 2 M HCl

Lewis acid sites [32-34]. The weak peaks at 1623 and 1455 cm^{-1} (appeared as shoulders) are corresponded to strong Lewis acid sites [32-34]. Brönsted acid sites (peaks at 1636 and 1546 cm^{-1}) were absent in these catalysts. At 498 K, the peaks corresponding to H-bonded pyridine and weak Lewis acid sites had almost disappeared and those associated with strong Lewis acid sites became prominent (Fig. 2.24).

2.5. Synthesis and Characterization of Manganese-containing SBA-12 and SBA-16 Molecular Sieves

2.5.1. Synthesis

Manganese-containing SBA-12 and SBA-16 silica molecular sieves were prepared by direct hydrothermal synthesis method.

2.5.1.1. Mn-SBA-12

In a typical preparation of Mn-SBA-12 (Si/Mn = 20), 8 g of Brij76 was dissolved in 40 g of distilled water and 160 g of 0.1 M HCl. The mixture was stirred at 313 K for 2 h and 17.6 g (TEOS, Aldrich 98%) of TEOS was added to it over 30 min. Then, 1.07 g of manganese nitrate ($\text{Mn}(\text{NO}_3)_2 \cdot 4\text{H}_2\text{O}$) was dissolved in 10 mL of water and added slowly. The stirring was continued for 20 h. The gel formed was transferred into a Teflon-lined stainless steel autoclave and heated at 373 K for 24 h. The solid formed was recovered by filtration, washed thoroughly with distilled water (2 - 3 L), dried at 373 K for 12 h, and calcined in the air at 823 K for 8 h.

2.5.1.2. Mn-SBA-16

In a typical synthesis of Mn-SBA-16 (Si/Mn = 30), 7.4 g of block-copolymer Pluronic F127 ($\text{EO}_{106}\text{PO}_{70}\text{EO}_{106}$) was dissolved in 384.3 g of 2 M HCl solution at 313 K. After 2 h of stirring, 28.34 g of tetraethyl orthosilicate (TEOS) was added drop wise over 30 min and stirring continued for 4 h. Then, 1.15 g of $\text{Mn}(\text{NO}_3)_2 \cdot 4\text{H}_2\text{O}$ was dissolved in 10 mL of water and added slowly. The stirring was continued for another 20 h. The gel formed was transferred into a Teflon-lined stainless steel autoclave. It was heated at 353 K for 48 h. The solid formed was separated by filtration, washed with distilled water (2 - 3 L), dried at 373 K overnight and calcined in air at 823 K for 8 h. Mn-SBA-16 with Si/Mn input ratio of

50, 40 and 20 were prepared in a similar manner taking appropriate amounts of the Si and Mn sources, respectively (see [Appendix at the end of this chapter](#)).

2.5.2. Characterization

2.5.2.1. Chemical Composition

Mn content in Mn-SBA-12 (Si/Mn = 20) and Mn-SBA-16 (Si/Mn = 20 – 80) was determined by ICP-OES analysis ([Table 2.6](#)). ICP-OES analysis revealed that only 6.3 to 14.8 mol% of input Mn was incorporated in the final composition of Mn-SBA-12 and Mn-SBA-16. Mn-SBA-16 (Si/Mn = 80) showed highest amount of manganese incorporation (about 14.8 mol%) in the structure ([Table 2.6](#)).

2.5.2.2. X-ray Powder Diffraction (XRD)

[Fig. 2.25](#) shows the low and wide-angle XRD patterns of manganese silicate materials. Mn-SBA-12 (Si/Mn = 20) showed an intense peak at 1.67° due to (002) reflection and two less resolved peaks at 2.67° and 3.0° attributed to (112) and (300) reflections, respectively [[Fig. 2.25 \(a\)](#)]. A weak shoulder to the main peak corresponding to (100) reflection was also observed for Mn-SBA-12 (Si/Mn = 20). These XRD patterns of Mn-SBA-12 can be indexed to an ordered, three-dimensional, hexagonal mesoporous structure with a space group of $p6_3/mmc$ [1]. Mn-SBA-16 (Si/Mn = 20 – 80) in the small-angle region ($0.5 - 5^\circ$) showed an intense main peak at 0.92° (for Mn-SBA-16 with Si/Mn ratio = 20) corresponding to (110) reflection and two less-resolved, weak peaks at 1.28° and 1.72° attributable to (200) and (211) reflections, respectively [[Fig. 2.25 \(b\)](#)]. These diffraction patterns of Mn-SBA-16 can be indexed to an ordered, three-dimensional, mesoporous, cubic structure with space group of $Im\bar{3}m$ [1]. The unit cell parameters of these manganese silicates (Mn-SBA-12 and Mn-SBA-16) are listed in [Table 2.6](#).

Wide-angle XRD pattern of Mn-SBA-12 [[Fig. 2.25\(a\)](#), inset] and Mn-SBA-16 [[Fig. 2.25 \(c\)](#)] showed no peaks due to bulk manganese oxide. This indicates that all the manganese are isolated.

2.5.2.3. N₂-Physisorption

N₂ physisorption isotherms of Mn-SBA-12 and Mn-SBA-16 and their pore size distribution curves (inset) are shown in the [Fig. 2.26](#). Mn-SBA-16 shows typical type-IV N₂ adsorption–desorption isotherms with a broad H₂ hysteresis loop

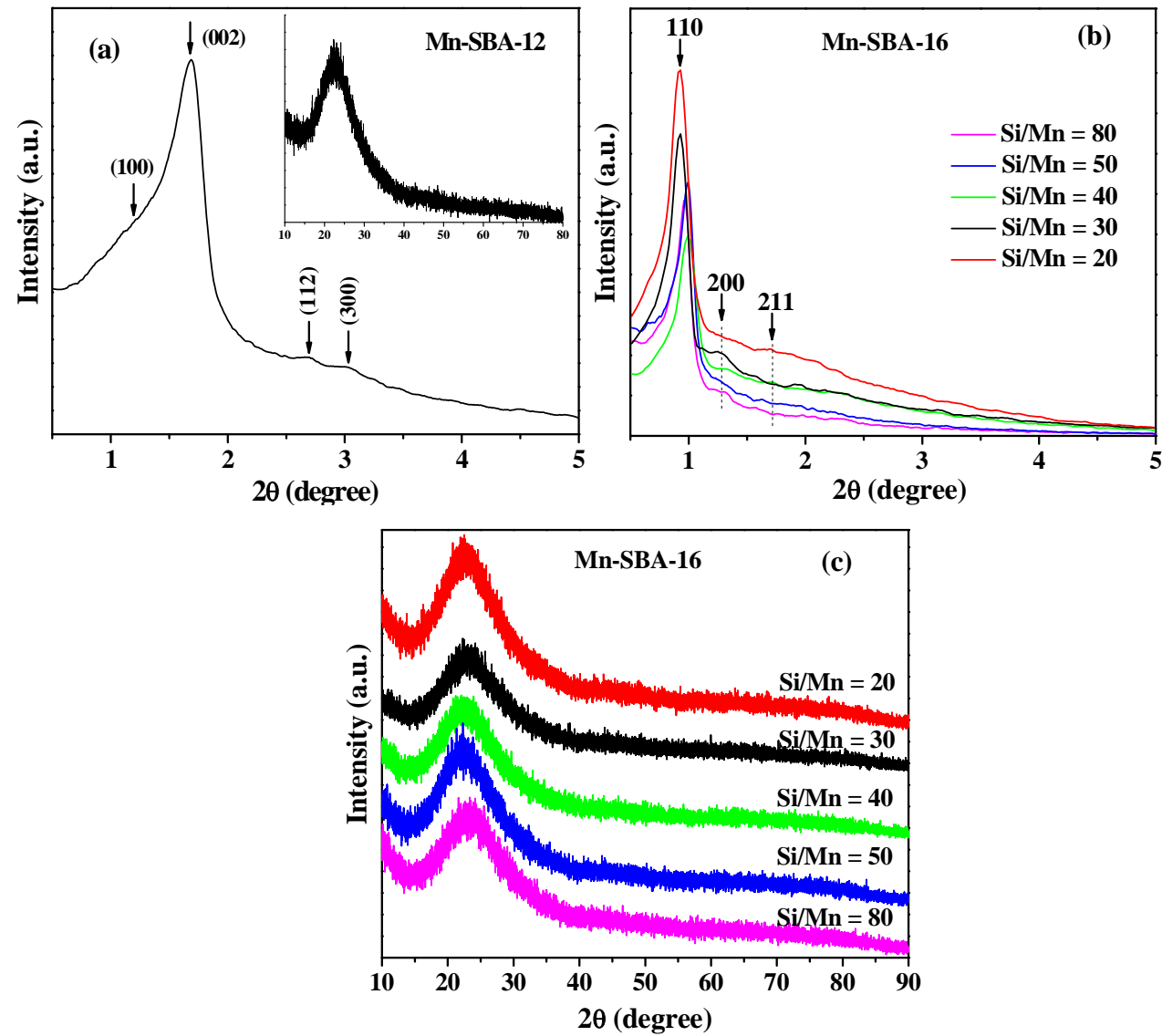


Fig. 2.25. Low and wide-angle XRD patterns: (a) Mn-SBA-12 (Si/Mn = 20), (b) & (c) Mn-SBA-16 with different Si/Mn molar ratios

which is characterized by a steep desorption branch and a smooth increasing adsorption branch. This has been corresponded to the existence of ink-bottle-type pores [15-19]. This H₂ type hysteresis loop reveals that Mn-SBA-16 has cubic cage-like interconnected mesopore structure. N₂ physisorption isotherms of Mn-SBA-12 showed typical type-IV isotherms with H₁ type hysteresis loop which is characteristics of hexagonal mesoporous materials (Fig. 2.26) [1, 18]. The textural properties of these materials are listed in Table 2.26. Mn-SBA-16 (Si/Mn = 20 – 80) has specific surface area (S_{BET}) in the range of 569 – 941 m²/g while Mn-SBA-12 (Si/Mn = 20) has a specific BET surface area of 969 m²/g (Table 2.6). All these materials showed a narrow BJH pore size distribution with an average pore size of 2.7 to 3.4 nm (Table 2.6). The wall thickness of these materials is varied from 7.4 to 8.7 nm. In general, S_{BET} decreased with Mn incorporation.

2.5.2.4. Scanning Electron Microscopy (SEM)

Fig. 2.27 shows SEM images of Mn-SBA-12 and Mn-SBA-16. Mn-SBA-12 showed triangular crystal shaped particle morphology but all the particles are not uniform in shape; particles size varied between 4 and 15 μm. Mn-SBA-16 (Si/Mn = 30 and 80) formed as planar sheets and worm-like morphologies with particle size in the range of 7 – 15 μm (Fig. 2.27). Mn-SBA-16 (Si/Mn = 50) has planar sheets and spherical shaped particles with a dimension of 10 – 20 μm.

2.5.2.5. High Resolution Transmission Electron Microscopy (HRTEM)

Fig. 2.28 shows HRTEM images of Mn-SBA-12 and Mn-SBA-16 with Si/Mn = 20. HRTEM images confirmed the long-range, three-dimensional, mesoporous ordering in these materials. While Mn-SBA-12 has hexagonally arranged pores, Mn-SBA-16 has cubic cage-like interconnected pore arrangement. The inset electron diffraction patterns show that the materials are highly crystalline in nature. No separate bulk manganese oxide particles were detected in the HRTEM images.

2.5.2.6. Diffuse Reflectance Ultraviolet Visible Spectroscopy (DRUV-vis)

The diffuse reflectance UV-vis spectra of Mn-SBA-12 and Mn-SBA-16 are shown in Fig. 2.29. The Mn-silicates showed four overlapping absorption bands at around 212 or 215, 270, 345 and 500 nm, respectively. The absorption bands at 212 or 215 and 270 nm could be assigned to O²⁻ → Mn³⁺ charge-transfer transitions for

Table 2.6. Composition, Structure and Textural Properties of Mn-SBA-12 and Mn-SBA-16

Catalyst	Molar conc. of HCl (M)	Si/Mn molar ratio		Structural data (XRD) ^a						Textural properties (N ₂ Physisorption)			
		Input	Output	Input	Inter planar spacing (nm)			Unit cell parameter (nm)		S _{BET} (m ² /g)	Pore volume (cc/g)	Average pore diameter (nm)	Wall thickness (nm) ^b
		(ICP-AES)	incorporated Mn (mol%)	d ₁₀₀	d ₀₀₂	d ₁₁₀	a	c					
Mn-SBA-12 (20)	0.1	20	230	9.1	7.0	5.3	-	8.0	10.6	969	0.78	3.2	7.4
Mn-SBA-16 (80)	2	80	548	14.8	-	-	9.0	12.8	-	941	0.75	3.2	7.9
Mn-SBA-16 (50)	2	50	736	6.9	-	-	8.9	12.6	-	627	0.81	3.4	7.5
Mn-SBA-16 (40)	2	40	649	6.3	-	-	8.9	12.6	-	569	0.39	2.7	8.2
Mn-SBA-16 (30)	2	30	348	8.9	-	-	9.5	13.4	-	585	0.45	3.1	8.5
Mn-SBA-16 (20)	2	20	278	7.5	-	-	9.6	13.6	-	625	0.48	3.1	8.7

^aMn-SBA-12 is defined by a three-dimensional hexagonal system with space group of $p6_3/mmc$. Mn-SBA-16 is described by a three-dimensional cubic system with space group of $Im\bar{3}m$. Unit cell parameter $a = 2d_{100}/\sqrt{3}$, $c = 2d_{002}$ for Mn-SBA-12 and $a = \sqrt{2} \times d_{110}$ for Mn-SBA-16. ^bWall thickness = $c - \text{average pore diameter}$ (for Mn-SBA-12) and $\sqrt{3}/2 a - \text{average pore diameter}$ (for Mn-SBA-16)

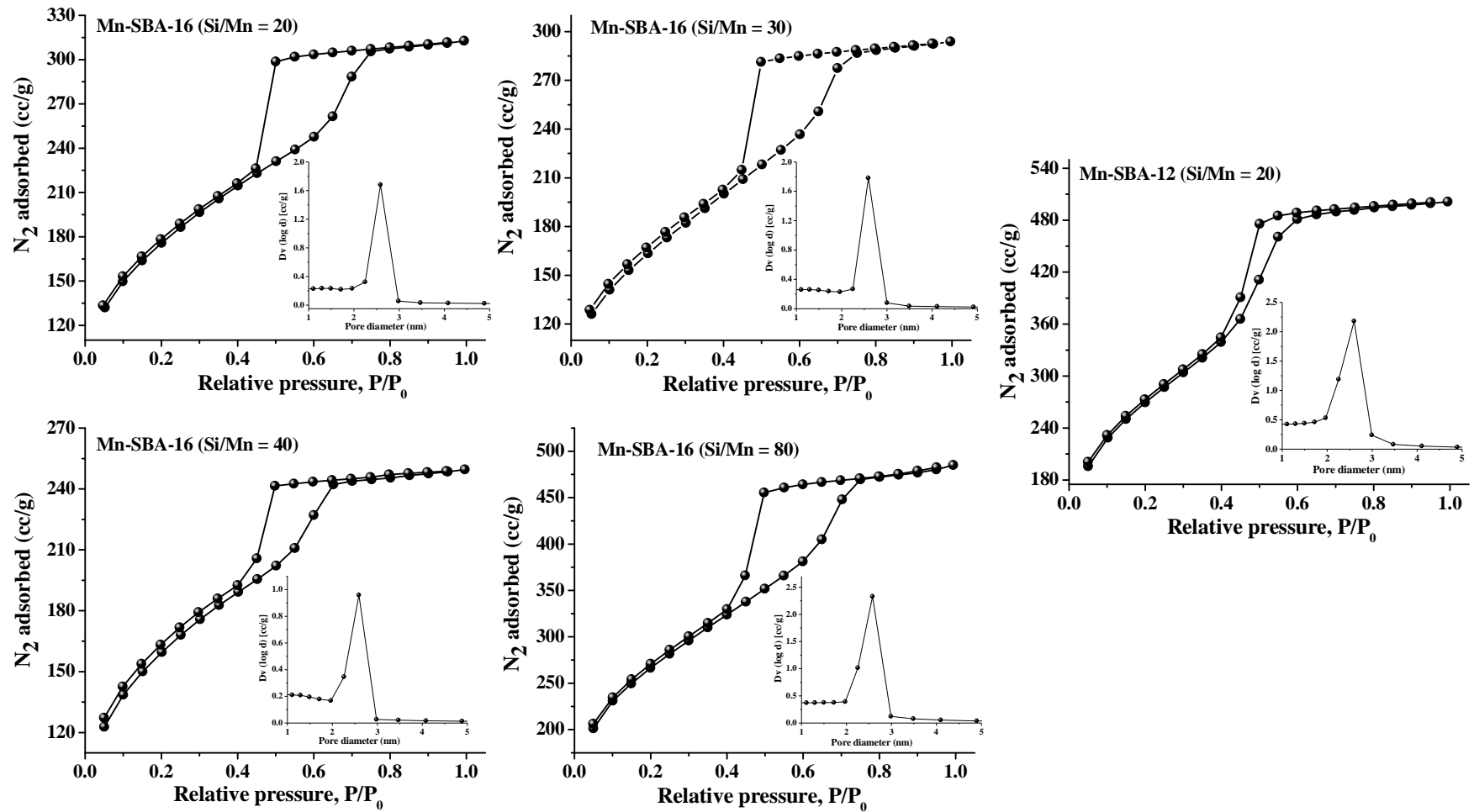


Fig. 2.26. Nitrogen adsorption-desorption isotherms of Mn-SBA-16 (Si/Mn = 20 – 80) and Mn-SBA-12 (Si/Mn = 20) and their pore size distribution curves (inset)

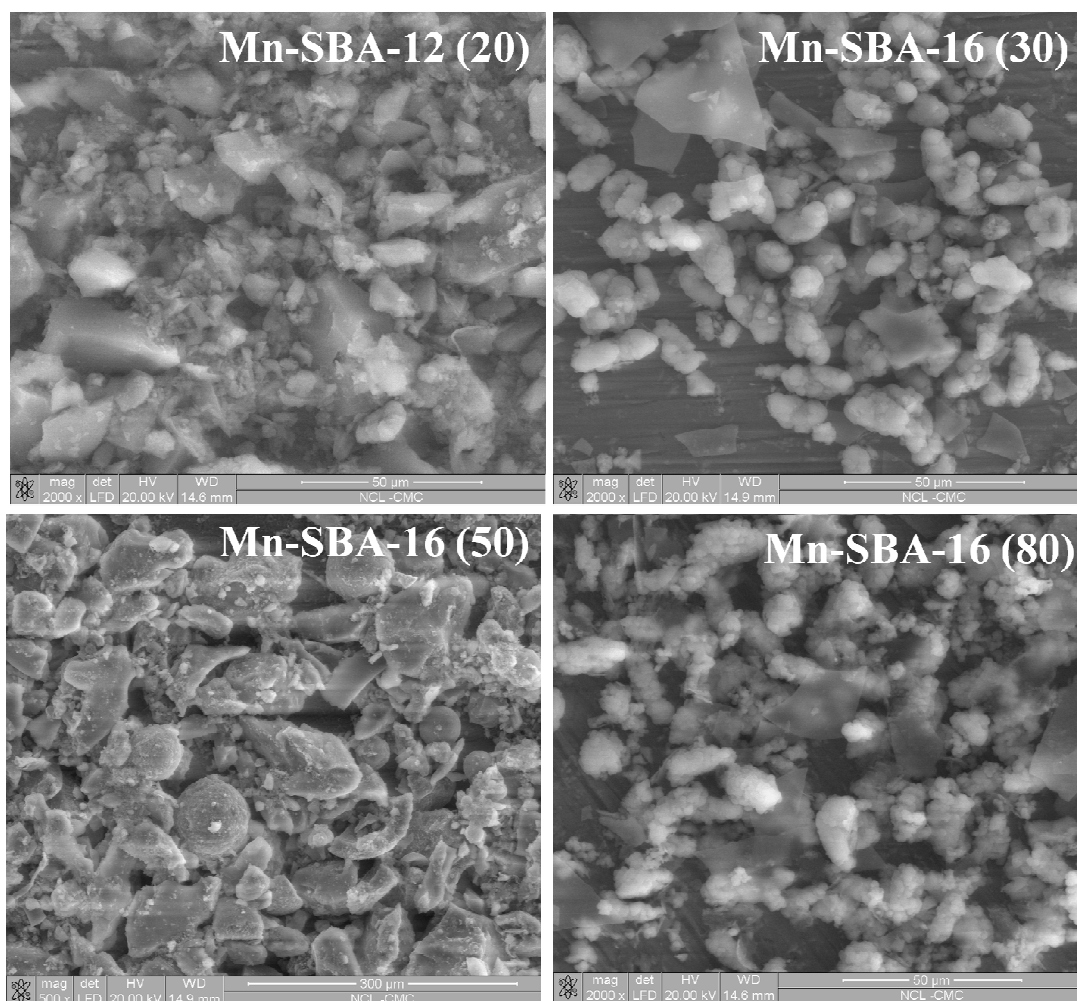


Fig. 2.27. SEM images of Mn-SBA-12 (Si/Mn = 20) and Mn-SBA-16 with Si/Mn molar ratio of 30, 50 and 80

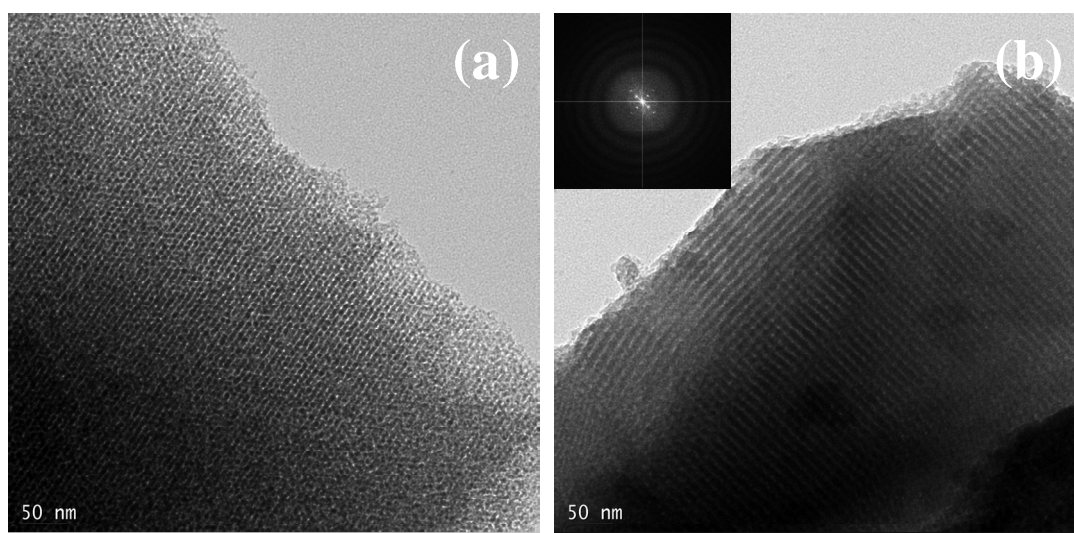


Fig. 2.28. HRTEM images of (a) Mn-SBA-12 (Si/Mn = 20) and (b) Mn-SBA-16 (Si/Mn = 20)

Mn ions with tetra-coordinated geometry [35]. The band at 345 nm is due to the charge transfer transition associated with Mn_3O_4 type species in which Mn is hexa-coordinated. A part of Mn is present also in +2 oxidation state and these ions showed ${}^6\text{A}_{1g} \rightarrow {}^4\text{T}_{2g}$ crystal field transition at 500 nm [35]. As Mn content increased the absorption bands have broadened and exhibited a red shift. Thus the spectral studies reveal that Mn in Mn-SBA-12 and Mn-SBA-16 are present in both +3 and +2 oxidation states and in disordered octahedral and tetrahedral coordination geometries.

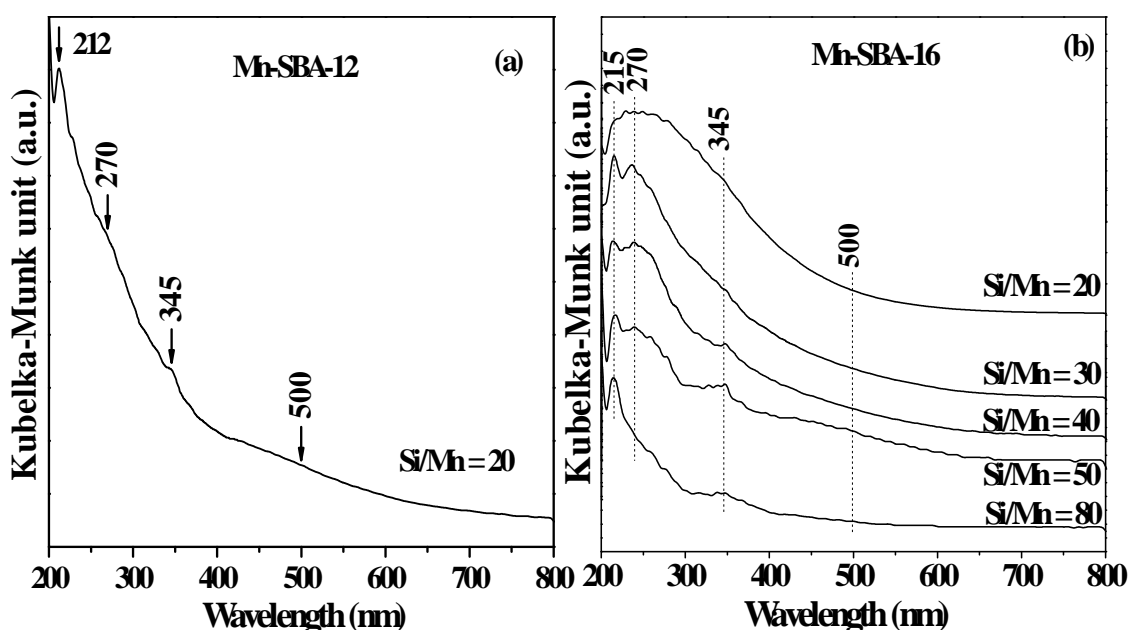


Fig. 2.29. DRUV-vis spectra of (a) Mn-SBA-12 (Si/Mn = 20) prepared using 0.1 M HCl and (b) Mn-SBA-16 (Si/Mn = 20 – 80) prepared in 2 M HCl

2.5.2.7. Electron Paramagnetic Resonance Spectroscopy (EPR)

Fig. 2.30 shows X-band EPR spectra of Mn-SBA-12 (Si/Mn = 20) and Mn-SBA-16 (Si/Mn = 30). In general, all the samples showed a sextet-line hyperfine pattern centered at $g_{av} = 2$ which is typical of Mn^{2+} ions ($3d^5$, $S = 5/2$, $I = 5/2$) in an octahedral environment of oxygen atoms [35-37]. However, the intensity of these signals per output Mn increased with increasing Mn content in the catalyst indicating that in catalysts with higher Si/Mn ratio, Mn is mainly in the +3 oxidation state while in the catalyst at lower Si/Mn ratio a significant amount of Mn is in +2 oxidation state. The sextet lines are not equally spaced due to second-order hyperfine interactions. Mn^{3+} which was detected by DRUV-vis spectroscopy is EPR (X-band)

silent, because, Mn^{3+} ($3d^4$, $S = 2$) with an integer spin is a non-Kramers ion, where the zero-field splitting is larger than the microwave quantum ($h\nu \sim 9.4$ GHz) [38]. DRUV-vis and EPR spectroscopy point out that both Mn^{3+} and Mn^{2+} species are present in these manganese silicate systems. At 77 K, the EPR signals became narrower and presence of forbidden transitions could be noticed in between the allowed transition signals. The framework substituted Mn is the +3 oxidation species and the extraframework one is the +2 oxidation state Mn species.

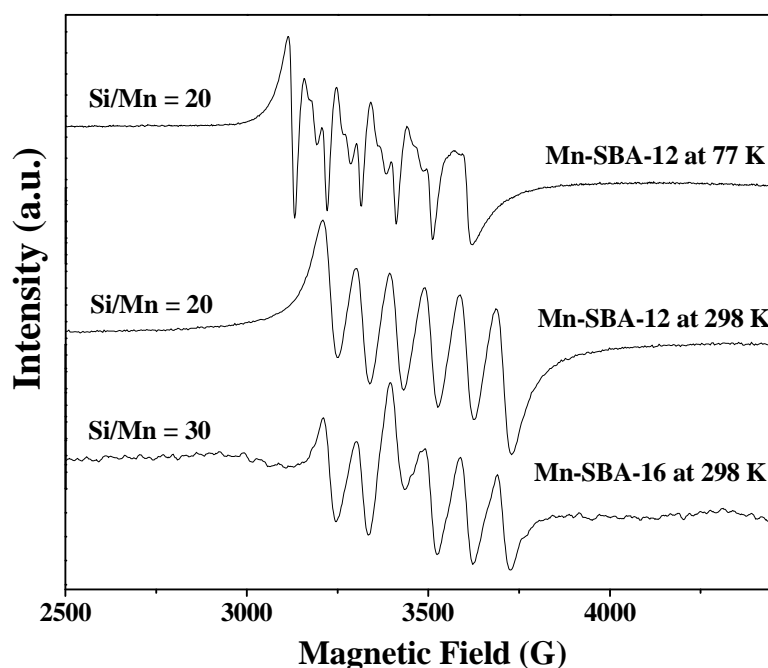


Fig. 2.30. EPR spectra of Mn-SBA-12 and Mn-SBA-16

2.5.2.8. Fourier Transform Infrared Spectroscopy (FTIR)

Fig. 2.31 shows the FTIR spectra of Mn-SBA-12 and Mn-SBA-16 materials. The absorption at $958 - 964 \text{ cm}^{-1}$ is due to stretching vibration mode of Si-O-Mn and Si-O-Si [39]. The FT-IR spectra of these materials showed characteristic absorption bands at $458 - 462$, 805 and 1078 cm^{-1} assigned to $\delta(\text{Si-O-Si})$, $\nu_s(\text{Si-O-Si})$ and $\nu_{as}(\text{Si-O-Si})$ vibrations, respectively. The absorption band at 1637 cm^{-1} is due to the deformation or bending vibration modes of adsorbed water molecules. The band at 3450 cm^{-1} is due to hydrogen-bonded surface silanol groups on manganese materials (Mn-SBA-12 and Mn-SBA-16).

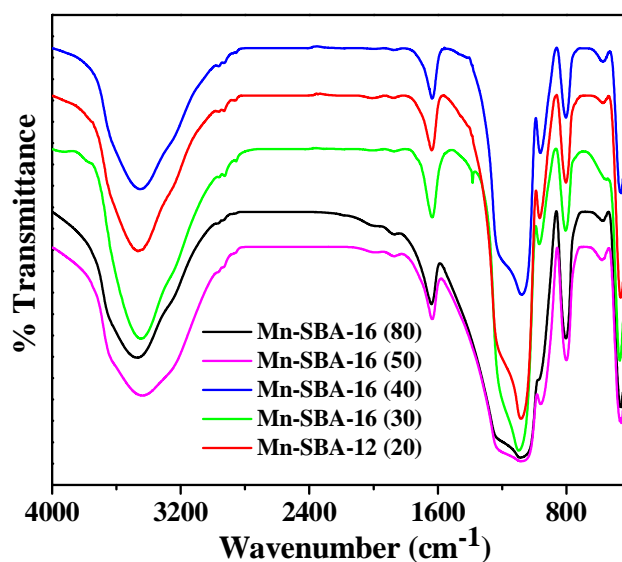


Fig. 2.31. FTIR spectra of Mn-SBA-12 and Mn-SBA-16

2.5.2.9. Fourier Transform Raman Spectroscopy (FT-Raman)

Fig. 2.32 shows FT-Raman spectra of Mn-SBA-12 and Mn-SBA-16 materials. Mn-incorporated SBA-12 and SBA-16 mesoporous silica show a new band at 955 cm^{-1} attributed to Si-O-Mn/Si-O-Si vibrations. In the FT-Raman spectrum, there are no peaks due to bulk manganese oxide [40]. This confirms that manganese ions are isolated and dispersed.

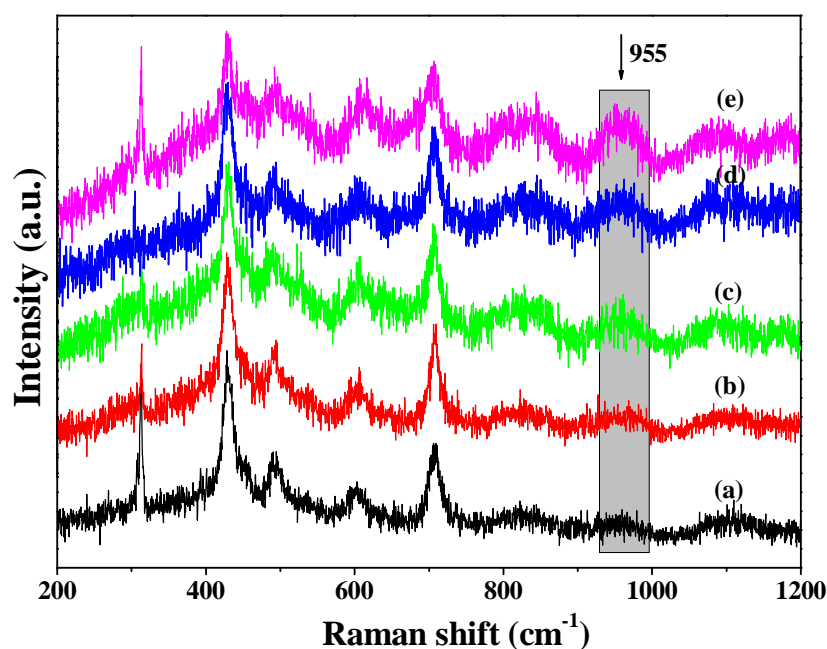


Fig. 2.32. FT-Raman spectra of (a) SBA-16, (b) Mn-SBA-16 (Si/Mn = 80), (c) Mn-SBA-16 (Si/Mn = 50), (d) Mn-SBA-16 (30) and (e) Mn-SBA-12 (Si/Mn = 20)

2.5.2.10. Thermal analysis (TGA)

Fig. 2.33 shows the thermogravimetric analysis of Mn-SBA-12 and Mn-SBA-16. The weight loss in the region 313 - 523 K is due to desorption of physisorbed water and that between 523 and 1273 K is due to condensation of silanol groups. All the Mn-containing materials showed a weight loss between 7.7 to 19.3%. Among manganese containing materials, Mn-SBA-16 (Si/Mn = 50) has the minimum weight loss of 7.7% (Table 2.7). Mn-SBA-12 (Si/Mn = 20) exhibited a weight loss of 10.1%.

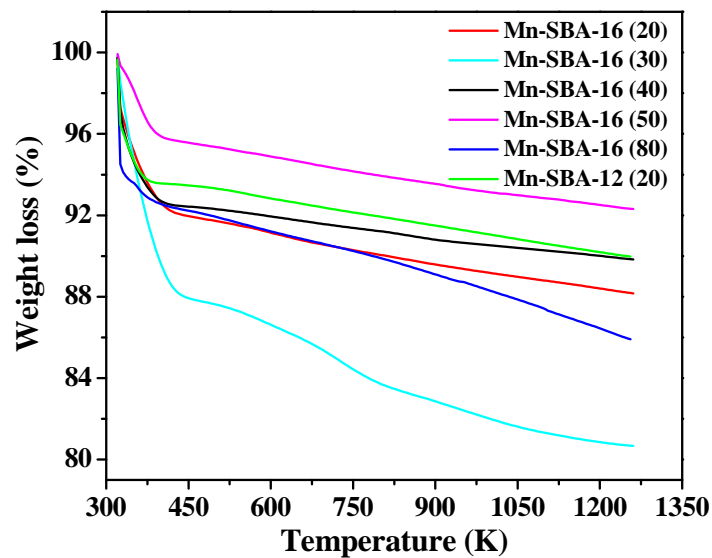


Fig. 2.33. Thermogravimetric analysis plots of Mn-SBA-12 and Mn-SBA-16

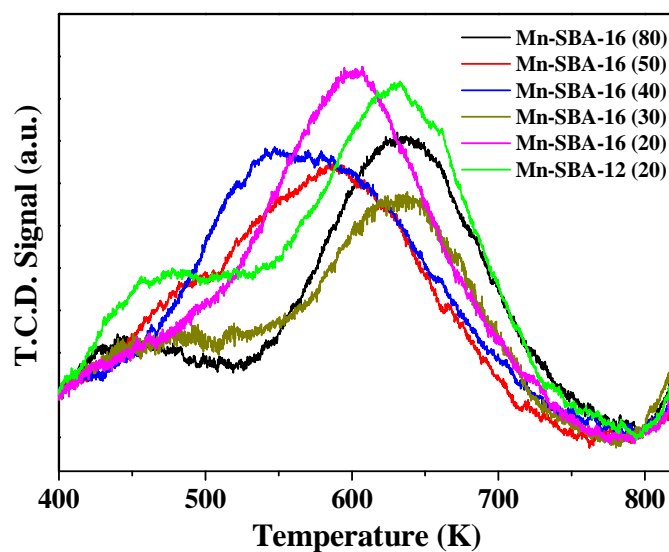


Fig. 2.34. NH_3 -TPD plots of Mn-SBA-12 and Mn-SBA-16

2.5.2.11. NH₃-TPD

The acidic properties of Mn-SBA-12 and Mn-SBA-16 materials were determined by NH₃-TPD (Fig. 2.34 and Table 2.7). Three NH₃ desorption peaks with maxima at 456, 600 and 645 K were observed (Fig. 2.34). While the first peak is attributed to ammonia desorbed from weakly acidic centres like silanols groups, the latter two peaks are attributed to that desorbed from relatively stronger acidic centers like isolated, framework-substituted, tetrahedral manganese ions. Table 2.7 provides the overall acidity value of these materials. Mn-SBA-12 (Si/Mn) was relatively more acidic (0.39 mmol/g) than Mn-SBA-16 (0.26 - 0.34 mmol/g) (Table 2.7).

Table 2.7. Thermogravimetric Analysis (TGA) and NH₃-TPD Data of Mn-SBA-12 and Mn-SBA-16

Catalyst (Si/Mn) input ratio	Conc. of HCl (M)	% Weight loss (TG) ^a			NH ₃ -TPD (mmol/g)
		< 523 K	523-1273 K	Total	
SBA-16	2	1.77	4.44	6.21	0.04
Mn-SBA-16 (80)	2	8.27	5.83	14.10	0.27
Mn-SBA-16 (50)	2	4.70	3.00	7.70	0.26
Mn-SBA-16 (40)	2	7.74	2.36	10.10	0.29
Mn-SBA-16 (30)	2	12.60	6.70	19.30	0.30
Mn-SBA-16 (20)	2	8.40	3.40	11.80	0.34
SBA-12	2	11.70	4.50	16.2	0.03
Mn-SBA-12 (20)	0.1	7.80	2.30	10.10	0.39

^aWeight loss below 523 K is due to loss of physisorbed water and between 523 to 1273 K is due to condensation of silanol groups

2.6. Synthesis and Characterization of Vanadium-containing SBA-12 Molecular Sieves

2.6.1. Synthesis

V-SBA-12 with varying Si/V molar ratio (20 – 80) were prepared by direct hydrothermal synthesis method.

2.6.1.1. V-SBA-12

In a typical preparation of V-SBA-12 (Si/V = 30), 8 g of Brij76 was dissolved in 40 g of distilled water and 160 g of 2 M HCl. The mixture was stirred at 313 K for 2 h and 17.6 g of TEOS was added to it over 30 min. Then, 0.33 g of

ammonium metavanadate (NH_4VO_3) was added to the above gel and stirring was continued for 20 h. The gel formed was transferred into a Teflon-lined stainless steel autoclave and heated at 373 K for 24 h. The solid formed was recovered by filtration, washed thoroughly with distilled water (2 - 3 L), dried at 373 K for 12 h, and calcined at 823 K for 8 h.

V-SBA-12 with Si/V input molar ratios of 80, 50, 40 and 20 were prepared in a similar manner as described above using appropriate quantities of Si and V sources (see [Appendix at the end of this chapter](#)). V-SBA-12 (Si/V = 30) was prepared also by varying the concentration of HCl used in the synthesis (0.1 to 1 M).

2.6.2. Characterization

2.6.2.1. Chemical Composition

The Si/V (input) content in these vanadosilicate materials was varied from 20 to 80. Chemical analysis by ICP-OES ([Table 2.8](#)) revealed that only 7.5 to 25.2 mol% of the input V was incorporated into the final compositions when the synthesis was carried out using 2 M HCl. When the molarity of HCl was decreased from 2 to 0.5 M, the amount of input V incorporated in the final products of V-SBA-12 (Si/V = 30) increased from ca., 2 to 4.4 times. In other words, this study reveals that by adjusting HCl concentration, one could alter the extent of V incorporation in the final compositions.

2.6.2.2. X-ray Powder Diffraction (XRD)

The crystallinity and phase purity of prepared vanadosilicates were confirmed from the XRD patterns. [Fig. 2.35](#) shows representative XRD patterns of V-SBA-12 in the small-angle region ($2\theta = 0.5 - 5^\circ$). Vanadium incorporation did not alter the integrity of the framework structure. But the peaks shifted to lower 2θ values. The unit cell parameters a and c for the hexagonal V-SBA-12 increased with increasing V content ([Table 2.8](#)). The increase in the unit cell parameters is due to the larger ionic radii of V than that of Si ($r_{\text{V}^{5+}} = 0.059$ nm). This observation provides an unequivocal evidence for the substitution of V for Si in the framework of mesoporous V-SBA-12. All these vanadosilicate materials showed a diffused XRD peak in the wide-angle region at 23° ([Fig. 2.36](#)) indicative of the presence of amorphous silica. Absence of peaks due to vanadium oxide phase in wide-angle region ($2\theta = 10 - 80^\circ$) confirms that vanadium is dispersed and isolated.

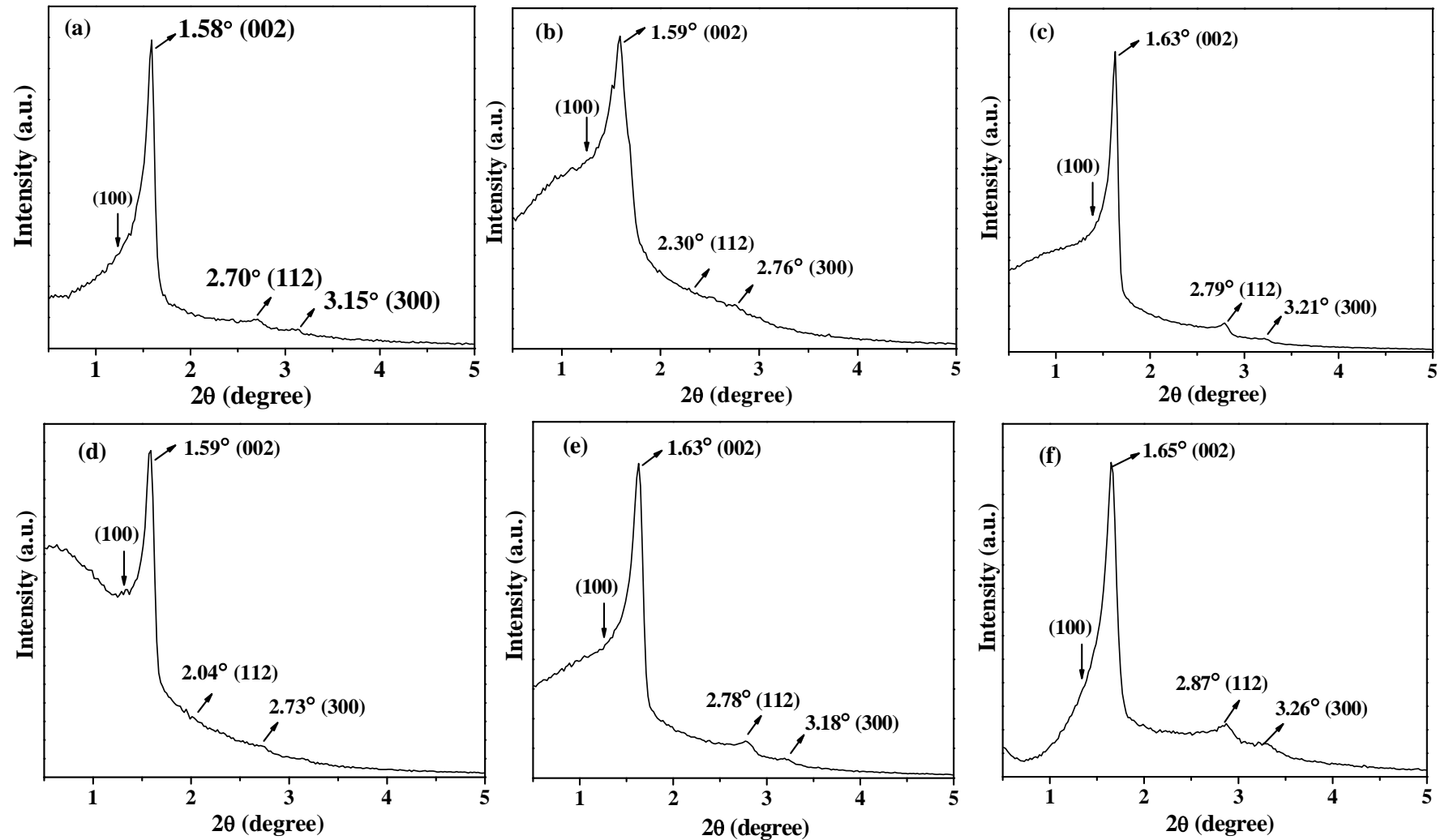


Fig. 2.35. Low-angle XRD patterns of (a) V-SBA-12 (Si/V = 20, 2 M), (b) V-SBA-12 (Si/V = 30, 2 M), (c) V-SBA-12 (Si/V = 40, 2 M), (d) V-SBA-12 (Si/V = 50, 2 M), (e) V-SBA-12 (Si/V = 80, 2 M), and (f) V-SBA-12 (Si/V = 30, 1 M)

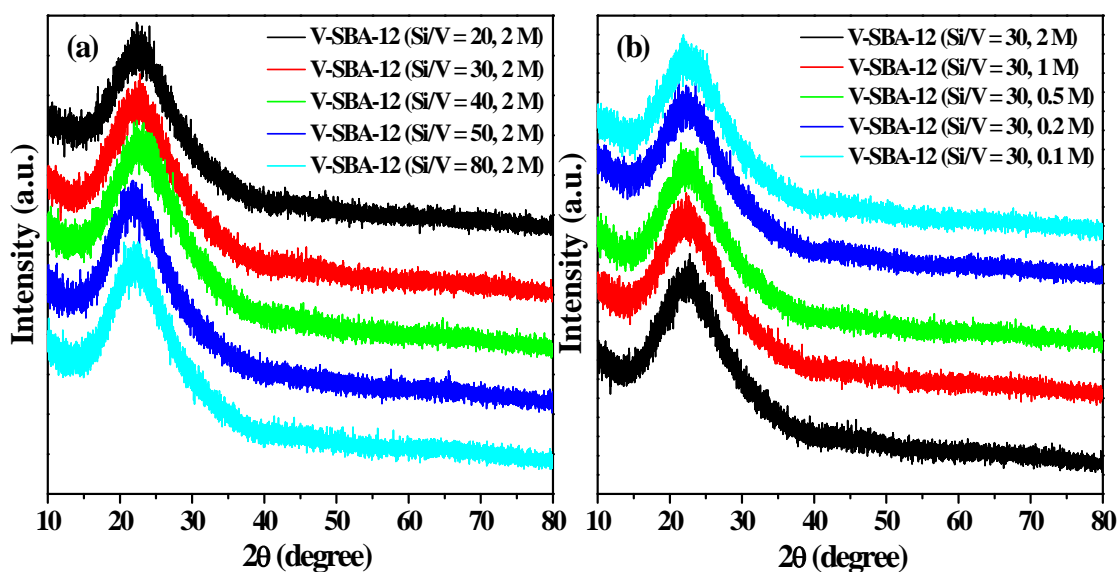


Fig. 2.36. Wide-angle XRD patterns: (a) V-SBA-12 (Si/V = 20 - 80) prepared using 2 M HCl, (b) V-SBA-12 (Si/V = 30) prepared using varying concentrations of HCl

2.6.2.3. N₂-Physisorption

Fig. 2.37 shows the N₂ adsorption-desorption isotherms of V-SBA-12 materials. All these vanadosilicates showed typical type-IV N₂ adsorption-desorption isotherms with a H₁-hysteresis loop characteristic of a hexagonal mesoporous material (Fig. 2.37) [1]. The textural properties of these materials are given in the Table 2.8. All these vanadium incorporated SBA-12 materials showed a narrow BJH pore size distribution with an average pore size of 3.3 - 8.1 nm (Fig. 2.37, inset). V-SBA-12 with varying Si/V molar ratio (20 – 80) showed increase in pore size (4.6 to 8.1 nm) as compared to pure SBA-12 (3.8 nm).

V-SBA-12 (Si/V = 30) prepared using 0.2 and 0.1 M HCl showed lower pore size (3.5 and 3.3 nm) than neat SBA-12 (3.8 nm). This may be due to the agglomeration of vanadium oxide nanocrystals residing in the mesopores of these materials. This fact is also supported by a decrease in the unit cell parameters of these materials (Table 2.8). The specific surface area for these materials varied between 557 and 752 m²/g. The total pore volume of these materials increased after vanadium incorporation (0.67 – 1.13 cc/g) except for V-SBA-12 (Si/V = 30) prepared using 0.1 M HCl. Again, formation of vanadium dioxide agglomerates at lower concentration of HCl is the possible cause for this behaviour in textural properties. In other words, both the V-content and molarity of HCl influenced the textural properties. The pore wall thickness of V-SBA-12 lays in the range 3.02 – 7.20 nm (Table 2.8).

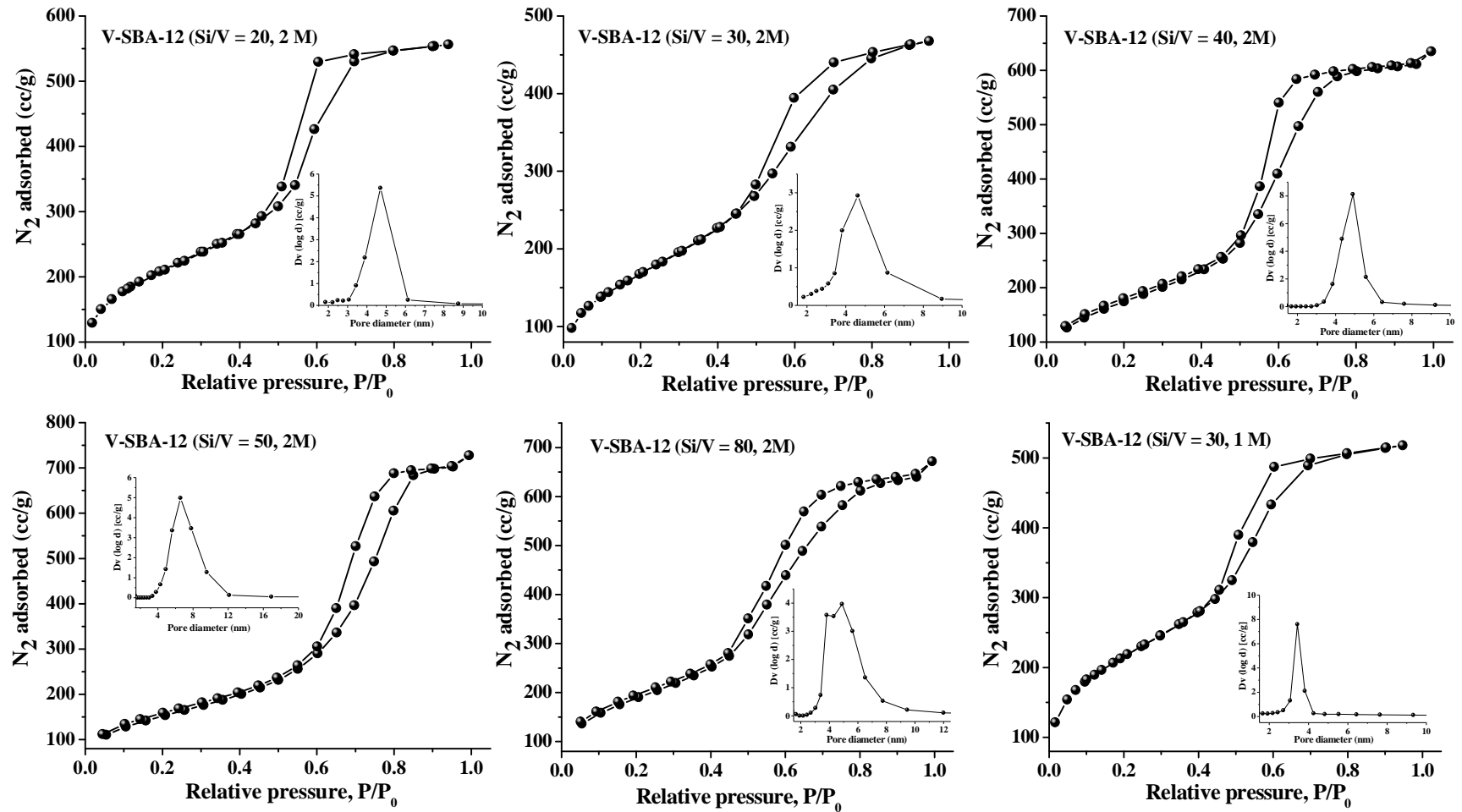


Fig. 2.37. N_2 adsorption-desorption isotherms of V-SBA-12 (Si/V = 20 – 80) prepared using 2 M HCl and V-SBA-12 (Si/V = 30) prepared using 1 M HCl

Table 2.8. Composition, Structure and Textural properties of V-SBA-12

Catalyst	Molar conc. of HCl (M)	Si/Mn molar ratio		Structural data (XRD) ^a				Textural properties (N ₂ Physisorption)				
		Input	Output (ICP-AES)	Input Incorporated V (mol %)	Inter planar spacing (nm)		Unit cell parameter (nm)		S _{BET} (m ² /g)	Average pore diameter (nm)	Pore volume (cc/g)	Wall thickness (nm) ^b
					d ₁₀₀	d ₀₀₂	a	c				
SBA-12	2	∞	∞	-	6.00	5.26	6.93	10.52	672	3.8	0.64	6.72
V-SBA-12 (80)	2	80	320	25.2	6.44	5.42	7.44	10.84	691	6.0	1.04	4.84
V-SBA-12 (50)	2	50	300	16.9	6.74	5.56	7.78	11.12	557	8.1	1.13	3.02
V-SBA-12 (40)	2	40	310	13.2	6.40	5.42	7.39	10.84	639	6.1	0.98	4.74
V-SBA-12 (30)	2	30	250	12.4	6.80	5.56	7.85	11.12	576	5.0	0.72	6.12
V-SBA-12 (20)	2	20	280	7.5	6.84	5.59	7.90	11.18	752	4.6	0.86	6.58
V-SBA-12 (30)	1	30	56	54.4	6.31	5.36	7.28	10.72	699	4.2	0.73	6.52
V-SBA-12 (30)	0.5	30	127	24.2	7.24	5.66	8.36	11.32	645	5.6	0.91	5.72
V-SBA-12 (30)	0.2	30	264	11.7	5.89	5.20	6.89	10.40	767	3.5	0.67	6.90
V-SBA-12 (30)	0.1	30	296	10.4	5.97	5.25	6.90	10.50	686	3.3	0.56	7.20

^aV-SBA-12 is defined by a three-dimensional hexagonal system with space group of $p6_3/mmc$. Unit cell parameter $a = 2d_{100}/\sqrt{3}$, $c = 2d_{002}$. ^bWall thickness = $c - \text{average pore diameter}$

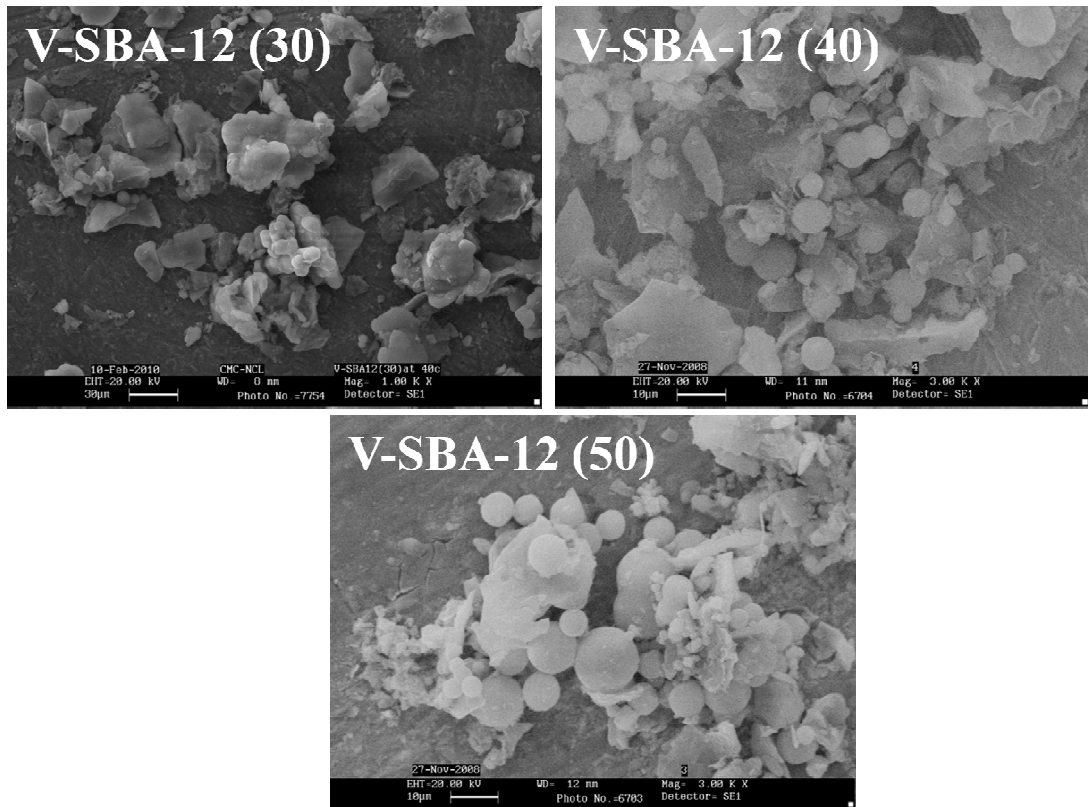


Fig. 2.38. SEM images of V-SBA-12

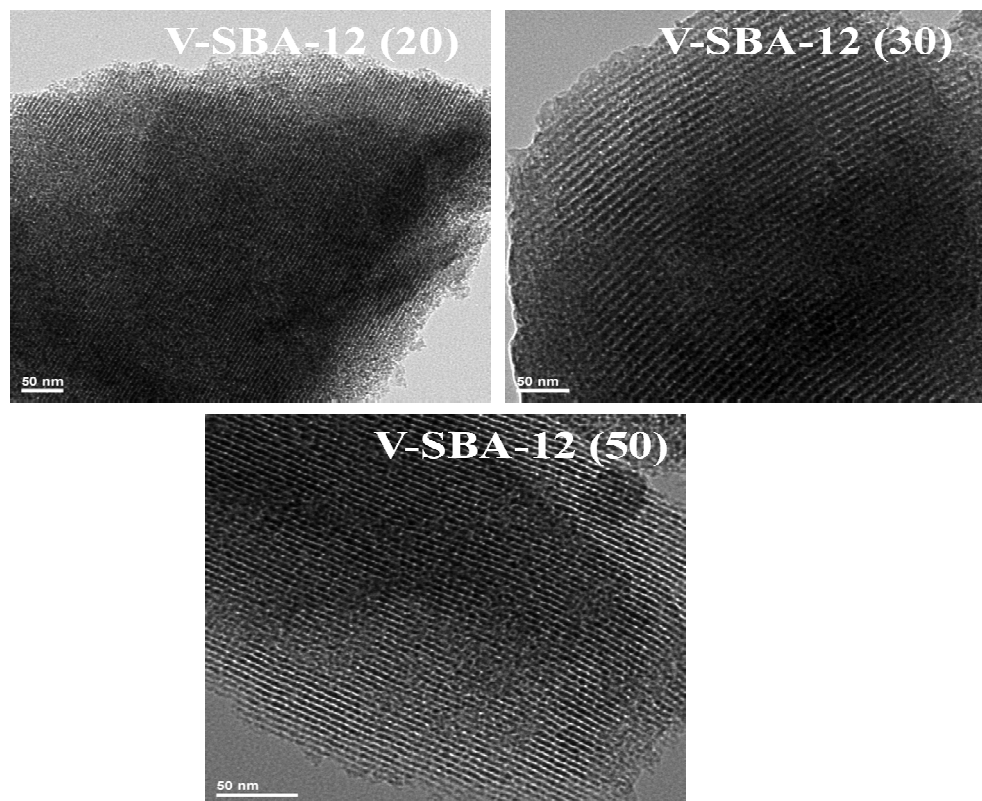


Fig. 2.39. HRTEM images of V-SBA-12

2.6.2.4. Scanning Electron Microscopy (SEM)

Fig. 2.38 shows the SEM images of V-SBA-12. V-SBA-12 (Si/V = 30) has a cubic crystalline morphology while those materials with Si/V = 40 and 50 have planar sheet and spherical morphology. The average particle size of these materials varied from 4 to 8 μm .

2.6.2.5. High Resolution Transmission Electron Microscopy (HRTEM)

HRTEM images (Fig. 2.39) confirmed the long-range, three-dimensional, mesoporous ordering in these materials. V-SBA-12 has hexagonally arranged pores with $p6_3/mmc$ space group. No separate bulk VO_x particles were detected in the HRTEM images.

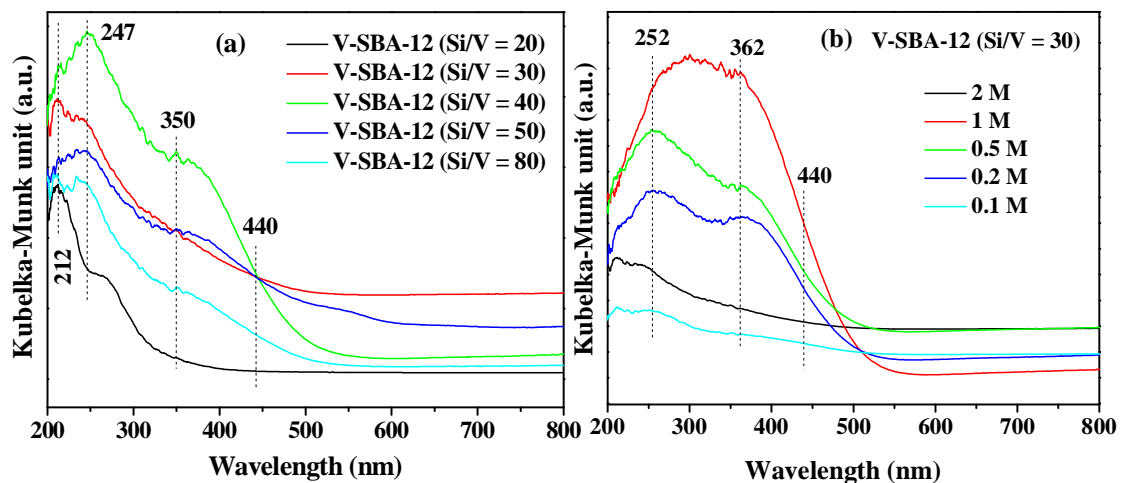


Fig. 2.40. DRUV-vis spectra of (a) V-SBA-12 (Si/V = 20 – 80) prepared using 2 M HCl and (b) V-SBA-12 (Si/V = 30) prepared using 0.1 to 2 M HCl

2.6.2.6. Diffuse Reflectance Ultraviolet Visible Spectroscopy (DRUV-vis)

Fig. 2.40 shows the DRUV-vis spectra of V-SBA-12 (Si/V = 20 – 80, 2 M) and V-SBA-12 (Si/V = 30, 0.1 – 2 M). Absorption band at 212 [Fig. 2.40 (a) and (b)] is due to the ligand to metal charge transfer transition ($\text{O}^{2-} \rightarrow \text{V}^{5+}$) confirming that a part of V^{5+} ions are isolated and in tetrahedral (T_d) coordination substituted in the framework of V-SBA-12 [41]. The absorption bands at 247 - 252 nm correspond to vanadium ions in pseudo-tetrahedral coordination (Fig. 2.40 (a) and (b)). The bands at 350 – 362 nm and 440 nm can be assigned to V^{5+} with penta or hexa coordination geometry and probably present as polymeric $(\text{V-O-V})_n$ clusters on the surface of the catalysts [41]. The absence of absorption bands at 550 – 800 nm indicate the absence of reduced vanadium (V^{4+}) ions in these materials [41, 42].

2.6.2.7. Fourier Transform Infrared Spectroscopy (FTIR)

Fig. 2.41 shows the FTIR spectra of V-SBA-12 materials. The FTIR band at 961 cm^{-1} is due to the stretching vibration mode of Si-O-V, which could be attributed to substituted vanadium species in these mesoporous V-SBA-12 materials [41 (b)]. The intensity of this band increased with increasing amount of vanadium in the framework of V-SBA-12 (Fig. 2.41).

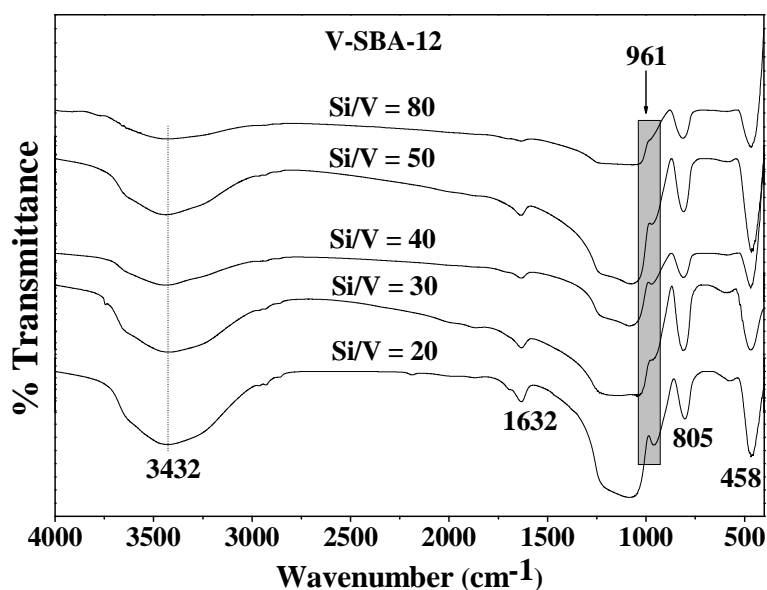


Fig. 2.41. FTIR spectra of V-SBA-12 (Si/V = 20 – 80) prepared in 2 M HCl

2.6.2.8. ^{29}Si MAS NMR Spectroscopy

Fig. 2.42 shows ^{29}Si MAS NMR spectra of V-SBA-12. These V-SBA-12 (Si/V = 20 – 80) materials showed peaks at -93.2, -103.2 and -111.3 ppm, which are attributable to Q^2 , Q^3 and Q^4 species, respectively (Fig. 2.42). These materials have mainly Q^4 type species in V-SBA-12 while pure SBA-12 showed mainly the Q^3 type of species (Table 2.9). The $\text{Q}^4/\text{Q}^2 + \text{Q}^3$ ratio of vanadium silicates are given in the Table 2.9. This ratio is highest for V-SBA-12 (Si/V = 80) and lowest for V-SBA-12 (Si/V = 30) prepared using 1 M HCl.

2.6.2.9. Thermal Analysis (TGA)

Fig. 2.43 shows the thermogravimetric analysis plots of V-SBA-12. V-SBA-12 (Si/V = 20) with high vanadium content showed lowest weight loss (8.32%) while V-SBA-12 (Si/V = 80) with less amount of vanadium showed the highest

weight loss (ca. 21%). This indicates that vanadium content has influenced the hydrophobic character of the catalyst (Table 2.9).

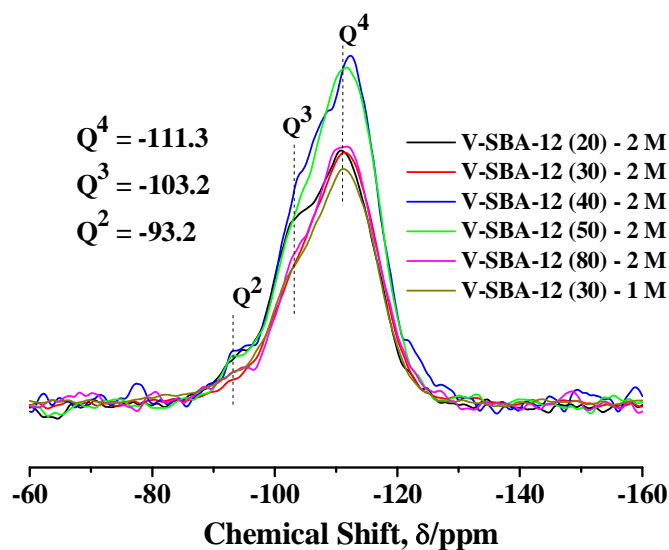


Fig. 2.42. ^{29}Si MAS NMR of V-SBA-12 mesoporous molecular sieves

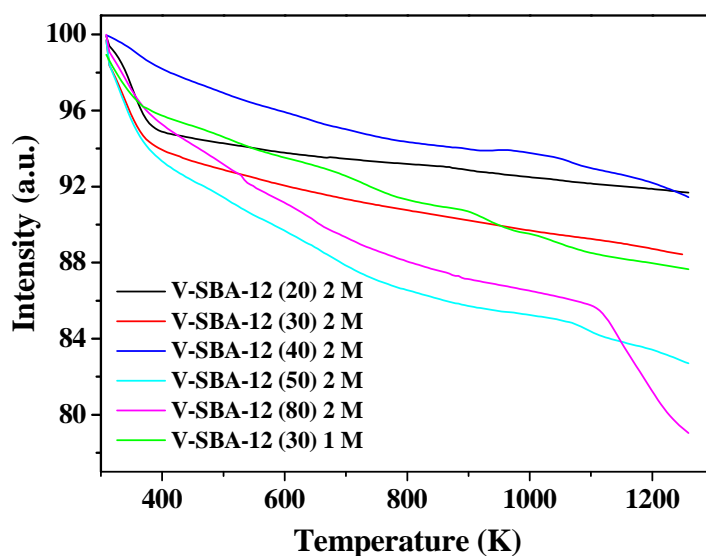


Fig. 2.43. TGA graph of V-SBA-12

2.6.2.10. NH_3 -TPD

The acidic properties of V-SBA-12 were determined by NH_3 -TPD (Fig. 2.44 and Table 2.9). Two desorption peaks with maxima at 474 and 636 K were observed (Fig. 2.44). While the first peak is attributed to ammonia desorbed from silanol groups, the latter peak is attributed to that desorbed from relatively stronger acid centers like isolated, framework-substituted, tetrahedral vanadium ions.

Table 2.9. ^{29}Si MAS NMR, Thermogravimetry (TG) and NH_3 -TPD Data of V-SBA-12

Catalyst (Si/V) input ratio	Concentration of HCl used in the synthesis (M)	% Intensity distribution of ^{29}Si MAS NMR signals				% Weight loss (TG) ^a			NH_3 -TPD (mmol/g)
		Q ²	Q ³	Q ⁴	Q ⁴ /Q ² + Q ³	< 523 K	523-1273 K	Total	
SBA-12	2	16.14	78.16	5.70	0.06	11.70	4.50	16.20	0.03
V-SBA-12 (80)	2	8.10	8.10	83.80	5.17	7.38	13.72	21.10	0.52
V-SBA-12 (50)	2	4.80	22.10	73.10	2.71	9.10	8.23	17.33	0.45
V-SBA-12 (40)	2	7.56	17.34	75.10	3.02	3.60	4.96	8.56	0.38
V-SBA-12 (30)	2	9.10	13.80	77.10	3.37	7.30	4.30	11.60	0.35
V-SBA-12 (20)	2	10.82	16.42	72.76	2.67	5.8	2.52	8.32	0.56
V-SBA-12 (30)	1	16.00	18.00	66.00	1.94	5.7	6.63	12.33	1.17
V-SBA-12 (30)	0.5	-	-	-	-	-	-	-	0.40
V-SBA-12 (30)	0.2	-	-	-	-	-	-	-	0.37
V-SBA-12 (30)	0.1	-	-	-	-	-	-	-	0.30

^aWeight loss below 523 K is due to loss of physisorbed water and between 523 and 1273 K is due to condensation of silanol groups

Table 2.9 provides the total acidity values of these vanadosilicates. Both vanadium content and concentration of HCl used in the synthesis have marked effect on the acidity of vanadosilicates.

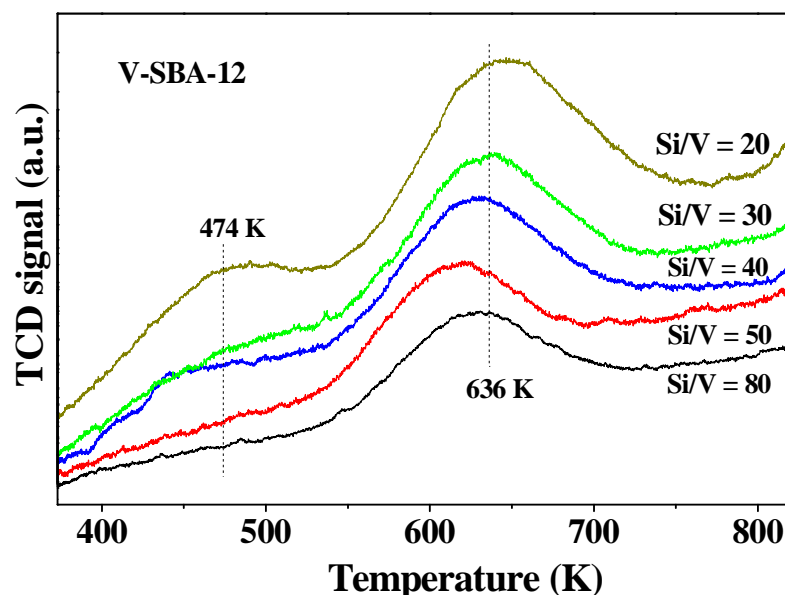


Fig. 2.44. NH_3 -TPD plots of V-SBA-12 prepared using 2 M HCl

2.7. Synthesis and Characterization of Fe-SBA-12 Molecular Sieves

2.7.1. Synthesis

2.7.1.1. Fe-SBA-12

Fe-SBA-12 was prepared by direct hydrothermal synthesis method. In a typical preparation of Fe-SBA-12 (Si/Fe = 20, 0.1M), 8 g of Brij76 was dissolved in 40 g of distilled water and 160 g of 0.1 M HCl. The mixture was stirred at 313 K for 2 h and 17.6 g of TEOS was added to it over 30 min. Then, 0.70 g of Iron (III) chloride anhydrous dissolved in 10 mL of water was added slowly. The stirring was continued for 20 h. The gel formed was transferred into a Teflon-lined stainless steel autoclave and heated at 373 K for 24 h. The solid formed was recovered by filtration, washed thoroughly with distilled water (2 - 3 L), dried at 373 K for 12 h, and calcined at 823 K for 8 h in the air.

2.7.2. Characterization

2.7.2.1. X-ray Powder Diffraction (XRD)

Fig. 2.45 shows representative low and wide-angle XRD patterns of Fe-SBA-12 (Si/Fe = 20). The low-angle XRD pattern showed an intense main peak at 1.67° corresponding to (002) reflection and two well-resolved, weak peaks at 2.82° and 3.25° attributable to (112) and (300) reflections, respectively. A weak shoulder (to the main peak) at 1.28° due to (100) reflection was also observed. All these characteristics of Fe-SBA-12 correspond to the ordered, three-dimensional, hexagonal mesoporous structure with a space group of $p6_3/mmc$ [1]. Fe incorporation did not alter the integrity of the framework structure. The unit cell parameters a and c for the hexagonal Fe-SBA-12 (Si/Fe = 20) are 8.0 and 10.6 nm, respectively. Wide-angle XRD showed a diffused XRD peak at 23° (Fig. 2.45, inset) indicative of the presence of amorphous silica. There are no peaks due to bulk iron oxide species confirming that iron in SBA-12 is in a dispersed state.

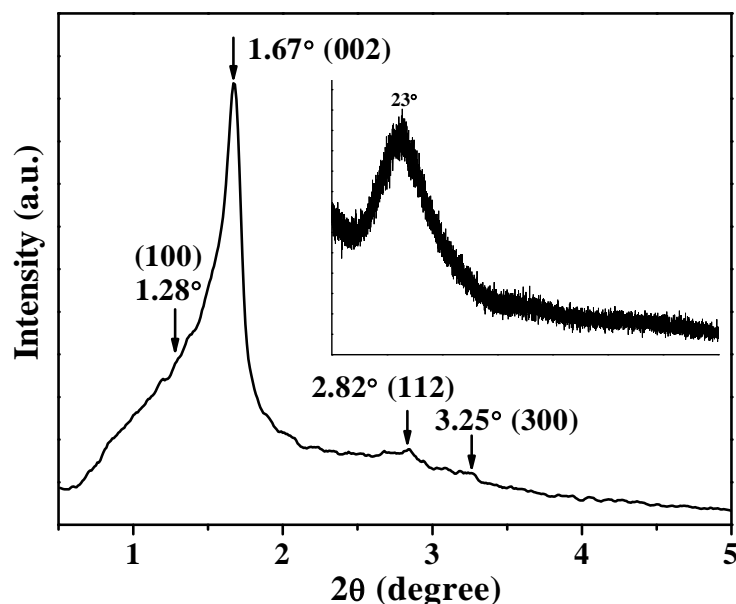


Fig. 2.45. Low and wide-angle XRD patterns of Fe-SBA-12 (Si/Fe = 20) prepared using 0.1 M HCl

2.7.2.2. N₂-Physisorption

N₂ adsorption-desorption isotherms of Fe-SBA-12 showed typical type-IV N₂ isotherms with a H₁-hysteresis loop, which are characteristics of a hexagonal mesoporous materials (Fig. 2.46) [1]. Fe-SBA-12 showed a narrow BJH pore size distribution with an average pore size of 3.8 nm (Fig. 2.46, inset). The specific BET surface area, pore volume and wall thickness are 982 m²/g, 0.94 cc/g and 6.8 nm, respectively.

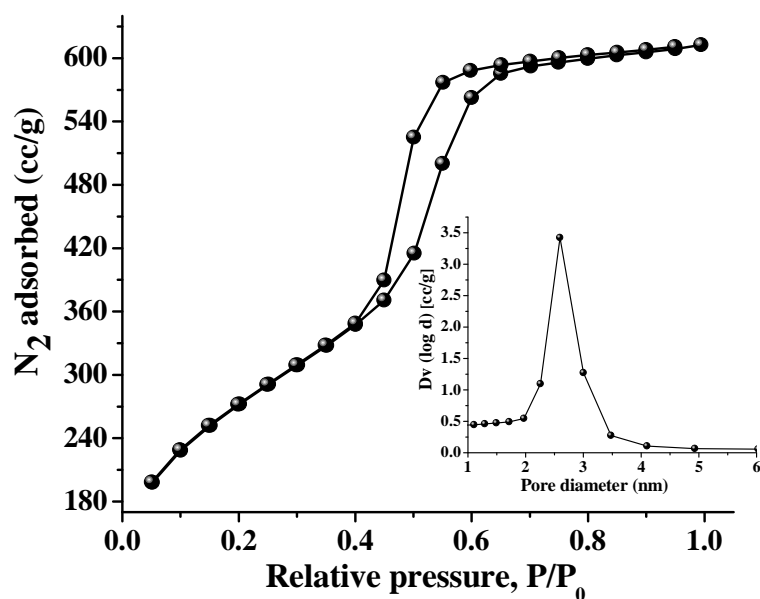


Fig. 2.46. N_2 adsorption-desorption isotherms and BJH pore size distribution plot (inset) of Fe-SBA-12 (Si/Fe = 20) prepared using 0.1 M HCl

2.7.2.3. Diffuse Reflectance Ultraviolet-Visible Spectroscopy (DRUV-vis)

Diffuse reflectance UV-visible spectra of Fe-SBA-12 (Si/Fe = 20) showed an absorption band at 268 nm which can be assigned to $O^{2-} \rightarrow Fe^{3+}$ charge-transfer transitions (Fig. 2.47) [43-45]. The band in the region 350 - 600 nm corresponds to the presence of Fe_2O_3 crystals which could not be detected by XRD.

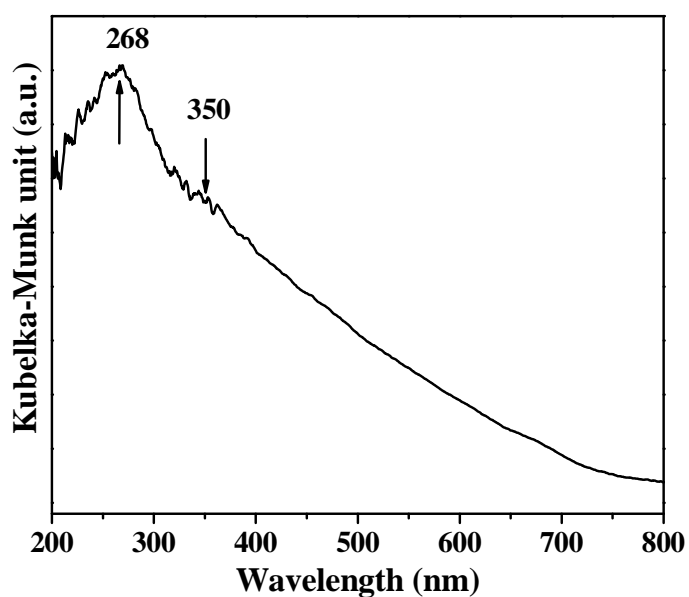


Fig. 2.47. DRUV-visible spectra of Fe-SBA-12 (Si/Fe = 20)

2.7.2.4. Fourier Transform Infrared Spectroscopy (FTIR)

Fe-SBA-12 showed an absorption band at 961 cm^{-1} assignable Si-O-Fe stretching vibrations (Fig. 2.48). The band at 3454 cm^{-1} is due to adsorbed water molecules.

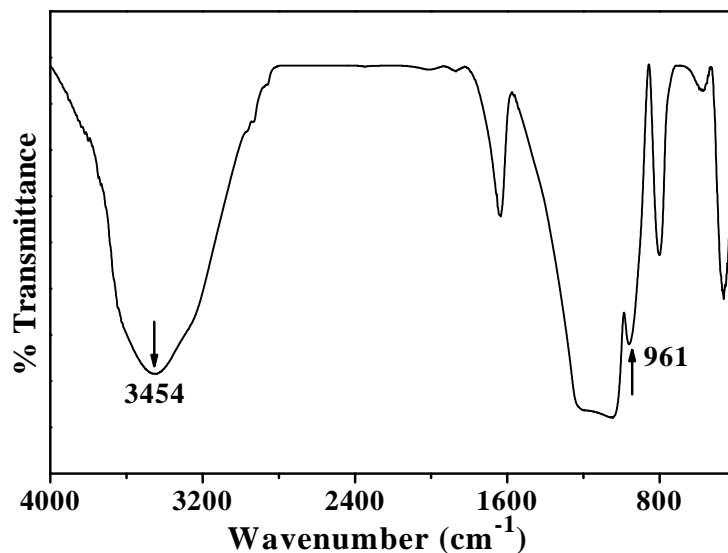


Fig. 2.48. FTIR spectrum of Fe-SBA-12 (Si/Fe = 20)

2.7.2.5. NH₃-TPD

The acidity of Fe-SBA-12 was determined by NH₃-TPD (Fig. 2.49). Two desorption peaks with maxima at 474 and 641 K were observed in NH₃-TPD studies (Fig. 2.49).

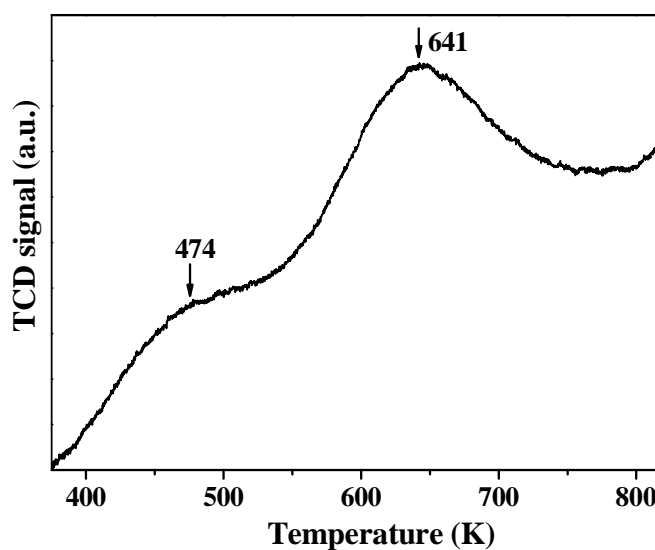


Fig. 2.49. NH₃-TPD profile of Fe-SBA-12 (Si/Fe = 20)

First peak is attributed to ammonia desorbed from weakly acidic silanols groups and the latter is attributed to that desorbed from relatively stronger acid centers like isolated, framework-substituted, tetrahedral Fe ions. The total acidity of Fe-SBA-12 (Si/Fe = 20) was found to be 0.38 mmol/g.

2.8. Conclusions

Ti, Mn, V and Fe incorporated mesoporous silica materials (SBA-12 and SBA-16) were prepared by direct hydrothermal synthesis method. These catalysts were characterized by ICP-OES, XRD, N₂-physisorption, DRUV-Vis, SEM, HRTEM, FTIR, FT-Raman, EPR and thermal analysis techniques. Acidity of these catalysts was determined by NH₃-TPD and DRIFT spectroscopy of adsorbed pyridine techniques.

2.9. References

1. D. Zhao, Q. Huo, J. Feng, B.F. Chmelka, G.D. Stucky, *J. Am. Chem. Soc.* 120 (1998) 6024.
2. C.F. Cheng, Y.C. Lin, H.H. Cheng, S.M. Liu, H.S. Sheu, *Chem. Lett.* 33 (2004) 262.
3. D. Zhao, J. Feng, Q. Huo, N. Melosh, G.H. Fredrickson, B.F. Chmelka, G.D. Stucky, *Science* 279 (1998) 548.
4. J.K. Satyarthi, L. Saikia, D. Srinivas, P. Ratnasamy, *Appl. Catal. A: Gen.* 330 (2007) 145.
5. A. Thangaraj, R. Kumar, S.P. Mirajkar, P. Ratnasamy, *J. Catal.* 130 (1991) 1.
6. S.K. Das, M.K. Bhunia, A. Bhaumik, *J. Solid State Chem.* 183 (2010) 1326.
7. Y. Sakamoto, M. Kaneda, O. Terasaki, D.Y. Zhao, J.M. Kim, G. Stucky, H.J. Shin, R. Ryoo, *Nature* 408 (2000) 449.
8. C. Yu, H. Chu, Y. Wan, D. Zhao, *J. Mater. Chem.* 20 (2010) 4705.
9. S. Shen, Y. Deng, G. Zhu, D. Mao, Y. Wang, G. Wu, J. Li, X.Z. Liu, G. Lu, D. Zhao, *J. Mater. Sci.* 42 (2007) 7057.
10. M. Taramasso, G. Perego, B. Notari, US Patent 4,410,501 (1993) to SNAM Progetti.
11. R. Millini, E.P. Massara, G. Perego, G. Bellussi, *J. Catal.* 133 (1992) 220, and 137 (1992) 497.
12. R. Millini, G. Perego, *Gazz. Chim. Ital.* 126 (1996) 133.

13. A. Thangaraj, S. Sivasanker, *J. Chem. Soc. Chem. Commun.* (1992) 123.
14. S.J. Gregg and K.S.W. Sing, *Adsorption, Surface Area and Porosity*, Academic Press, New York, 1982, Ch. 3.
15. P.I. Ravikovitch, A.V. Neimark, *Langmuir* 18 (2002) 9830.
16. K. Morishige, N. Tateishi, S. Fukuma, *J. Phys. Chem. B* 107 (2003) 5177.
17. T.-W. Kim, R. Ryoo, M. Kruk, K.P. Gierszal, M. Jaroniec, S. Kamiya, O. Terasaki, *J. Phys. Chem. B* 108 (2004) 11480.
18. K. Flodström, H. Wennerström, C.V. Teixeira, H. Amenitsch, M. Lindén, V. Alfredsson, *Langmuir* 20 (2004) 10311.
19. K. Morishige, N. Tateishi, *J. Chem. Phys.* 119 (2003) 2301.
20. C.G.V. Burgess, D.H. Everett, S. Nuttall, *Pure Appl. Chem.* 61 (1989) 1845.
21. W.D. Machin, *Langmuir* 10 (1994) 1235.
22. K. Chaudhari, R. Bal, T.Kr. Das, A. Chandwadkar, D. Srinivas, S. Sivasanker, *J. Phys. Chem. B* 104 (2000) 11066.
23. P. Ratnasamy, D. Srinivas, H. Knözinger, *Adv. Catal.* 48 (2004) 1.
24. (a) Z. Luan, L. Kevan, *Micropor. Mesopor. Mater.* 44-45 (2001) 337. (b) R. Millini, E. Previde Massara, G. Perego, G. Bellussi, *J. Catal.* 137 (1992) 497. (c) M.A. Camblor, A. Corma, J. Perez Pariente, *Zeolites* 13 (1993) 82.
25. N.T. Trukhan, A.L. Panchenko, E. Roduner, *Langmuir* 21 (2005) 10454.
26. (a) Z. Luan, E.M. Maes, P.A.W. van der Heide, D. Zhao, R.S. Czernuszewicz, L. Kevan, *Chem. Mater.* 11 (1999) 3680. (b) C. Li, G. Xiong, J. Liu, P. Ying, Q. Xin, Z. Feng, *J. Phys. Chem. B* 105 (2001) 2993.
27. D.W. Sindorf, G.E. Maciel, *J. Phys. Chem.* 86 (1982) 5208.
28. B.R. Jermly, S.Y. Kim, K.V. Bineesh, D.W. Park, *Micropor. Mesopor. Mater.* 117 (2009) 661.
29. G. Valerio, A. Goursot, R. Vetrivel, O. Malkina, V. Malkin, D.R. Salahub, *J. Am. Chem. Soc.* 120 (1998) 11426.
30. J. Klinowski, *Ann. Rev. Mater. Sci.* 18 (1988) 189.
31. C.A. Fyfe, J.M. Thomas, J. Klinowski, G.C. Gobbi, *Angew. Chem. Int. Ed. Engl.* 22 (1983) 259.
32. A. Corma, V. Fornés, M.T. Navarro, J. Pérez-Pariente, *J. Catal.* 148 (1994) 569.
33. M. Hunger, U. Schenk, M. Breninger, R. Gläser, J. Weitkamp, *Micropor.*

- Mesopor. Mater. 27 (1999) 261.
34. A. Taguchi, F. Schüth, Micropor. Mesopor. Mater. 77 (2005) 1.
 35. (a) Q. Jhang, Ye Wang, S. Itsuki, T. Shishido, K. Takehira, J. Mol. Catal. A: Chem. 188 (2002) 189. (b) K.M. Parida, S.S. Das, J. Mol. Catal. A: Chem. 306 (2009) 54.
 36. M. Selvaraj, T.G. Lee, J. Phys. Chem. B 110 (2006) 21793.
 37. A. Ramanathan, T. Archipov, R. Maheswari, U. Henefeld, E. Roduner, R. Gläser, J. Phys. Chem. C 112 (2008) 7468.
 38. D.P. Goldberg, J. Telser, J. Krzystek, A.G. Montalban, L.-C. Brunel, A.G. M. Barrett, B. M. Hoffman, J. Am. Chem. Soc. 119 (1997) 8722.
 39. K.M. Parida, S.S. Dash, S. Singha, Appl. Catal. A: Gen. 351 (2008) 59.
 40. F. Buciuman, F. Patcas, R. Craciun, D.R.T. Zahn, Phys. Chem. Chem. Phys. 1 (1999) 185.
 41. (a) F. Gao, Y. Zhang, H. Wan, Y. Kong, X. Wu, L. Dong, B. Li, Y. Chen, Micropor. Mesopor. Mater. 110 (2008) 508. (b) S. Shylesh, A.P. Singh, J. Catal. 233 (2005) 359. (c) K.J. Chao, C.N. Wu, H. Chang, J. Phys. Chem. B 101 (1997) 6341.
 42. Y. Zhua, Y. Donga, L. Zhaoa, F. Yuana, J. Mol. Catal. A: Chem. 315 (2010) 205.
 43. Y. Li, Z. Feng, Y. Lian, K. Sun, L. Zhang, G. Jia, Q. Yang, C. Li, Micropor. Mesopor. Mater. 84 (2005) 41.
 44. T. Kawabata, Y. Ohishi, S. Itsuki, N. Fujisaki, T. Shishido, K. Takaki, Q. Zhang, Y. Wang, K. Takehira, J. Mol. Catal. A: Chem. 236 (2005) 99.
 45. M.S. Hamdy, G. Mul, J.C. Jansen, A. Ebaid, Z. Shan, A.R. Overweg, T. Maschmeyer, Catal. Today 100 (2005) 255.

APPENDIX-I

Quantities of Silica and Metal Sources Used in the Synthesis of Various Catalysts

Catalyst (Si/M)	Concentration of HCl used in the synthesis (M)	Amount of TEOS (g)	Amount of metal source (g)
<i>Pure mesoporous silica molecular sieves</i>			
SBA-12 (∞)	2	17.60	-
SBA-16 (∞)	2	28.34	-
SBA-15 (∞)	2	17.00	-
MCM-41 (∞)	Basic medium	14.17	-
<i>Titanosilicate molecular sieves (Titanium iso-propoxide as a Ti source)</i>			
Ti-SBA-12 (80)	2	17.60	0.30
Ti-SBA-12 (50)	2	17.60	0.48
Ti-SBA-12 (40)	2	17.60	0.60
Ti-SBA-12 (30)	2	17.60	0.8 g
Ti-SBA-12 (20)	2	17.60	1.20
Ti-SBA-12 (30)	1	17.60	0.8 g
Ti-SBA-12 (30)	0.5	17.60	0.8 g
Ti-SBA-12 (30)	0.2	17.60	0.8 g
Ti-SBA-12 (30)	0.1	17.60	0.8 g
Ti-SBA-12 (30)	0.05	17.60	0.8 g
Ti-SBA-16 (80)	2	28.34	0.48
Ti-SBA-16 (50)	2	28.34	0.77
Ti-SBA-16 (40)	2	28.34	0.96
Ti-SBA-16 (30)	2	28.34	1.28
Ti-SBA-16 (20)	2	28.34	1.93
Ti-SBA-16 (30)	2	28.34	1.28
Ti-SBA-16 (30)	1	28.34	1.28
Ti-SBA-16 (30)	0.5	28.34	1.28
Ti-SBA-16 (30)	0.2	28.34	1.28
Ti-SBA-16 (30)	0.1	28.34	1.28
Ti-SBA-16 (30)	0.05	28.34	1.28

Ti-SBA-15 (20)	2	17.00	1.16
Ti-SBA-15 (30)	2	17.00	0.77
Ti-SBA-15 (40)	2	17.00	0.58

Ti-MCM-41 (20)	Basic medium	14.17	0.96
Ti-MCM-41 (30)	Basic medium	14.17	0.64
Ti-MCM-41 (40)	Basic medium	14.17	0.48

Manganese silicate molecular sieves (Manganese nitrate as a Mn source)

Mn-SBA-12 (20)	0.1	17.60	1.07
Mn-SBA-16 (80)	2	28.34	0.43
Mn-SBA-16 (50)	2	28.34	0.69
Mn-SBA-16 (40)	2	28.34	0.86
Mn-SBA-16 (30)	2	28.34	1.15
Mn-SBA-16 (20)	2	28.34	1.72

Vanadosilicate molecular sieves (Ammonium metavanadate as a V source)

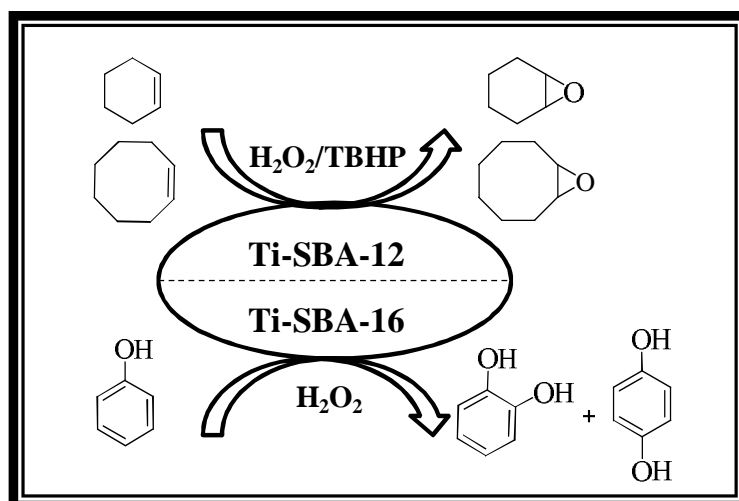
V-SBA-12 (80)	2	17.60	0.12
V-SBA-12 (50)	2	17.60	0.20
V-SBA-12 (40)	2	17.60	0.25
V-SBA-12 (30)	2	17.60	0.33
V-SBA-12 (20)	2	17.60	0.50
V-SBA-12 (30)	1	17.60	0.33
V-SBA-12 (30)	0.5	17.60	0.33
V-SBA-12 (30)	0.2	17.60	0.33
V-SBA-12 (30)	0.1	17.60	0.33

Iron silicate molecular sieve (Iron (III) chloride anhydrous as a Fe source)

Fe-SBA-12 (20)	2	17.60	0.70
----------------	---	-------	------

CHAPTER – 3

Catalytic Properties of Ti-SBA-12 & Ti-SBA-16 in Oxidation Reactions



3.1. Introduction

Oxidation is one of the important reactions in organic chemistry [1-6]. Traditionally, oxidation processes are carried out using stoichiometric amount of oxidants such as chromates, permanganates, osmium reagents, acids and peracids, which are not acceptable from environmental considerations as they are toxic/corrosive and produce large quantities of waste materials [7-10]. Selective oxidation of organic molecules using hydrogen peroxides, organic peroxides, air or molecular oxygen is a cleaner and greener approach [11]. The first example of liquid phase catalytic oxygen transfer was reported in 1936 [12(a)]. The so-called Milas reagents were formed by reaction of transition metal oxides (osmium tetroxides) with a solution of H₂O₂ in *tert.*-butanol resulting in soluble inorganic peracids [12]. These catalysts were used for the vicinal dihydroxylation of olefins. But with some transition metal oxides like MoO₃ or WO₃, selective epoxidation was observed. From these basics, a great deal of effort has been put into for developing transition metal-based homogeneous and heterogeneous catalysts for oxidation reactions [13, 14].

Titanium-containing materials have shown promise as potential catalysts in the area of selective oxidation. The best-known homogeneous Ti-catalyst is the Sharpless catalyst [15], which epoxidizes allylic alcohols with enantiomeric excess over 95% using *tert.*-butyl hydroperoxide (TBHP) as the oxidizing agent. The catalyst is prepared *in situ* from an optically active tartrate and a titanium(IV) alkoxide. The active catalyst, however, is not sufficiently stable to be stored over longer periods of time and is very sensitive to water. The first heterogeneous titanium oxidation catalyst [Ti(IV)/SiO₂] was patented by Shell Oil in 1971 for the epoxidation of propylene using organic peroxide as oxidant [16]. This catalyst was prepared by impregnating silica with TiCl₄ or an organo-titanium compound, followed by calcination. The obtained titanium catalyst was highly active but becomes a true heterogeneous catalyst only after a certain time-on-stream [17]. The titanosilicate molecular sieves with isolated tetrahedral Ti species in the zeolite framework with MFI topology (TS-1) was first synthesized by Taramasso et al. [18] at EniChem company in 1983 which was one of the major breakthroughs in the area of heterogeneous catalysis. This microporous material (TS-1) with elliptical pore openings (0.51 nm × 0.57 nm) can be used to catalyze the liquid-phase oxidation of various organic molecules in the presence of 30% aqueous hydrogen peroxide [19,

20] at mild conditions. However, the small aperture of the pores in TS-1 (~ 0.6 nm) restricts the use of this catalyst to the oxidation of small molecules. Due to the unique oxidation property of TS-1 catalyst, it has been commercialized for the industrial oxidation of phenol to dihydroxybenzenes, cyclohexanone to cyclohexanone oxime and propylene to propylene oxide [18, 21, 22]. After the discovery of microporous TS-1 catalyst, various titanium containing zeolitic molecular sieves, TS-2 or Ti-ZSM-11 (Ti-MEL) [23], Ti-ZSM-48 [24], Al-Ti- β [25], TS-12 or Ti-ZSM-12 (Ti-MTW) [26], Ti-APSO-5 [27], Ti- β (Ti-BEA) [28], Ti-SSZ-33 [29], Ti-mordenite (Ti-MOR) [30], Ti-ITQ-7 (Ti-ISV) [31], Ti-MCM-22 (Ti-MWW) [32] and Ti-MCM-68 (Ti-MSE) [33] have been synthesized by direct hydrothermal synthesis, dry-gel conversion or by post synthetic modifications for the oxidation of various organic molecules using aqueous hydrogen peroxide or alkyl hydroperoxide as oxidant. The possibilities of molecular sieves containing titanium as oxidation catalysts were extended after the synthesis of Ti- β . With micropores slightly larger than in TS-1, Ti- β can be used for the oxidation of cycloalkenes and cycloalkanes such as cyclododecane [34-36]. Nevertheless, the use of 12-membered ring Ti- β in oxidation catalysis is limited to molecules with kinetic diameters less than about 0.7 nm. The presence of aluminium in the lattice leads to certain acidity which can reduce the selectivity of the products obtained (forming diols by epoxide opening).

Oxidation of bulkier substrates requires catalysts with extra-large pores. In this context, mesoporous titanosilicate molecular sieves containing Ti ions in various structural and geometric locations have been synthesized and their physical, chemical and catalytic properties have been investigated. A few of the mesoporous titanosilicate synthesized are Ti-MCM-41 [37], Ti-HMS [38], Ti-MCM-48 [39], Ti-MSU [40], mesoporous mesophase materials (Ti-MMM) [41], Ti-SBA-15 [42], Ti-SBA-1 [43], Ti-TUD-1 [44], amorphous SiO₂-TiO₂ mixed oxides [45] and Ti-KIT-n (n = 5,6) [46]. However, mesoporous M41S-type titanosilicates are not only less stable but show lower intrinsic catalytic activity and selectivity toward the use of hydrogen peroxide in epoxidation reactions than microporous TS-1 owing to their high hydrophilicity [47, 48]. Among several, SBA-12 and SBA-16 attract attention due to their outstanding stability and three-dimensional mesopore structure [49, 50]. Ti-SBA-12 and Ti-SBA-16 are the three-dimensional, mesoporous, titanosilicates and can provide better mass transfer kinetics for bulkier molecules as compared to

the known 2-D titanosilicates [37, 42]. In this chapter, the catalytic properties of Ti-SBA-12 and Ti-SBA-16 for the oxidation of cyclic olefins (cyclohexene and cyclooctene) and hydroxylation of phenol have been investigated.

3.2. Epoxidation of Cyclic Olefins

The catalytic electrophilic addition of oxygen to the carbon-carbon double bond of alkenes in the presence of a catalyst using an oxidant is known as epoxidation. The catalytic epoxidation of cyclic olefins has been a subject of growing interest in the fundamental chemistry and modern industrial processes since epoxides are key building blocks in organic fine chemical synthesis [51]. Moreover, epoxide compounds are commercially important intermediates used in the synthesis of products such as pharmaceuticals, pesticides, epoxy paints and agrochemicals [1-6, 52, 53]. Cytochromes are highly efficient biocatalysts for their selective synthesis [54]. Their synthesis using solid catalysts instead of homogeneous catalysts is a desirable approach [46(b), 55-67]. Microporous TS-1 shows high activity and selectivity. But its application is limited to small molecular transformations. Most of the known mesoporous titanosilicates including Ti-MCM-41 and Ti-SBA-15 are less active and selective. However, silylation of the surface of Ti-MCM-41 and removal of water from the reaction media improve the catalytic activity of these materials [68, 69]. However, there is a need to develop more efficient ordered, mesoporous silica materials with Ti substituted in their framework for transformation of bulky organic molecules of pharmaceutical interest. There are a few articles in the literature on the synthesis, characterization and catalytic applications of Ti containing SBA-16 materials [70], but none of them reported the epoxidation of cyclic olefins. Development of more efficient mesoporous Ti-containing molecular sieves is a challenge for the selective epoxidation. In this chapter the application of Ti-SBA-12 and Ti-SBA-16 for the selective epoxidation of bulkier cyclic olefins (cyclohexene and cyclooctene) is investigated for the first time. The details on the synthesis and characterization of Ti-SBA-12 and Ti-SBA-16 titanosilicates have been provided in the [Chapter 2](#).

3.2.1. Experimental Section

3.2.1.1. Reaction Procedure

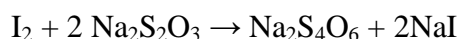
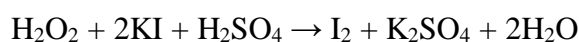
In a typical reaction, the substrate (cyclohexene or cyclooctene), solvent, catalyst and oxidizing agent were taken in a 50 mL double-necked round-bottom flask placed in a temperature-controlled oil bath and fitted with a water-cooled condenser. The reactions were conducted at a specified temperature for a desired period of time with stirring. Some reactions were also done in the absence of solvent.

3.2.1.2. Product Analysis

After completion of the reaction, the catalyst was separated by centrifugation and the liquid products were identified by GC-MS (Shimadzu GCMS-QP5050A, HP-5 column: 30 m-long x 0.25 mm i.d. x 0.25 μ m thickness) and quantified by gas chromatography (Varian 3400, CP-SIL8CB column: 30 m-long and 0.53 mm i.d.). For those reactions conducted in the absence of solvent, a specific amount of the reaction mixture was dissolved in CH_2Cl_2 and then it was analyzed in the same manner described as above.

Estimation of Peroxide Content

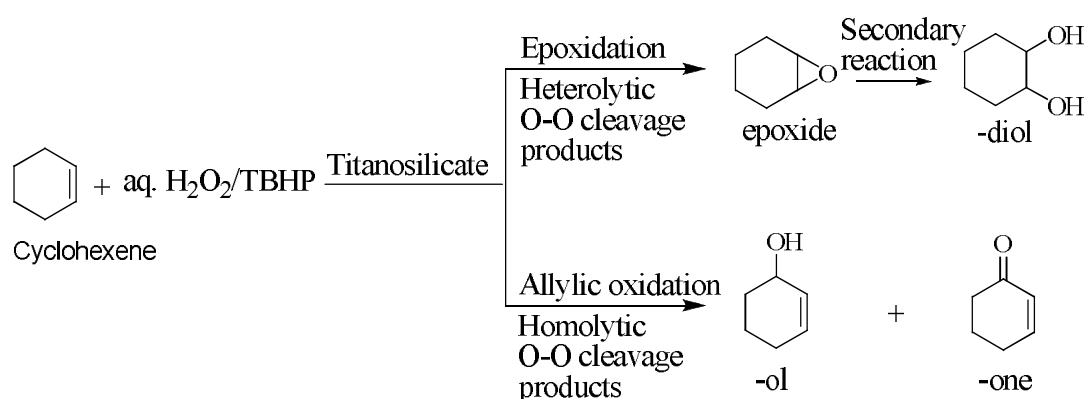
After completion of the reaction, catalyst was removed by filtration. Unreacted H_2O_2 or TBHP present in the filtrate was estimated by iodometric titration. The principle involved in the iodometric titration is that, H_2O_2 or TBHP oxidizes iodide to iodine in the presence of acid and molybdate catalyst. The iodine formed is titrated with thiosulfate solution, using starch as indicator. The reactions involved are:



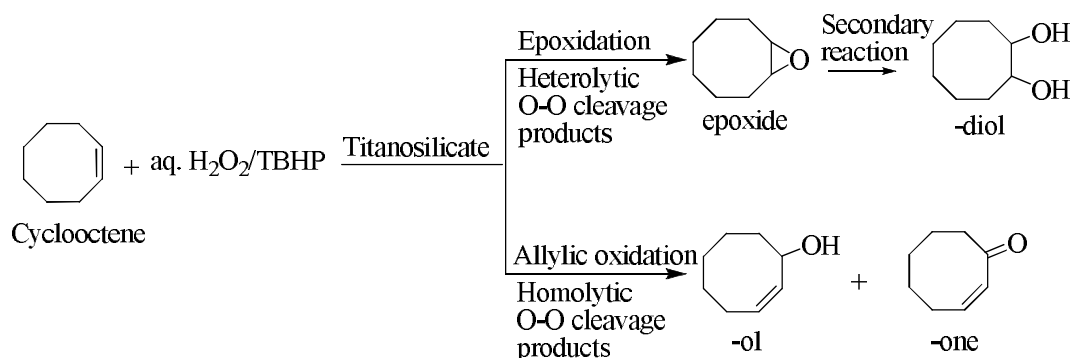
In this procedure, required chemical solutions were prepared as follows. KI solution (1% w/v) was prepared by dissolving 2 g of KI in 200 mL of double-deionized water and stored in a capped volumetric flask in a cool and dark place. The light yellow tinge of the solution (air oxidized KI to I_2) was removed by adding 1 - 2 drops of dilute sodium thiosulfate solution to it. Ammonium molybdate solution was prepared by dissolving 9 g of ammonium molybdate in 10 mL of 6 N NH_4OH . To it, 24 g of ammonium nitrate was added and the solution was diluted to 100 mL with double-distilled water. 5 N H_2SO_4 solution was prepared in a separate volumetric flask. 0.1

N sodium thiosulfate solution was prepared by dissolving 6.25 g of the salt in 250 mL of water, and standardized by titrating against potassium dichromate (0.1 N) solution.

In a typical titration, the whole reaction mixture was taken in a 100 mL volumetric flask and diluted up to the mark with deionized water. 10 mL of the diluted solution was pipetted out into the Erlenmeyer flask. To this, 20 mL of double-distilled water, 10 mL of 5 N sulfuric acid solution and 10 mL of potassium iodide solution and 2 drops of molybdate solution were added. The mixture was kept for 15-20 min in a dark place. The liberated iodine was immediately titrated against 0.1 N sodium thiosulfate solution (which was taken in a burette and already standardized with 0.1 N potassium dichromate solution) to faint yellow color. At this point, about 2 mL of freshly prepared starch indicator was added and the titration was continued until the disappearance of blue color.



Scheme 3.1. Oxidation of cyclohexene and their products



Scheme 3.2. Oxidation of cyclooctene and their products

3.2.2. Catalytic Activity

Three-dimensional mesoporous titanasilicates, Ti-SBA-12 and Ti-SBA-16 were used as catalysts for the epoxidation of cyclohexene and cyclooctene. The activity of these catalysts was compared with that of the known micro- and mesoporous titanasilicates. Influence of various reaction parameters on catalytic activity was studied.

3.2.2.1. Epoxidation of Cyclohexene

Oxidation of carbon-carbon double bond of cyclic olefins (cyclohexene and cyclooctene, for example) with peroxides yields the corresponding epoxide which upon further reaction with water produces diols (Schemes 3.1 and 3.2). Oxidation of the allylic C-H bond results in alcohol (-ol) which can get further oxidized to a ketone product (-one) [71]. Selective epoxidation over titanasilicates occur via heterolytic cleavage of the O-O bond of hydroperoxo/superoxo-Ti species. Allylic C-H bond oxidations proceed via homolytic O-O bond cleavage (Scheme 3.1 and 3.2) [72-74]. Due to differences in electronic structure, tetrapodal Ti in titanasilicates [Ti(OSi)₄] facilitate heterolytic O-O bond cleavage while the tripodal Ti sites [Ti(OH)(OSi)₃] facilitate homolytic cleavage of the O-O bond [71]. When both these species co-exist, all the four oxidation products of cyclic olefins will be formed (Scheme 3.1 and 3.2).

Table 3.1. Oxidation of Cyclohexene over Different Titanasilicates^a

Catalyst (Si/Ti)	Conv., wt% (TOF, h ⁻¹)	Product selectivity, wt%			
		Epoxide	Diol	-Ol	-One
TS-1 (33) ^b	19.2 (3)	5.9	69.3	9.7	15.1
Ti-MCM-41 (40) ^b	34.2 (7)	12.9	60.3	20.0	6.8
Ti-SBA-12 (30) ^b	93.2 (14)	17.3	33.9	34.6	14.2

^aReaction conditions: catalyst = 0.1 g, cyclohexene = 0.82 g, substrate : oxidant = 2 : 1.2, acetone = 5 mL, reaction temperature = 333 K, reaction time = 12 h. ^bOxidant = 30% aq. H₂O₂, solvent = acetone

3.2.2.1.1. Influence of Different Titanasilicates

Table 3.1 shows the effect of different titanasilicates on the catalytic activity in cyclohexene oxidation. Ti-SBA-12 with three-dimensional hexagonal mesoporous structure resulted in 93.2% conversion of cyclohexene with 30% aqueous H₂O₂ as an oxidant. Conversions of only 19.2 and 34.2% were obtained over microporous TS-1

and two-dimensional hexagonal mesoporous Ti-MCM-41, respectively (Table 3.1). The selectivity for (epoxide + diol) was, however, lower over Ti-SBA-12 (51.2%) than on TS-1 (75.2%). Ti-SBA-12, contains more tripodal Ti sites [Ti(OH)(OSi)₃] than TS-1 (Chapter 2, Fig. 2.14). These Ti species facilitate the homolytic cleavage of O—O bond in reactive oxo-Ti intermediates and thereby, the radical mechanism yielding allylic oxidation products. Catalytic activity of Ti-SBA-12 prepared by direct synthesis exhibited higher selectivity than that prepared by post-synthesis method. Oxidation reactions with 30% H₂O₂ gave very low epoxide selectivity due to simultaneous hydrolysis of epoxide into the corresponding diol product. Therefore, in the subsequent work oxidation of cyclohexene was carried out with *tert.*-butylhydroperoxide (TBHP, 5.5 M in decane and 70% in aqueous medium) as oxidant.

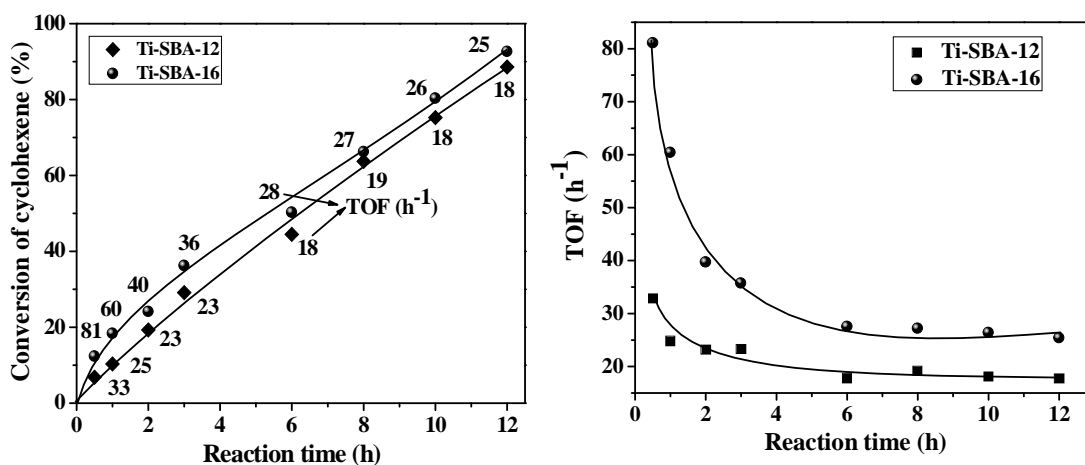


Fig. 3.1. Comparative catalytic activities of Ti-SBA-12 (Si/Ti = 30) and Ti-SBA-16 (Si/Ti = 30) in the oxidation of cyclohexene with TBHP (5.5 M in decane). Reaction conditions: catalyst = 0.1 g, cyclohexene = 0.82 g, cyclohexene: oxidant (molar ratio) = 2: 1, reaction time = 12 h, reaction temperature = 313 K, solvent (dichloromethane) = 5 mL and oxidant = 0.90 g

3.2.2.1.2. Influence of Reaction Time

Fig. 3.1 shows the effect of reaction time on the conversion of cyclohexene over Ti-SBA-12 and Ti-SBA-16. The reaction was conducted at 313 K and using dichloromethane as solvent and TBHP (5.5 M in decane) as an oxidizing agent. The conversion of the cyclohexene increased gradually with reaction time. Ti-SBA-16 (with cubic interconnected cage-like pore arrangement) was more active than Ti-SBA-12 (with hexagonal pore arrangement). It may be recalled (from ²⁹Si MAS

NMR studies) that Ti-SBA-16 is relatively more hydrophobic than Ti-SBA-12 (Chapter 2, Fig. 2.18, Table 2.5) Thus, the pore structure which controls the diffusion of reactant and product molecules and the surface structure do play important roles on the oxidation activity of titanosilicates. At 313 K and 12 h of reaction time, a cyclohexene conversion of 92.7% and 88.6% was achieved over Ti-SBA-16 and Ti-SBA-12 catalysts. The epoxide selectivity was 100% in both the cases.

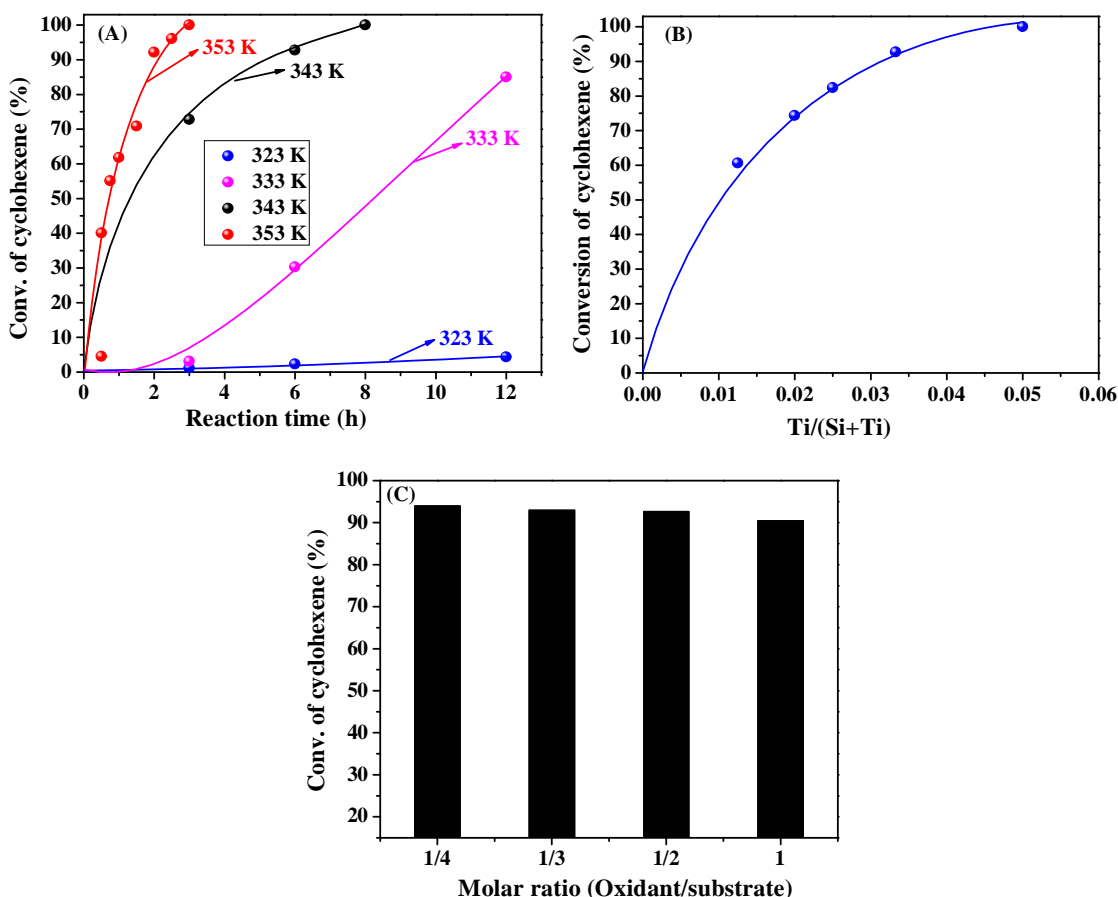


Fig. 3.2. Influence of reaction parameters on the oxidation of cyclohexene over Ti-SBA-16 (Si/Ti = 30). Reaction conditions for A: catalyst = 0.1 g, cyclohexene = 0.82 g, cyclohexene: oxidant (molar ratio) = 2: 1, solvent (dichloroethane) = 5 mL and oxidant (70% aq. TBHP) = 0.64 g. Reaction conditions for B: same as for A except that reaction time = 12 h, reaction temperature = 313 K, solvent (dichloromethane) = 5 mL and oxidant (TBHP, 5.5 M in decane) = 0.90 g. Reaction conditions for C: same as for A except that oxidant: cyclohexene (molar ratio) = 0.25–1, reaction time = 12 h, reaction temperature = 313 K, solvent (dichloromethane) = 5 mL, oxidant (TBHP, 5.5 M in decane) = 0.45–1.80 g

3.2.2.1.3. Influence of Reaction Temperature, Si/Ti and Oxidant/Substrate Molar Ratio

The influence of reaction parameters on the oxidation of cyclohexene is depicted in Fig. 3.2. With increasing Ti/(Si + Ti) ratio, the activity of the catalyst increased and this increase was more significant for the change in molar ratio from 0.01 to 0.033 than beyond that. When the TBHP to substrate ratio was increased from 0.25 to 1, a decrease in conversion from near 100 to 90% was observed. Some part of TBHP got decomposed when it was taken in stoichiometric ratios than in the oxidant depleting conditions. Temperature has a major effect on the reaction. While it took more than 12 h at 333 K, a shorter period of time (~3 h) itself is enough to get complete conversion of cyclohexene to its epoxide when the reaction was carried out at 353 K. Such high conversions and epoxide selectivities have not been reported so far over earlier known titanosilicate catalysts. A linear correlation was observed between catalytic activity and the content of framework, tetrahedral Ti ions (Fig. 3.3).

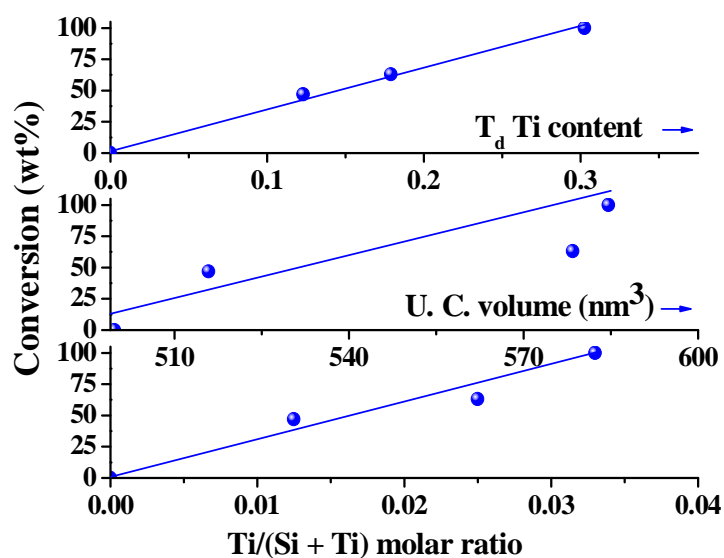


Fig. 3.3. Correlation of catalytic activity (cyclohexene conversion) with variation in molar ratio of Ti, unit cell volume (XRD) and area of tetrahedral Ti (diffuse reflectance UV-visible spectroscopy). Reaction conditions: catalyst = 0.1 g, cyclohexene = 0.82 g, oxidant = 5.5 M TBHP in decane = 0.90 g, substrate to oxidant molar ratio = 2, solvent = dichloromethane (5 mL), reaction temperature = 333 K, and reaction time = 12 h

3.2.2.1.4. Influence of Solvent and Oxidant

Solvent and the nature of oxidant (70% aq. TBHP verses 5.5 M TBHP in decane) showed a remarkable effect on the oxidation reactions over Ti-SBA-12 and Ti-SBA-16 (Table 3.2). These reactions did not occur in the absence of a catalyst. Conversions were higher while using 5.5 M TBHP in decane than with 70% aq. TBHP. This difference is more apparent in the case of Ti-SBA-12 than with hydrophobic Ti-SBA-16 catalyst (Table 3.2). The relative ordering of catalytic activity in different solvents decreased in the order: $\text{CH}_2\text{Cl}_2 > \text{CHCl}_3 > (\text{CH}_2)_2\text{Cl}_2 > \text{C}_6\text{H}_5\text{CH}_3 > \text{CH}_3\text{COCH}_3 > \text{CH}_3\text{CN} > \text{CH}_3\text{OH}$. The lower activity with acetonitrile and methanol solvents is perhaps due to higher competitive adsorption of these solvents (than the other solvents) on the catalyst surface. The conversion of cyclohexene increased with decreasing amount of the solvent in the reaction medium. Cyclohexene conversion and epoxide selectivity were 100% when the reaction was conducted in the absence of solvent (Table 3.3). Reactions over Ti-MCM-41 had showed a similar trend in cyclohexene conversion. But, in terms of intrinsic activity (TOF) and TBHP efficiency, Ti-SBA-16 was found superior to Ti-SBA-12 and Ti-MCM-41 (Table 3.3).

3.2.2.2. Epoxidation of Cyclooctene

Table 3.4 shows the oxidation of cyclooctene with aqueous and non-aqueous peroxides over Ti-SBA-12 and Ti-SBA-16 catalysts. Cyclooctene is a bulkier cyclic olefin and it could be converted into its epoxide with high efficiency (Table 3.4). Solvent and the nature of the oxidant (30% aq. H_2O_2 , 70% aq. TBHP verses 5.5 M TBHP in decane) influenced even this oxidation reaction. The reaction goes more effectively when 5.5 M TBHP was used as oxidant. Dichloromethane was found to be the best solvent when 70% aq. TBHP and 5.5 M TBHP in decane was used as oxidant. Cyclooctene oxide formed with 100% selectivity. The conversion of cyclooctene was 92% and 87% in CH_2Cl_2 solvent by using 5.5 M TBHP as oxidant over Ti-SBA-16 and Ti-SBA-12 catalysts, respectively. It was only 45% (over Ti-SBA-16) and 44% (over Ti-SBA-12) with 70% aq. TBHP. Reactions with 30% aqueous H_2O_2 showed poor results, only 2.6% conversion of cyclooctene was

Table 3.2. Influence of Solvent, Oxidant and Silica Structure on the Oxidation of Cyclohexene^a

Solvent	Ti-SBA-12				Ti-SBA-16			
	TBHP (70%, aqueous)		TBHP (5.5 M, decane)		TBHP (70%, aqueous)		TBHP (5.5 M, decane)	
	Conversion (wt%)	TOF (h ⁻¹)	Conversion (wt%)	TOF (h ⁻¹)	Conversion (wt%)	TOF (h ⁻¹)	Conversion (wt%)	TOF (h ⁻¹)
Dichloromethane	80.4	16	90.6	18	92.1	25	92.7	25
Chloroform	74.1	15	88.2	18	90.0	25	91.6	25
1,2-Dichloroethane	60.5	12	84.7	17	85.0	23	90.0	25
Toluene	49.6	10	78.0	15	70.5	19	82.4	23
Acetone	46.0	9	72.4	14	33.8	9	76.0	21
Acetonitrile	27.3	5	44.8	9	30.6	8	62.2	17
Methanol	5.0	1	7.1	1	6.5	2	8.1	2

^aReaction conditions: catalyst (Ti-SBA-12 or Ti-SBA-16, input Si/Ti = 30) = 0.1 g, cyclohexene = 0.82 g, cyclohexene: oxidant (molar ratio) = 2: 1, solvent = 5 mL, reaction time = 12 h, reaction temperature = 313 K (for dichloromethane) and 333 K (rest of the solvents). Conversion = theoretical conversion of cyclohexene. Epoxide selectivity = 100%. Turnover frequency (TOF) = moles of cyclohexene converted per mole of Ti (output) in the catalyst per hour

Table 3.3. Influence of Amount of Solvent on the Oxidation of Cyclohexene with TBHP (5.5 M in Decane)^a

Catalyst (Si/Ti, output)	Amount of solvent (CH ₂ Cl ₂ in mL)	Conversion (wt%)		TOF (h ⁻¹)	TBHP efficiency (%)	Product selectivity (wt%)			
		Cyclohexene	TBHP			epoxide	-diol	-ol	-one
Ti-SBA-12 (39.1)	5	90.6	96	18	94.4	100	-	-	-
	3	93.8	97	19	96.7	100	-	-	-
	1	94.7	98	19	96.6	100	-	-	-
	0	100	100	20	100.0	100	-	-	-
Ti-SBA-16 (53.8)	5	92.7	97	25	95.6	100	-	-	-
	3	94.1	98	26	96.0	100	-	-	-
	1	98.7	100	27	98.7	100	-	-	-
	0	100	100	27	100.0	100	-	-	-
Ti-MCM-41 (33)	5	87.6	94	15	93.2	95.0	-	3.0	2.0
	3	90.3	96	15	94.1	93.2	-	2.9	3.9
	1	92.4	98	16	94.3	92.6	-	2.7	4.7
	0	95.0	100	16	95.0	91.0	-	2.5	6.5

^aReaction conditions: catalyst = 0.1 g, cyclohexene = 0.82 g, cyclohexene: oxidant (molar ratio) = 2: 1, reaction time = 12 h, reaction temperature = 313 K, reaction time = 12 h. TBHP conversion was determined by iodometric titrations. Cyclohexene conversion (theoretical value). Turnover frequency (TOF) = moles of cyclohexene converted per mole of Ti (output) in the catalyst per hour. TBHP efficiency = (moles of oxidation products of cyclohexene formed/moles of TBHP consumed) × 100

obtained over Ti-SBA-12 catalyst with dichloromethane as a solvent. 7.8% conversion of cyclooctene was obtained with 30% aqueous H₂O₂ by using acetonitrile as a polar solvent over Ti-SBA-12.

Solvents are usually used to keep both reactants and products in a single phase. Apart from enabling the proper mixing of the reactants, solvents are known to affect conversions and product selectivities through interaction with the active sites and the transition state. Atoguchi and Yao [75] investigated the effect of solvents (various mixtures of H₂O and CH₃OH) on the oxidation of phenol catalyzed by TS-1 both experimentally and by DFT calculations. Water addition to methanol increased the dielectric constant of the reaction medium and accelerated the catalytic oxidation of phenol. Solvents can influence the reactivity of the hydroperoxo-Ti species. In solvents with high dielectric constants, the heterolytic cleavage of the O-O bond is probably dominant when the partially or totally ionic intermediates are stabilized by the solvent. Wu and Tatsumi [76] reported the influence of solvents of varying polarity on the epoxidation of allyl alcohol catalyzed by TS-1, Ti-beta and Ti-MWW. In the present case the reactions did go well in the presence of solvents with low polarity and low to moderate dielectric constant. The surface structure and pore architecture of Ti-SBA-12 and Ti-SBA-16 and the relative adsorption capacity of reactant as against the solvent play a dominant role on the oxidation of cyclic olefins over the present catalysts.

3.2.2.3. Tentative Reaction Mechanism

Fig.3.4 shows the tentative reaction mechanism of oxidation of cyclic olefins (cyclohexene and cyclooctene, for example) with hydrogen peroxide or alkyl hydroperoxide over mesoporous titanosilicates (Ti-SBA-12 and Ti-SBA-16). Titanosilicates form hydroperoxo/superoxo-Ti species when they react with H₂O₂ or alkylhydroperoxide. The formation of superoxo-Ti species on titanosilicates (TS-1, Ti-MCM-41, Ti-SBA-12 and Ti-SBA-16) in the presence of H₂O₂ or alkylhydroperoxide have been identified by EPR spectroscopy and have been discussed in Chapter 2 (Fig. 2.14). The breaking of the O-O bond in hydroperoxo/superoxo-Ti species plays a crucial role in the oxidation reactions in determining the product pattern. Electron-donating or withdrawing ligands either on the Ti atom (such as OSi, OH, or H₂O) or the peroxy moiety (such as the alkyl group in TBHP) can influence the scission of the O-O bond.

Table 3.4. Oxidation of Cyclooctene: Influence of Reaction Conditions^a

Solvent	Ti-SBA-12		Ti-SBA-16						
	H ₂ O ₂ (30%, aqueous)	TBHP (70%, aqueous)		TBHP (5.5 M, decane)		TBHP (70%, aqueous)		TBHP (5.5 M, decane)	
	Conv. (wt%)	Conv. (wt%)	TOF (h ⁻¹)	Conv. (wt%)	TOF (h ⁻¹)	Conv. (wt%)	TOF (h ⁻¹)	Conv. (wt%)	TOF (h ⁻¹)
Dichloromethane	2.6	44.0	4	87.0	9.0	45.0	6	92.0	13
Chloroform	2.1	43.1	4	82.5	8	43.3	6	87.0	12
1,2-Dichloroethane	5.4	39.0	4	76.8	8	33.7	5	79.5	11
Toluene	-	36.5	4	66.1	6	29.3	4	66.7	9
Acetone	-	42.9	4	48.5	5	32.0	4	40.8	6
Acetonitrile	7.8	39.4	4	40.2	4	27.7	3	33.2	4
Methanol	-	5.5	1	6.0	1	5.0	1	13.7	2

^aReaction conditions: catalyst (Ti-SBA-12 or Ti-SBA-16, input Si/Ti = 30) = 0.1 g, cyclooctene = 1.1 g, cyclooctene: oxidant (molar ratio) = 2: 1, solvent = 10 mL, reaction time = 24 h, reaction temp.= 313 K (for dichloromethane) and 333 K (rest of solvents). Conversion = theoretical conversion of cyclooctene. Epoxide selectivity = 100%. Turnover frequency (TOF) = moles of cyclooctene converted per mole of Ti (output) in the catalyst per hour

In other words, the type of Ti site (tetra-, tripodal, etc.) or oxidant (H_2O_2 , TBHP) influences the homolytic vs. heterolytic cleavage. The open structured, tripodal titanium sites form penta- or hexa-coordinated species such as $[\text{Ti}(\text{OSi})_3(\text{H}_2\text{O})_2(\text{OH})]$ more easily than the closed tetrapodal Ti structures. The coordinated water and OH groups enhance electron density at Ti center and the O–O bond, favoring homolytic O–O bond cleavage and $\cdot\text{OH}$ radical formation. In cycloalkenes, homolytic O–O bond cleavage favors non-selective allylic C–H bond oxidation resulting in alcohol (-ol) which can get further oxidized to a ketone product (-one) [72]. Tetrapodal Ti in titanasilicates $[\text{Ti}(\text{OSi})_4]$ with less electron density at Ti center as compared to tripodal Ti sites $[\text{Ti}(\text{OH})(\text{OSi})_3]$ favors the heterolytic O–O cleavage. Ionic species (^+OH) species are the reactive species in this cleavage and act as electrophile and susceptible to attack by nucleophile (in cycloalkenes carbon-carbon double bond acting as nucleophile) resulting in the epoxide formation which can further get converted into diol in the presence of water (while using aqueous peroxides as oxidants) in the reaction medium. When both the tripodal and tetrapodal sites co-exist, all the four oxidation products of cyclic olefins will be formed (Scheme 3.1 and 3.2) [72].

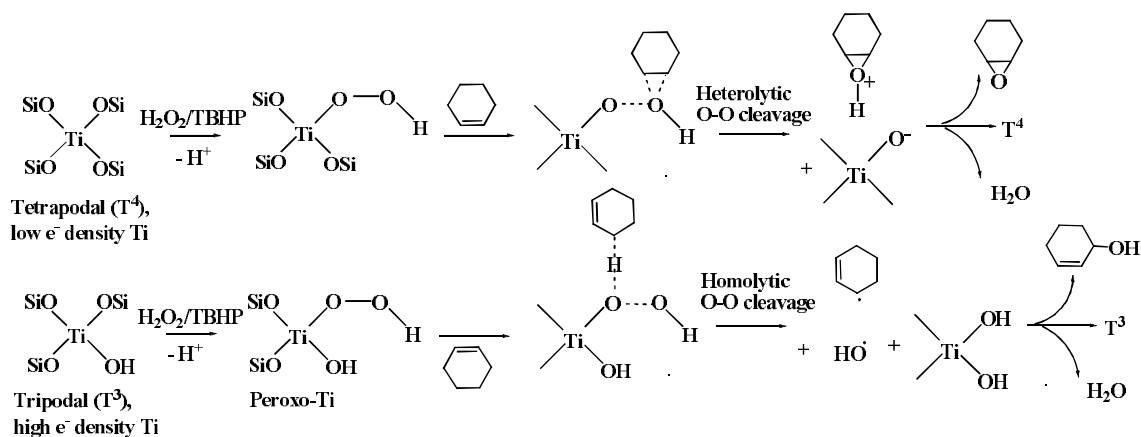
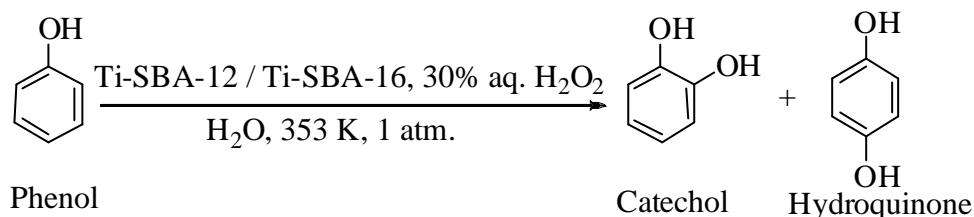


Fig. 3.4. Tentative mechanism of oxidation of cyclic olefins over Ti-SBA-12 and Ti-SBA-16 catalysts

3.3. Hydroxylation of Phenol

Hydroxylation of phenol is an industrially important reaction as the product diphenols, *viz.*, catechol and hydroquinone (Scheme 3.3), are widely used as

photography chemicals, antioxidants, polymerization inhibitors, flavouring agents and drug intermediates [77].



Scheme 3.3. Hydroxylation of phenol and their products

Since the 1970's, phenol hydroxylation has been widely investigated using various homogeneous and heterogeneous catalysts. In *Brichima process* (now EniChem, Italy) [78, 79], the salts of Fe^{2+} and Co^{2+} are used as catalysts for phenol hydroxylation using 60% aqueous H_2O_2 as oxidizing agent. In the *Rhône-Poulenc process* [80, 81], strong mineral acids such as phosphoric acid and catalytic amount of perchloric acid are employed with 70% aqueous H_2O_2 . In the *Hamilton process* [82], Fenton reagent is used as a catalyst. In the *Ube-Rhone-Poulenc process* [83], this reaction is carried out with ketone peroxides (α -hydroxy hydroperoxides) formed *in situ* from a ketone and 60% aqueous H_2O_2 in the presence of an acid catalyst (sulphuric or sulphonic acid). But these homogeneous catalysts are difficult to separate and recover from the reaction mixture. Heterogeneous catalysts are particularly attractive in the hydroxylation of phenol due to their engineering and catalyst reusability advantages. Since the discovery of TS-1 molecular sieves by Taramasso et al. [18] in 1983, TS-1 has been widely investigated due to its remarkable catalytic activity for oxidation reactions at mild conditions using aqueous hydrogen peroxide as oxidant [19, 20]. Hydroxylation of phenol catalyzed by TS-1 and TS-2 using 30% aqueous H_2O_2 as the oxidant created an environmentally benign route for the production of catechol and hydroquinone [84-88]. The hydroxylation of phenol to catechol and hydroquinone has already been commercialized by EniChem, Italy in 1986. The application of microporous titanasilicate is, however, limited to molecules with smaller dimensions due to inherent constraints on pore size (0.54 nm). Mesoporous M41S-type titanosilicates are less stable and also show a lower intrinsic catalytic activity and selectivity toward the use of H_2O_2 in phenol hydroxylation [20]. Hence, there is a need to develop more efficient, ordered

mesoporous silica materials with Ti substituted in their framework for transformation of bulky organic molecules of pharmaceutical interest.

In this chapter, liquid phase hydroxylation of phenol with 30% H₂O₂ catalyzed by three-dimensional, mesoporous, Ti-SBA-12 and Ti-SBA-16 titanasilicate is presented.

3.3.1. Experimental Section

3.3.1.1. Reaction procedure

Liquid phase hydroxylation of phenol was carried out in a 50 mL glass round-bottom flask fitted with a water-cooled condenser and placed in a temperature-controlled oil bath. In a typical reaction, 10 mmol (0.94 g) of phenol, 10 mL of distilled water and 0.1 g of catalyst were taken in the glass reactor. To it, a known quantity of 30% aqueous H₂O₂ was added in one lot. The temperature of the reaction mixture was raised to a specific value and the reaction was conducted while stirring for a desired period of time.

3.3.1.2. Product Analysis

The progress of the reaction was monitored by gas chromatographic technique (GC - Varian 3400; CP-SIL8CB column; 30 m-long and 0.53 mm-i.d.). Prior to GC analysis, solid catalyst particles, if any, in the aliquot sample were removed by centrifugation followed by filtration. Solvent (water) was separated by treating the liquid portion of the reaction mixture with diethyl ether. Unreacted phenol and the oxidation products remained in the ether layer, which were then separated. Ether was distilled out under reduced pressure using a rotavapor. The reaction mixture thus recovered was diluted with a known quantity of methanol and analyzed by GC. Identification of the products was done by GC-MS (Varian CP-3800; 30 m-long, 0.25 mm-i.d., and 0.25 µm-thick CP-Sil8CB capillary column) and by comparing with the standard samples. A typical mass balance of greater than 98% was obtained.

3.3.2. Catalytic Activity

Liquid phase hydroxylation of phenol was carried out in the presence of Ti-SBA-12 and Ti-SBA-16 catalysts using 30% aqueous H₂O₂ as oxidant (Tables 3.5–3.7). Catechol (CAT) and hydroquinone (HQ) were the only products formed in the hydroxylation reaction (Scheme 3.3). Surprisingly, benzoquinones, the over

oxidation products, were not detected. The reaction occurred in the presence of water as solvent. Controlled experiments confirmed that no reaction takes place without a catalyst under same reaction conditions. Also no reaction was detected when all-silica SBA-12 and SBA-16 or bulk TiO₂ (Ti in octahedral geometry) was used as a catalyst in place of Ti-SBA-12 and Ti-SBA-16. All these observations reveal that isolated Ti with pseudo tetrahedral geometry present in framework positions of Ti-SBA-12 and Ti-SBA-16 are the active sites for the hydroxylation reaction to occur.

3.3.2.1. Influence of Si/Ti Molar Ratio

In general, the catalytic activity (phenol conversion) increased with increasing Ti content (i.e., decreasing Si/Ti molar ratio) for both Ti-SBA-12 and Ti-SBA-16 catalysts (Table 3.5). Except for Si/Ti = 80, the intrinsic catalytic activity (phenol conversion or TOF) of Ti-SBA-12 is double than that of Ti-SBA-16. Based on stoichiometry, one expects a HQ/CAT product molar ratio of about 0.5 in the reaction. In fact, this is, actually, the case with Ti-SBA-16. Ti-SBA-12 was found to be a *para*-selective catalyst. HQ/CAT molar ratio in the case of Ti-SBA-12 was in the range 0.67 - 1.14. The higher amount of *para*-product formation suggests that the extent of reaction is occurring mainly in the mesopores of Ti-SBA-12 than on the external particle surface. This conclusion on shape selectivity is made in line with the similarities observed in the case of *para*-selective TS-1 catalyst for the hydroxylation of phenol [20, 84-90]. H₂O₂ selectivity is nearly the same (~ 90 mol%) irrespective of Ti content in the catalyst. This is because the Ti ions are isolated even at higher concentrations. The small amount of anatase-like TiO₂ present in Ti-SBA-12 at Si/Ti ≤ 50 hardly influenced the decomposition of H₂O₂. Irrespective of Si/Ti molar ratio, the TOF values are nearly the same.

3.3.2.2. Influence of Reaction Time and Temperature

Fig. 3.5 shows the effect of reaction time and temperature on phenol conversion. Phenol hydroxylation reaction were conducted over Ti-SBA-12 (Si/Ti = 20) catalyst at four different temperatures (333, 343, 353 and 363 K). As seen from Fig. 3.5, temperature has a marked effect on phenol hydroxylation activity. Phenol conversion increased with increasing reaction time and temperature. Phenol conversion of 16.7, 21.7, 24.1 and 26.5% was obtained at different reaction temperatures 333, 343, 353 and 363 K in 24 h, respectively. The HQ/CAT selectivity has also increased with temperature (Fig. 3.5).

Table 3.5. Hydroxylation of Phenol over Ti-SBA-12 and Ti-SBA-16 Catalysts: Influence of Si/Ti Molar Ratio^a

Si/Ti molar ratio ^b	Ti-SBA-12						Ti-SBA-16					
	Phenol conv. (mol%)	H ₂ O ₂ efficiency (mol%) ^c	Product (mol%)		selectivity HQ/ CAT	TOF (h ⁻¹) ^d	Phenol conv. (mol%)	H ₂ O ₂ efficiency (mol%) ^c	Product selectivity (mol%)			TOF (h ⁻¹) ^d
			CAT	HQ					CAT	HQ	HQ/ CAT	
20	24.1	90.3	47.1	53.9	1.1	2.8	13.3	90.0	66.0	34.0	0.5	1.3
30	16.7	87.0	56.0	44.0	0.8	2.6	10.2	91.2	64.3	35.7	0.6	1.4
40	11.7	92.1	59.0	41.0	0.7	2.0	8.4	89.7	70.0	30.0	0.4	1.5
50	14.0	89.2	52.1	47.9	0.9	2.8	7.9	90.1	66.7	33.3	0.5	1.6
80	6.7	93.0	59.7	40.3	0.7	2.4	8.1	92.8	71.8	28.2	0.4	3.1

^aReaction conditions: catalyst (prepared using 2 M HCl) = 0.1 g, phenol = 0.94 g (10 mmol), oxidant = 30 wt% aqueous H₂O₂ (0.37 g), phenol/H₂O₂ (molar ratio) = 3, solvent = water (10 mL), reaction temperature = 353 K, reaction time = 24 h; CAT = catechol, HQ = hydroquinone. ^bValues in parenthesis are output molar ratios for Ti-SBA-12 and Ti-SBA-16, respectively. ^cH₂O₂ efficiency determined by means of iodometric titrations. H₂O₂ efficiency = (moles of hydroxylation products of phenol formed/moles of H₂O₂ consumed) × 100. ^dTurnover frequency (TOF) = moles of phenol converted per mole of Ti (output) in the catalyst per hour

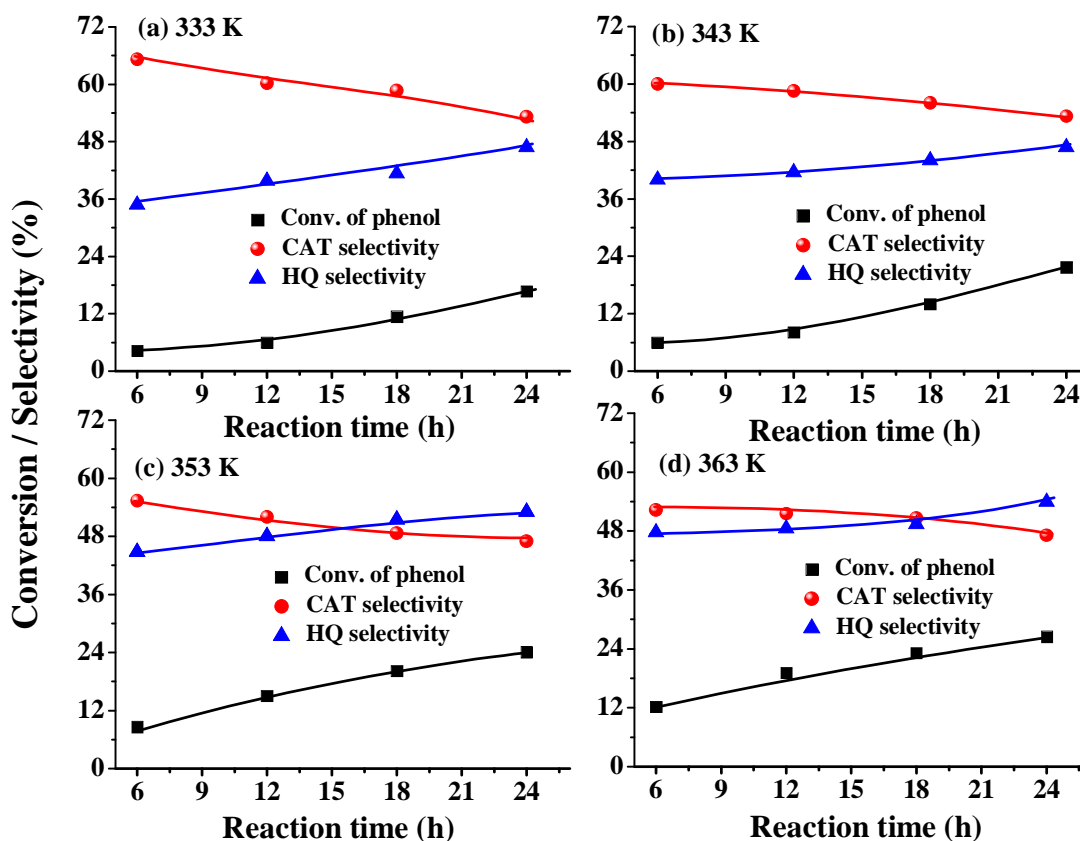


Fig. 3.5. Effect of reaction time and temperature on phenol conversion and products selectivity. Reaction conditions: catalyst = 0.1 g [Ti-SBA-12 (Si/Ti = 20)], phenol = 10 mmol (0.94 g), oxidant = 30% aqueous H_2O_2 (0.37 g), phenol/ H_2O_2 (molar ratio) = 3 and solvent = water (10 mL). CAT = catechol and HQ = hydroquinone

3.3.2.3. Influence of Catalyst and Oxidant Amount

The influences of catalyst/phenol (wt/mol) and phenol/ H_2O_2 (mol/mol) ratios on phenol hydroxylation activity are provided in Table 3.6. Phenol conversion increased with increasing amount of the catalyst. With increasing H_2O_2 amount, the conversion of phenol increased while HQ/CAT molar ratio had decreased. H_2O_2 efficiency was lower at higher amount of oxidant concentrations as a part of the oxidant decomposed into water and molecular oxygen.

Table 3.6. Influence of Catalyst and Oxidant Amounts on the Hydroxylation of Phenol over Ti-SBA-12

Catalyst/phenol (g.mol ⁻¹) ^a	Phenol conv. (mol%)	Product selectivity (mol%)			TOF (h ⁻¹) ^c
		CAT	HQ	HQ/CAT	
5	4.8	57.5	42.5	0.7	4.4
10	8.6	52.3	47.7	0.9	3.9
15	10.2	51.0	49.0	1.0	3.1
20	11.8	50.4	49.6	1.0	2.7
Phenol/H ₂ O ₂ (molar ratio) ^b					
4	15.1	44.1	55.9	1.3	1.7
3	24.1	47.1	53.9	1.1	2.8
2	31.2	46.5	53.5	1.2	3.6
1	55.0	57.0	43.0	0.8	6.3

^aReaction conditions: catalyst = Ti-SBA-12 (Si/Ti = 20, 2 M; 0.1 g), phenol = 0.94 g (10 mmol), oxidant = 30 wt% aqueous H₂O₂, phenol/H₂O₂ (molar ratio) = 3, solvent = water (10 mL), reaction temperature = 353 K, reaction time = 6 h, CAT = Catechol, HQ = Hydroquinone. ^bReaction conditions: same as those of *a* except for phenol/H₂O₂ (molar ratio) = 1 to 4 and reaction time = 24 h. ^cTurnover frequency (TOF) = moles of phenol converted per mole of Ti (output) in the catalyst per hour

3.3.2.4. Comparative Catalytic Activity of Ti-SBA-12 and Ti-SBA-16

A comparison of catalytic activity of mesoporous Ti-SBA-12 and microporous TS-1 is reported in Table 3.7. The reaction was conducted with phenol/H₂O₂ molar ratio of 3. Under these conditions, for 100% of H₂O₂ consumption, one would get 33.3 mol% of phenol conversion with HQ and CAT as the only products. As seen from Table 3.7, a phenol conversion of 31 mol% was obtained in just 12 h over TS-1 while Ti-SBA-12 required more than 24 h for such a phenol conversion. In other words, the initial rate of reaction and intrinsic catalytic activity (TOF) of TS-1 is higher than that of Ti-SBA-12. A similar observation was also found with other mesoporous titanosilicates like Ti-MCM-41 [20]. Clerici et al. [91] proposed that the intrinsic activity of titanium sites declines progressively with increasing pore diameter. It is interesting to note that at similar conversions, the

Table 3.7. Comparative Catalytic Activity Data of Ti-SBA-12 and TS-1 for the Hydroxylation of Phenol^a

Reaction time (h)	Ti-SBA-12					TS-1				
	Phenol conv. (mol%)	Product selectivity (mol%)			TOF (h ⁻¹) ^b	Phenol conv. (mol%)	Product selectivity (mol%)			TOF (h ⁻¹) ^b
		CAT	HQ	HQ/CAT			CAT	HQ	HQ/CAT	
1	-	-	-	-	-	6.0	70.5	29.5	0.4	11.9
3	4.8	55.0	45.0	0.8	4.4	21.7	60.0	40.0	0.7	14.3
6	8.6	52.3	47.7	0.9	3.9	26.7	56.7	43.3	0.8	8.8
12	15.0	51.5	48.5	0.9	3.4	31.0	52.3	47.3	0.9	5.1
18	20.2	50.6	49.4	1.0	3.1	31.4	52.4	48.6	0.9	3.5
24	24.1	47.1	53.9	1.1	2.8	32.0	48.0	52.0	1.1	2.6

^aReaction conditions: catalyst, Ti-SBA-12 (Si/Ti = 20, 2 M) and TS-1 (Si/Ti = 30) = 0.1 g, phenol = 0.94 g (10 mmol), oxidant = 30 wt% aqueous H₂O₂ (0.37 g), phenol/H₂O₂ (molar ratio) = 3, solvent = water (10 mL), reaction temperature = 353 K, CAT = catechol, HQ = hydroquinone. ^bTurnover frequency (TOF) = moles of phenol converted per mole of Ti (output) in the catalyst per hour

HQ/CAT selectivity is higher over Ti-SBA-12 than over TS-1 (Fig. 3.6, right panel). A systematic increase in HQ/CAT selectivity with increasing phenol conversion was observed on both TS-1 and Ti-SBA-12. Such an interesting variation was not found in the case of Ti-SBA-16 (Fig. 3.6, left panel).

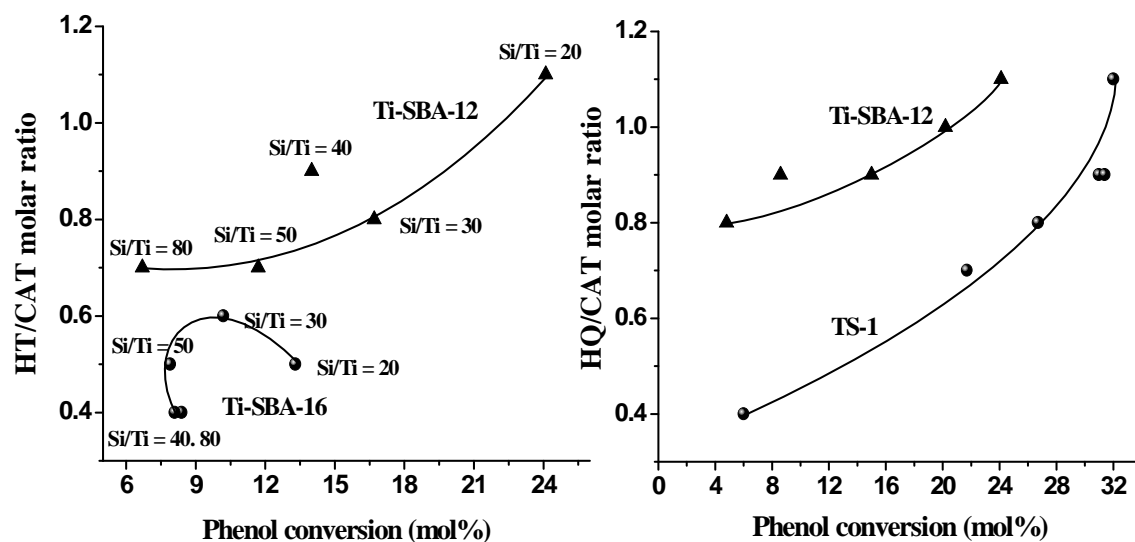


Fig. 3.6. Variation of HQ/CAT molar ratio as a function of phenol conversion: (Left) for Ti-SBA-12 and Ti-SBA-16, data and reaction conditions taken from Table 3.5 and (Right) for Ti-SBA-12 and TS-1, data and reaction conditions taken from Table 3.7.

3.3.2.5. Catalyst Reusability Study

The reusability of Ti-SBA-12 (Si/Ti = 20) was studied in five recycling experiments. At the end of each run, the catalyst was separated by centrifugation, dried at 373 K for 4 h and then reused in a subsequent recycle experiment. As seen from Fig. 3.7, Ti-SBA-12 is quite stable even after the 5th recycle. No loss in phenol conversion and variation in product selectivity were detected. The spent Ti-SBA-12 catalyst (after the 5th recycle) was characterized by ICP-OES, XRD, thermal analysis and FTIR. No loss in Ti content was detected in the reused catalyst (ICP-OES). While the XRD pattern of the reused catalyst is nearly the same as that of a fresh catalyst, a decrease in intensity of the XRD peaks with a back ground signal below 1.5° becoming more prominent was observed (Fig. 3.8). In thermal analysis, the spent catalyst (at the end of 5th recycle) showed an additional weight loss of 40% in the temperature range of 450 – 900 K. FTIR spectrum of the reused catalyst showed

additional bands at around 1100 and 1600 cm^{-1} and a broad band at 3300 – 3450 cm^{-1} corresponding to the characteristic peaks of the product dihydroxybenzenes (Fig. 3.8). In spite of this adherence of product molecules, the spent catalyst showed activity similar to that of a fresh catalyst. The active Ti sites are not buried or obscured by the adsorbed product molecules.

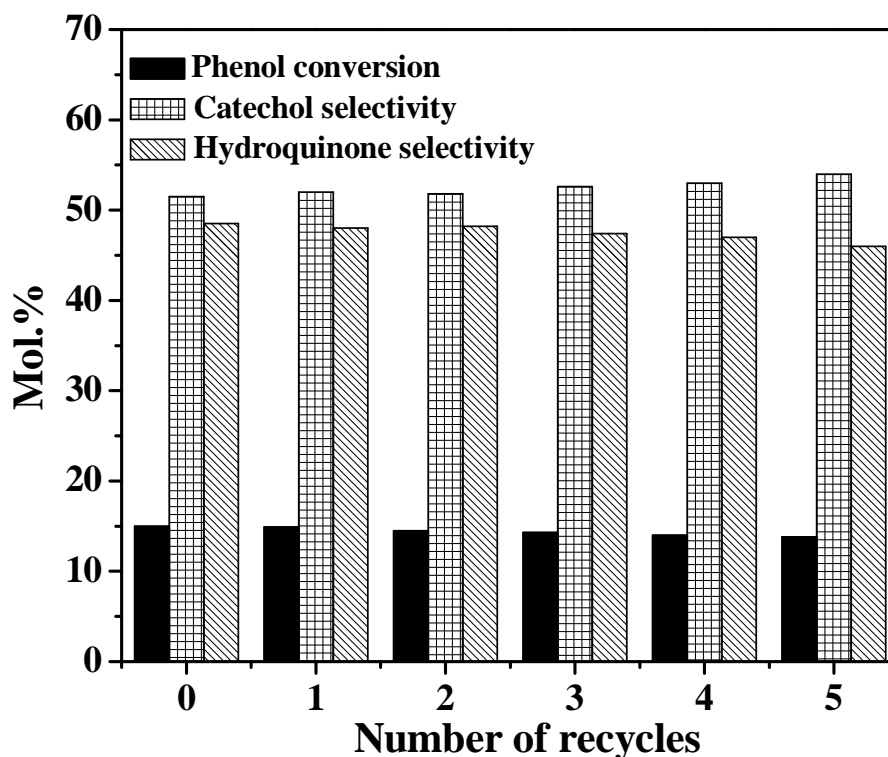


Fig. 3.7. Catalyst reusability study in the hydroxylation of phenol. Reaction conditions: catalyst = 0.1 g [Ti-SBA-12 (Si/Ti = 20)], phenol = 10 mmol, oxidant = 30 wt% aqueous H_2O_2 (0.37 g), phenol/ H_2O_2 (molar ratio) = 3, solvent = water (10 mL), reaction temperature = 353 K, and reaction time = 12 h

It is interesting to note that with microporous TS-1 catalyst, about 30% weight gain due to adsorption of product molecules was observed at the end of one reuse itself. However, the weight gain in the case of mesoporous titanosilicate catalyst of the present study at the end of one recycle was lower by nearly four times to that of TS-1 catalyst. Although the intrinsic catalytic activity is lower, mesoporosity of Ti-SBA-12 enables prolonged usage of the catalyst. Thus, the three-dimensional pore structure benefits in the catalytic applications by reducing the pore-blockage and prolonging the catalyst life.

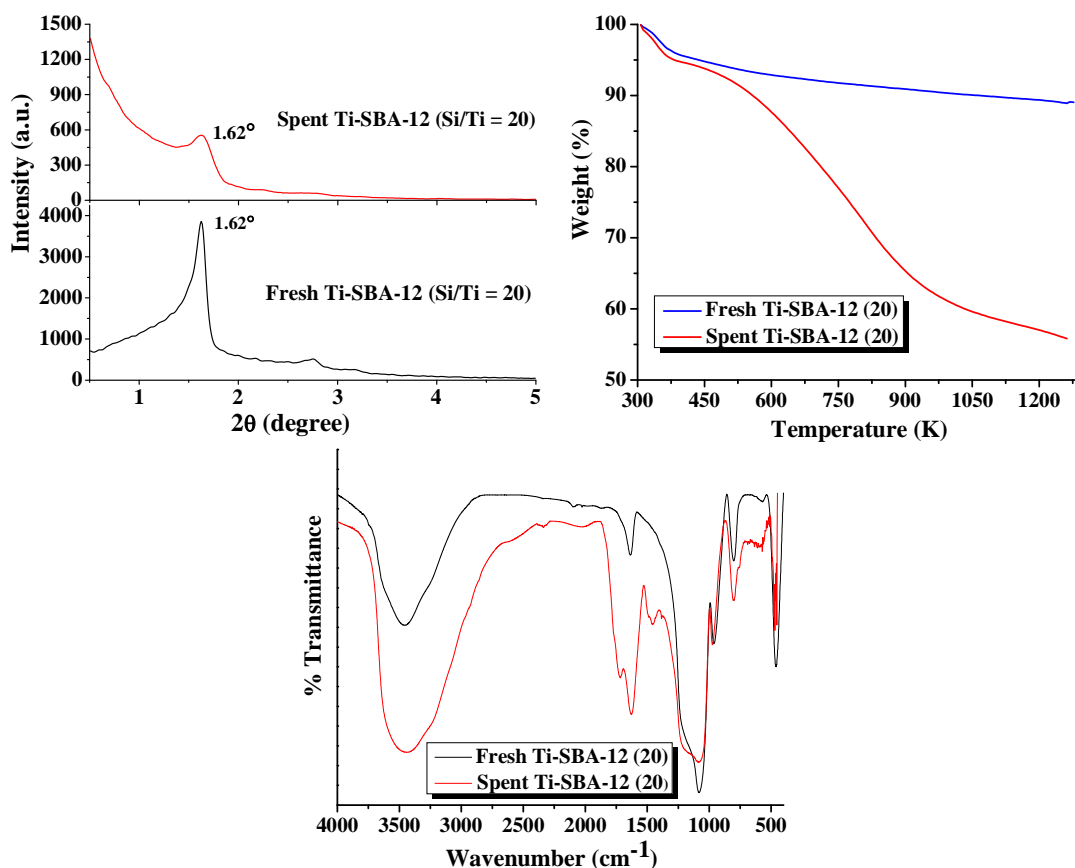


Fig. 3.8. Low-angle X-ray diffraction (XRD), thermal analysis and FTIR of fresh and spent Ti-SBA-12 (Si/Ti = 20) catalyst after 5th recycle

Tuel and Ben Taarit [92] proposed that steric hindrance of transition complex favors the formation of para-isomer, HQ which can further undergo isomerization into the ortho-isomer, CAT on the external surface of TS-1. Kerton et al. [93] stated that phenol oxidation occurs on the exterior crystallite surface or within the pores close to the surface of the crystallites. In order to find whether any such isomerization is happening in the case of catalysts of the present study, CAT or HQ were taken as substrate and carried out the reaction under similar conditions in liquid phase with and without H_2O_2 . No isomerization product was detected in this case. Therefore, the differences in HQ/CAT molar ratio can arise due to the following reasons: (1) difference in the binding of CAT and HQ molecules on the catalyst surface and (2) differences in the rates of conversion of ortho- and para-dihydroxy compounds to corresponding quinones and their polymerized products. Non-detection of benzoquinone products at our reaction conditions suggests that the latter

cannot be the cause for higher values of HQ/CAT in the case of Ti-SBA-12. Hence, differences in the desorption rates of HQ and CAT from the surface of Ti-SBA is the possible cause for variation in HQ/CAT selectivity. Based on thermal and NMR studies (Chapter-2, Table 2.5) it can be realized that TiSBA-12 is relatively more hydrophilic than Ti-SBA-16. Ortho-hydroxy compound (CAT) must be more strongly adsorbed than the para-hydroxy compound (HQ) on hydrophilic Ti-SBA-12 surface than on hydrophobic Ti-SBA-16. Hence, the HQ/CAT ratio in the product is higher in the case of Ti-SBA-12 than with Ti-SBA-16. The increase in HQ/CAT selectivity ratio with increase in phenol conversion is also because of these differences in the adsorption characteristics. Tsai et al. [94] have also observed such differences in diphenol product selectivities over post-treated TS-1 catalysts. They too have attributed these changes in product selectivity as due to changes in textural properties and pore structure of the TS-1 catalyst samples.

The possible reason for the higher activity of Ti-SBA-12 is due to its larger pore size than that of Ti-SBA-16. Differences in pore arrangement in these two titanosilicate molecular sieves (Ti-SBA-12 has a hexagonal mesopore structure while Ti-SBA-16 has a cage-like cubic interconnected pore structure) could be the other reason. Under similar experimental (353 K, 24 h, phenol/H₂O₂ = 3; Si/Ti = 20) while Ti-MCM-41 showed a phenol conversion of 1.5%, Ti-SBA-12 exhibited a conversion of 24.1 mol%. To demonstrate the importance of three-dimensional pore architecture, phenol hydroxylation was carried out in the presence of Ti-SBA-15 (Si/Ti = 30 and 20), a two-dimensional mesoporous titanosilicate catalyst at reaction conditions of catalyst = 0.1 g, phenol = 10 mmol, H₂O₂ (30% aqueous) = 0.37 g, phenol/H₂O₂ (molar ratio) = 3, reaction temperature = 353 K, reaction time = 24 h and H₂O = 10 mL. Catalytic activity of Ti-SBA-15 was found inferior to Ti-SBA-12 confirming that the three-dimensional pore network of Ti-SBA-12 facilitates diffusion of the reactant and product molecules and accessibility of active sites. Unlike that with Ti-SBA-12, over Ti-SBA-15 catechol formed in higher amounts than hydroquinone (Ti-SBA-15 (Si/Ti = 30): phenol conversion = 6.6 mol%, CAT = 72 mol% and HQ = 28 mol%, HQ/CAT = 0.39; Ti-SBA-15 (Si/Ti = 20): phenol conversion = 7.8 mol%, CAT = 73 mol% and HQ = 27 mol%, HQ/CAT = 0.37). Thus the three-dimensional, mesoporous titanosilicates (Ti-SBA-12 and Ti-SBA-16) of the present study are more active than Ti-MCM-41 and Ti-SBA-15 catalysts [20, 95].

3.4. Conclusions

Catalytic activities of three-dimensional, mesoporous titanosilicates, Ti-SBA-12 and Ti-SBA-16, for liquid phase oxidation of cyclic olefins and hydroxylation of phenol have been investigated. Cyclohexene and cyclooctene were epoxidized with high selectivities using tert.-butyl hydroperoxide. Catalytic activity of these titanosilicates is superior to the well known microporous TS-1 and two-dimensional mesoporous Ti-MCM-41. Although both these mesoporous titanosilicates are highly active for hydroxylation of phenol, their intrinsic catalytic activity is lesser than that of microporous TS-1 but they are relatively more active than Ti-MCM-41. Catechol and hydroquinone are the only products of phenol hydroxylation. The para selective hydroxylation was more predominant over Ti-SBA-12 than on TS-1 and Ti-SBA-16. The mesoporous Ti catalysts of this work are reusable with little loss in activity and product selectivity in at least the fifth recycling experiments. Isolated framework Ti with tetrahedral geometry and three-dimensional, ordered mesoporosity are the unique characteristic features responsible for the highly efficient oxidation activity of Ti-SBA-12 and Ti-SBA-16 catalysts.

3.5. References

1. R.A. Sheldon, J.K. Kochi, *Metal Catalyzed Oxidations of Organic Compounds*, Academic Press, New York, 1981.
2. (a) Ullmann F (2003) *Ullmann's encyclopedia of industrial chemistry*. Wiley-VCH Verlag, Weinheim. (b) Kroschwitz JI (1992) *Kirth Othmer encyclopedia of chemical technology*, vol 4, 4th edn. Wiley-Interscience, New Delhi.
3. R.A. Sheldon, J. Dakka. *Catal. Today* 19 (1994) 215.
4. B. Notari, *Adv. Catal.* 41 (1996) 253.
5. R.A. Sheldon, I.W.C.E. Arends, A. Dijkstra, *Catalysis Today* 57 (2000) 157.
6. Z. Du, J. Ma, J. Gao, J. Xu, *Green Chemistry* 12 (2010) 590.
7. J. Muzart, *Chem. Rev.* 92 (1992) 113.
8. A. Corma, H. Garcia, *Chem. Rev.* 102 (2002) 3837.
9. B.S. Lane, K. Burgess, *Chem. Rev.* 103 (2003) 2457.
10. R.A. Sheldon, in: L.I. Simandi (Ed.), *Dioxygen Activation and Homogeneous Catalytic Oxidation*, Elsevier, Amsterdam, 1991, p. 573.
11. (a) G. Strukul, *Catalytic Oxidations with Hydrogen Peroxide as Oxidant*, Kluwer, (Dordrecht), 1992. (b) P. Ratnasamy, D. Srinivas and H. Knözinger,

- Adv. Catal. 48 (2004) 1.
12. (a) N.A. Milas, S. Sussman, *J. Am. Chem. Soc.* 58 (1936) 1302. (b) N.A. Milas, S. Sussman, *J. Am. Chem. Soc.* 59 (1937) 2345.
 13. K.A. Jørgensen, *Chem. Rev.* 89 (1989) 431.
 14. H.E.B. Lempers, R.I. Garcia, R.A. Sheldon, *J. Org. Chem.* 63 (1998) 1408.
 15. (a) T. Katsuki, K.B. Sharpless, *J. Am. Chem. Soc.* 102 (1980) 5974. (b) S.V. Pedersen, J.C. Dewan, R.R. Eckman, K.B. Sharpless, *J. Am. Chem. Soc.* 109 (1987) 1279. (c) M.G. Finn, K.B. Sharpless, *J. Am. Chem. Soc.* 113 (1991) 113.
 16. Shell Oil, British Patent, 1,249,079 (1971).
 17. R.A. Sheldon, *J. Mol. Catal.* 7 (1980) 107.
 18. M. Taramasso, G. Perego, B. Notari, US Pat. 4,410,501 (1983) to SNAM Progetti.
 19. J.M. Thomas, G. Sankar, *Acc. Chem. Res.* 34 (2001) 571.
 20. A. Corma, *Chem. Rev.* 97 (1997) 2373.
 21. M.G. Clerici, G. Bellussi, U. Romano, *J. Catal.* 129 (1991) 159.
 22. M.G. Clerici, U. Romano, US Patent 4,824,976 (1989) to Eniricerche S.p.A. and ENIchem Sintesi S.p.A.
 23. (a) J.S. Reddy, R. Kumar, P. Ratnasamy, *Appl. Catal.*, 58 (1990) L1. (b) J. S. Reddy, R. Kumar, *J. Catal.* 130 (1991) 440.
 24. D.P. Serrano, H.-X. Li, M.E. Davis, *J. Chem. Soc., Chem. Commun.* (1992) 745.
 25. (a) M.A. Camblor, A. Corma, J.P.-Pariante, SP Pat. 9101798, 1991. (b) M. A. Camblor, A. Corma, A. Martinez, J.P.-Pariante. *J. Chem. Soc. Chem. Commun.* (1992) 589.
 26. A. Tuel, *Zeolites* 15 (1995) 236.
 27. A. Tuel, *Zeolites* 15 (1995) 228.
 28. M.A. Camblor, M. Costantini, A. Corma, L. Gilbert, P. Esteve, A. Martínez, S. Valencia *Chem. Commun.* (1996) 1339.
 29. C.B. Dartt, M.E. Davis, *Appl. Catal. A: Chem.* 143 (1996) 53.
 30. P. Wu, T. Komatsu, T. Yashima, *J. Phys. Chem.* 100 (1996) 10316.
 31. M.-J. Díaz-Cabañas, L.A. Villaescusa, M.A. Camblor, *Chem. Commun.* (2000) 761.
 32. (a) P. Wu, T. Tatsumi, T. Komatsu, T. Yashima, *J. Phys. Chem. B* 105 (2001) 2897. (b) P. Wu, T. Tatsumi, *Chem. Commun.* (2002) 1026. (c) P. Wu, T.

- Miyaji, Y. Liu, M. He, T. Tatsumi, *Catal. Today* 99 (2005) 233.
33. Y. Kubota, Y. Koyama, T. Yamada, S. Inagaki, T. Tatsumi, *Chem. Commun.* (2008) 6224.
 34. A. Corma, M.A. Camblor, P. Esteve, A. Martinez, J.P.-Pariente, *J. Catal.* 145 (1994) 151.
 35. T. Tatsumi, M. Yako, M. Nakamura, Y. Yuihara, H. Tominaga, *J. Mol. Catal.* 78 (1993) L41.
 36. N. Jappar, Q. Xia, T. Tatsumi, *J. Catal.* 180 (1998) 132.
 37. (a) A. Corma, M.T. Navarro, J.P. pariente, *J. Chem. Soc. Chem. Commun.* 147 (1994). (b) A.T. Blasco, A. Corma, M.T. Navarro, J. Pérezpariente, *J. Catal.* 156 (1995) 65.
 38. (a) P.T. Tanev, M. Chibwe, T.J. Pinnavaia, *Nature* 368 (1994) 317. (b) S. Gontier, A. Tuel, *Zeolites* 15 (1995) 601. (c) J.S. Reddy, A. Dicko, A. Sayari, in “Synthesis of Porous Materials: Zeolites, Clays and Nanostructures” (M. Occelli and H. Kessler, Eds.), p. 405–415. Marcel Dekker, New York, 1997.
 39. K.A. Koyano, T. Tatsumi, *Chem. Commun.* 145 (1996).
 40. (a) S.A. Bagshaw, E. Prouzet, T.J. Pinnavaia, *Science* 269 (1995) 1242. (b) S.A. Bagshaw, F.D. Renzo, F. Fajula, *Chem. Commun.* (1996) 2209.
 41. (a) O.A. Kholdeeva, A.Y. Derevyankin, A.N. Shmakov, N.N. Trukhan, E.A. Paukshtis, A. Tuel, V.N. Romannikov, *J. Mol. Catal. A: Chem.* 158 (2000) 417. (b) N.N. Trukhan, A.Y. Derevyankin, A.N. Shmakov, E.A. Paukshtis, O.A. Kholdeeva, V.N. Romannikov, *Micropor. Mesopor. Mater.* 44/45 (2001) 603. (c) N.N. Trukhan, V.N. Romannikov, E.A. Paukshtis, A.N. Shmakov, O.A. Kholdeeva, *J. Catal.* 202 (2001) 110.
 42. (a) M.S. Morey, S. O’Brien, S. Schwarz, G.D. Stucky, *Chem. Mater.* 12 (2000) 898. (b) Z. Luan, L. Kevan, *Micropor. Mesopor. Mater.* 44/45 (2001) 337. (c) B. L. Newalkar, J. Olanrewaju, S. Komarneni, *Chem. Mater.* 13 (2001) 552.
 43. D. Ji, T. Ren, L. Yan, J. Suo, *Mater. Lett.* 57 (2003) 4474.
 44. Z. Shan, J.C. Jansen, L. Marchese, T. Maschmeyer, *Micropor. Mesopor. Mater.* 48 (2001) 181.
 45. (a) R. Hutter, T. Mallat, D. Dutoit, A. Baiker, *Top. Catal.* 3 (1996) 421. (b) A. Welch, N.R. Shiju, I.D. Watts, G. Sankar, S. Nikitenko, W. Bras, *Catal. Lett.* 105 (2005) 179. (c) A.R. Oki, Q. Xu, B. Shpeizer, A. Clearfield, X. Qiu, S.

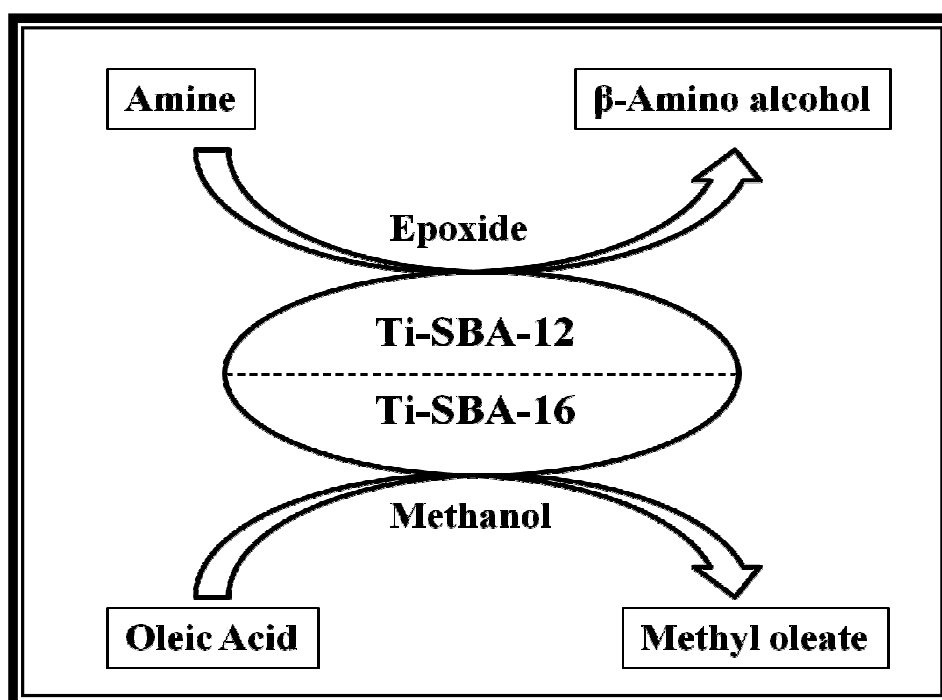
- Kirumakki, S. Tichy, *Catal. Commun.* 8 (2007) 950.
46. (a) A. Vinu, P. Srinivasu, V.V. Balasubramanian, K. Ariga, T. Mori, Y. Nemoto, *Chemistry Lett.*, 37 (2008) 1016. (b) C. Anand, P. Srinivasu, G.P. Mane, S.N. Talapaneni, D.S. Dhawale, M.A. Wahab, S.V. Priya, S. Varghese, Y. Sugi, A. Vinu, *Micropor. Mesopor. Mater.* 160 (2012) 159.
 47. T. Blasco, A. Corma, M.T. Navarro, J. Pérez Pariente, *J. Catal.* 156 (1995) 65.
 48. T. Tatsumi, K.A. Koyano, N. Igarashi, *Chem. Commun.* (1998) 325.
 49. D. Zhao, Q. Huo, J. Feng, B.F. Chmelka, G.D. Stucky, *J. Am. Chem. Soc.* 120 (1998) 6024.
 50. Y. Sakamoto, I. Diaz, O. Terasaki, D. Zhao, J.P. Pariente, J.M. Kim, G.D. Stucky, *J. Phys. Chem. B* 106 (2002) 3118.
 51. G. Clerici, in: M.G. Guisnet Jr., J. Barrault, C. Bouchoule, D. Duprez, G. Perot, C. Montassier (Eds.), *Heterogeneous Catalysis and Fine Chemicals III*, vol. 78, Elsevier, Amsterdam, 1993, p. 78.
 52. M. Dusi, T. Mallat, A. Baiker, *Catal. Rev. Sci. Eng.* 42 (2000) 213.
 53. J. Gao, Y. Chen, B. Hau, Z. Feng, C. Li, N. Zhou, S. Gao, Z. Xi, *J. Mol. Catal. A: Chem.* 210 (2004) 197.
 54. R. Fasan, *ACS Catal.* 2 (2012) 647.
 55. L. Raboin, J. Yano, T. D. Tilley, *J. Catal.* 285 (2012) 168.
 56. P.J. Cordeiro, T. D. Tilley, *ACS Catal.* 1 (2011) 455.
 57. H. Zhou, L. Xiao, X. Liu, S. Li, H. Kobayashi, X. Zheng, J. Fan, *Chem. Commun.* 48 (2012) 6954.
 58. K. Wada, S. Sakugawa, M. Inoue, *Chem. Commun.* 48 (2012) 7991.
 59. S. Sakugawa, K. Wada, M. Inoue, *J. Catal.* 275 (2010) 280.
 60. Z. Wang, L. Xu, J.-G. Jiang, Y. Liu, M. He, P. Wu, *Micropor. Mesopor. Mater.* 156 (2012) 106.
 61. J. Wang, L. Xu, K. Zhang, H. Peng, H. Wu, J.-G. Jiang, Y. Liu, P. Wu, *J. Catal.* 288 (2012) 16.
 62. Y. Wu, Y. Zhang, J. Cheng, Z. Li, H. Wang, Q. Sun, B. Han, Y. Kong, *Micropor. Mesopor. Mater.* 162 (2012) 51.
 63. S. Chen, C. Ma, M. Qin, H. Yang, H. Xie, J. Guan, *Reac. Kinet. Mech. Cat.* 106 (2012) 245.
 64. F. Carniato, C. Bisio, L. Sordelli, E. Gavrilova, M. Guidotti, *Inorganica Chimica*

- Acta 380 (2012) 244.
65. V. Sazo, C. M. López, M. De Quesada, J. M. Vieira, *Catal. Today* 172 (2011) 8.
 66. L. Kumaresan, A. Prabhu, M. Palanichamy, V. Murugesan, *J. Taiwan Inst. Chem. Eng.* 41 (2010) 670.
 67. F. Bérube, A. Khadhraoui, M.T. Janicke, F. Kleitz, S. Kaliaguine, *Ind. Eng. Chem. Res.* 49 (2010) 6977.
 68. T. Tatsumi, K.A. Koyano, N. Igarashi, *Chem. Commun.* (1998) 325.
 69. A. Corma, M. Domine, J.A. Gaona, J.L. Jordá, M.T. Navarro, F. Rey, J. Pérez-Pariente, J. Tsuji, B. McCulloch, L.T. Nemeth, *Chem. Commun.* (1998) 2211.
 70. (a) S. Shen, Y. Deng, G. Zhu, D. Mao, Y. Wang, G. Wu, J. Li, X.Z. Liu, G. Lu, D. Zhao, *J. Mater. Sci.* 42 (2007) 7057. (b) J.C. Amezcua, L. Lizama, C. Salcedo, I. Puente, J. M. Domínguez, T. Klimova, *Catal. Today* 107-108 (2005) 578. (c) A.T. Shah, B. Li, Z.E.A. Abdalla, *J. Coll. Int. Sci.* 336 (2009) 707. (d) J. Ma, L.S. Qiang, X.B. Tang, H.Y. Li, *Catal. Lett.* 138 (2010) 88.
 71. T. Tatsumi, Y. Watanabe, Y. Himasawa, J. Tsuchiya, *Res. Chem. Intermed.* 24 (1998) 529.
 72. P. Ratasamy, D. Srinivas, H. Knözinger, *Adv. Catal.* 48 (2004) 1.
 73. Z. Luan, E.M. Maes, P.A.W. van der Heide, D. Zhao, R.S. Czernuszewicz, L. Kevan, *Chem. Mater.* 11 (1999) 3680.
 74. V.N. Shetti, P. Manikandan, D. Srinivas, P. Ratnasamy, *J. Catal.* 216 (2003) 461.
 75. A. Atoguchi, S. Yao, *J. Mol. Catal. A: Chem.* 176 (2001) 173.
 76. P. Wu, T. Tatsumi, *J. Catal.* 214 (2003) 317.
 77. H. Fiegel, H.-W. Voges, T. Hamamoto, S. Umemura, T. Iwata, H. Miki, Y. Fujita, H.-J. Buysch, D. Garbe, W. Paulus, *Phenol Derivatives in Ullmann's Encyclopedia of Industrial Chemistry*; Wiley-VCH: New York, 26 (2002) 521.
 78. P. Maggioni, US Pat. 3,914,323 (1972), assigned to Brichima.
 79. P. Maggioni, F. Minisci, *Chim. Ind. (Milan)* 59 (1977) 239.
 80. F. Bourdin, M. Costantini, M. Jouffret, G. Lartigan, Ger, Pat. DE 064,497 (1971), assigned to Rhone-Paulenc, France.
 81. J. Varagnat, *J. Ind. Eng. Chem. Prod. Res. Dev.* 15 (1976) 212.
 82. G.A. Hamilton, J.P. Friedman, P.M. Campbell, *J. Am. Chem. Soc.* 88 (1966) 5266.
 83. S. Umemura, N. Takamitsu, T. Hamamoto, N. Kuroda, U.S. Patent 4,078,006,

- 1978, to UBE Industries. U.S. 5714641.
84. A. Thangaraj, R. Kumar, P. Ratnasamy, *J. Catal.* 131 (1991) 294.
 85. A. Thangaraj, R. Kumar, P. Ratnasamy, *Appl. Catal.* 57 (1990) L1.
 86. A. Thangaraj, R. Kumar, S. P. Mirajkar, P. Ratnasamy, *J. Catal.* 130 (1991)1.
 87. J.S. Reddy, R. Kumar, *Zeolites* 12 (1992) 95.
 88. J.S. Reddy, S. Sivasankar, P. Ratnasamy, *J. Mol. Catal.* 71 (1992) 373.
 89. U. Wilkenhöner, G. Langhendries, F.V. Laar, G.V. Baron, D.W. Gammon, P.A. Jacobs, E.V. Steen, *J. Catal.* 203 (2001) 201.
 90. A. Tuel, S.M.-Khouzami, Y.B. Taarit, C. Naccache, *J. Mol. Catal.* 68 (1991) 45.
 91. M.G. Clerici, R.A. Sheldon, H. van Bekkum, (Eds.) *Fine Chemicals through Heterogeneous Catalysis*, Wiley-VCH, Weinheim, 2001, p. 538.
 92. A. Tuel, Y. Ben Taarit, *Appl. Catal.* 102 (1993) 69.
 93. O.J. Kerton, P. McMorn, D. Bethell, F. King, F. Hancock, A. Burrows, C. J. Kiely, S. Ellwood, G. Hutchings, *Phys. Chem. Chem. Phys.* 7 (2005) 2671.
 94. S.-T. Tsai, P.-Y. Chao, T.-C. Tsai, I. Wang, X. Liu, X.-W. Guo, *Catal. Today* 148 (2009) 174.
 95. S. Song, W. Zhao, L. Wang, J. Chu, J. Qu, S. Li, L. Wang, T. Qi, *J. Colloid. Inter. Sci.* 354 (2001) 686.

CHAPTER – 4

Acid Catalyzed Reactions over Ti-SBA-12 & Ti-SBA-16



4.1. Introduction

Acid catalysts play an important role in oil refining, petrochemistry and fine chemical industry. Homogeneous Lewis acids such as AlCl_3 , BF_3 , FeCl_3 , TiCl_4 , ZnCl_2 , etc., and Brønsted acids like HF, H_2SO_4 and polyphosphoric acid have been widely used as catalysts in alkylation, acylation, esterification and isomerization reactions [1]. Homogeneous catalysts are highly active but have disadvantages due to their corrosive nature, high cost of separation of products, non-reusability and safe disposal. From environmental and economic points of view, solid acid catalysts overcome most of the above disadvantages. Solid acid catalysts such as zeolites, aluminophosphates, mixed metal oxides, resins, sulfonic acid functionalized mesoporous silica, sulfated metal oxides, metal containing micro and mesoporous molecular sieves have been used for many organic transformations in fine chemical and pharmaceutical industries [2-5].

Titanium containing micro and mesoporous molecular sieves are a class of solid Lewis acid and redox catalyst systems which are of considerable interest. Since the discovery of microporous titanosilicate zeolite (TS-1) by Taramasso et al. in 1983 [6, 7], many such molecular sieves viz., TS-2, Ti-ZSM-48, Ti- β , Ti-ZSM-12, Ti-MCM-41, Ti-HMS, Ti-MCM-48, Ti-MSU, Ti-SBA-15, Ti-MMM, Ti-MWW, Ti-TUD-1, Ti-MCM-68 (Ti-MSE) and hierarchical TS-1 zeolites have been synthesized and their physical, chemical and catalytic properties have been investigated [4, 8, 9]. The potential applications of these titanosilicates (Ti^{4+} ions in framework positions) for a variety of oxidation reactions was extensively studied under heterogeneous conditions using dilute H_2O_2 as oxidant [4, 8, 9]. However, the utility of these titanium silicates in areas other than oxidation catalysis has not been studied in depth. There are a few reports in the open literature of their use as solid Lewis acid catalysts. The transformation of oximes to lactams (the Beckmann rearrangement) was one of the earliest such acid-catalyzed reactions reported with TS-1 and TS-2 catalysts [10, 11]. The rearrangement of cyclohexanone oxime to 1-caprolactam proceeds with high selectivity in the presence of TS-1, with high catalyst stability. Srivastava et al. [12] and Srinivas et al. [13] reported the application of TS-1, Ti-MCM-41 and $\text{TiO}_2\text{-SiO}_2$ in transesterification reactions and in the synthesis of cyclic carbonates. Sashidharan and Kumar [14] reported the application of titanosilicate molecular sieves in carbon-carbon bond formation reactions like Mukaiyama-type aldol reactions between silyl enol ethers and aldehydes to give β -hydroxy

esters/aldols, Michael addition reactions of silyl enol ethers with various α , β -unsaturated carbonyl compounds and formation of pinacols from alkenes catalyzed by various titanosilicates [15, 16]. In 2005, Garro et al. [17] reported Lewis acid catalyzed solvent-free Mukaiyama-type aldol condensation using Ti-MCM-41 and amorphous Ti-silicate materials. Recently, Sasidharan and Bhaumik [18] reported alkylation and acylation of silyl enol ethers under liquid-phase conditions catalyzed by microporous TS-1, TS-2, Ti- β and Sn-MFI catalysts. Bayense et al. [19] disclosed an esterification process catalyzed by Engelhard Corporation titanium based zeolites ETS-4, ETS-10 and ETAS-10. Kawabata et al. [20] reported esterification of carboxylic acids with alcohols over Montmorillonite-enwrapped titanium catalyst.

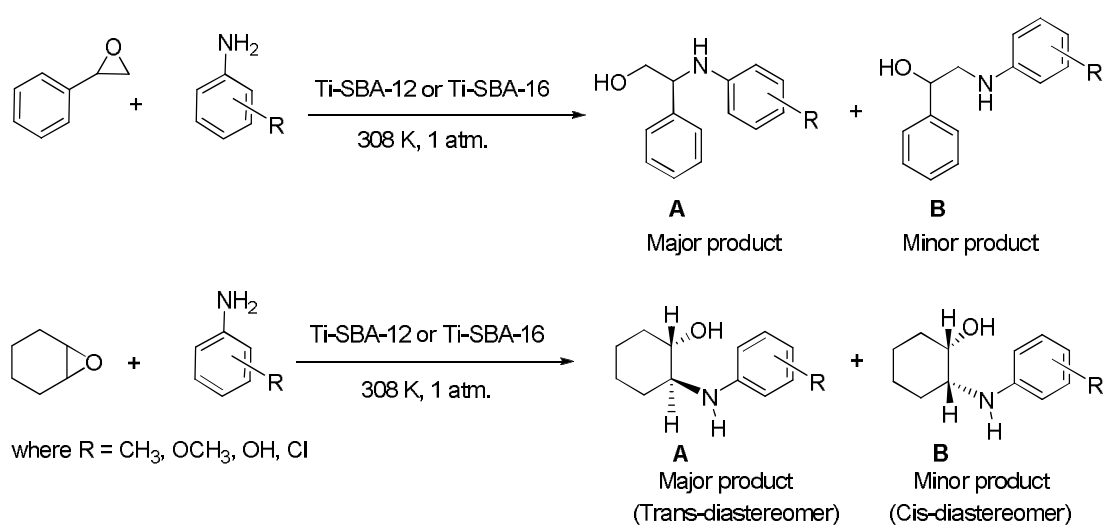
In this chapter, a novel application of Ti-SBA-12 and Ti-SBA-16 three-dimensional, mesoporous, titanosilicates in two different acid-catalyzed reactions viz., aminolysis of epoxides and esterification of oleic acid with methanol is reported.

4.2. Ring-Opening of Epoxides with Amines

Epoxides are versatile and important organic intermediates in the pharmaceutical and agrochemical industries. The three-membered heterocyclic ring of an epoxide is strained and offers an uncommon combination of reactivity, synthetic flexibility and atom economy. This strained epoxide ring can be attacked by a range of nucleophiles including nitrogen- (ammonia, amines and azides), oxygen- (water, alcohols, phenols and acids) and sulfur- (thiol)-containing compounds leading to bifunctional molecules of great industrial value. Ring-opening of epoxides with amines or aminolysis of epoxides yields β -amino alcohols which are versatile intermediates for the synthesis of various biologically active natural products, unnatural amino acids, β -blockers, insecticidal agents, chiral auxiliaries and oxazolines [21-25]. Oxycontin, Coreg and Toprol-XL are a few examples of active pharmaceutical ingredients (APIs) that contain a β -amino alcohol unit in their structure. Zyvox and Skelaxin are a few others that can be formed through β -amino alcohol precursors. Among several synthetic strategies, the most straightforward approach for the synthesis of β -amino alcohols is the direct reaction of epoxide with an excess amount of amine at elevated temperatures and in the presence of solvents [24, 26, 27]. This approach is not always favorable especially when the reactants contain temperature-sensitive functional groups. Further, this method is less effective

for weakly nucleophilic amines and yields low regioselectivity [24, 25]. Several Lewis and Brønsted acid catalysts including metal halides, metal perchlorates, metal triflates, Bu_3P , ionic liquids, sulfamic acid, etc., have been reported to catalyze this transformation [28-31]. Solid acid catalysts including resins and zeolites have also been reported [32-35]. However, many of these methods suffer from one or more of the following disadvantages: poor regio-selectivity, requirement of extended reaction times, elevated temperatures, high pressures and stoichiometric amount of catalyst, and the use of expensive reagents or catalysts. Hence, there is need to develop more efficient and reusable solid catalysts that are active at low temperatures and avoid the use of solvent. Ti-MCM-41 and sulfonic acid functionalized SBA-15 catalysts have been used for the ring-opening reaction of epoxides with amines [36-38]. Ti-MCM-41 showed more efficient activity than the sulfonic acid functionalized SBA-15. Mechanistic investigations revealed that both epoxide and amines compete for adsorption on acid functionalities on the catalyst surface. Polar solvent molecules, when present, also compete for adsorption with the reactant molecules [37].

In this chapter the catalytic application of solid, Lewis acidic Ti-SBA-12 and Ti-SBA-16 for the activation and ring-opening of epoxides with amines is reported. A range of β -amino alcohols are synthesized in high yields over Ti-SBA-12 and Ti-SBA-16 at ambient temperatures under solvent free conditions by the ring opening of symmetrical and an unsymmetrical epoxides (aliphatic as well as aromatic) with amines (Scheme 4.1).



Scheme 4.1. Regio- and stereoselective ring opening of epoxides with amines

4.2.1. Experimental Section

Details on the preparation and characterization of Ti-SBA-12 and Ti-SBA-16 are reported in [Chapter 2](#).

4.2.1.1. Reaction Procedure

In a typical reaction, epoxide and amine in equimolar quantities (20 mmol) and a known amount of catalyst were taken in a double-necked, glass, round-bottom flask (50 mL) placed in a temperature-controlled oil bath and fitted with a water-cooled condenser. The reaction was conducted at a specific temperature and for a desired period of time. Some experiments were conducted in the presence of solvent (5 mL).

4.2.1.2. Product Analysis

The progress of the reaction was monitored by taking out aliquots of the sample, diluting it with a known quantity of dichloromethane, separating the catalyst by centrifugation and subjecting the diluted liquid to gas chromatographic analysis (Varian 3400; CP-SIL8CB column; 30 m-long and 0.53 mm-i.d.). The products were identified using GC-MS (Varian CP-3800; 30 m-long, 0.25 mm-i.d., and 0.25 μ m-thick CP-Sil8CB capillary column). They were also isolated by column chromatography (eluent: petroleum ether-ethyl acetate mixture) and characterized by ^1H NMR studies (see [Appendix-I](#) at the end of this chapter).

4.2.2. Catalytic Activity

A range of β -amino alcohols were synthesized by the aminolysis of epoxides at ambient temperature under solvent-free conditions ([Scheme 4.1](#)). Styrene oxide and cyclohexene oxide were chosen as representative epoxides. Aniline and its derivatives and also some aliphatic amines were chosen as representative amines. Two regio-/stereoisomers, A and B can be obtained ([Scheme 4.1](#)). The conversion of an epoxide and the selectivity of the products depend on the nature and type of the amine molecules. Steric hindrance or electronic structure (inductive and conjugative effect) and nucleophilicity of amines can affect the reactivity. Influences of different reaction parameters on the conversion and product selectivity are given below.

4.2.2.1. Aminolysis of Styrene oxide with Aniline over Different Catalysts

For comparison, aminolysis of styrene oxide with aniline was carried out over different homogeneous and heterogeneous catalysts (titanosilicates with different pore structure). Controlled experiments revealed that this reaction occurs to a lesser extent without any catalyst (styrene oxide conversion = 7.3 wt%). But the selectivity for A and B isomers was nearly the same (Table 4.1, entry no. 1).

Table 4.1. Aminolysis of Styrene Oxide with Aniline over Different Catalysts^a

Entry No.	Catalyst	Styrene oxide conv. (wt%)	Product selectivity (wt%)		TOF (h ⁻¹)
			A	B	
1	Nil	7.3	53.3	46.7	-
2	TiO ₂	20.8	86.2	13.9	1
3	TiO ₂ ^b	13.5	83.5	16.5	9
4	TS-1 (30)	39.1	88.1	11.9	52
5	Ti-MCM-41(30)	92.0	95.8	4.2	121
6	Ti-SBA-15 (30)	90.2	92.1	7.9	109
7	Ti-SBA-12 (30) ^c	93.7	92.9	7.1	147
8	Ti-SBA-16 (30) ^d	86.9	93.5	6.5	187
9	Anhydrous AlCl ₃	76.9	99.1	0.9	7
10	ZnCl ₂	73.4	96.5	3.5	7
11	MnCl ₂ .4H ₂ O	45.6	85.4	14.6	6

^aReaction conditions: Catalyst = 50 mg, styrene oxide = 20 mmol, aniline = 20 mmol, reaction time = 6 h, reaction temperature = 308 K. ^bReaction conditions: Same as above except 4 mg of catalyst was used. ^cMolarity of HCl used in Ti-SBA-12 preparation = 0.1 M. ^dMolarity of HCl used in Ti-SBA-16 preparation = 2 M. Turnover frequency (TOF) = moles of styrene oxide converted per mole of metal in the catalyst per hour

In the presence of a catalyst, isomer-A formed with high selectivity. Nature and type of catalyst influenced the epoxide conversion and isomer-A selectivity. Titanosilicates showed higher catalytic activity (turnover frequency, TOF) than bulk TiO₂ and the conventional homogeneous, Lewis acid catalysts – AlCl₃, ZnCl₂ and MnCl₂ (Table 4.1, entry nos. 2, 3, 9, 10 and 11). The TOF of different titanosilicates

decreased in the order: Ti-SBA-16 (187) > Ti-SBA-12 (147) > Ti-MCM-41 (121) > Ti-SBA-15 (109) > TS-1 (52) (Table 4.1). The lowest activity of TS-1 among these titanasilicate catalysts is perhaps due to its microporous structure. The highest activities of Ti-SBA-16 and Ti-SBA-12 are due to their three-dimensional, mesoporous structure. Ti-MCM-41 and Ti-SBA-15 have two-dimensional, mesoporous structure. Hence, mesoporosity and higher dimensionality are the two important characteristics that enable better accessibility of the active sites and facile diffusion of reactant and product molecules. Even if a small quantity of anatase-like TiO₂ was present that would not have contributed much to the overall catalytic activity of Ti-SBA-16 and Ti-SBA-12.

Table 4.2. Effect of Si/Ti Molar Ratio on the Aminolysis of Styrene Oxide^a

Si/Ti (molar ratio)	Ti-SBA-12, reaction time = 6 h				Ti-SBA-16, reaction time = 2 h			
	Epoxide conv. (wt%)	TOF (h ⁻¹)	Product		Epoxide conv. (wt%)	TOF (h ⁻¹)	Product	
			selectivity				selectivity	
			A	B			A	B
20	28.8	53	94.2	5.8	69.5	339	95.8	4.2
30	30.3	74	94.9	5.1	43.7	282	94.7	5.3
40	18.2	50	94.5	5.5	42.5	370	95.7	4.3
50	19.0	61	93.9	6.1	33.2	321	95.4	4.3

^aReaction conditions: Ti-SBA-12 or Ti-SBA-16 (2 M HCl) = 50 mg, styrene oxide = 20 mmol, aniline = 20 mmol, reaction temperature = 308 K. Turnover frequency (TOF) = moles of styrene oxide converted per mole of Ti (output) in the catalyst per hour

4.2.2.2. Influence of Si/Ti Molar Ratio

The influence of Si/Ti molar ratio of the catalysts on the epoxide conversion is reported in Table 4.2. It may be noted that all these titanosilicates reported in Table 4.2 were prepared using the same concentration of HCl (2 M) in the synthesis gel. In general, the conversion of styrene oxide increased with increasing Ti content (i.e., decreasing Si/Ti molar ratio) in the catalyst. Catalytic activities (styrene oxide conversion and TOF) of Ti-SBA-16 were higher than those of Ti-SBA-12. This is

because Ti-SBA-16 has higher amount of framework-substituted, isolated, tetra-coordinated Ti ions than Ti-SBA-12 (Chapter 2, Table 2.5).

4.2.2.3. Influence of Method of Preparation

Table 4.3 shows the influence of method of preparation (i.e., molar concentration of HCl used in the synthesis) on the aminolysis activity. It may be noted that Ti-SBA-12 (Si/Ti = 30) prepared using 0.1 M HCl is highly active than the other Ti-SBA-12 catalysts. Ti-SBA-16 (Si/Ti = 20) prepared using 2 M HCl showed the highest activity. Superior activities of these two titanasilicate compositions are due to the higher amount of framework-substituted, isolated, tetra-coordinated Ti ions present in them.

Table 4.3. Influence of Method of Preparation on the Aminolysis of Styrene Oxide with Aniline^a

Entry No.	Molar conc. of HCl used in catalyst preparation	Epoxide conv. (wt%)	Product selectivity		TOF (h ⁻¹)
			A	B	
1.	2	30.3	94.9	5.1	74
2.	1	20.7	93.4	6.6	42
3.	0.5	20.7	93.7	6.3	39
4.	0.2	41.3	93.7	6.3	70
5.	0.1	93.7	92.9	7.1	147
6.	0.05	25.8	93.2	6.8	38

^aReaction conditions: Ti-SBA-12 (Si/Ti = 30) = 50 mg, styrene oxide = 20 mmol, aniline = 20 mmol, reaction time = 6 h, reaction temperature = 308 K. Turnover frequency (TOF) = moles of styrene oxide converted per mole of Ti (output) in the catalyst per hour

4.2.2.4. Influence of Pore Structure

Fig. 4.1 shows the time-on-stream catalytic activity profiles of TS-1, Ti-MCM-41, Ti-SBA-12 and Ti-SBA-16. Styrene oxide conversion increased with increasing reaction time (Ti-SBA-16 > Ti-SBA-12 > Ti-MCM-41 > TS-1). There is a marginal decrease in product selectivity (by about 5 wt%) over a period of 6 h indicating that at higher conversions a part of A got isomerized into B over the acidic catalysts. From the plots, it is obvious that three-dimensional mesoporous titanosilicates Ti-SBA-12 and Ti-SBA-16 are more active than the microporous TS-1 and two-dimensional Ti-MCM-41. The three-dimensional pore system and mesoporous architecture have influenced the catalytic activity of these titanosilicates due to fast mass transfer kinetics into their pore system and easy accessibility of catalytic active sites.

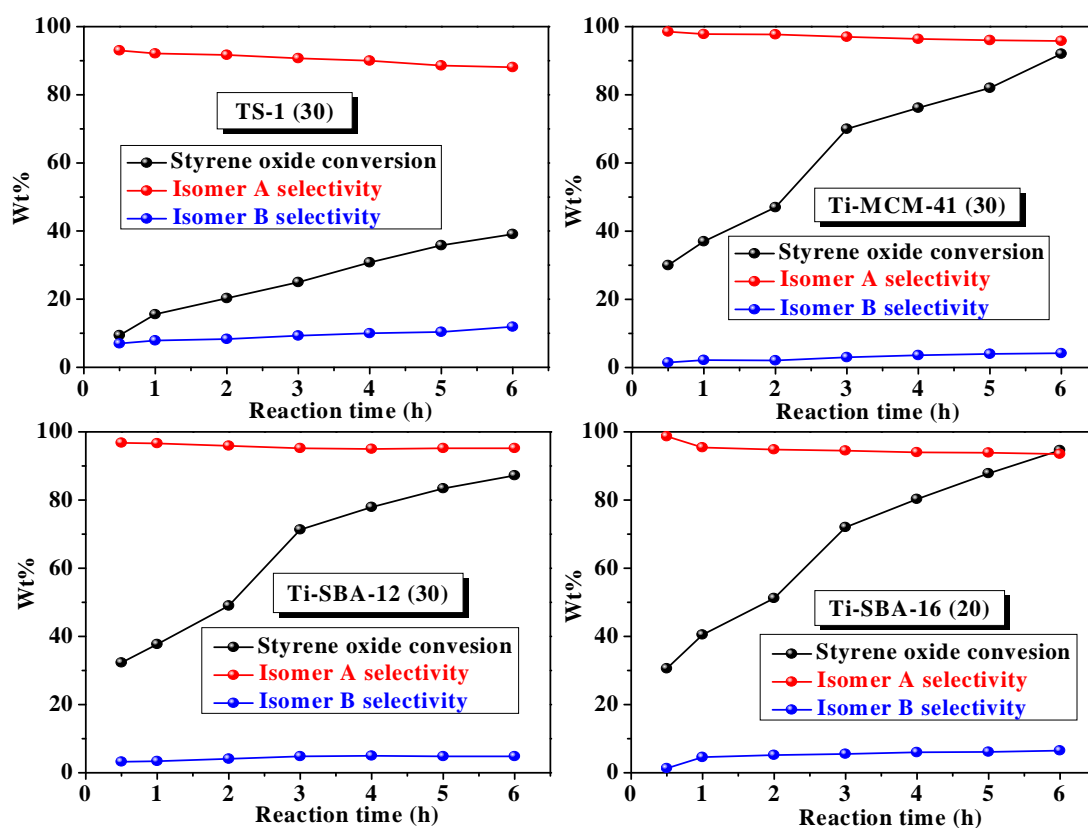


Fig. 4.1. Catalytic activity of different titanosilicate catalysts in the aminolysis of styrene oxide with aniline. Reaction conditions: catalyst [TS-1 (30), Ti-MCM-41 (30), Ti-SBA-12 (30, 0.1 M), Ti-SBA-16 (20, 2 M)] = 50 mg, styrene oxide = 20 mmol, aniline = 20 mmol, reaction temperature = 308 K

4.2.2.5. Influence of Reaction Temperature

Fig. 4.2 shows the effect of temperature on the conversion and product selectivity in the aminolysis of styrene oxide in 2 h. Over Ti-SBA-12 (Si/Ti = 30, 0.1 M), as the temperature was raised from 308 to 343 K, the conversion of styrene oxide increased from 56.2 to 92.0 wt% and TOF from 264 to 432 h⁻¹. Over Ti-SBA-16 (Si/Ti = 20, 2 M), this increase in conversion was from 69.5 to 96.6 wt% and TOF from 338 to 470 h⁻¹. In other words, Ti-SBA-16 (Si/Ti = 20, 2 M) is a superior catalyst to Ti-SBA-12 (Si/Ti = 30, 0.1 M). In fact, the activity of Ti-SBA-16 is higher than the hitherto known solid catalysts for this reaction. It is interesting to note that unlike in the conventional process, the ring-opening reaction of epoxides occurs even at ambient conditions with high yields and selectivity for isomer-A. The selectivity of isomer-A is nearly the same over Ti-SBA-12 (Si/Ti = 30, 0.1 M) and Ti-SBA-16 (Si/Ti = 20, 2 M).

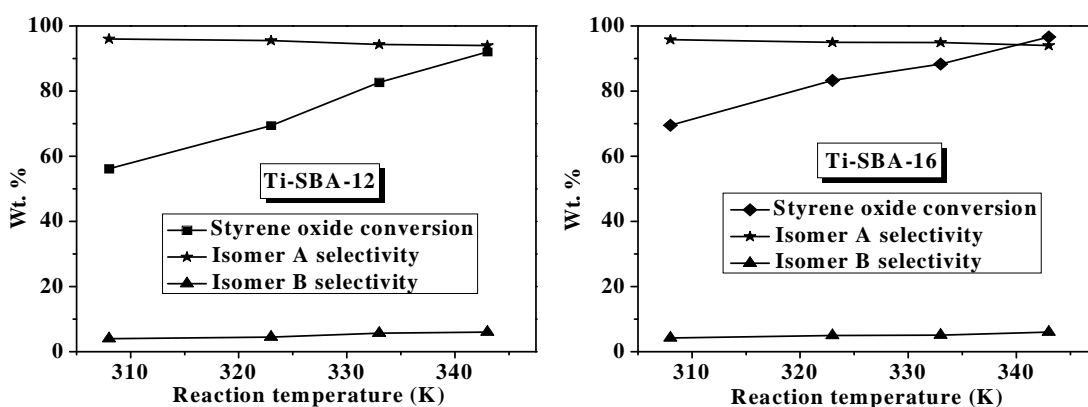


Fig. 4.2. Effect of reaction temperature on the aminolysis of styrene oxide with aniline. Reaction conditions: catalysts, Ti-SBA-12 (Si/Ti = 30, 0.1 M) or Ti-SBA-16 (Si/Ti = 20, 2 M) = 50 mg, styrene oxide = 20 mmol, aniline = 20 mmol, reaction time = 2 h

4.2.2.6. Influence of Solvent

The influence of solvent on the conversion and product selectivity is given in the Table 4.4. When solvent was used, lowering in styrene oxide conversion was observed. This lowering was relatively more for Ti-SBA-12 (Si/Ti = 30, 0.1 M) than for Ti-SBA-16 (Si/Ti = 20, 2 M) (Table 4.4). Non-polar solvents had a little effect compared to polar solvents. ²⁹Si MAS NMR and thermogravimetric studies (Chapter 2, Table 2.5 and Fig. 2.21) revealed that Ti-SBA-16 is relatively more hydrophobic

than Ti-SBA-12. The difference in surface structure is perhaps the cause for the differences observed in solvent effects.

Table 4.4. Effect of Solvent on the Reaction of Styrene Oxide with Aniline^a

Solvent	Ti-SBA-12 (Si/Ti = 30, 0.1 M)				Ti-SBA-16 (Si/Ti = 20, 2 M)			
	Epoxide	TOF	Product		Epoxide	TOF	Product	
	conv.	(h ⁻¹)	selectivity		conv.	(h ⁻¹)	selectivity	
	(wt%)		(wt%)		(wt%)		(wt%)	
		A	B			A	B	
Nil	93.7	147	92.9	7.1	96.1	156	93.0	7.0
CCl ₄	90.6	142	98.3	1.7	95.4	155	91.4	8.6
Toluene	84.2	132	98.9	1.1	95.5	155	92.2	7.8
Chloroform	63.6	99	98.7	1.3	83.4	135	91.3	8.7
Dichloromethane	59.7	93	99.0	1.0	72.9	118	91.5	8.5
Dichloroethane	53.4	84	99.0	1.0	63.8	104	90.4	9.6
Acetonitrile	50.2	79	98.2	1.8	49.8	81	90.5	8.5
Methanol	28.8	45	86.1	13.9	39.8	65	89.0	11
Acetone	28.3	44	29.3 ^b	3.2 ^b	28.3	46	53.7	4.1 ^b

^aReaction conditions: Catalyst = 50 mg, styrene oxide = 20 mmol, aniline = 20 mmol, solvent = 5 mL, reaction time = 6 h, reaction temperature = 308 K. ^bSelectivity for other product formed by condensation of acetone and aniline = 67.5% (for Ti-SBA-12) and 42.2% (for Ti-SBA-16). Turnover frequency (TOF) = moles of styrene oxide converted per mole of Ti (output) in the catalyst per hour

In an earlier study, using SBA-15-*pr*-SO₃H and Ti-MCM-41 catalysts, Saikia et al. [37] reported that both epoxide and amine compete for adsorption on acidic functionalities on the catalyst surface. Polar solvent molecules, when present, also compete for adsorption with the reactant molecules and thereby reduce epoxide conversion. Epoxide adsorption and activation on acid sites are essential for the reaction to occur. A linear correlation between styrene oxide conversion and dielectric constant was found especially in the case of non-polar solvents (Fig. 4.3). Polar, protic solvents deviated from this linear relationship as they induce some side reactions (Table 4.4).

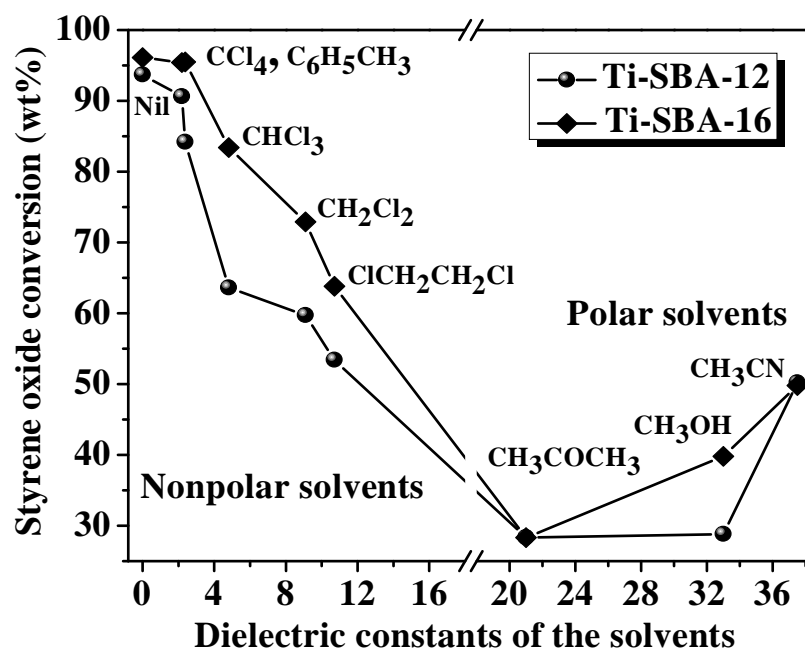
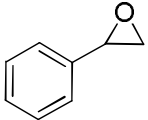
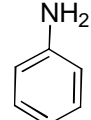
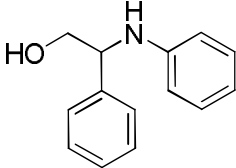
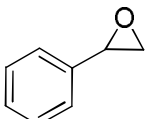
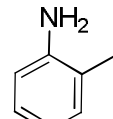
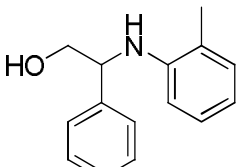
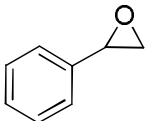
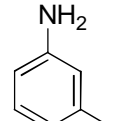
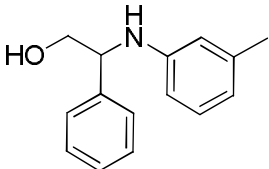
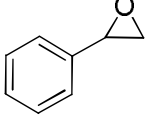
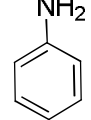
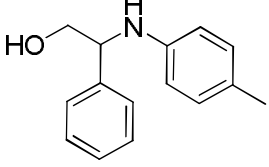


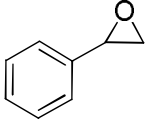
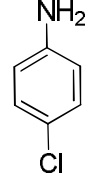
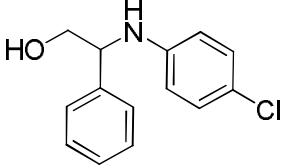
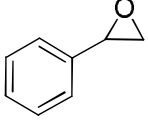
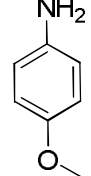
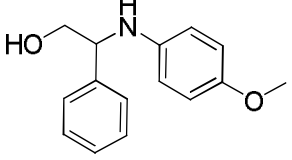
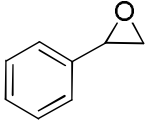
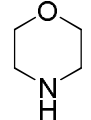
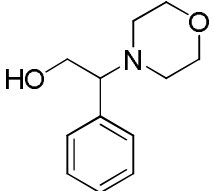
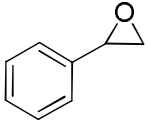
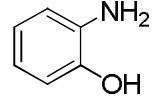
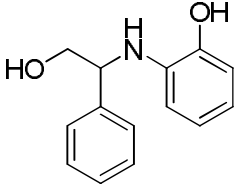
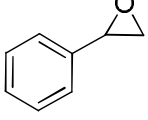
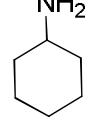
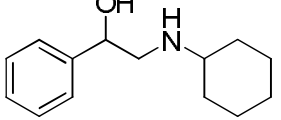
Fig. 4.3. Influence of dielectric constant of solvent on the conversion of styrene oxide in the aminolysis reaction with aniline over Ti-SBA-12 (Si/Ti = 30, 0.1 M) and Ti-SBA-16 (Si/Ti = 20, 2 M) catalysts. Reaction conditions: catalyst = 50 mg, styrene oxide = 20 mmol, aniline = 20 mmol, solvent = 5 mL, reaction time = 6 h, reaction temperature = 308 K

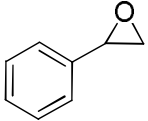
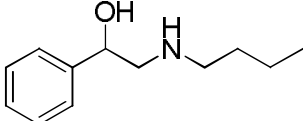
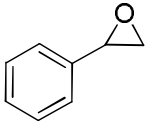
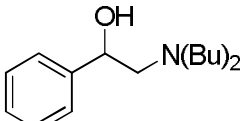
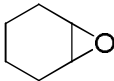
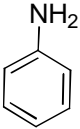
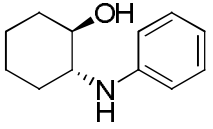
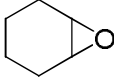
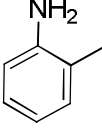
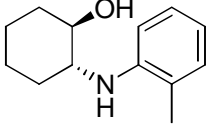
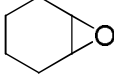
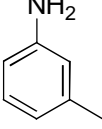
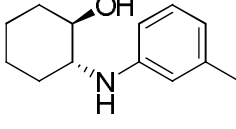
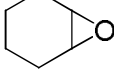
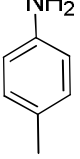
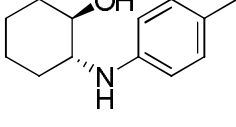
4.2.2.7. Influence of Substrate Structure

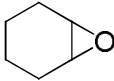
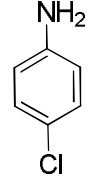
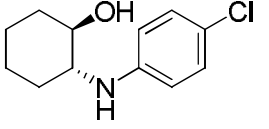
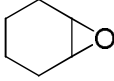
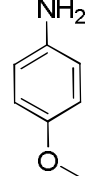
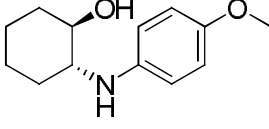
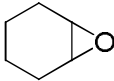
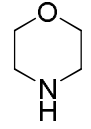
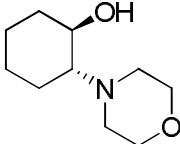
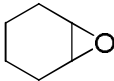
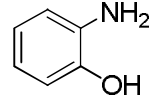
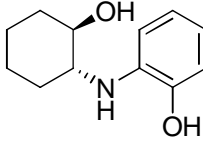
The influence of substrate structure on the aminolysis of epoxides is listed in the Table 4.5. The three-dimensional, mesoporous titanasilicate catalysts were highly active for the aminolysis of epoxides with a range of bulkier amines. Very high conversions of epoxide and product selectivity for the A-isomer were obtained. The conversion and selectivity of the products depended on the nature and type of the amine molecules. The reaction of styrene oxide with aniline or substituted aniline gives two types of regio-isomer A and B (Scheme 4.1). Aromatic amines preferentially attack on a more stable benzylic carbon (carbocation as intermediate or favorable S_{N}^1 mechanism) of styrene oxide at α position, resulting in the formation of corresponding β -amino alcohols or regio-isomer A (primary alcoholic products). In the similar way, aromatic amines can attack on the less stable benzylic β -carbon which gives the secondary alcoholic minor products as regio-isomer B. With cyclohexylamine, n-butylamine and dibutylamine, regio-isomer-B was the selective product. Cyclohexylamine, n-butylamine and dibutylamine are aliphatic amines and

Table 4.5. Aminolysis of Epoxides over Ti-SBA-12 and Ti-SBA-16^a

Epoxide	Amine	Major Product	Ti-SBA-12 (Si/Ti = 30, 0.1 M)				Ti-SBA-16 (Si/Ti = 20, 2 M)			
			Epoxide conv. (wt%)	TOF (h ⁻¹)	Product selectivity (wt%)		Epoxide conv. (wt%)	TOF (h ⁻¹)	Product selectivity (wt%)	
					A	B			A	B
			93.7	113	92.9	7.1	96.1	156	93.0	7.0
			83.0	100	92.5	7.5	88.2	143	93.2	6.8
			78.5	95	93.5	6.5	85.8	139	91.6	8.4
			80.6	126	93.5	6.5	87.0	141	92.5	7.5

			55.1	86	98.2	1.8	83.5	136	96.3	3.7
			81.3	127	91.0	9.0	65.9	107	90.6	9.4
			62.9	98	99.6	0.4	67.8	110	99.4	0.6
			32.7	51	98.0	2.0	33.5	54	99.2	0.8
			35.5	55	10.2	89.8	33.2	54	8.4	91.6

	n-BuNH ₂		11.5	18	3.5	96.5	13.0	21	1.1	98.9
	(Bu) ₂ NH		23.5	37	4.4	95.6	29.9	49	11.4	88.6
			71.1	111	100	0	72.3	117	100	0
			63.0	99	100	0	66.5	108	100	0
			61.7	97	100	0	63.7	103	100	0
			60.6	95	100	0	65.4	106	100	0

			53.0	83	100	0	54.2	88	100	0
			48.5	76	100	0	49.0	80	100	0
			2.5	4	100	0	2.4	4	100	0
			11.5	18	100	0	12.0	18	100	0

^aReaction conditions: Catalyst = 50 mg, epoxides = 20 mmol, amine = 20 mmol, reaction temperature = 308 K, reaction time = 6 h.

Turnover frequency (TOF) = moles of epoxide converted per mole of Ti (output) in the catalyst per hour. Bu = Butyl

undergo acid-catalyzed ring-opening through a S_N^2 reaction mechanism favoring the more substituted alcohol. In this case regio-isomer B was the major product. Thus, less nucleophilic aromatic amines were found to react selectively at the benzylic carbon of styrene oxide whereas the aliphatic amines being more nucleophilic, favor the reaction at the terminal carbon following S_N^2 mechanism. This is because the aliphatic amines are harder Lewis base than the aromatic amines, which enhance their preferential adsorption on the surface of the catalysts over the epoxide.

In all these transformation, the catalytic activity (TOF) of Ti-SBA-16 was significantly higher than Ti-SBA-12 and the earlier reported SBA-15-*pr*-SO₃H and Ti-MCM-41 catalysts [37]. However, the reactivity (TOF) depended on the nature and type of amine molecule. Cyclohexene oxide is a symmetrical epoxide. Reaction with amines yielded cis- and trans-diastereomeric products (Scheme 4.1). Only the trans-diastereo isomer (A) formed with 100% selectivity over these catalysts.

Table 4.6. Catalyst Reusability Studies: Reaction of Styrene Oxide with Aniline^a

Recycle No.	Ti-SBA-12 (Si/Ti = 30, 0.1 M)				Ti-SBA-16 (Si/Ti = 20, 2 M)			
	Epoxide conv. (wt%)	TOF (h ⁻¹)	Product selectivity (wt%)		Epoxide conv. (wt%)	TOF (h ⁻¹)	Product selectivity (wt%)	
			A	B			A	B
0	92.9	145	94.0	6.0	96.0	156	95.1	4.9
1	91.6	143	92.2	7.8	95.3	155	95.1	4.9
2	91.4	143	92.2	7.8	95.3	155	94.3	5.7
3	88.9	139	93.0	7.0	94.5	153	96.5	3.5
4	88.7	139	94.0	6.0	95.2	155	93.5	6.5
5	88.4	138	93.5	6.5	93.4	152	92.5	7.5
6	87.5	137	92.4	7.6	93.0	151	91.7	8.3

^aReaction conditions: Catalyst = 50 mg, styrene oxide = 20 mmol, aniline = 20 mmol, solvent = nil, reaction time = 6 h, reaction temperature = 308 K. Turnover frequency (TOF) = moles of epoxide converted per mole of Ti (output) in the catalyst per hour

4.2.2.8. Catalyst Reusability

Catalyst recycle experiments were undertaken to establish the stability of these catalysts (Table 4.6). At the end of each recycling experiment, 10 mL of dichloromethane was added and the catalyst was separated by centrifugation/filtration. Then it was washed with acetone, dried at 373 K overnight and then, reused in subsequent recycle experiment. As seen from Table 4.6, the titanosilicate catalysts [especially Ti-SBA-16 (20, 2 M)] showed stable activity even after 6th recycle [TOF = 156 h⁻¹ (fresh) and 151 h⁻¹ (6th cycle)]. No leaching of titanium (ICP-OES) and structural collapse (XRD) was observed.

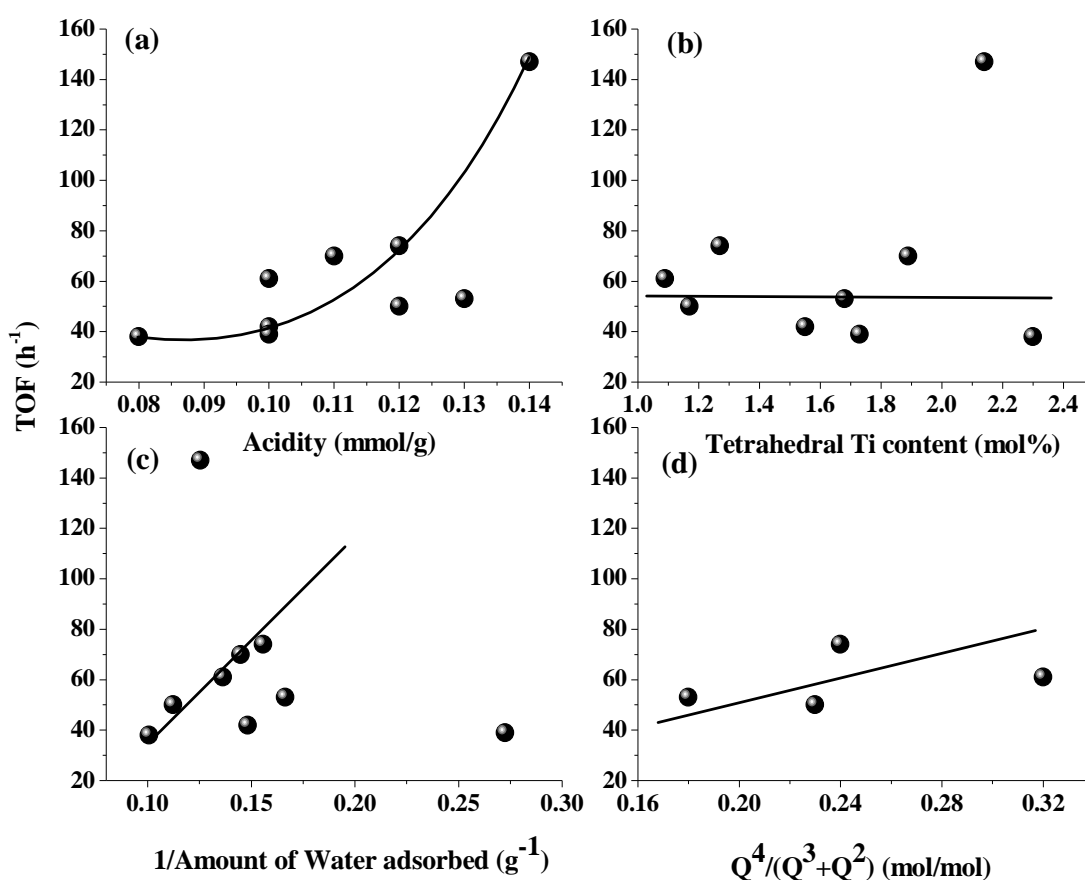


Fig. 4.4. Correlation between turnover frequency (TOF) and (a) acidity (from NH₃-TPD), (b) tetrahedral Ti content (from ICP-OES and DRUV-vis.), (c) water adsorption capacity (thermogravimetric analysis) and (d) ²⁹Si MAS NMR signal intensity of Ti-SBA-12 catalysts

4.2.2.9. Structure-Activity Correlations

To understand the factors influencing catalytic activity (TOF) of mesoporous titanosilicates, variation of TOF as a function of acidity (NH_3 -TPD), hydrophobicity (estimated based on water adsorption and ^{29}Si MAS NMR) and tetrahedral Ti content (estimated from ICP-OES and DRUV-vis. data) of Ti-SBA-12 catalysts was plotted (Fig. 4.4). Reaction conditions are the same for all these data points (Tables 4.2 and 4.3). As seen from Fig. 4.4 (traces a, c and d), catalytic activity increased with increasing acidity and hydrophobicity of the catalyst. The values of TOF should be the same irrespective of the amount of tetrahedral Ti content in the catalysts as TOF is expressed per unit of Ti concentration. However, a marginal decrease in TOF with increasing tetrahedral Ti content was observed indicating that all the Ti sites in the catalysts are probably not equally active at higher Ti concentrations. This study, thus, reveals that the high efficiency of the catalysts of the present work is due to the combined effects of framework-substituted tetrahedral Ti ions, strong Lewis acidity and surface hydrophobicity.

4.2.2.10. Tentative Reaction Mechanisms

Aminolysis of epoxides is a bimolecular reaction. Most of the reactions of epoxides involve the opening of the epoxide ring, the addition of a proton to the epoxide oxygen and the deprotonated molecule of the substrate (amine in this case) to one of the carbon atoms of the oxirane ring [39]. The reaction can occur under neutral, basic or acidic conditions. Reaction under neutral or basic conditions, involves the attack of a nucleophile on one of the epoxide carbon atoms. Under acidic conditions (Lewis acidic Ti^{4+} ions in the present case), the addition of the nucleophile is considerably accelerated due to the reversible formation of the more reactive conjugate acid of the epoxide [37]. The ring-opening reactions of epoxides take place by ionic mechanisms. The bond, which is broken, is the highly polar carbon–oxygen bond, which would be expected to break ionically. Earlier, Saikia et al. [37] found that both epoxide and amine compete for adsorptions on the acidic sites. While the amine adsorption is detrimental, epoxide adsorption and activation on acid sites are more crucial processes [37]. A tentative reaction mechanism for aminolysis of epoxides over Lewis acidic titanosilicate catalysts is shown in Fig. 4.5.

The changes in the optical spectra of Ti-SBA-12 and Ti-SBA-16 during the reaction were monitored. In these *in situ* experiments, the titanosilicate sample

activated at 573 K (for 4 h) was contacted with styrene oxide, aniline and styrene oxide + aniline (1 : 1) and the spectra were recorded. The electronic transitions of the ligand (π - π^* and n - π^*) dominated and masked the spectral features of the catalyst samples and no useful information could be derived. The optical spectra of these samples have given in the Fig. 4.6.

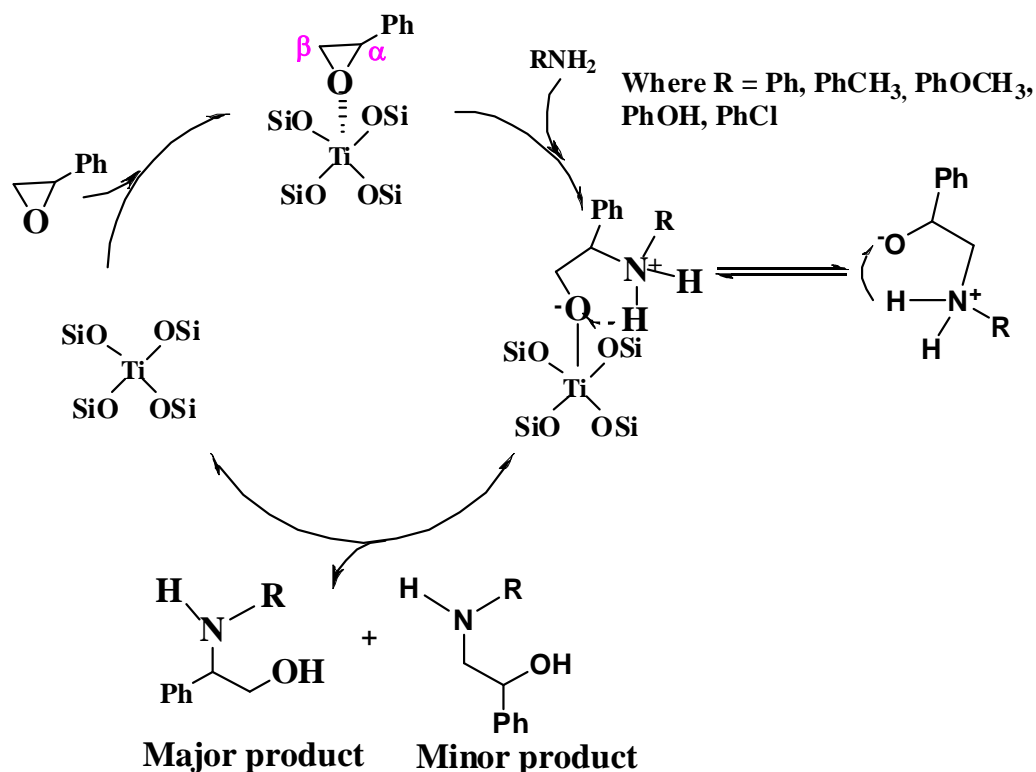


Fig. 4.5. Tentative reaction mechanism for the ring-opening of epoxides with amines

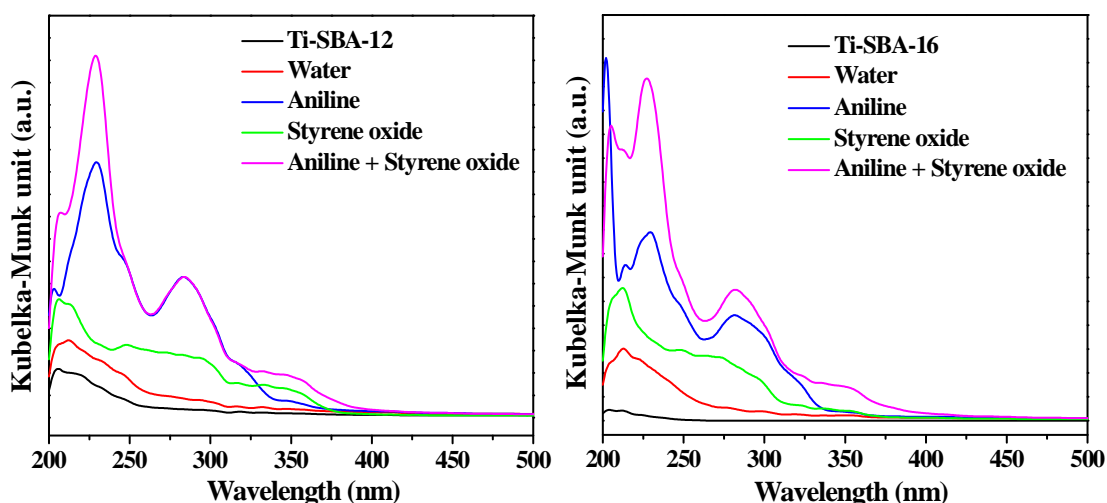


Fig. 4.6. DRUV-vis. spectra of Ti-SBA-12 and Ti-SBA-16 contacted with water, styrene oxide, aniline and the mixture of styrene oxide and aniline (1:1)

4.3. Esterification of Oleic Acid with Methanol

Fatty acids are the major components used in the preparation of a wide variety of products, such as soaps, surfactants, lubricants, plasticizers, paints, coatings, pharmaceuticals, foods, agricultural, industrial and personal care products [40]. Biodiesel (fatty acid methyl esters, FAME) can also be produced from fatty acids by esterification with methanol [41]. Biodiesel is a sustainable, non-petroleum based fuel and it comes with many advantages: (1) low emissions, (2) biodegradability, (3) non-toxicity, and (4) better lubricity [42, 43]. Conventionally, biodiesel is produced by transesterification of refined/edible oils with methanol using an alkali catalyst like NaOH, NaOCH₃ or KOH. [44-47]. However, this process has several disadvantages including non-recoverability of the catalyst for its reuse, generation of waste water (in washing step) and salt by-products (in neutralization step) and production of low-quality glycerin co-product. Moreover, the production cost of biodiesel is still higher than the petroleum-based diesel. To overcome these disadvantages, homogeneous alkali should be replaced with solid catalysts and less-expensive feedstocks such as non-edible oils (Jatropha oil and Karanja oil, for example) or animal fat should be used instead of edible oils. Non-edible oils and fats contain significant amount of free fatty acids (FFAs). The Jatropha oil contains 23% saturated fatty acids and 77% unsaturated ones. The unsaturated fatty acid, oleic acid, is the most abundant (44.7%) followed by linoleic acid (31.4%), palmitic acid (15.1%) and stearic acid (7.1%) [48, 49]. Oleic acid which is derived from Jatropha oil could be used as raw material to produce biodiesel by esterification reaction using low molecular weight alcohol such as methanol, ethanol, etc. The FFAs react with the homogeneous alkali catalysts in the conventional process forming unwanted soap by-products and deactivate the catalyst. In addition, water, sometimes present in non-edible, unrefined or waste vegetable oils also leads to the deactivation of homogeneous catalysts.

In conventional esterification processes, strong acids are used as catalysts. Homogeneous acidic catalysts such as H₂SO₄, HF, and HNO₃ have high catalytic activity and are used as effective catalysts when raw oils contain large amounts of water and fatty acids [50, 51]. The issues in this process are corrosiveness, environmental pollution, and difficulty in catalyst recovery. Solid acid catalysts have advantages over homogeneous catalyst because they are easily separable, reusable and ecofriendly. Zeolites have attracted great attention in the field of catalysis due to

their unique pore structure, high surface area and high stability [52]. However, these materials present severe limitations when large reactant molecules like fatty compounds are employed. Mass transfer is a severe issue with these microporous materials. Several solid acid catalysts like zeolites, sulfated zirconia, supported heteropoly acids, mixed and supported metal oxides, sulfonic acid functionalized mesoporous silica etc. have been used for this esterification reaction [53-64]. Sulfated catalysts have leaching problems in the reaction medium. Recently, many research articles have been published for the esterification of free fatty acid catalyzed by solid acid catalysts [65-71]. However, these solid catalysts showed lower catalytic activity. Problems associated with these catalysts are mass transfer limitations in microporous materials (zeolites) and leaching problems with sulfonic acid functionalized catalytic materials. Hence, there is a need to develop stable mesoporous solid catalysts with high catalytic activity and reusability. Ti-SBA-12 and Ti-SBA-16 are 3-D, mesoporous, titanosilicates which can enable easy diffusion and accessibility of active sites for bulky fatty molecules in esterification reactions.

4.3.1. Experimental Section

Details on the preparation and characterization of Ti-SBA-12 and Ti-SBA-16 are reported in [Chapter 2](#).

4.3.1.1. Reaction Procedure

Esterification of oleic acid with methanol was carried out in a batch reactor. In a typical reaction, 0.15 g of catalyst, 17.7 mmol of oleic acid and methanol (oleic acid to methanol molar ratio = 1 : 10) were taken in a Teflon-lined, stainless-steel autoclave (100 mL). The reaction was conducted by mounting the autoclave in a rotating hydrothermal reactor (Hiro Co., Japan; 50 rpm). At the end of the reaction, the autoclave was cooled to room temperature (298 K) and the catalyst was separated by filtration. Methanol from the reaction mixture was removed using a rotavapor and the remaining reaction mixture was used to determine the fatty acid conversion.

4.3.1.2. Product Analysis

The oleic acid conversion was determined by acid value estimation. The acid values of the reaction mixture at the beginning and at the end of the reaction were determined by titration with 0.1 N NaOH solution and using phenolphthalein as the indicator.

To determine the acid value of free fatty acid, 0.5 g or 1 g of sample was weighed and taken in a conical flask. A solvent mixture containing equal parts of isopropyl alcohol and toluene (v/v%), 3 to 5 drops of phenolphthalein indicator (1%, Merck, India) was added to it. Then the solution was titrated against 0.1 N standardized sodium hydroxide solution. Acid value of the sample can be calculated by the formula,

$$\text{Acid Value} = 56.1 \times N_{\text{NaOH}} \times V_{\text{NaOH}} / W_{\text{Sample}}$$

where 56.1 is the molecular weight of potassium hydroxide as acid value is always reported as mg of KOH per g of sample. N_{NaOH} = normality of NaOH, V_{NaOH} = volume of NaOH used in the titration, W_{Sample} = weight of the sample taken for titration. Percentage of fatty acid content was determined assuming that the molecular weight of fatty acids as 282 [72].

$$\% \text{ of Fatty acid} = (N_{\text{NaOH}} \times V_{\text{NaOH}} \times 282 / W_{\text{Sample}}) \times 100$$

4.3.2. Catalytic Activity

Oleic acid (OA, $C_{18.1}$) with eighteen carbon atoms and one double bond between C_9 and C_{10} carbon atoms is a major constituent of several vegetable oils including soybean, rapeseed and corn. So it was taken in this study as a representative fatty acid present in edible and non-edible vegetable oils. Esterification of OA with methanol (a monohydric alcohol) results in methyl oleate ester which is a suitable substitute for the conventional petroleum diesel. Methyl oleate has lower cold flow properties than palmitate ($C_{16.0}$) and stearate ($C_{18.0}$) esters and better oxidation stability than linolic ($C_{18.2}$) and linolenic ($C_{18.3}$) esters [73]. The esterification reaction of OA with methanol (Eq. 1) produces water as by-product. Most of the acid catalysts get destabilized in the presence of water and cannot be reused in a long run [74]. Ti-SBA-12 and Ti-SBA-16 titanosilicates were examined for the catalytic performance in this reaction. The effect of Ti content in these SBA catalysts, reaction time, reaction temperature and catalyst reusability on esterification activity was examined.



4.3.2.1. Influence of Si/Ti Molar Ratio

Table 4.7 presents the catalytic activity data of Ti-SBA-12 and Ti-SBA-16 with varying Si/Ti molar ratio for the esterification of OA with methanol at 443 K

Table 4.7. Catalytic Activity of Ti-SBA-12 and Ti-SBA-16 for Esterification of Oleic Acid with Methanol^a

Entry No.	Catalyst	Catalytic Activity			
		OA conv. (mol%)	TOF (h ⁻¹)		
			Based on total output Ti	Based on framework Ti	Based on acidity
1	SBA-12	18.1	-	-	-
2	Ti-SBA-12 (80)	26.0	269	283	372
3	Ti-SBA-12 (50)	40.9	232	260	493
4	Ti-SBA-12 (40)	41.2	201	247	408
5	Ti-SBA-12 (30)	29.7	129	163	294
6	Ti-SBA-12 (20)	32.3	104	132	305
7	SBA-16	17.5	-	-	-
8	Ti-SBA-16 (80)	27.5	293	293	345
9	Ti-SBA-16 (50)	29.2	167	167	398
10	Ti-SBA-16 (40)	16.8	84	84	197
11	Ti-SBA-16 (30)	21.5	83	85	238
12	Ti-SBA-16 (20)	19.7	56	64	201

^aReaction conditions: catalyst = 0.15 g; oleic acid (OA) = 5 g; oleic acid : methanol (molar ratio) = 1 : 10; reaction temperature = 443 K and reaction time = 1 h. Turnover frequency (TOF) = moles of OA converted per mole of total or framework substitute Ti or acidity of the catalyst per hour

for 1 h. The reaction occurs even without a catalyst at our experimental conditions. However, OA conversion was 16 mol% only. No significant improvement in OA conversion was found when the reaction was carried out in the presence of all silica SBA-12 and SBA-16 (Table 4.7, entry nos. 1 and 7). This suggests that silanol groups on these silica materials are not catalytically active. A marked increase in OA conversion was observed when the reaction was performed in the presence of titanium-containing SBA-12 and SBA-16 (Table 4.7). OA conversion increased from 16.1 (without any catalyst) to 29.2 with Ti-SBA-16 (50), (Table 4.7, entry no. 9) and 41.2 mol% with Ti-SBA-12 (40), (Table 4.7, entry no. 4). Ti-SBA-12 are relatively more active than Ti-SBA-16. This study, thus, reveals that Lewis acidic Ti are the

active sites in the mesoporous titanosilicates. The intrinsic catalytic activity (turnover frequency, TOF) was calculated based on total amount of Ti present in the catalyst, Ti presently exclusively in framework locations as tetrahedral sites and acidity estimated from NH₃-TPD measurements (Chapter 2, Table 2.2 and 2.5).

In general, the TOF values estimated based on acidity of the catalysts have been found to be higher than those calculated using the Ti content (Table 4.7). Further, the values estimated based on framework Ti have been found to be higher than those based on total amount of Ti. The intrinsic catalytic activity of Ti (TOF values) decreased with decrease in Si/Ti molar ratio revealing that all Ti ions in titanosilicate catalysts do not have the same activity. Their intrinsic activity decreased with increasing Ti content in the catalyst sample. Ti-SBA-12 having large pore diameter, specific surface area and pore volume than Ti-SBA-16 (Chapter 2, Table 2.4) showed higher catalytic activity (conversion and TOF) for esterification of OA with methanol. This is possibly due to more facile diffusion of fatty acid molecules inside the mesoporous silica matrix and accessibility of all the active Ti sites inside the pores. Neat anatase titania (TiO₂) and microporous TS-1 were not active for this reaction. This suggests that only the dispersed and framework substituted, tetraordinated Ti sites and the mesoporous architecture facilitate the catalytic esterification reaction.

4.3.2.2. Influence of Reaction Time and Temperature

Reactions were conducted at four different temperatures (413, 423, 433 and 443 K). Conversion of OA was monitored as a function of time (Fig. 4.7). Conversion of OA increased with increasing reaction time and temperature. At 443 K, about 90 mol% of OA got converted into its methyl ester when the reaction was carried out for 8 h. From the conversion versus time plots, the initial rates of reaction at different temperatures were determined. Then the rate constant (k) was calculated using the pseudo-first order rate law. Note that methanol was taken in excess in all these reactions (OA : methanol molar ratio = 1 : 10). Employing the Arrhenius equation, activation energy values (E_a) were determined (Fig. 4.8). The E_a values for Ti-SBA-12 (40) and Ti-SBA-16 (50) were estimated to be 42.7 and 25.6 KJ/mol, respectively. Detailed characterization studies (thermal analysis and ²⁹Si MAS NMR) reported in (Chapter-2, Fig. 2.21) revealed that Ti-SBA-16 is relatively more hydrophobic than Ti-SBA-12. Hence, the byproduct water generated in the

esterification reaction (eq. 1) doesn't compete for adsorption with the reactants on Ti-SBA-16 surface and thereby, lowers the activation energy compared to that for Ti-SBA-12.

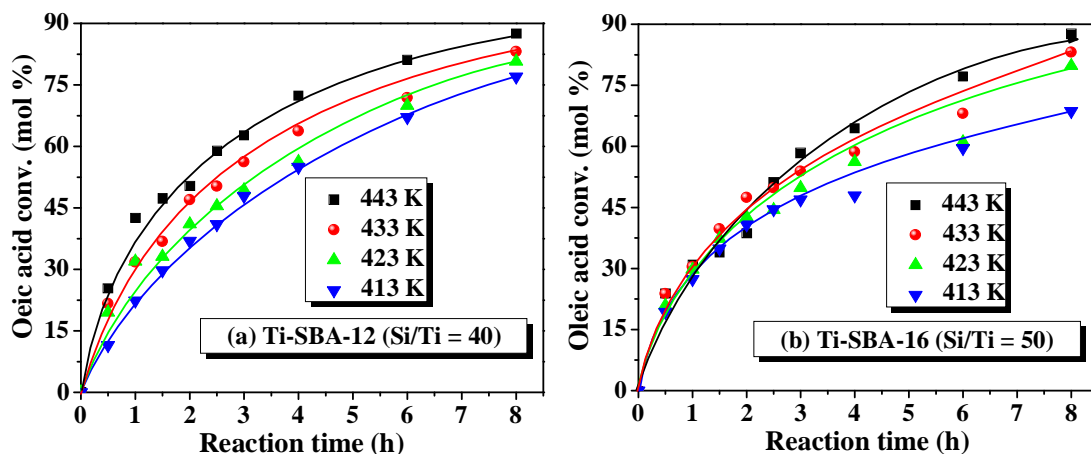


Fig. 4.7. Effect of reaction time and temperature on the esterification of oleic acid with methanol. ^aReaction conditions: catalyst = [Ti-SBA-12 (40) or Ti-SBA-16 (50)] = 0.15 g, OA : methanol (molar ratio) = 1 : 10

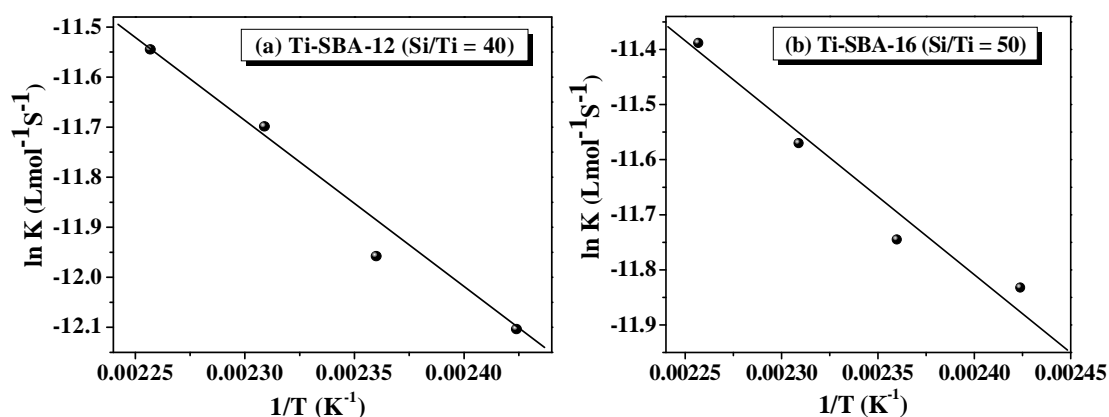


Fig. 4.8. Arrhenius plots for the calculation of energy of activation (E_a)

4.3.2.3. Catalyst Reusability

Reusability of the catalysts was investigated in four recycling experiments. After each reaction, the catalyst was separated from the reaction mixture by filtration, washed with methanol, dried at 373 K for 3 h and then, reused in the subsequent recycle. As seen from Fig. 4.9, the esterification activities (OA conversion) of both Ti-SBA-12 (40) and Ti-SBA-16 (50) were almost the same in all

the four recycling experiments. No leaching of Ti ions from the solid catalyst was detected (ICP-OES).

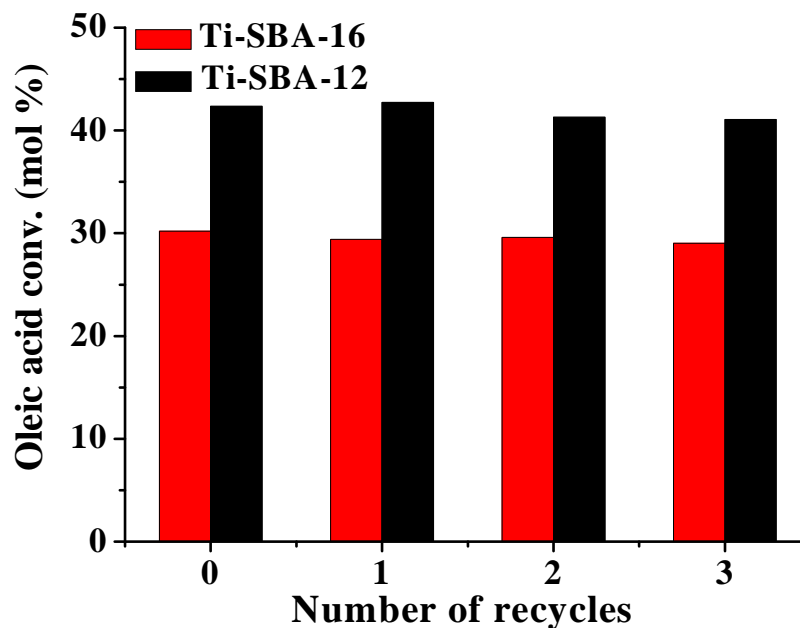


Fig. 4.9. Catalyst reusability study in the esterification of oleic acid (OA) with methanol. Reaction conditions: catalyst [Ti-SBA-12 (40) or Ti-SBA-16 (50)] = 0.15 g, OA = 5 g, OA : methanol (molar ratio) = 1 : 10, reaction temperature = 443 K, reaction time = 1 h

4.4. Conclusions

A range of β -amino alcohols with high regio- and stereoselectivity were synthesized in solvent-free reaction conditions over three-dimensional mesoporous titanosilicates, Ti-SBA-12 and Ti-SBA-16 by reacting symmetric or unsymmetric epoxides with aromatic as well as aliphatic amines. Structure-function relationships reveal that the superior activity of Ti-SBA-16 is possibly due to its high amount of framework-substituted tetrahedral Ti ions, higher acidity and surface hydrophobicity.

Esterification of oleic acid with methanol was investigated over Ti-SBA-12 and Ti-SBA-16 catalysts. Energy of activation (E_a) was estimated to be 42.7 and 25.6 kJ/mol for Ti-SBA-12 and Ti-SBA-16, respectively. Higher amount of surface hydrophobicity is the cause of more efficient activity of Ti-SBA-16 than Ti-SBA-12.

These titanosilicates are highly efficient catalyst for their application in Lewis acid-catalyzed synthesis of β -amino alcohols and production of fatty acid methyl ester (FAME, biodiesel).

4.5. References

1. J. Clark, D. Macquarrie (Eds.), *Hand Book of Green Chemistry and Technology*, Blackwell, UK, 2002, xviii.
2. G. Busca, *Chem. Rev.* 107 (2007) 5366.
3. K. Tanabe, W.F. Hölderich, *Appl. Catal. A: Gen.* 181 (1999) 399.
4. P. Ratnasamy, D. Srinivas, H. Knözinger, *Adv. Catal.* 48 (2004) 1.
5. R.A. Sheldon, *Pure Appl. Chem.* 72 (2000) 1233.
6. M. Taramasso, G. Perego, B. Notari, U.S. Patent 4410501, 1983.
7. M. Taramasso, G. Perego, B. Notari, U.K. Patent GB. 2071 B (1983), assigned to SNAM Progetti, Italy.
8. Y. Kubota, Y. Koyama, T. Yamada, S. Inagaki, T. Tatsumi, *Chem. Commun.* (2008) 6224.
9. H. Xin, J. Zhao, S. Xu, J. Li, W. Zhang, X. Guo, E.J.M. Hensen, Q. Yang, C. Li, *J. Phys. Chem. C* 114 (2010) 6553.
10. A. Thangaraj, S. Sivasanker, P. Ratnasamy, *J. Catal.* 137 (1992) 252.
11. J. S. Reddy, R. Ravishanker, S. Sivasanker, P. Ratnasamy, *Catal. Lett.* 17 (1993) 139.
12. R. Srivastava, D. Srinivas, P. Ratnasamy, *Catal. Lett.* 91 (2003) 133.
13. D. Srinivas, R. Srivastava, P. Ratnasamy *Catal. Today* 96 (2004) 127.
14. M. Sasidharan, R. Kumar, *J. Catal.* 220 (2003) 326.
15. T. Mukaiyama, K. Bano, K. Narasaka, *J. Am. Chem. Soc.* 96 (1974) 7503.
16. M. Sasidharan, P. Wu, T. Tatsumi, *J. Catal.* 209 (2002) 260.
17. R. Garro, M.T. Navarro, J. Primo, A. Corma, *J. Catal.* 233 (2005) 342.
18. M. Sasidharan, A. Bhaumik, *J. Mol. Catal. A: Chem.* 346 (2011) 87.
19. C.R. Bayense, H. Hinnekens, J. Martens, U.S. Patent 5508457 (1996).
20. T. Kawabata, T. Mizugaki, K. Ebitani, K. Kaneda, *Tetrahedron Lett.* 44 (2003) 9205.
21. O. Mitsunobu, in: B. M. Trost, I. Fleming (Eds.), *Comprehensive Organic Synthesis*, vol. 6, Springer, New York, 1991, p. 88.
22. E.J. Corey, F.-Y. Zhang, *Angew. Chem. Int. Ed. Engl.* 38 (1999) 1931.
23. P. O'Brien, *Angew. Chem. Int. Ed. Engl.* 38 (1999) 326.
24. D.J. Ager, I. Prakash, D.R. Schaad, *Chem. Rev.* 96 (1996) 835.
25. S.C. Bergmeier, *Tetrahedron* 56 (2000) 2561.

26. M.W. Bedore, N. Zaborenko, K.F. Jensen, T.F. Jamison, *Org. Proc. Res. Dev.* 14 (2010) 432.
27. N. Zaborenko, M.W. Bedore, T.F. Jamison, K.F. Jensen, *Org. Proc. Res. Dev.* 15 (2011) 131.
28. A. Procopio, M. Gaspari, M. Nardi, M. Oliverio, O. Rosati, *Tetrahedron Lett.* 49 (2008) 2289.
29. M.J. Bhanushali, N.S. Nandurkar, M.D. Bhor, B.M. Bhanage, *Tetrahedron Lett.* 49 (2008) 3672.
30. J. Agarwal, A. Duley, R. Rani, R. Peddinti, *Synthesis* 16 (2009) 2790.
31. M. Moghadam, S. Tangestaninejad, V. Mirkhani, I. Mohammadpoor-Baltork, S. Gorjipoor, P. Yazdani, *Syn. Commun.* 39 (2009) 552.
32. M. Vijender, P. Kishore, P. Narender, B. Satyanarayana, *J. Mol. Catal. A: Chem.* 266 (2007) 290.
33. R.I. Kureshy, S. Singh, N.H. Khan, S.H.R. Abdi, E. Suresh, R.V. Jasra, *J. Mol. Catal. A: Chem.* 264 (2007) 162.
34. M.W.C. Robinson, D.A. Timms, S.M. Williams, A.E. Graham, *Tetrahedron Lett.* 48 (2007) 6249.
35. R. Chakravarti, H. Oveisi, P. Kalita, R.R. Pal, S.B. Halligudi, M.L. Kantam, A. Vinu, *Micropor. Mesopor. Mater.* 123 (2009) 338.
36. J.K. Satyarthi, L. Saikia, D. Srinivas, P. Ratnasamy, *Appl. Catal. A: Gen.* 330 (2007) 145.
37. L. Saikia, J.K. Satyarthi, D. Srinivas, P. Ratnasamy, *J. Catal.* 252 (2007) 148.
38. L. Saikia, J.K. Satyarthi, R. Gonnade, D. Srinivas, P. Ratnasamy, *Catal. Lett.* 123 (2008) 24.
39. R.E. Parker, N.S. Isaacs, *Chem. Rev.* 59 (1959) 737.
40. An Ullmann's Encyclopedia, *Industrial Organic Chemicals: Starting Materials and Intermediates*, Wiley-VCH, Weinheim, Germany, Vol. 4, 1999, pp. 2481.
41. D. Kusdiana, S. Saka, *Appl. Biochem. Biotechnol.* 113–116 (2004) 781.
42. G. Knothe, C.A. Sharp, T.W. Ryan III, *Energy Fuels* 20 (2006) 403.
43. A.A. Kiss, A.C. Dimian, G. Rothenberg, *Adv. Synth. Catal.* 348 (2006) 75.
44. A.W. Schwab, M.O. Bagby, B. Freedman, *Fuel* 66 (1987) 1372.
45. B. Freedman, R.O. Butterfield, E.H. Pryde, *J. Am. Oil Chem. Soc.* 63 (1986)

- 1375.
46. C. Stavarache, M. Vinatoru, R. Nishimura, Y. Maed, *Ultrason. Sonochem.* 12 (2005) 367.
 47. H.A. Aksoy, I. Becerik, F. Karaosmanoglu, H.C. Yamaz, H. Civelekoglu, *Fuel* 69 (1990) 600.
 48. A. Thomas, "Fats and Fatty Oils" *Ullmann's Encyclopaedia of Industrial Chemistry* (2000).
 49. N. Foidl, G. Foidl, M. Sanchez, M. Mittelbach, S. Hackel, *Bioresour. Technol.* 58 (1996) 77.
 50. U.R. Unnithan, K.K. Tiwari, *Indian J. Technol.* 25 (1987) 477.
 51. B. Chemseddine, R. Audinos, *Catal. Today* 25 (1995) 417.
 52. G.J. Suppes, M.A. Dasari, E.J. Doskocil, P.J. Mankidy, M.J. Goff, *Appl. Catal. A: Gen.* 257 (2004) 213.
 53. A. Brito, M.E. Borges, N. Otero, *Energy Fuels* 21 (2007) 3280.
 54. T.S. Koh, K.H. Chung, *J. Kor. Ind. Eng. Chem.* 19 (2008) 214.
 55. D.E. López, J.G. Goodwin Jr., D.A. Bruce, S. Furuta, *Appl. Catal. A: Gen.* 339 (2008) 76.
 56. I. Jimenez-Morales, M.A. del Rio-Tejero, P. Braos-Garcia, *Fuel Process. Technol.* 97 (2012) 65.
 57. C.S. Caetano, I.M. Fonseca, A.M. Ramos, *Catal. Commun.* 9 (2008) 1996.
 58. S.A. Fernandes, A.L. Cardoso, da Silva, M. Jose, *Fuel Process. Technol.* 96 (2012) 98.
 59. A. Sarkar, S.K. Ghosh, K. Sudip, P. Pramanik, *J. Mol. Catal. A: Chem.* 327 (2010) 73.
 60. I.J.-Morales, J.S.-Gonzalez, P.M.-Torres, *Appl. Catal. A: Gen.* 379 (2010) 61.
 61. S. Furuta, H. Matsushashi, K. Arata (2004) *Catal. Commun.* 5 (2004) 721.
 62. W.D. Bossaert, D.E. De Vos, W.M.V. Rhijn, J. Bullen, P.J. Grobet, P.A. Jacobs, *J. Catal.* 182 (1999) 156.
 63. I. Diaz, C. Marquez-Alvarez, F. Mohino, *J. Catal.* 193 (2000) 295.
 64. J. Pérez-Pariente, I. Diaz, F. Mohino, E. Sastre, *Appl. Catal. A: Gen.* 254 (2003) 173.
 65. L. Afanador, S. Ortega, R. Gómez, M.E. Niño-Gómez, *Fuel* 100 (2012) 43.
 66. K.-H. Chung, B.-G. Park, *Ind. Eng. Chem. Res.* 15 (2009) 388.

67. B. Chang, J. Fu, Y. Tian, X. Dong, *Appl. Catal. A: Gen.* 437-438 (2012) 149.
68. M.G.M. D'Oca, R.M. Soares, R.R. de Moura, V.de F. Granjão, *Fuel* 97 (2012) 884.
69. J.R. Kastner, J. Miller, D.P. Geller, J. Locklin, L.H. Keith, T. Johnson, *Catal. Today* 190 (2012) 122.
70. K.V. Thiruvengadaravi, J. Nandagopal, P. Baskaralingam, V.S.S. Bala, S. Sivanesan, *Fuel* 98 (2012) 1.
71. C. Pirez, J.-M. Caderon, J.-P. Dacquin, A.F. Lee, K. Wilson, *ACS Catal.* 2 (2012) 1607.
72. J. Mendham, R.C. Denney, J.D. Barnes, M.J.K. Thomas, *Vogel's Textbook of Quantitative Chemical Analysis*, 6th Ed., Pearson Education limited (2006).
73. A. Demirbas, *Biofuels: Securing the Planet's Future Energy Needs* Springer-Verlag, London, 2009.
74. M. Di Serio, R. Tesser, L. Pengmei, E. Santacesaria, *Energy Fuels* 22 (2008) 207.

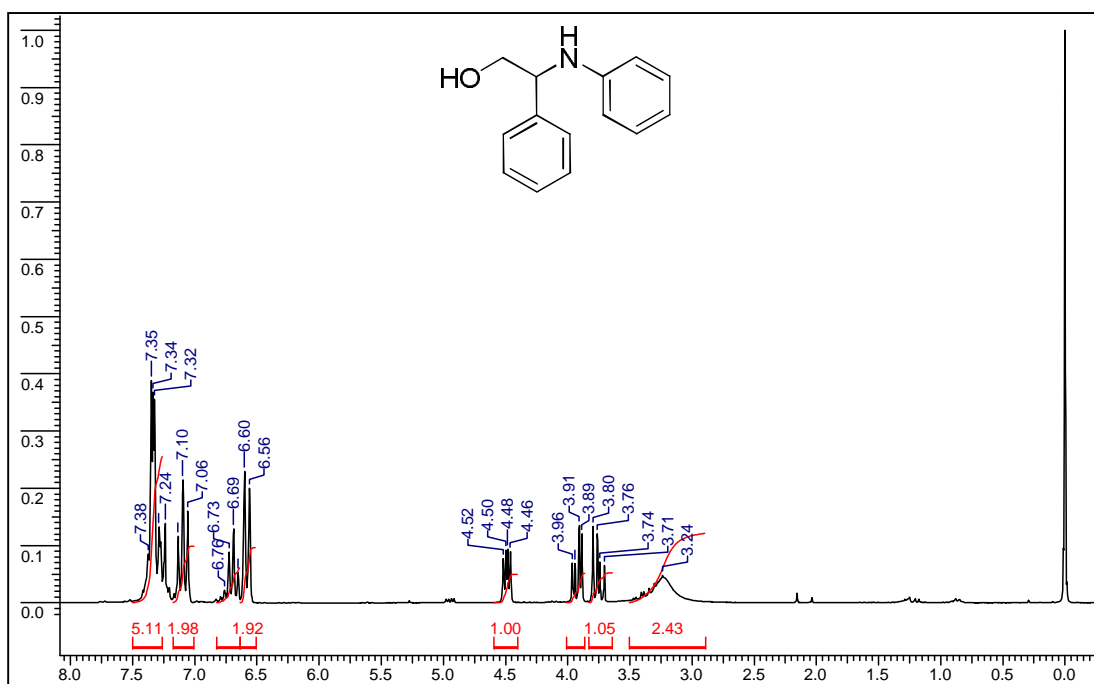
APPENDIX-I

 ^1H NMR Characteristics of Some Isolated β -amino Alcohol Products

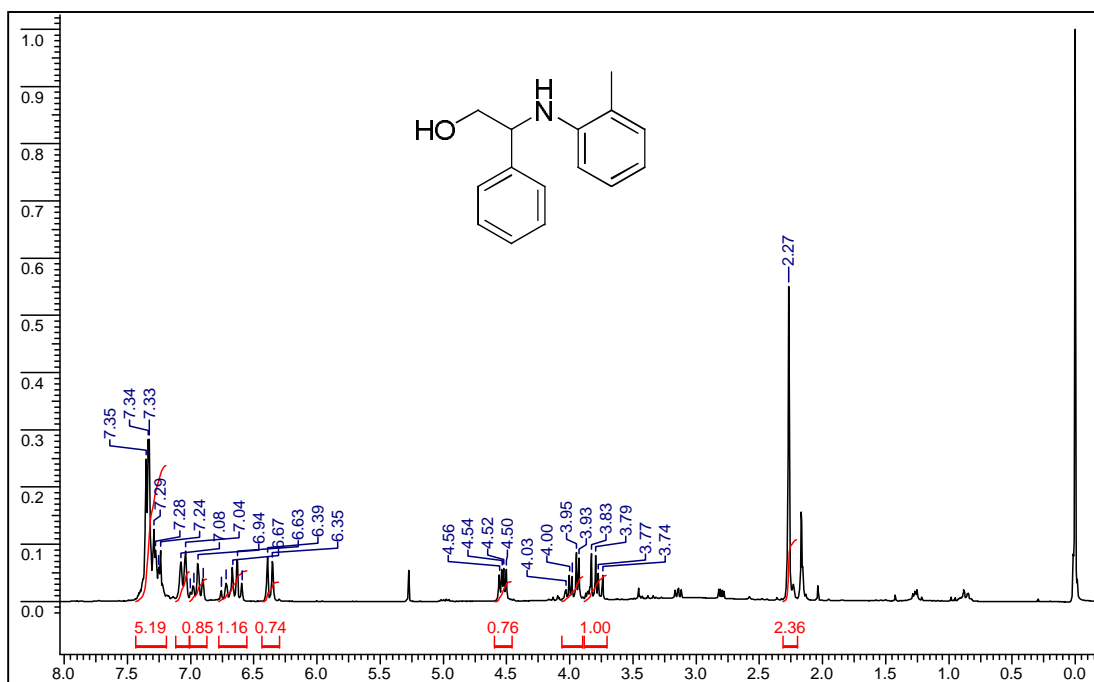
^1H NMR spectral data of some isolated β -amino alcohol compounds in CDCl_3 are given below. Spectra were recorded on a 200 or 500 MHz Bruker Avance NMR spectrometer using $(\text{CH}_3)_4\text{Si}$ as a reference.

Compound 1: 2-Phenylamino-2-phenylethanol

^1H NMR (CDCl_3 , 200 MHz): $\delta = 3.71\text{--}3.80$ ppm (dd, $J = 11.24$ and 7.20 Hz, 1H), $3.89\text{--}3.96$ ppm (dd, $J = 11.24$ and 4.17 Hz, 1H), $4.46\text{--}4.52$ ppm (dd, $J = 7.07$ and 4.17 Hz, 1H), $6.56\text{--}6.60$ ppm (d, $J = 7.83$ Hz, 2H), $6.65\text{--}6.73$ ppm (t, $J = 7.20$ Hz, 1H), $7.06\text{--}7.14$ ppm (t, $J = 7.71$ Hz, 2H), $7.24\text{--}7.36$ ppm (m, 5H).

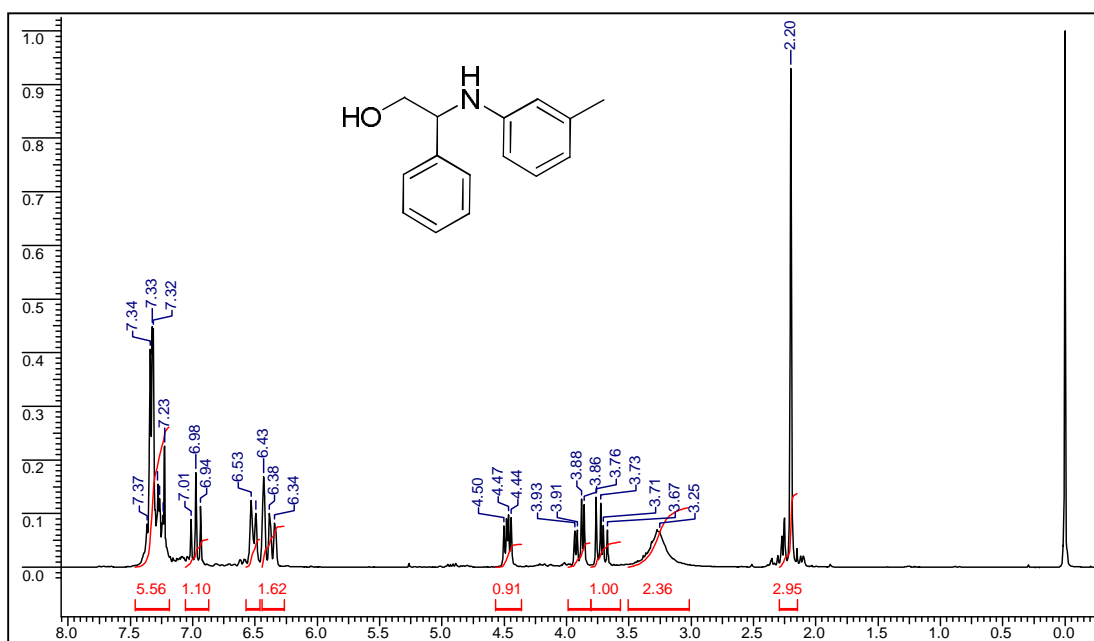
**Compound 2:** 2-(2-Methylphenylamino)-2-phenylethanol

^1H NMR (CDCl_3 , 200 MHz): $\delta = 2.27$ ppm (s, 3H), $3.74\text{--}3.83$ ppm (dd, $J = 11.12$ and 7.07 Hz, 1H), $3.93\text{--}4.0$ ppm (dd, $J = 11.0$ and 4.17 Hz, 1H), $4.50\text{--}4.56$ ppm (dd, $J = 7.08$ and 4.17 Hz, 1H), $6.35\text{--}6.39$ ppm (d, $J = 7.96$ Hz, 1H), $6.59\text{--}6.67$ ppm (t, $J = 7.32$ Hz, 1H), $6.91\text{--}6.98$ ppm (t, $J = 7.58$ Hz, 1H), $7.04\text{--}7.08$ ppm (d, $J = 7.33$ Hz, 1H), $7.24\text{--}7.36$ ppm (m, 5H).



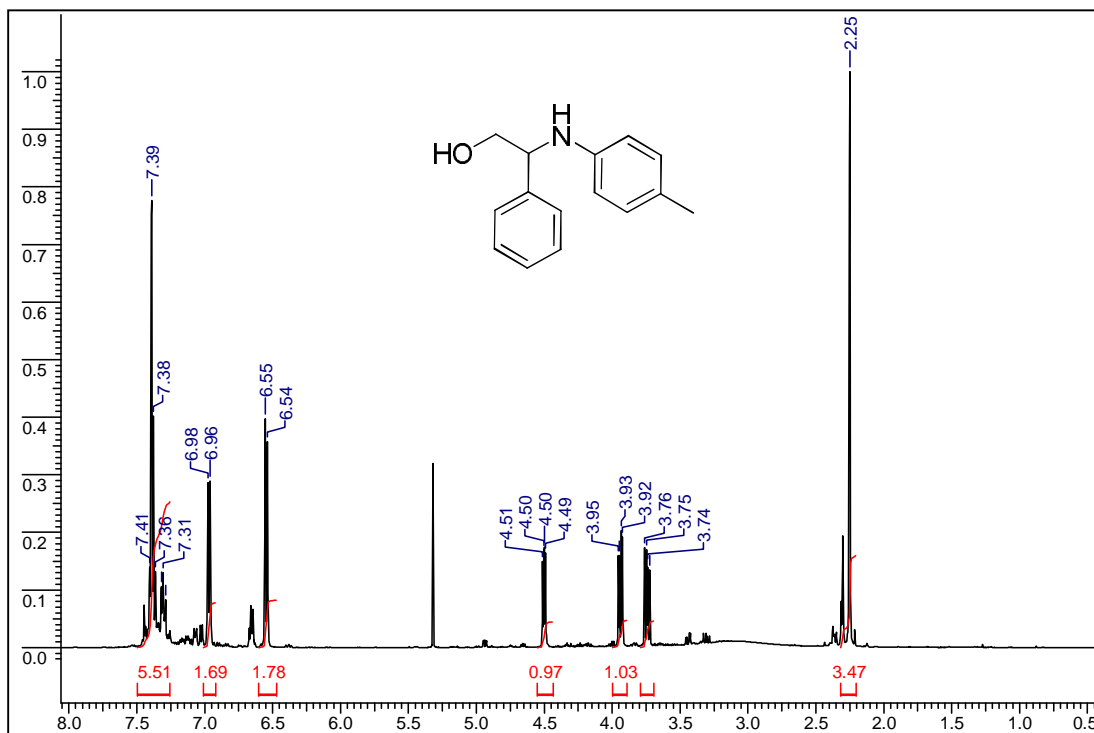
Compound 3: 2-(3-Methylphenylamino)-2-phenylethanol

^1H NMR (CDCl₃, 200 MHz): δ = 2.20 ppm (s, 3H), 3.67–3.76 ppm (dd, J = 11.11 and 7.20 Hz, 1H), 3.86–3.93 ppm (dd, J = 11.12 and 4.17 Hz, 1H), 4.44–4.50 ppm (dd, J = 7.08 and 4.30 Hz, 1H), 6.34–6.43 ppm (t, J = 8.09 Hz, 2H), 6.49–6.53 ppm (d, J = 7.45 Hz, 1H), 6.94–7.01 ppm (t, J = 7.70 Hz, 1H), 7.23–7.36 ppm (m, 5H).

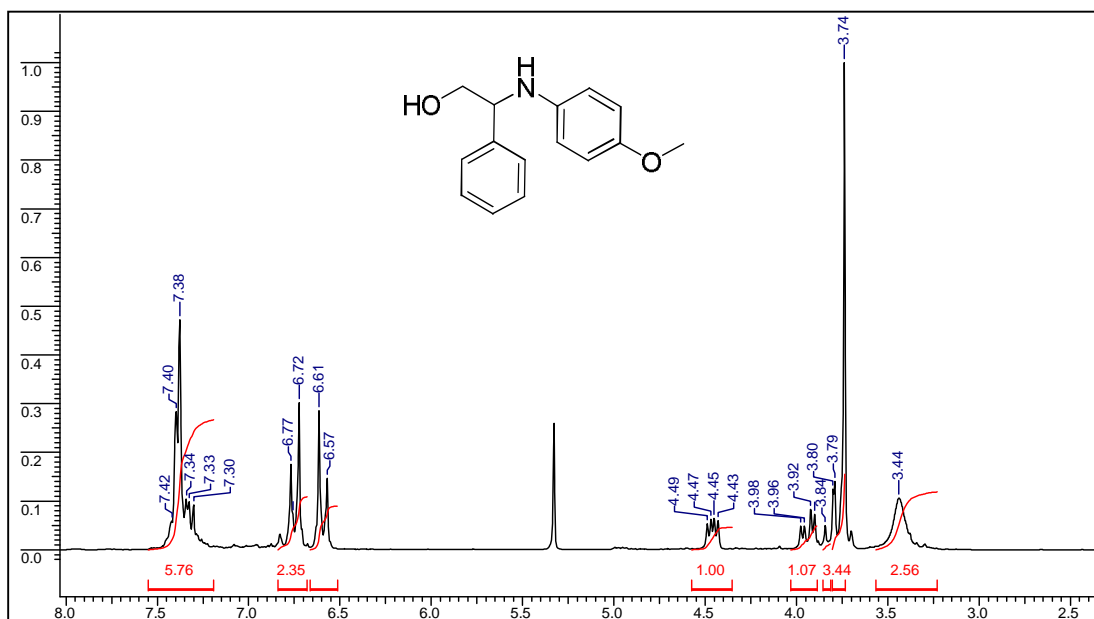


Compound 4: 2-(4-Methylphenylamino)-2-phenylethanol

^1H NMR (CDCl_3 , 500 MHz): δ = 2.25 ppm (s, 3H), 3.72–3.76 ppm (dd, J = 11.30 and 7.32 Hz, 1H), 3.92–3.95 ppm (dd, J = 11.0 and 4.27 Hz, 1H), 4.49–4.51 ppm (dd, J = 7.32 and 4.27 Hz, 1H), 6.54–6.55 ppm (d, J = 8.24 Hz, 2H), 6.96–6.98 ppm (d, J = 7.94 Hz, 2H), 7.31–7.41 ppm (m, 5H).

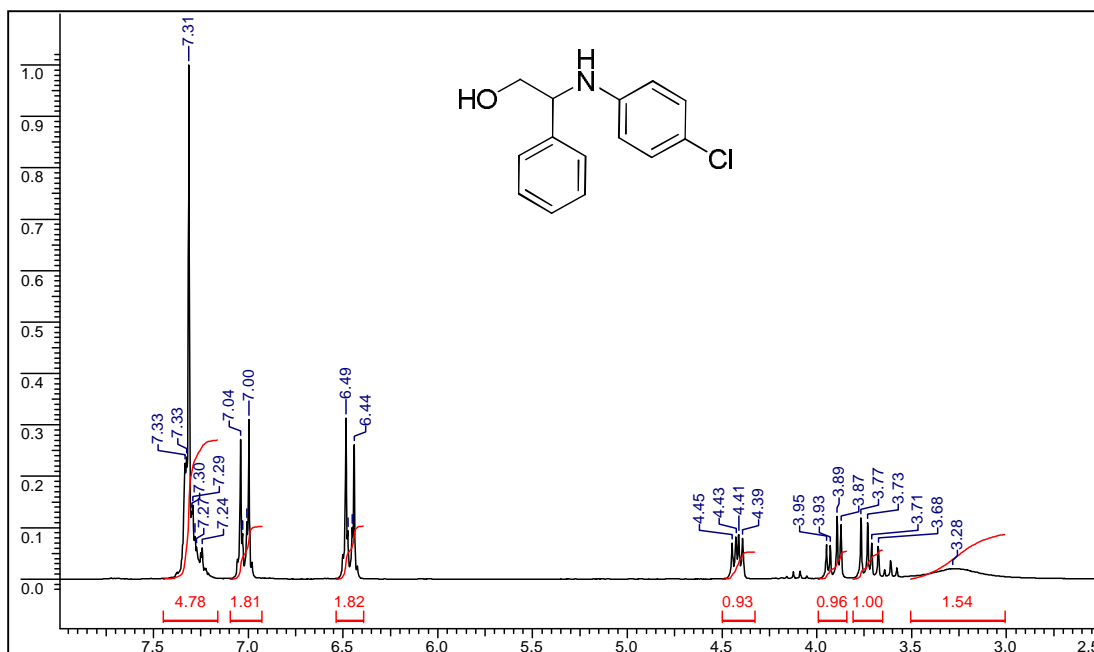
**Compound 5:** 2-(4-Methoxyphenylamino)-2-phenylethanol

^1H NMR (CDCl_3 , 200 MHz): δ = 3.74 ppm (s, 3H), 3.76–3.80 ppm (dd, 1H), 3.90–3.98 ppm (dd, J = 11.12 and 4.17 Hz, 1H), 4.43–4.49 ppm (dd, J = 7.58 and 4.17 Hz, 1H), 6.57–6.61 ppm (d, J = 8.97 Hz, 2H), 6.72–6.77 ppm (d, J = 8.96 Hz, 2H), 7.30–7.40 ppm (m, 5H).



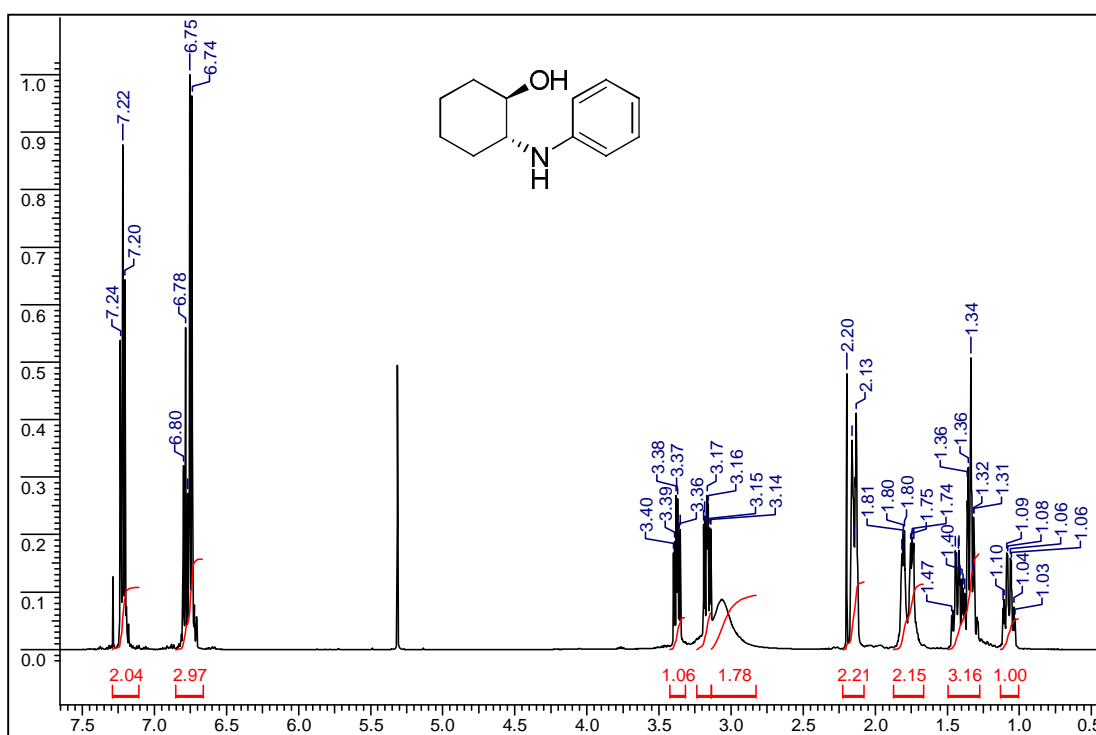
Compound 6: 2-(4-Chlorophenylamino)-2-phenylethanol

¹H NMR (CDCl₃, 200 MHz): δ = 3.68–3.77 ppm (dd, J = 11.12 and 7.95 Hz, 1H), 3.87–3.95 ppm (dd, J = 11.24 and 4.04 Hz, 1H), 4.39–4.45 ppm (dd, J = 6.95, 4.04 Hz, 1H), 6.44–6.49 ppm (d, J = 8.84 Hz, 2H), 7.0–7.04 ppm (d, J = 8.84 Hz, 2H), 7.22–7.33 ppm (m, 5H).

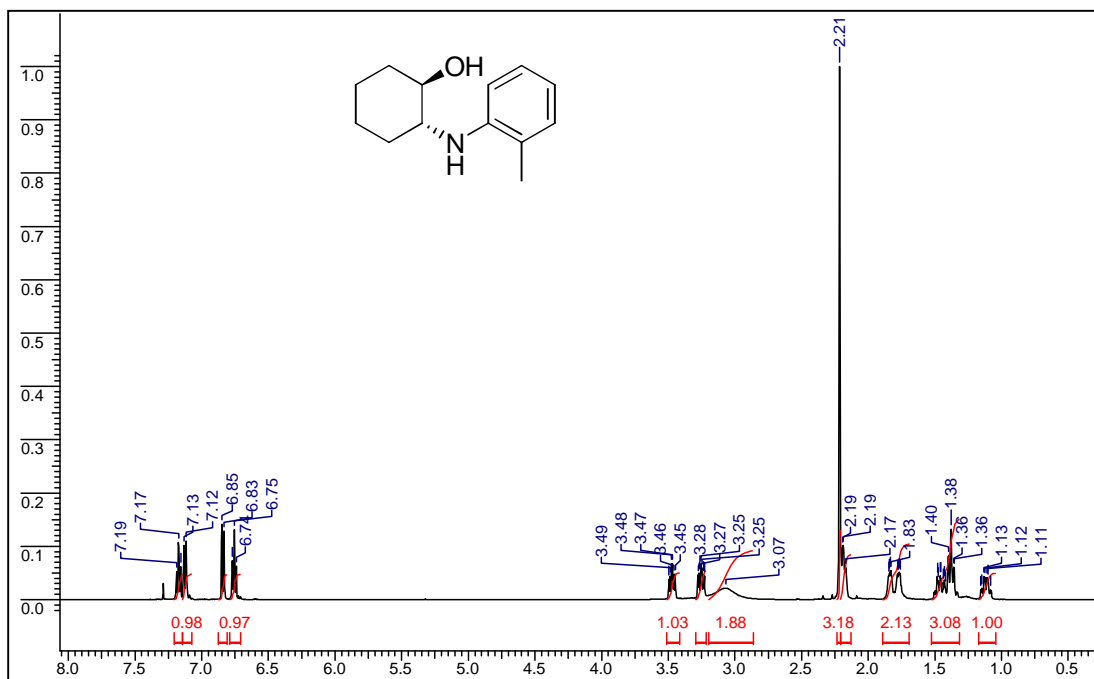


Compound 7: *trans*-2-(Phenylamino)cyclohexanol

^1H NMR (CDCl_3 , 500 MHz): δ = 1.03–1.11 ppm (m, 1H; CH_2), 1.29–1.47 ppm (m, 3H; CH_2), 1.73–1.82 ppm (m, 2H; CH_2), 2.13–2.16 ppm (m, 2H; CH_2), 3.06 ppm (bs, 2H, NH and OH), 3.14–3.19 ppm (ddd, J = 11.30, 9.15 and 3.97 Hz, 1H; CH), 3.35–3.40 ppm (ddd, J = 9.46, 9.46 and 4.27 Hz, 1H; CH), 6.74–6.80 ppm (m, 3H; ArH), 7.18–7.24 ppm (m, 2H; ArH).

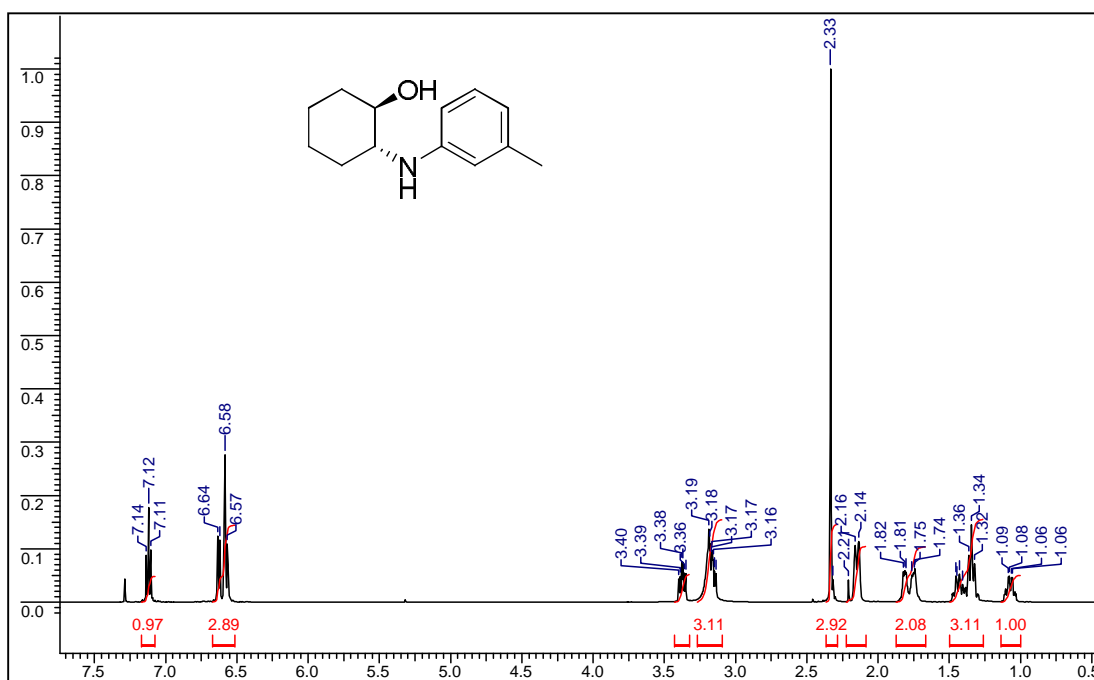
**Compound 8:** *trans*-2-(2-Methylphenylamino)cyclohexanol

^1H NMR (CDCl_3 , 500 MHz): δ = 1.08–1.16 ppm (m, 1H; CH_2), 1.33–1.51 ppm (m, 3H; CH_2), 1.76–1.85 ppm (m, 2H; CH_2), 2.17–2.19 ppm (m, 2H; CH_2), 2.21 ppm (s, 3H; CH_3), 3.07 ppm (bs, 2H, NH and OH), 3.23–3.28 ppm (ddd, J = 10.98, 9.46 and 3.96 Hz, 1H; CH), 3.45–3.49 ppm (ddd, J = 10.37, 9.77 and 4.57 Hz, 1H; CH), 6.74–6.77 ppm (m, 1H; ArH), 6.83–6.85 ppm (d, 1H; ArH), 7.12–7.19 ppm (m, 2H; ArH).



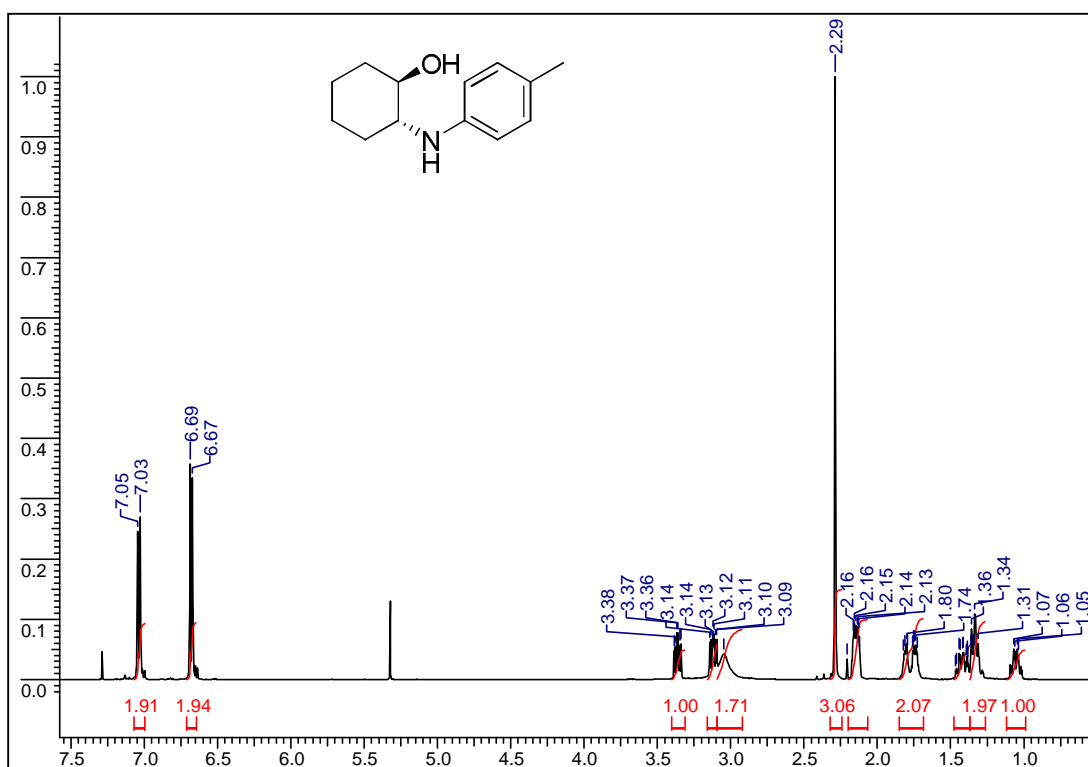
Compound 9: *trans*-2-(3-Methylphenylamino)cyclohexanol

¹H NMR (CDCl₃, 500 MHz): δ = 1.03–1.11 ppm (m, 1H; CH₂), 1.30–1.48 ppm (m, 3H; CH₂), 1.74–1.82 ppm (m, 2H; CH₂), 2.16 ppm (m, 2H; CH₂), 2.33 ppm (s, 3H; CH₃), 3.14–3.17 ppm (m, 1H; CH), 3.19 ppm (bs, 2H, NH and OH), 3.35–3.40 ppm (ddd, J = 10.37, 9.77 and 4.57 Hz, 1H; CH), 6.57–6.58 ppm (d, 2H; ArH), 6.62–6.64 ppm (d, 1H; ArH), 7.11–7.14 ppm (t, 1H; ArH).

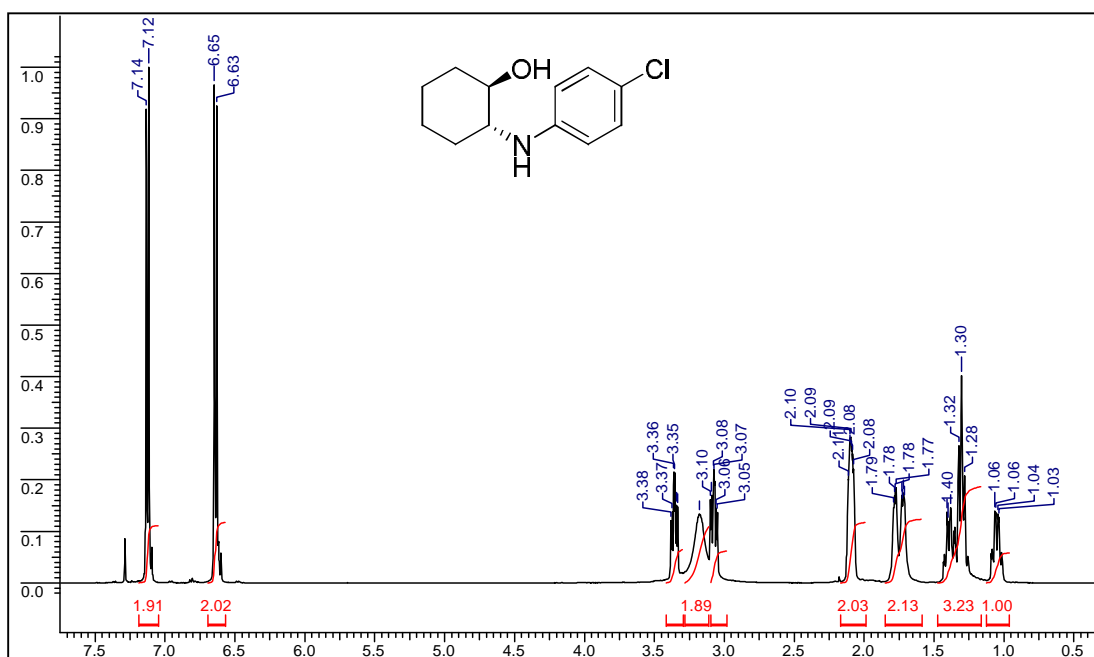
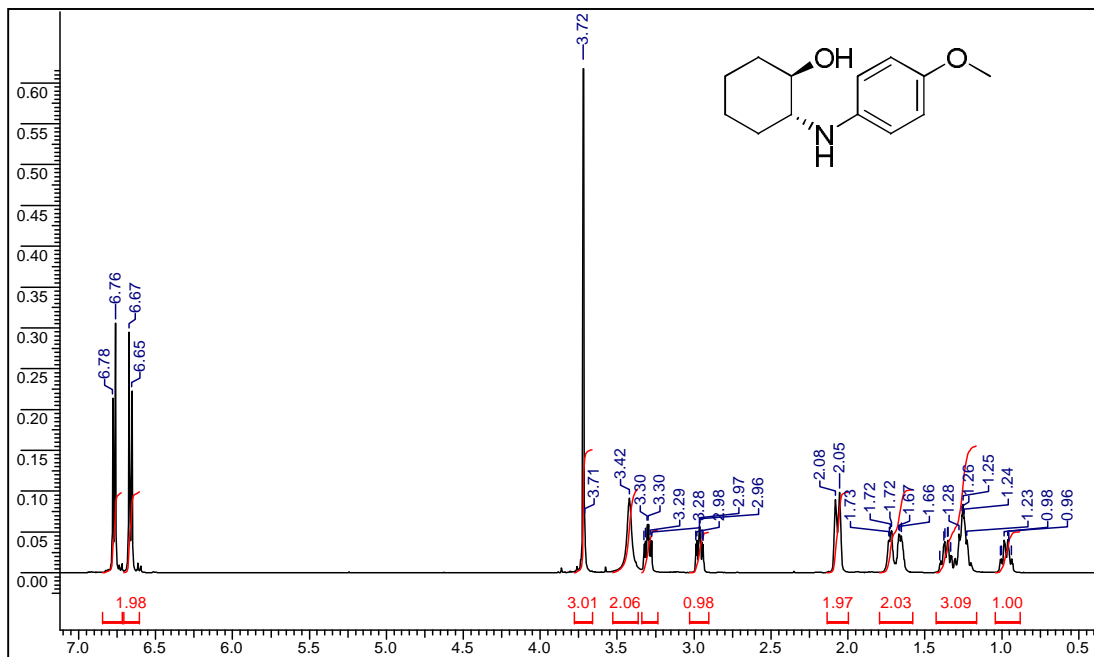


Compound 10: *trans*-2-(4-Methylphenylamino)cyclohexanol

^1H NMR (CDCl_3 , 500MHz): $\delta = 1.01\text{--}1.09$ ppm (m, 1H; CH_2), 1.28–1.47 ppm (m, 3H; CH_2), 1.73–1.82 ppm (m, 2H; CH_2), 2.12–2.16 ppm (m, 2H; CH_2), 2.29 ppm (s, 3H; CH_3), 3.05 ppm (bs, 2H, NH and OH), 3.09–3.14 ppm (m, 1H; CH), 3.34–3.39 ppm (ddd, $J = 10.38, 9.46$ and 4.28 Hz, 1H; CH), 6.67–6.69 ppm (d, 1H; ArH), 7.03–7.05 ppm (d, 1H; ArH).

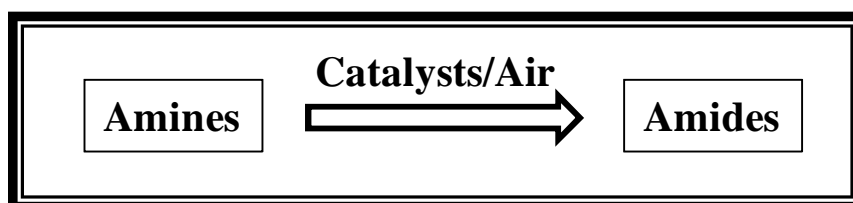
**Compound 11:** *trans*-2-(4-Methoxyphenylamino)cyclohexanol

^1H NMR (CDCl_3 , 500 MHz): $\delta = 0.93\text{--}1.01$ ppm (m, 1H; CH_2), 1.20–1.40 ppm (m, 3H; CH_2), 1.65–1.73 ppm (m, 2H; CH_2), 2.05–2.08 ppm (m, 2H; CH_2), 2.94–2.99 ppm (ddd, $J = 10.99, 9.46$ and 3.97 Hz, 1H; CH), 3.28–3.33 ppm (ddd, $J = 10.38, 9.46$ and 4.58 Hz, 1H; CH), 3.42 ppm (bs, 2H, NH and OH), 3.72 ppm (s, 3H; CH_3), 6.65–6.67 ppm (d, 2H; ArH), 6.76–6.78 ppm (d, 2H; ArH).



CHAPTER – 5

Aerobic Oxidation of Amines to Amides



5.1. Introduction

Aerobic oxidation of amines to amides is an important reaction because amides are valuable synthetic intermediates in chemistry as well as in biology. Amides are widely used in the synthesis of peptide and proteins, intensifiers of perfume, anti-block reagents, color pigments for inks, detergents and lubricants [1]. (Meth)acrylamide and caprolactum are two amide group-containing monomeric compounds of great industrial relevance in the preparation of polymers [2]. Compounds of amides are known to have excellent anthropol-controlling activity and application in treatment of HIV disease, cardiovascular disease, hypertension and high blood pressure [3]. Although, there have been several methods to prepare amides, their preparation under neutral conditions without generating waste by-products is a challenging one. Amides are mostly prepared by the reaction of amines with activated acid derivatives such as acid chlorides and anhydrides [4]. They can also be produced by acid-catalyzed Beckmann rearrangement of ketoximes to *N*-substituted amides [5, 6], the Aube-Schmidt rearrangement [4] and the Staudinger ligation [4]. This reaction generates equimolar quantity of acid by-product, which needs further processing steps to neutralize and separate from the desired amide product. Further, this reaction becomes sluggish and often fails to take place if the amine is deactivated due to presence of electron withdrawing substituents in it.

In 2001, Mori et al. [7] reported the oxidation of primary amines to their corresponding nitriles and hydration of nitriles to amides over hydroxyapatite-bound ruthenium (RuHAP) catalysts. In 2007, Gunanathan et al. [8] have reported the direct synthesis of amides from primary alcohols and amines using PNN pincer-type ruthenium complex. Subsequently, in the same year, Fujiwara et al. [9] reported the one-pot synthesis of primary amides from various kinds of aldoximes in water over rhodium hydroxide supported on alumina ((Rh(OH)_x/Al₂O₃) catalysts. In 2008, Kim et al. [10] reported the direct oxygenation of primary amines to primary amide by molecular oxygen (from air) in presence of water and ruthenium hydroxide supported on alumina catalyst. However, these processes are expensive because of the use of precious metal complexes as catalysts.

There are reports for the synthesis of primary amides from primary alcohols and ammonia in the presence of manganese oxide based octahedral molecular sieves (OMS-2) which have a 2 x 2 hollandite structure and one dimensional pore system [11]. Recently, Wang et al. [12] reported the OMS-2 catalyzed direct transformation

of primary amines to amides through the sequence of oxidative dehydrogenation and successive hydration.

However, it is difficult to oxidize amines into amides selectively because in benzylamine, amine group is more reactive than α -methylene. In earlier reports by Tanaka et al. [13], amine group was protected with *tert.*-butoxycarbonyl group (Boc) and then oxygenated using *in situ* generated RuO₄ followed by deprotection of the Boc group. There are only a few reports in the open literature regarding the oxidation of amines [14].

Amide compounds have also been produced by hydrating the corresponding nitrile over a reduced metal catalyst (Cu, for example), amorphous manganese oxides (MnO₂), supported gold catalysts, etc. [15]. In recent times, nitrile hydratase-containing microorganisms are also being used in their production [16]. There have been some reports on the direct synthesis of amides from alcohols and amines in the presence of metal catalysts [8, 17]. There are very recent reports on the synthesis of primary amides from different starting materials using manganese oxide based catalysts [18-20]. Oxygenation of amines is an efficient route for amides synthesis. This transformation possibly proceeds by a tandem process of oxidative dehydrogenation of amines to nitriles, followed by hydration to produce the corresponding amides [12]. In view of the importance of amide compounds in industrial applications and drawbacks of the known processes which include use of expensive metals, mineral acids or bases for rearrangements, low structural stability and microporosity of catalysts, it is desirable to have a more efficient catalytic process.

Amines are desirable starting materials for the synthesis of amides because they are readily available and inexpensive. The aerobic oxidation of benzylamine over three-dimensional, mesoporous, Mn-SBA-16, Mn-SBA-12, V-SBA-12 and Fe-SBA-12 molecular sieves is reported, for the first time, in this chapter. Benzylamine can be converted into benzamide using these catalysts (Scheme 5.1). In this procedure molecular oxygen (from air) is the sole oxidant and water is the co-product theoretically which makes the process environmental benign.

5.2. Experimental Section

Details on the preparation and characterization of Mn-SBA-12, Mn-SBA-16, V-SBA-12 and Fe-SBA-12 are reported in Chapter 2.

5.2.1. Reaction Procedure

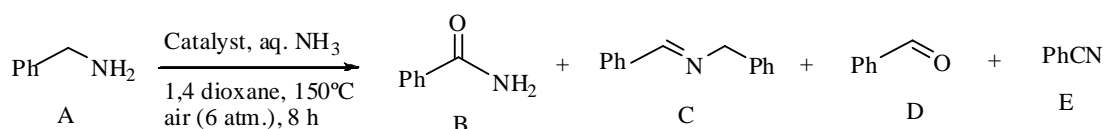
In a typical aerobic oxidation reaction, known quantities of benzylamine, solvent (1,4-dioxane), aqueous ammonia (25 wt%) and catalyst were charged into a Parr reactor (100 mL). It was then pressurized with air, temperature was raised to a desired value and the reaction was conducted for a desired period of time.

5.2.2. Product Analysis

After completion of the reaction, the Parr reactor was depressurized, catalyst was separated by filtration and the liquid product was analyzed by gas chromatography (Varian 3400; CP-SIL8CB column; 30 m-long and 0.53 mm-i.d.) and identified by using GC-MS (Varian CP-3800; 30 m-long, 0.25 mm-i.d., and 0.25 μ m-thick CP-Sil8CB capillary column) and standard product samples.

5.3. Catalytic Activity

Benzylamine can be converted directly into benzamide by reacting with air and aqueous ammonia in the presence of a catalyst (Scheme 5.1). 1,4-dioxane was the suitable solvent because of the high solubilities of benzylamine, ammonia and water [11]. Four oxidation products of benzylamine (A) [benzamide (B), benzylidenebenzylamine (C), benzaldehyde (D) and benzonitrile (E)] are possible (Scheme 5.1). But, in the present study, formation of only B, C and D products was observed. In other cases, some unknown product was also detected.



where A = benzylamine, B = benzamide, C = benzylidenebenzylamine, D = benzaldehyde and E = benzonitrile

Scheme 5.1. Oxidation of benzylamine and the possible reaction products

5.3.1. Influence of Si/Mn Molar Ratio

Table 5.1 shows the oxidation of benzylamine over Mn-SBA-16 catalysts with varying Si/Mn molar ratio. Blank, controlled experiments revealed that the oxidation of benzylamine (A) does not take place in the absence of a catalyst. It is clear from Table 5.1 that the conversion of benzylamine is 100%, even in the presence of bulk MnO₂. But benzamide (B) selectivity was significantly low (4.7% only). Further, turnover frequency (TOF) with MnO₂ is also low (<1 h⁻¹). Mn-SBA-

16 catalysts were highly active with TOF varying between 43 and 138 h⁻¹; benzamide (B) selectivity varied between 19.3 and 40.3 mol%. The catalyst with Si/Mn = 50 exhibited the highest activity (TOF) and benzamide selectivity. This study revealed that the isolated Mn ions in silica matrix provide the desired product while the extra-lattice manganese oxide species yields the undesired products (C and D). Mn-SBA-16 (Si/Mn = 80) catalyst resulted in an unknown product with 5.5 mol% selectivity (Table 5.1).

Table 5.1. Influence of Si/Mn Molar Ratio on the Conversion of Benzylamine and Product Selectivity^a

Catalyst (Si/Mn molar ratio)	Conversion of A (mol%)	TOF (h ⁻¹)	Product selectivity (mol%)			
			B	C	D	Others
Mn-SBA-16 (20)	100	43	25.6	68.9	6.4	-
Mn-SBA-16 (30)	100	65	19.3	78.0	1.7	-
Mn-SBA-16 (40)	100	122	34.0	51.1	14.9	-
Mn-SBA-16 (50)	100	138	40.3	44.7	15.0	-
Mn-SBA-16 (80)	100	103	36.0	46.9	11.6	5.5
MnO ₂	100	<1	4.7	95.3	0	-

^aReaction conditions: Catalyst = 0.2 g, benzylamine = 5 mmol (0.53 g), aqueous NH₃ (25%) = 1 mL, solvent = 1,4 dioxane (15 mL), stirring speed (rpm) = 600, reaction pressure = 6 atm, reaction temperature = 423 K and reaction time = 8 h. Mn-SBA-16 (Si/Mn = 20 to 80) were prepared by using 2 M HCl solution. TOF (turn over frequency) = number of moles of benzylamine converted per mole of Mn (output) present in the catalyst per hour

5.3.2. Influence of Different Catalysts

Table 5.2 shows the influence of catalyst on the catalytic activity and product selectivity in the oxidation of benzylamine. Benzylamine conversion was nearly 100% for all the catalysts investigated but the product selectivity varied (Table 5.2). V-SBA-12 (Si/V = 30) showed a high level of product selectivity (42.5%) as compared to the rest of the catalysts. This difference in product selectivity may be due to the differences in the adsorption of reactants on the catalyst surface for the reaction to occur.

Table 5.2. Influence of Different Catalysts on the Conversion of Benzylamine and Product Selectivity^a

Catalyst (Si/M molar ratio, M = Mn, Fe and V)	Conversion of A (mol%)	TOF (h ⁻¹)	Product selectivity (mol%)			
			B	C	D	Others
Mn-Al-SBA-16 (30)	100	-	24.5	54.3	9.7	11.5
Mn-SBA-16 (30)	100	65	19.3	78.0	1.7	-
Mn-SBA-12 (20)	100	52	30.9	62.3	6.8	-
Fe-SBA-12 (20)	100	-	31.2	56.9	11.9	-
V-SBA-12 (30)	100	47	42.5	40.9	16.6	-

^aReaction conditions: Catalyst = 0.2 g, benzylamine = 5 mmol (0.53 g), aqueous NH₃ (25%) = 1 mL, solvent = 1,4 dioxane (15 mL), stirring speed (rpm) = 600, reaction pressure = 6 atm, reaction temperature = 423 K and reaction time = 8 h. Mn-Al-SBA-16 (30) and V-SBA-12 (Si/V = 30) were prepared using 2 M HCl solution while Mn and Fe-incorporated SBA-12 were prepared using 0.1 M HCl solution (Chapter 2). TOF (turn over frequency) = number of moles of benzylamine converted per mole of Mn/V (output) present in the catalyst per hour

5.3.3. Influence of Reaction Time

Table 5.3 shows the effect of reaction time on the conversion of benzylamine and benzamide product selectivity. Complete conversion of benzylamine was achieved in just 2 h (Table 5.3). Benzamide selectivity increased from 34.0 to 47.1% with an increase in reaction time from 2 to 10 h.

5.3.4. Influence of Reaction Temperature

Table 5.4 shows the effect of reaction temperature on the catalytic activity of Mn-SBA-16 (Si/Mn = 50). Only 10.2% of benzylamine conversion was obtained at 373 K with benzylidenebenzylamine (C) as the only product. With increasing reaction temperature from 373 to 403 K, a significant increase in benzylamine conversion from 10.2 to 90% was observed. At 403 K, product selectivities for B (benzamide) and C (benzylidenebenzylamine) were 14.5 and 73.8%, respectively. At higher temperatures, the product C decomposes into aldimine (possible reaction intermediate) which through oxidative dehydrogenation and successive hydration in the presence of aqueous ammonia forms benzamide [11]. Complete conversion of

benzylamine was observed at 423 K with benzamide selectivity of 40.3%. At this temperature, selectivity of product C had decreased to 44.7%; product D (benzaldehyde) formed with a selectivity of 15.0% (Table 5.4). With increasing reaction temperature from 373 to 423 K, TOF had increased from 14 to 138 h⁻¹.

Table 5.3. Influence of Reaction Time on the Conversion of Benzylamine and Product Selectivity^a

Entry No.	Reaction time (h)	Conversion of A (mol%)	TOF (h ⁻¹)	Product selectivity (mol%)		
				B	C	D
1	2	100	552	34.0	36.0	30.0
2	4	100	276	39.5	30.0	31.5
3	6	100	184	42.4	36.2	21.4
4	8	100	138	40.3	31.3	28.4
5	10	100	110	47.1	35.9	17.0

^aReaction conditions: Catalyst, Mn-SBA-16 (Si/Mn = 50, 2 M) = 0.2 g, benzylamine = 5 mmol (0.53 g), aqueous NH₃ (25%) = 0.5 mL, solvent = 1,4 dioxane (15 mL), reaction pressure = 6 atm, stirring speed (rpm) = 600 and reaction temperature = 423 K. TOF (turn over frequency) = number of moles of benzylamine converted per mole of Mn (output) present in the catalyst per hour

Table 5.4. Influence of Reaction Temperature^a

Entry No.	Reaction Temperature (K)	Conversion of A (mol%)	TOF (h ⁻¹)	Product selectivity (mol%)		
				B	C	D
1	373	10.2	14	-	100.0	-
2	403	90.0	124	14.5	73.8	-
3	423	100.0	138	40.3	44.7	15.0

^aReaction conditions: Catalyst, Mn-SBA-16 (Si/Mn = 50, 2 M) = 0.2 g, benzylamine = 5 mmol (0.53 g), aqueous NH₃ (25%) = 1 mL, solvent = 1,4 dioxane (15 mL), stirring speed (rpm) = 600, reaction pressure = 6 atm and reaction time = 8 h. TOF (turn over frequency) = number of moles of benzylamine converted per mole of Mn (output) present in the catalyst per hour

5.3.5. Influence of Reaction Pressure

Table 5.5 shows the influence of reaction pressure on the catalytic activity of Mn-SBA-16 (Si/Mn = 50). Pressure doesn't affect the conversion of benzylamine and even at 6 atm, complete conversion of benzylamine was observed at 423 K and reaction time of 8 h (Table 5.5). Pressure had a marginal effect on product B selectivity which increased from 40.3 to 44.0% with rise in pressure from 6 to 10 atm. (Table 5.5). Under these conditions, a major decrease in product C selectivity was observed. At high pressure (ca., 8 - 10 atm), an unknown compound had also formed, identity of which could not be made at this point of time.

Table 5.5. Influence of Reaction Pressure on the Conversion of Benzylamine and Product Selectivity^a

Entry No.	Reaction pressure (atm.)	Conversion of A (mol%)	TOF (h ⁻¹)	Product selectivity (mol%)			
				B	C	D	Others
1	6	100	138	40.3	44.7	15.0	-
2	8	100	138	42.9	6.9	19.1	31.1
3	10	100	138	44.0	4.5	25.2	26.3

^aReaction conditions: Catalyst, Mn-SBA-16 (Si/Mn = 50, 2 M) = 0.2 g, benzylamine = 5 mmol (0.53 g), aqueous NH₃ (25%) = 1 mL, solvent = 1,4 dioxane (15 mL), stirring speed (rpm) = 600, reaction temperature = 423 K and reaction time = 8 h. TOF (turn over frequency) = number of moles of benzylamine converted per mole of Mn (output) present in the catalyst per hour

5.3.6. Reaction Mechanism and Structure - Activity Relationship

Fig. 5.1 shows the possible reaction mechanism for the formation of amides from amines. According to this mechanism, amine (A) is converted into an intermediate aldimine through oxidative dehydrogenation. This intermediate undergoes further transformation by two reaction pathways. According to the first pathway, it can get hydrolyzed in presence of water into an aldehyde (D) which can then react with the initial reactant amine (A) resulting in a condensed product, alkylimine (C). Product C can also decompose into aldimine intermediate in the presence of ammonia. According to the second pathway, aldimine undergoes one more oxidative dehydrogenation resulting in the formation of a nitrile intermediate

(**E**) which through further hydration and amination (in presence of ammonia) forms a stable amide (**B**) [12].

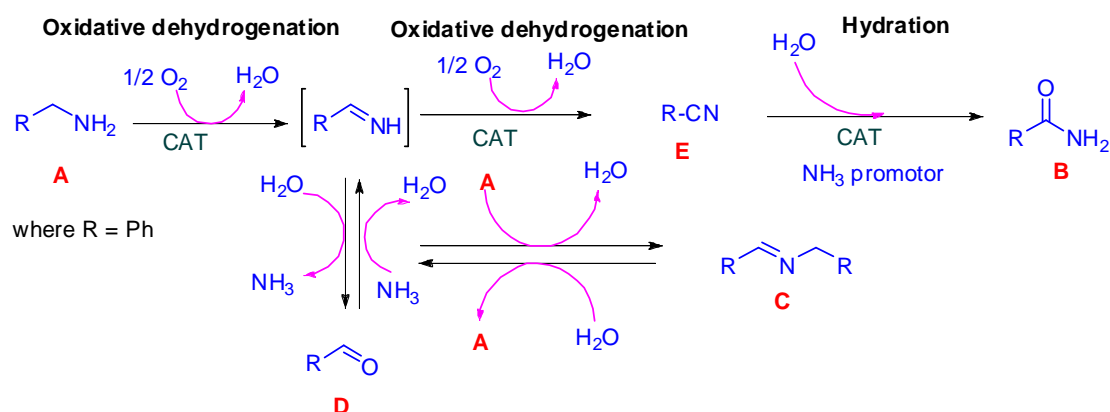


Fig. 5.1. Possible reaction mechanisms for the formation of primary amides from primary amines

Complete conversion of benzylamine (**A**) was achieved with all the Mn-SBA-16/12 catalysts investigated. However, the product selectivity was different. As shown in Fig. 5.1, oxidative dehydrogenation which is dependent on the metal redox behavior and hydrolysis/reaction with amine which are dependent on the acidic behavior of the catalyst are the two competing reactions controlling the product selectivity. Complete conversion with all the Mn catalysts indicates that the first step i.e., amine to aldimine formation (oxidative dehydrogenation) is a facile reaction. Acidity vs redox behavior of the catalyst decides whether aldimine undergoes hydrolysis to benzaldehyde (**D**) which further reacts with A to form benzylidenebenzylamine (**C**) or follows the other route. The backward reaction of benzaldehyde (**D**) to aldimine can also take place in presence of ammonia. However, benzylamine is relatively more basic than ammonia [$pK_b = 4.66$ (benzylamine) and 4.75 (ammonia)] and hence, formation of **C** is preferred over acid catalysts than the reverse reaction of **D** to aldimine. Moreover, aldimine could not be detected in the product. So it is an intermediate under our experimental conditions. Under mild acidic conditions and Mn with a facile redox state, further oxidative dehydrogenation followed by hydrolysis and amination converts aldimine into benzamide. In other words, the catalyst for this reaction should possess facile redox behavior and weak acidity for amides (**B**) to form with high selectivity.

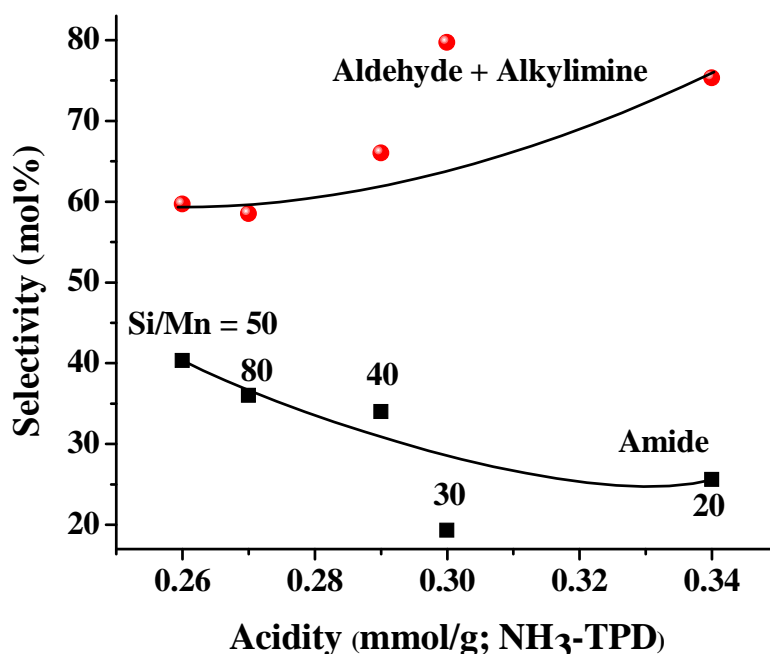


Fig. 5.2. Correlation between product selectivity and acidity of Mn-SBA-16 catalyst

Fig. 5.2 shows a correlation between product selectivity and acidity of the catalyst. With increasing acidity of the catalyst higher amounts of benzylidenebenzylamine (C) + benzaldehyde (D) products have formed and the selectivity for benzamide (B) has decreased. As noted in Chapter 2, with decreasing Si/Mn ratio, the concentration of Mn²⁺ showing an electronic band at 500 nm in the DRUV-vis spectrum and paramagnetic sextet-line pattern in the EPR spectrum increased. The framework substituted Mn is in +3 oxidation state. At higher Mn contents (lower Si/Mn ratio), only a small part of Mn is in framework +3 oxidation state and the remaining is present as extraframework Mn²⁺ species. While both the Mn species are active for the conversion of benzylamine to aldimine, only the +3 state Mn species facilitates amide (B) formation while the extraframework +2 state Mn leads to benzylidenebenzylamine (C) + benzaldehyde (D) products formation. Thus, this study reveals that weak acidity and high amount of framework substituted +3 state Mn ions are the key characteristic features of Mn-SBA-16/12 catalysts to be active in amine to amide oxidation reactions.

5.4. Conclusions

Aerobic oxidation of benzylamine to benzamide was carried out over different transition metals (Mn, Fe and V) incorporated three-dimensional SBA-12 and SBA-16 molecular sieves. While the framework substituted Mn facilitated benzamide formation, the extraframework Mn led to the undesired products – benzylidenebenzylamine and benzaldehyde. The effect of reaction parameters on catalytic activity and product selectivity was investigated. Mild acidity and Mn in +3 oxidation state are key factors for Mn-SBA-16 catalysts to be highly active and selective in the oxidation of primary amines to amides.

5.5. References

- (a) C. E. Mabermann in *Encyclopedia of Chemical Technology*, Vol. 1 (Eds.: J.I. Kroschwitz), Wiley, New York, 1991, p. 251. (b) D. Lipp in *Encyclopedia of Chemical Technology*, Vol. 1 (Eds.: J.I. Kroschwitz), Wiley, New York, 1991, p. 266. (c) R. Opsahl in *Encyclopedia of Chemical Technology*, Vol. 2 (Eds.: J. I. Kroschwitz), Wiley, New York, 1991, p. 346.
- (a) U.S. Patent 5,626,836 (1997). (b) U.S. Patent 6,225,429 (2001).
- (a) U.S. Patent 5,196,438 (1993). (b) E. Valeur, M. Bradley, *Chem. Soc. Rev.* 38 (2009) 606.
- (a) M.B. Smith, J. March, *March's Advanced Organic Chemistry: Reactions, Mechanisms, and Structure*, 6th ed., Wiley, Hoboken, NJ, 2007. (b) M.B. Smith, *Organic Synthesis*, 2nd ed., Mc-Graw-Hill Companies, New York, 2002.
- (a) O. Meth-Cohn, B. Narine, *Synthesis* 133 (1980). (b) R. E. Gawley, *Org. React.* 1 (1988) 1. (c) L. De Luca, G. Giacomelli, A. Porcheddu, *J. Org. Chem.* 67 (2002) 6272. (d) S. Chandrasekhar, K. Gopalaiah, *Tetrahedron Lett.* 44 (2003) 755. (e) Y. Furuya, K. Ishihara, H. Yamamoto, *J. Am. Chem. Soc.* 127 (2005) 11240.
- Y. Izumi, H. Ichihashi, Y. Shimazu, M. Kitamura and H. Sato, *Bull. Chem. Soc. Jpn.* 80 (2007) 1280.
- K. Mori, K. Yamaguchi, T. Mizugaki, K. Ebitani, K. Kaneda, *Chem. Commun.* (2001) 461.
- C. Gunanathan, Y. B.-David, D. Milstein, *Science* 317 (2007) 790.
- H. Fujiwara, Y. Ogasawara, K. Yamaguchi, N. Mizuno, *Angew. Chem. Int.*

- Ed. 46 (2007) 5202.
10. J.W. Kim, K. Yamaguchi, N. Mizuno, *Angew. Chem. Int. Ed.* 47 (2008) 9249.
 11. K. Yamaguchi, H. Kobayashi, T. Oishi, N. Mizuno, *Angew. Chem. Int. Ed.* 51 (2012) 544.
 12. Y. Wang, H. Kobayashi, K. Yamaguchi, N. Mizuno, *Chem. Commun.* 48 (2012) 2642.
 13. K.-I. Tanaka, S. Yoshifuji, Y. Nitta, *Chem. Pharm. Bull.* 36 (1988) 3125.
 14. M. T. Schumperli, C. Hammond, I. Hermans, *ACS Catal.* 2 (2012) 1108.
 15. (a) U.S. Patent 3,642,894 (1972). (b) U.S. Patent Re. 32,640 (1988). (c) T. Subramanian, K. Pitchumani, *Catal. Commun.* 29 (2012) 109. (c) K. Yamaguchi, Y. Wang, H. Kobayashi, N. Mizuno, *Chem. Lett.* 41 (2012) 574. (d) Y.-M. Liu, L. He, M.-M. Wang, Y. Cao, H.-Y. He, K.-N. Fan, *ChemSusChem* 5 (2012) 1.
 16. K. Ingvørsen, J. Kamphuis, in *Enzyme Catalysis in Organic Synthesis: A Comprehensive Handbook*, ed. by K. Drauz, H. Waldmann, VCH, Weinheim, 1995, Vol. 1, pp. 365.
 17. J.-F. Soulé, H. Miyamura, S. Kobayashi, *J. Am. Chem. Soc.* 133 (2011) 18550.
 18. Y. Wang, K. Yamaguchi, N. Mizuno, *Angew. Chem. Int. Ed.* 51 (2012) 7250.
 19. R. Nie, J. Shi, S. Xia, L. Shen, P. Chen, Z. Hou, F.-S. Xiao, *J. Mater. Chem.*, 22 (2012) 18115.
 20. K. Yamaguchi, Y. Wang, N. Mizuno, *Chem. Lett.* 41 (2012) 633.

CHAPTER – 6

Summary and Overall Conclusions

Ordered mesoporous silica or silicate materials should overcome the limitations of zeolites for applications in transformation of bulky organic molecules of pharmaceutical interest. In principle, the pore size and surface structure of these porous solids can be tailored to suit for their application. However, most of the materials known today (MCM-41 series, for example) are less active and thermally less stable compared to zeolites. Hence, development of efficient mesoporous solids remains a changing task in Catalysis and Material Chemistry research. Three-dimensional ordered mesoporous systems enable better diffusion and availability active sites to reactant molecules than the two-dimensional solids. In this context, synthesis, characterization and catalytic activity investigation of transition metal incorporated SBA-12 and SBA-16 have been undertaken in this work. SBA-12 and SBA-16 belong to the class of three-dimensional, ordered mesoporous silica systems with thick pore walls. They have higher stability than MCM-41. However, as these materials are synthesized in highly acidic conditions, incorporation of metal (M) in their framework to induce redox and Lewis acidic functionalities is a challenging task. It is shown in the present work that by suitably adjusting the synthesis conditions a variety of metal (M = Ti, Mn, V and Fe)-containing SBA-12 and SBA-16 materials with Si/M input ratio in the range of 20 – 80 can be synthesized. The catalytic applications of these new porous solids in selective oxidation and acid catalyzed reactions have been investigated. It has been found that the catalysts of the present study are more active than the hitherto known mesoporous silicates. A brief summary and conclusions of the present work is provided below.

Transition metal (Ti, Mn, V and Fe) incorporated SBA-12 and SBA-16 mesoporous silica materials were prepared by direct hydrothermal synthesis method ([Chapter 2](#)). The composition, structure and textural properties of the materials were determined by ICP-OES, XRD, HRTEM, N₂-physisorption, FTIR, FT-Raman, DRUV-vis, ²⁹Si MAS NMR, EPR and TG-DTA techniques. Acidic properties of the solid catalysts were evaluated by NH₃-TPD and DRIFT spectroscopy of adsorbed pyridine. A linear increase in unit cell parameters and unit cell volume of SBA-12 and SBA-16 was observed with increasing metal ion content providing an unequivocal evidence for the substitution of metal ions in the framework of M-SBA-12 and M-SBA-16. Metal incorporation has also affected the textural properties. TG-DTA and ²⁹Si MAS NMR studies revealed that M-SBA-16 are relatively more hydrophobic than M-SBA-12. The extent of metal incorporation in the framework is

higher in the case of Ti than with Mn, V and Fe. Framework substituted metal ion content is more in Ti-SBA-16 than in Ti-SBA-12. Acidity measurement revealed the presence of weak and strong Lewis acid sites. Brönsted acidity was not detected.

Catalytic properties of Ti-SBA-12 and Ti-SBA-16 were investigated in the liquid phase oxidation reactions viz., (1) epoxidation of cyclic olefins (cyclohexene and cyclooctene) and phenol hydroxylation (Chapter 3). Cyclohexene and cyclooctene were epoxidized with high selectivity at 100% conversion using *tert.*-butylhydroperoxide as oxidant. Activity of these titanosiicates was superior to microporous TS-1 and mesoporous Ti-MCM-41. TBHP (5.5 M) in decane was found to be the best oxidant. Solvent has the marked effect on catalytic activity. Dichloromethane was found to be the best solvent. These catalysts were also found highly active for selective hydroxylation of phenol. Their intrinsic catalytic activity was lower than that of microporous TS-1. But they were superior to most of the know mesoporous titanosilicates. Catechol and hydroquinone were the only products in phenol hydroxylation. Over oxidation to benzoquinones did not occur. The *para* selective hydroxylation was more predominant over Ti-SBA-12 than on TS-1 and Ti-SBA-16. The mesoporous Ti catalysts were reusable with little loss in activity and product selectivity. Isolated framework Ti with tetrahedral geometry and three-dimensional, ordered mesoporosity are the unique characteristic features responsible for the highly efficient oxidation activity of Ti-SBA-12 and Ti-SBA-16 catalysts.

Two types of acid catalyzed reactions viz., (1) aminolysis of epoxides and (2) esterification of oleic acid with methanol were investigated using Ti-SBA-12 and Ti-SBA-16 catalysts (Chapter 4). A range of β -amino alcohols with high regio- and stereo-selectivity were synthesized in solvent-free reaction conditions using Ti-SBA-12 and Ti-SBA-16, by reacting symmetric or unsymmetric epoxides with aromatic as well as aliphatic amines at ambient conditions. Structure-function relationships revealed that the superior activity of Ti-SBA-16 is possibly due to its high amount of framework-substituted tetrahedral Ti ions, higher acidity and surface hydrophobicity. Catalyst reusability study up to 6th recycling experiment revealed that these titanosilicates are stable and reusable catalysts. They were more efficient than the hitherto known mesoporous titanosilicate catalysts for the aminolysis of epoxides. Both Ti-SBA-12 and Ti-SAB-16 showed high catalytic activity for the esterification of oleic acid (a representative fatty acid) with methanol. Methyl oleate ester (biodiesel) yields as high as 90 mol% were obtained at 443 K. Energy of activation

(E_a) for the esterification reaction was estimated to be 42.7 and 25.6 kJ/mol for Ti-SBA-12 and Ti-SBA-16, respectively. Higher amount of surface hydrophobicity is the cause of more efficient activity of Ti-SBA-16 than Ti-SBA-12.

Aerobic oxidation of benzylamine was carried out over different transition metals (Mn, Fe and V) incorporated three-dimensional SBA-12 and SBA-16 molecular sieves. While the framework substituted Mn facilitated benzamide formation, the extraframework Mn led to other products – benzylidenebenzylamine and benzaldehyde. Structure-activity correlations revealed that mild acidity and Mn in +3 oxidation state are the key features of Mn-SBA-16 to be a highly selective catalyst in the direct oxidation of amines to amides ([Chapter 5](#)).

By and large, this thesis contributes the synthesis and characterization of transition metal (Ti, Mn, V and Fe) incorporated three-dimensional mesoporous silica materials, SBA-12/SBA-16. These metallosilicates have been found to be more efficient than the known mesoporous metallosilicates in certain industrially relevant organic transformations. Structure-function correlations revealed that the framework substituted metal ions as well as the unique pore structure and hydrophilic-hydrophobic properties are responsible for the high activity and product selectivity of these novel catalysts. In general, the work presented in this thesis contributes to the area of new materials and sustainable catalytic processes.

List of Research Publications

1. Synthesis of framework Ti-substituted, 3-D hexagonal, mesoporous Ti-SBA-12 for selective catalytic oxidation
A. Kumar, D. Srinivas, P. Ratnasamy
Chem. Commun. (2009) 6484 – 6486.
2. Selective oxidation of cyclic olefins over framework Ti-substituted, three-dimensional, mesoporous Ti-SBA-12 and Ti-SBA-16 molecular sieves
A. Kumar, D. Srinivas
Catal. Today 198 (2012) 59 – 68.
3. Aminolysis of epoxides catalyzed by three-dimensional, mesoporous titanosilicates, Ti-SBA-12 and Ti-SBA-16
A. Kumar, D. Srinivas
J. Catal. 293 (2012) 126 – 140.
4. Hydroxylation of phenol with hydrogen peroxide catalyzed by Ti-SBA-12 and Ti-SBA-16
A. Kumar, D. Srinivas
J. Mol. Catal. A: Chem. 368 – 369 (2013) 112 – 118.
5. Three-dimensional mesoporous titanosilicates as catalyst for producing biodiesel and biolubricants
Mahejabeen Kotawal, **Anuj Kumar**, Darbha Srinivas
Manuscript communicated.
6. Aerobic oxidation of amines to amides over three-dimensional, mesoporous Mn-SBA-12 and Mn-SBA-16 catalysts
Anuj Kumar, Devadutta Nepal, Darbha Srinivas
Manuscript under preparation for communication.

List of Patents

1. Ordered mesoporous titanosilicate and the process for the preparation thereof
Darbha Srinivas, **Anuj Kumar**
International Publication Number WO 2012/011124 A1
2. Process for producing amides compounds
Darbha Srinivas, **Anuj Kumar**, Devadutta Nepak
India, US and EP - Appl. No. 602DEL2012